Application of Environmental Technology Management (ETM) to Automobile Exhaust Emission Reduction

by

Meshari AL-Harbi

A thesis

presented to the University of Waterloo

in fulfillment of the

thesis requirement for the degree of

Doctor of Philosophy

in

Chemical Engineering

Waterloo, Ontario, Canada, 2010

AUTHOR'S DECLARATION

I hereby declare that I am the sole author of this thesis. This is a true copy of the thesis, including any required final revisions, as accepted by my examiners. I understand that my thesis may be made electronically available to the public.

Abstract

Vehicle emissions, arising from incomplete fuel combustion and reactions between N_2 and O_2 leading to NO_X, have detrimental effects on human health and environment quality. Engine exhaust contains a variety of regulated components, such as hydrocarbons, CO, nitrogen oxides (NO_X), and particulate matter (PM). Government environmental agencies have been continuously establishing regulations for automobile manufacturers to reduce these emissions. Lean-burn engines operate with an excess of oxygen, which makes the reduction of NO_X, challenging, with a coincident challenge for diesel engines being PM. Diesel particulate filters have been successfully employed to reduce PM. NO_X storage and reduction (NSR) catalysts and selective catalytic reduction (SCR) catalysts are two promising technologies used to mitigate NO_X emissions. A diesel oxidation catalyst (DOC) is usually placed upstream of these to reduce hydrocarbons and CO emissions and oxidize NO to NO_2, which leads to improved performance over these catalysts.

In this study, the performance of DOCs and NSR catalysts, individually and in series, has been investigated as a function of temperature, gas composition, catalyst length, and catalyst configuration. The catalytic oxidation of CO, hydrocarbons, and NO, both individually and in mixtures with NO_2, was investigated over a monolith-supported DOC. The data clearly show mutual inhibition effects between these species. Addition of each gas to the inlet gas mixture caused an increase in the light-off temperatures of the other species, mainly due to site adsorption competition. CO was less affected by other species because its light-off temperatures began prior to those of NO_X and other

hydrocarbons, and it is likely the primary surface species poisoning the active sites at low temperature.

Hydrogen production via hydrocarbon steam reforming and water gas shift reactions was also investigated over a DOC during steady-state and cycling conditions (to mimic NSR catalyst operation) along the catalyst length. C_3H_6 and dodecane steam reforming started at 375 and 450°C, respectively, whereas the water gas shift reaction started at 225°C, and proceeded further than hydrocarbon steam reforming in terms of H_2 production. It should be mentioned that H_2 production via the hydrocarbon steam reforming and water gas shift reactions during cycling experiments, was higher than that observed during steady-state experiments. According to temperature programmed oxidation experiments performed after steam reforming, the better performance during cyclic operation is because less coke was deposited compared to that with steady-state experiments.

Experiments were also performed over a NSR catalyst. The evaluations included testing the performance as a function of NO_X source, NO or NO_2, testing different regeneration protocols, and evaluating different reducing agents (hydrocarbons, H_2, or CO). For NO and NO_2 as the NO_X source, the trapping and reduction performance was better when NO_2 was used at all operating temperatures except 300°C, likely due to high NO oxidation activity and rapid trapping of NO_2 at 300°C. Numerous reasons were provided to explain the improved performance with NO_2 at other tested temperatures. The foremost reason though, is treating the monolith as an integral reactor. With NO_2 as the NO_X source, NO_2 can be readily trapped at the very inlet and along the catalyst length, resulting in a higher trapping amount. Along the same concept, the released NO_X

from the inlet of the catalyst has more residence time and contact with downstream Pt sites, but more importantly more interaction between reductant and stored NO_X. In the second set of experiments, different regeneration protocols were used. Different regeneration times, 4, 8 and 16 seconds with 4, 2, and 1% H_2 as the reductant amounts, and constant lean times were evaluated. The data clearly show an improvement with longer regeneration times in both NO_X trapping and overall reduction performance at all temperatures except 500°C, where the more significant NO_X release resulted in an overall decrease in NO_X conversion with increasing regeneration time. The improved performance at the lower temperatures is due to more extensive nitrate/nitrite decomposition with longer regeneration times, thus leading to more extensive surface cleaning. The performance of the NSR catalyst was also investigated using hydrocarbons, H_2, or CO as reducing agents. H_2 was found the best at $T \leq 250$°C, where the decreased performance with CO and hydrocarbons was due to Pt site poisoning at 200°C and as a result of slow kinetics at 250°C. CO and hydrocarbons, however, proved to regenerate the catalyst as efficiently as H_2 at $T \geq 300$°C. Hydrogen production via steam reforming experiments can not explain the improved performance with hydrocarbons, since propylene steam reforming occurred at 375°C, with only a small amount of H_2 generated, and dodecane or m-xylene reforming did not occur below 450°C. TPR data show that propylene started to activate as low as 217°C and the complete reduction of NO by propylene was achieved at 287°C. For surface chemisorbed NO_X species, propylene was observed to reduce these species at $T > 200$°C, with high rates by 264°C, with this activity eventually leading to comparable performance with either CO or H_2 at similar temperatures during NO_X cycling experiments.

The performance of two different hybrid DOC+NSR systems was also investigated. In the first configuration, a DOC and NSR catalyst were placed in series while in the other configuration, the DOC and NSR catalysts were divided into two equal volumes and placed in series (DOC + NSR + DOC + NSR). Overall, the data show an increase in the NO_X performance with the split configuration at all temperatures tested, with small changes at 200°C due to poisoning effects of Pt and Ba sites by CO and hydrocarbons being significant. The improved performance with the split configuration was related to further NO oxidation occurring over the 2nd DOC, more H_2 formed from steam reforming and WGS reactions, and reduced inhibition of the WGS reaction by hydrocarbons.

Acknowledgements

I would never have been able to finish my dissertation without the guidance and support of ALLAH (GOD) throughout my study.

I am and will be heartily thankful and grateful to my supervisor, William S. Epling, whose encouragement, valuable comments, guidance, patience, supervision and support from the preliminary to the concluding level enabled me to develop an understanding of the subject. The good seeds you planted in me will be always the ignition source of my success.

I would like to express my immense appreciation and thanks to my supervisory committee members: Professor Kevin Smith, Professor John Wen, Professor Ali Elkamel, and Professor Zhongwei Chen.

Special thanks and appreciation to my wife (Manal), who left her job, family, and friends, to join me on this journey. She is the source of love, inspiration, and support. She was always there cheering me up and stood by me through the good times and bad.

I would also like to thank my parents, brothers and sisters, and my best friend Musaed AL-Fadly. They were always supporting me and encouraging me with their best wishes. I am grateful to all my friends who I knew in Waterloo, for being the surrogate family during the many years I stayed there and for their continued moral support there after. My deep appreciation also goes to all my friends in Catalysis Research Groups, and secretaries and technicians in the chemical engineering department.

Finally, I would like to thank Kuwait University, Natural Sciences and Engineering Research Council of Canada Discovery Grant Program, and Auto 21 for financial support, and Johnson Matthey and Umicore for the samples provided.

Dedication

To my beloved parents,

my beloved wife…Manal,

and my lovely son…Mohammed

Table of Contents

Chapter-3: Competitive NO, CO and hydrocarbon oxidation reactions over a diesel oxidation catalyst

Chapter-4: Hydrogen generation and coke formation over a diesel oxidation catalyst under fuel rich conditions

Chapter-5: Investigating the Effect of NO Versus NO₂ on the Performance of a Model NOₓ Storage/Reduction Catalyst

Chapter-6: Effects of Different Regeneration Timing Protocols on the Performance of a Model NOₓ Storage/Reduction Catalyst

Chapter-7: Regeneration of a Model NOₓ Storage/Reduction Catalyst   Using Hydrocarbons as the Reductant

Chapter-8: DeNO$_X$ Performance in Different Hybrid DOC+NSR Systems

Chapter-9: Conclusions and Recommendations

Appendix A

List of Figures

List of Tables

Chapter 1: Introduction

1.1 Environmental Technology Management (ETM)

Environmental Technology Management (ETM) is a multidisciplinary science that combines three interrelated fields; environmental science, environmental management, and environmental technology. Environmental science is the field that studies the environment (air, water, and land) and the interaction between the environment and humans [1]. Environmental management is an approach to environmental stewardship which deals with prevention and resolution of environmental problems, establishing limits, and identifying new technologies or policies that are useful [2]. Environmental technology is defined as any technology that reduces risks to humans and environmental ecology, improves process efficiency, and creates products that are environmentally friendly [3]. These disciplines collectively aim to provide a comprehensive understanding of environmental issues for air, water, and land and solutions to those issues.

The focus of the research to be described is a proposed solution to control emissions from automobiles. Figure 1.1 describes an example of application of the ETM concept to motor vehicle emissions. In the rest of this section, automobile emissions and the approaches to manage automobile emissions via stipulating standards and regulations will be discussed. Finally, the feasibility of using different technologies to control these emissions, specifically for diesel engines, will be evaluated.

Environmental Technology Management

Environment → Automobile Emission → Health & Safety → **Management** → Automobile Management → Standards & Regulation → **Technology** → Automobile Technology

Diesel Engine → DOC, NSR, SCR

Gasoline Engine → TWC

Evaluation — Yes → Commercialized / NO
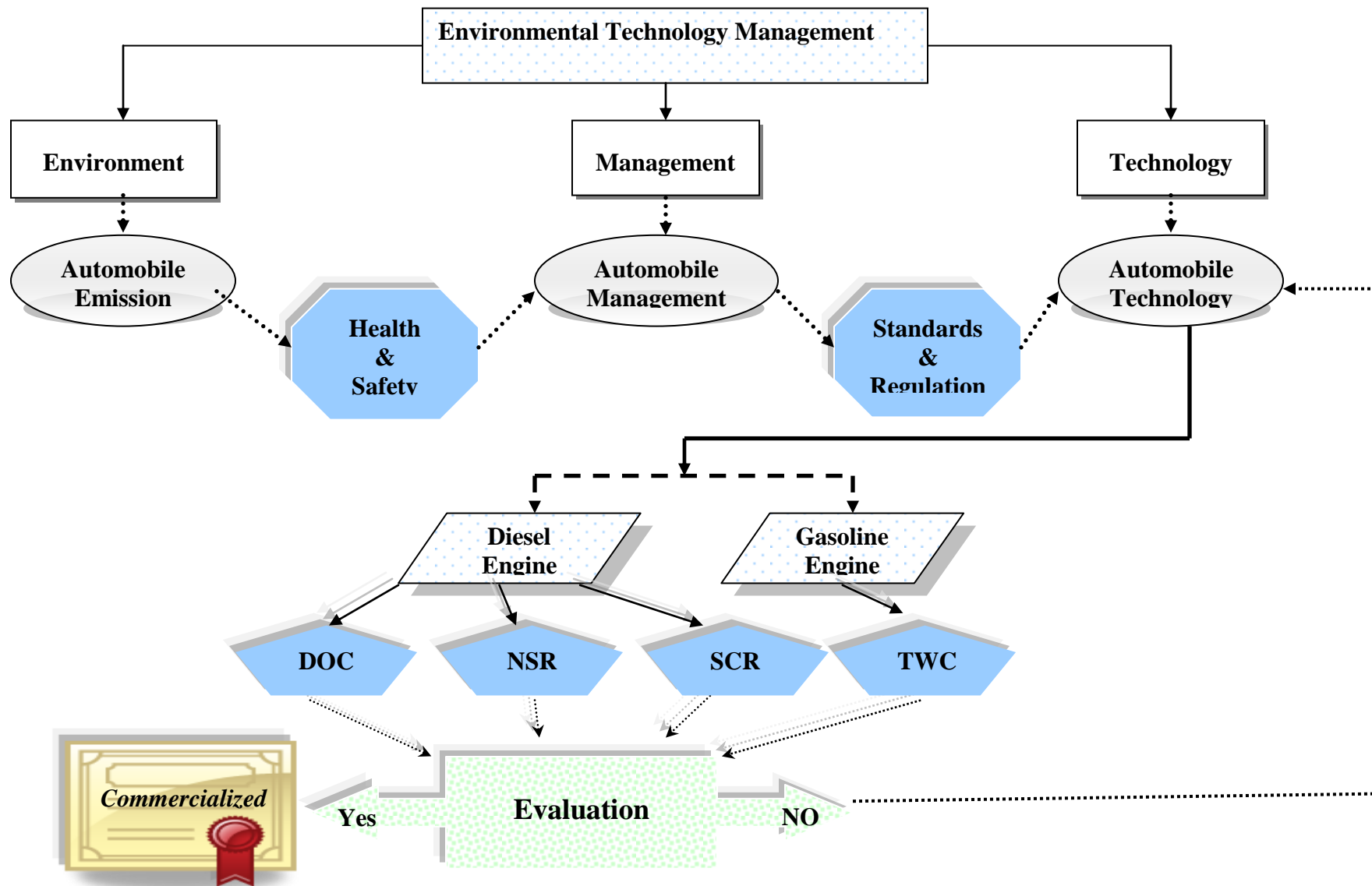
Figure 1.1 Application of the environmental technology management concept to automobile emissions

1.2 Environment

1.2.1   Automobile Emissions

Automobile emissions are the largest contributor to urban air contaminant emissions and one of the largest sources of greenhouse gases [4,5]. In 2002, about 67.4% of CO, 60% of nitrogen oxides, and 7.1% of particulate matter (PM) emitted came from automobiles, as cited by the Environmental Protection Agency (EPA) with highlights in Table 1.1 [6]. Additionally, automotive CO_2 emissions are considered a significant contributor to global warming and thus climate change. Compounding this is the increasing numbers of vehicles on the road and different emissions regulations in different countries.

Table 1.1 Automobile Emissions Relative to Total Emission Sources (Kilotons) in 2002

Emission Source	CO	NO$_X$	VOCs	PM	SOx
On Road Vehicle	**62,957**	**8,133**	**4,660**	**14.433**	**257.6**
Non Road Vehicle	**22,414**	**4,517**	**2,623.7**	**301.8**	**515**
Fires	14,520	16.1	3,036	1,230	102
Residential Wood Consumption	2,704	36.7	1,222.8	338	5.1
Industrial Processes	2,414	1,158	1,680	491	1,233.8
Waste Disposal	2,018	120	464	273.9	26

Fossil Fuel Combustion	1,499	2,419	146	190.8	2,028
Electricity Generation	652	4,668.9	49	500	10,411.9
Miscellaneous	33	2.3	1,200	1099.9	0.754
Solvent use	3.3	9	4,267.9	7	1
Total All sources	73,218.8	21,082	19,350	4,448	14,581.9
Total vehicle sources	**49,372.8**	**12,650.8**	**7,284**	**316**	**772**
Percent Vehicle Sources (%)	67.4	60	37.6	7.1	5.29

1.2.2 Pollutants and Their Effects

As discussed in the previous section, automobile emissions account for a significant portion of some pollutants. Pollutants are typically classified as either primary or secondary. Primary pollutants are substances that are released directly into the atmosphere from their sources. Common examples include SO_2, CO, nitrogen oxides (NO_X), particulate matter less than 10 μm in diameter (PM-10), and volatile organic compounds (VOCs). Secondary pollutants are not directly emitted from sources, but form in the atmosphere as a result of chemical and photochemical reactions between other emitted molecules. A common example of secondary pollutants is ground level ozone.

In our research, NO_X is used as a generic term for mononitrogen oxides, NO and NO_2. NO_X is one of the major contributors to ground-level ozone, which forms when NO_X reacts with VOCs in the presence of sunlight.

VOCs + NO_X + Sunlight → Ozone   (1-1)

In addition, NO_X is a major component of smog. Smog is a mixture of poisonous gases (e.g. hydrocarbons, SO_2, and CO_2) with ground-level ozone as the main component. NO_X can also react with atmospheric water to form acid which falls to earth as rain, fog, or dry particles.

These pollutants, whether primary or secondary, have harmful effects on human, plant, and animal life. They can cause breathing problems, dizziness, severe headaches, irritate the respiratory system, and at high concentrations can cause death.

1.3 Management of Automobile Emissions

Although the emissions per automobile have decreased over time, due to the large increase in the number of automobiles on the road, the overall emissions are still high. Therefore, it is still essential to manage and control these emissions to minimize the adverse impact to human health and the environment.

Environmental agencies begin the management scheme by evaluating the effect of automobile emissions on human health and the environment. Then, they develop standards and regulations and impose them on automobile manufacturers. Automobile manufacturers then try to find and develop solutions or technologies that meet the

5

regulatory requirements. The third step in the management scheme is evaluating these technologies and whether they meet the requirements or not. The last step is implementation and subsequently monitoring, which is accomplished in two ways. The first is installing on-board diagnostic (OBD) systems; in some cases these are sensors that can detect emissions levels. The second is emissions test programs established by government agencies, which has been done in many countries such as the US, Canada, and Japan.

1.3.1 Standards and Regulations

Standards and regulations for automobile emissions are set by accounting for the effects of each pollutant on public health and the environment. Due to the increase in the number of automobiles and a recognized need for better air quality, government environmental agencies have been continuously imposing tighter regulations to reduce emissions from vehicle engines. Overall, automobile manufacturers have made remarkable progress in reducing pollutant emissions via advanced engine design and using cleaner fuels and highly developed exhaust aftertreatment technologies. Table 1.2 summarizes the history of heavy-duty, diesel-fueled vehicle emissions legislation in the U.S, Europe, and Canada from 1998 to 2010 [7, 8].

Table 1.2 History of automobile legislations, g/KW-hr

United States (US)				
Year	**HC**	**NO$_X$**	**CO**	**PM**
1998	1.75	5.4	20.8	0.13
2004	0.67	3.35	20.8	0.13
2007	0.187	1.6	20.8	0.013
2010	0.187	0.26	20.8	0.013
Europe				
2000 (Euro III)	0.66	5.0	2.1	0.10
2005 (Euro IV)	0.46	3.5	1.5	0.02
2008 (Euro V)	0.25	2.0	1.5	0.02
Canada				
1998-2004	1.75	5.4	20.8	0.13
2005	HC + NO$_X$ = 1.0		19.3	0.13
2008-2010	0.187	0.26	19.3	0.013

1.4 Technology

In the previous sections, automobile emissions and how these emissions are managed and controlled by environmental agencies were discussed. The ultimate step is finding

suitable pollution control technologies to mitigate these emissions and meet the regulatory requirements.

1.4.1 Diesel Automobile

The interest in diesel engines has recently increased due to their better fuel economy, and associated reduced CO_2 emissions, relative to gasoline engines. Switching to diesel powered vehicles could reduce CO_2 emissions from the transportation sector by 25% from their current levels [9]. Diesel engines not only emit less CO_2, but also less hydrocarbon (HC), CO, and NO_X as shown in Table 1.3 [9].

Table 1.3 Heavy duty diesel vs heavy duty gasoline engine emissions

Emissions (g/KW-h)	Diesel Engine	Gasoline Engine
HC	0.2	1.08
CO	2	40.5
NOx	4.6	5.76
PM	0.09	-

1.4.2 Diesel Exhaust Emissions Technologies

Despite the fact that the diesel engine is promising from a fuel economy standpoint, further efforts are needed to reduce emissions in order to meet recently imposed, and upcoming, regulations. The following sections will describe some exhaust aftertreatment technologies that could be, and have already been, applied to diesel engines to minimize emissions.

1.4.2.1 Three-Way Catalytic Converter

The three-way catalytic (TWC) converter is used to clean exhaust from most gasoline vehicles. The TWC converter contains precious metals, such as platinum, palladium and rhodium, for chemically converting some pollutants in the exhaust gases, such as CO, unburned hydrocarbons, and NO_X, into harmless compounds. The basic chemical reactions occurring on the TWC can be described as follows:

$$2\,NO_X \rightarrow xO_2 + N_2 \tag{1-2}$$

$$CO + {}^1\!/_2\,O_2 \rightarrow CO_2 \tag{1-3}$$

$$2C_xH_y + (2x + y/2)\,O_2 \rightarrow 2xCO_2 + yH_2O \tag{1-4}$$

TWC converters have been used in cars since 1980 [10] and have had a significant impact in the reduction of NO_X, CO and hydrocarbons from engine exhaust. The TWC converter is designed for use in exhaust that is net-free of oxygen, in other words the engine operates with a stoichiometric air to fuel ratio. Diesel engines operate with excess air, therefore there is a significant amount of O_2 in the exhaust. In the literature, there is a consensus that the TWC converter can reduce only a small fraction of lean-burn engine NO_X emissions due to its design focus on operation where little to no oxygen is present during reaction.

1.4.2.2 Selective Catalytic Reduction (SCR)

Selective catalytic reduction (SCR) is a process where a reductant such as ammonia (NH_3) or a hydrocarbon is added to the engine's exhaust gas to reduce NO_X emissions. Some available vehicle models utilizing SCR technology are the Mercedes-Benz E320

and Vision GL 320. In NH_3-based SCR, NH_3 can either be injected as NH_3 or originate from the decomposition of injected urea. The reductants, NH_3 or hydrocarbons, react selectively with NO_X to form N_2 and H_2O. NH_3-based SCR can meet the regulations being imposed, however there is currently no catalyst for hydrocarbon-based SCR that has the efficiencies required to meet today's regulations. NH_3 SCR reactions take place in the presence of a catalyst, which is commonly a Fe or Cu-doped zeolite catalyst.

Several SCR reaction pathways have been suggested. The three primary ones are:

$4NH_3 + 4NO + O_2 \rightarrow 4N_2 + 6H_2O$ (standard reaction)   (1-5)

$2NH_3 + NO_2 + NO \rightarrow 2N_2 + 3H_2O$ (fast reaction)   (1-6)

$8 NH_3 + 6 NO_2 \rightarrow 7 N_2 + 12 H_2O$ (slow reaction)   (1-7)
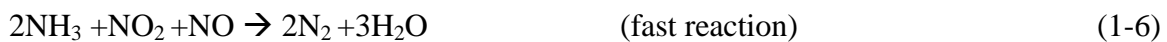
The first reaction pathway is called the "standard reaction" [11] and is considered relatively slow, especially at low temperature. The second is called the "fast reaction" [12] and is considered much faster than the standard SCR reaction, especially at low operating temperature (~200˚C). The third pathway reaction involves the reaction of NH_3 with NO_2 and is slow relative to the others. This reaction tends to occur at temperatures greater than 250°C and when NO_2 exceeds 50% of the total NO_X ($NO+NO_2$) [13,14].

Although SCR technology can achieve significant reductions in NOx emissions, it has some associated problems:

ω SCR technology would require a distribution network for urea or NH_3. In addition, there are toxicity, storage and refueling problems with these reductants [15].

ω NH_3 slip, and an associated odor [16], can occur and consequently SCR requires a very accurate injection system for urea or NH_3 to assure that all the NH_3 is consumed.

1.4.2.3 Diesel Oxidation Catalyst

Diesel oxidation catalysts (DOCs) are used in most diesel engine exhaust clean-up technologies. DOCs are typically comprised of precious metals dispersed on Al_2O_3 or zeolite [9]. The DOC is effective for the control of CO, hydrocarbons, and the soluble organic fraction of PM.

As the name implies, DOCs are effective oxidation catalysts, with the common reactions including CO, hydrocarbon and NO oxidation. CO and hydrocarbon emissions are thus reduced. NO oxidation, as will be discussed in greater detail in the literature review section, is also a desired reaction, as several downstream technologies are more efficient with NO_2 as the NO_X source, relative to NO.

The incorporation of zeolite into the formulation is a recent development. Zeolites adsorb hydrocarbons at low temperature and release them at about 250°C, where they can then be oxidized by the precious metals [17]. The adsorption at low temperature helps reduce cold start hydrocarbon emissions.

1.4.2.4 NSR Catalyst Technology

NO_X storage/reduction (NSR) is a relatively new catalyst technology for NO_X emission abatement from lean-burn engines. NSR catalysts were first placed on both the Dodge

Ram and GM's Humvee in 2007 are expected to be used more wide-spread in the near future to meet 2007 and 2010 emissions standards in the US, Europe, and Japan. Reduction of NO_X to N_2 over a NSR catalyst is accomplished in sequential reaction steps [18]. Key reactions include storage of NO_X by adsorption onto alkali and/or alkaline earth components, such as Ba, in the form of nitrate or nitrite species, and an intermittent addition of reductant to reduce the surface NO_X species to N_2. This technology operates in two phases; called lean and rich. The lean phase is the trapping or storage phase and the rich phase is the regeneration or reduction phase. In NSR, one cycle takes approximately ½ to 2 minutes, with 1 to 5 seconds for the rich phase. The lean phase can be considered normal engine operation where the exhaust gas includes CO_2, H_2O, O_2, N_2 and NO_X species. The NO_X species react with the alkali or alkaline earth species to form nitrites and nitrates. With time, the storage materials become saturated with NO_X species. Thus, the rich phase is needed to clean the storage materials from adsorbed NO_X, thereby beginning a new cycle where the storage species are nitrate-free and are able to adsorb entering NO_X species again. This rich phase contains many of the same gas species, except there should be some form of reductant, such as fuel, CO, or H_2, but little or no O_2. In NSR, the reductants react with surface NO_X species and convert them to N_2. These reductants originate in the exhaust via combustion of the extra fuel and air.

1.5 Motivation

Emissions from vehicles have become a societal concern. In many cities, the automobile is the single greatest polluter, as emissions from millions of vehicles on the road add up. In the U.S. for example, 28% of all US greenhouse gases come from the transportation

sector [19]. Despite the fact that new vehicles emit significantly less pollutants compared with older-model vehicles, due to the continuing growth in the number of vehicles and total distance traveled by each vehicle, the total emissions remain high.

In diesel-powered automobiles, the DOC can significantly reduce the amounts of unburned hydrocarbons and CO. However, it is very difficult to dissociate the nitrogen oxides to elemental N_2 and O_2 due to the oxygen present in diesel engine exhaust. Consequently, different catalyst technologies, such as SCR and NSR have been developed to reduce NO_X to N_2 in lean exhaust.

1.6 Objectives

The aim of this study is to evaluate the effect of operating conditions on, and integration of, the DOC and NSR catalyst on NO_X emissions. The investigation included effects of temperature, gas composition, and cycling times on the overall conversion efficiencies for key reactants.

The specific objectives as related to DOC research are:

1. Investigate the oxidation of NO, CO, and hydrocarbons individually and in mixtures with NO_2 under oxidizing conditions.
2. Study hydrocarbon steam reforming and water gas shift reactions, quantify the production of H_2, and probe carbon deposition and regeneration during steady-state and cycling operations.

The specific objectives as related to the NSR catalyst are:

1. Evaluate the effect of NO_X source (NO or NO_2) on the overall conversion to N_2.

2. Investigate the influence of different rich times with same reductant type and amount on the overall reduction to N_2.

3. Investigate the effect of HC species during the regeneration event on catalyst performance.

DOC and NSR in series

The aim of this part of the study is to evaluate performance when both the DOC and NSR catalyst are placed in series, which represents the actual configuration in NSR-equipped diesel automobiles. Two configurations of a DOC and NSR catalyst were compared. In the first configuration, the DOC and NSR catalyst were placed in series. In the second configuration, the DOC and NSR catalysts were divided into two equal volumes and placed in alternating series.

1.7 Research Contribution

This research provides unique contributions in developing advanced aftertreatment technologies that mitigate diesel automobile emissions. These include the following highlights:

- Competitive reactions between NO, NO_2, CO and hydrocarbons are evaluated, leading to a more representative understanding of the mechanisms on a DOC in practice.

- Hydrogen production via the hydrocarbon steam reforming and water gas shift reactions over the DOC during rich conditions is evaluated. This will demonstrate

the amount of hydrogen formed, which would subsequently be used as a reductant to reduce NO_X species in the downstream NSR catalyst. This also provides insight about any fuel penalty associated with NO_X traps.

- A systematic and comprehensive understanding of the performance of a NSR catalyst when either NO or NO_2 is used as the feed NO_X source is provided. The comparison was made between the two when the same amount of NO_X is trapped so that the effects during the regeneration phase could also be observed.

- The effects of regeneration-phase time, while keeping the total amount of reductant introduced during the regeneration phase the same, is evaluated. Such a study provides guidance for control strategies that could help minimize fuel penalties associated with NSR technology.

- Regenerating the NSR catalyst using hydrocarbons is systemically investigated. This will show at what temperatures WGS and steam reforming reactions become important, and if the direct reaction between the HC and the surface is key, rather than the indirect intermediate route, both of which are still proposed in the literature.

- Integrated systems containing both DOC and NSR catalysts, which represents the actual configuration in NSR-equipped diesel automobiles, is studied. A novel configuration was also evaluated, by alternating DOC and NSR catalysts in series, taking advantage of increased NO oxidation and H_2 evolution through more extensive WGS and steam reforming reactions.

1.8 Thesis Outline

This thesis is divided into nine chapters and it is organized as follows:

Chapter 1: **Introduction and Background**

This chapter provides an introduction and background about automobile emissions and their effect, standards and regulations to manage and control these emissions, and a brief description about some automobile aftertreatment emission reduction technologies. It also provides the motivation for this research, research objectives, contributions, and organization of the thesis.

Chapter 2: **Literature Review**

This chapter presents a detailed background and a review of several relevant previous studies for DOCs and NSR catalysts.

Chapter 3-4: **Diesel Oxidation Catalyst (DOC)**

In Chapter 3, competitive reactions between NO, NO_2, CO and different hydrocarbons (C_3H_6, dodecane, and xylene) are discussed. Hydrogen production via the SR and WGS reactions is extensively discussed in Chapter 4. The main focus is to compare and quantify the amount of hydrogen formed during steady-state and cyclic operation. As a part of this study, coke formation and regeneration was investigated after these experiments to explain the observed differences.

Chapter 5-7:   **NO_X Storage and Reduction (NSR) Catalyst**

In Chapter 5, the performance of a model NSR catalyst as a function of NO_X source, NO versus NO_2, is discussed. The assessment included comparison with constant cycling times and trapping the same amount of NO_X during the lean phase. In Chapter 6 the effect of regeneration time, while keeping the total amount of reductant introduced during the regeneration phase the same, is evaluated. The evaluation included trapping performance, NO_X release and formation of NH_3. In Chapter 7, the regeneration of a NSR catalyst using representative HCs, propylene for short chain, dodecane for long chain and m-xylene for cyclic species, is discussed. Hydrogen and CO were also used for comparison with the HCs. Hydrocarbon steam reforming and temperature programmed reduction (TPR) experiments were also performed to characterize the performance changes observed as a function of temperature.

Chapter 8:   **DOC and NSR Catalyst in Series**

In this chapter, the performance when both the DOC and NSR catalyst are placed in series, which represents the actual configuration in NSR-equipped diesel automobiles, is presented. Two configurations of a DOC and NSR catalyst were compared. In the first configuration, the DOC and NSR catalyst are placed in series, while in the second configuration, the DOC and NSR

catalysts were divided into two equal volumes and were placed in alternating series

Chapter 9: **Conclusions and Recommendations**

In this chapter, the overall conclusions from this research and recommendations for future work are listed.

Note: Chapters 3 through 8 have been or will be submitted individually for journal publication. Therefore, each of these chapters is "stand-alone" and includes its own introduction, experimental methodology and reference sections.

References

1. S. E. Jørgensen and I. Johnsen, Principles of Environmental Science and Technology, Published by Elsevier, 1989, page11.

2. C. J. Barrow, Environmental Management: Principles and Practice, Published by Routledge, 1999, page18.

3. D. W. Gottlieb, Environmental Technology Resources, Published by Lewis Publishers, 2003, Preface page.

4. E. T. Chanlett, Enviromental Protection, Published by McGraw-Hill, 1973, page 1973.

5. R. D. Griffin, Principles of air quality management, Published by Lewis, 1994, page 324.

6. Environment Protection Agency: http://www.epa.gov/air/emissions/dex.htm

7. S. Chatterjee, A. P. Walker and P.G. Blakeman, SAE Technical Paper Series 2008-28-0021.

8. Dieselnet website: http://www.dieselnet.com/standards/ca/#ldv.

9. W. A. Majewski and M. K. Khair, Diesel emissions and their control, SAE International, 2006, page 20, 90, and 150.

10. Dieselnet website: http://www.dieselnet.com/tech/cat_diesel.html.

11. C. Ciardelli, I. Nova, E. Tronconi, D. Chatterjee, B. Bandl-Konrad, and M. Weibel, B. Krutzsch, Applied Catalysis B: Environmental 70(2007)80.

12. J. Hagen, Industrial catalysis: A practical approach, Published by Whleyvch, 2nd edition, 2006, page 318.

13. A. Grossale, I. Nova, and E. Tronconi, Catalysis Today 136(2008)18.

14. E. Tronconi, I. Nova, C. Ciardelli, D. Chatterjee , M. Weibel, Journal of Catalysis 245(2007)1.

15. M. A Gómez-García, V. Pitchon, and A. Kiennemann, Environmental International 31(2005)445.

16. M. Radojevic, Environmental Pollution 102(1998)685.

17. R. M. Heck and R. J. Farrauto, Applied Catalysis A: General 221(2001)443.

18. W. S. Epling, L. E. Campbell, A. Yezerets, N. W.Currier, and J. E. Parks II, Catalysis Review 46(2004)163.

19. Green Car Congrss: http://www.greencarcongress.com/2008/03/epa-us-greenhouse.html.

Chapter 2: Literature Review

The literature review includes discussion of both diesel oxidation catalyst (DOC) technology and NO_X storage and reduction catalyst (NSR) technology. The first section will focus on the DOC and highlight the oxidation reactions, competitive reactions, catalyst formulation, and the effect of thermal degradation on DOC performance. In the next section, a detailed review on the five sequential reaction steps in NSR catalysis and a technique by which the chemistry of an NSR catalyst can be axially resolved is presented.

2.1 Diesel Oxidation Catalyst

DOCs were originally used to oxidize CO and hydrocarbons (HCs) into CO_2 and H_2O and help eliminate odors associated with diesel exhaust. DOCs are now also used with NO_X and PM control systems. Their role in these systems is as preheating devices for diesel particulate filters (DPFs) and SCR and NSR catalysts [1,2], as well as for NO oxidation. The heat is generated from exothermic HC oxidation reactions, with HC amounts controlled either by directly injecting fuel into the exhaust stream or adjusting the combustion strategy in the engine [1,3,4]. NO oxidation is desired for better low temperature SCR performance (as mentioned in the Introduction, the "fast SCR" reaction requires an equimolar mixture of NO-NO_2 and diesel engine exhaust contains on the order of 5-10% NO_2) and also results in more efficient NSR catalyst performance as will be discussed below.

2.1.1 Reactions on a Diesel Oxidation Catalyst

Due to the complicated nature of diesel fuel and combustion, a vast number of species are emitted from the combustion process. For most applications, a DOC is the first catalyst in the aftertreatment system. Key reactions that occur over the DOC include the following [5]:
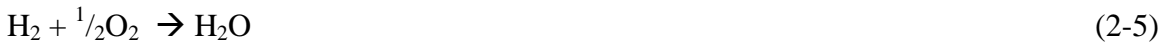
$$2C_xH_y + (2x + y/2) \, O_2 \rightarrow 2xCO_2 + yH_2O \tag{2-1}$$

$$CO + {}^1/_2 \, O_2 \rightarrow CO_2 \tag{2-2}$$

$$NO + {}^1/_2 O_2 \rightarrow NO_2 \tag{2-3}$$

$$SO_2 + {}^1/_2 O_2 \rightarrow SO_3 \tag{2-4}$$

$$H_2 + {}^1/_2 O_2 \rightarrow H_2O \tag{2-5}$$

$$C_nH_m + 2nH_2O \rightarrow (2n +m/2) \, H_2+nCO_2 \tag{2-6}$$

In general, DOCs can achieve more than 90% reduction in CO and HC emissions at exhaust temperatures higher than ~300°C [6]. At lower operating temperatures however, as in the case of low-speed driving and engine start-up, the catalytic oxidation of HC and CO remains a significant challenge [7,8]. One solution to overcome the low operating temperature difficulty is incorporating zeolites into the catalyst formulation [9,10]. Zeolites can adsorb and trap HCs at low operating temperatures. Then as the temperature rises, to about 250ºC, which is above the light-off temperature (the temperature necessary to initiate the catalytic reaction) for most HCs over Pt [11], HCs desorb and are oxidized to H_2O and CO_2. Another proposed solution for low temperature HC and CO emissions control is using an electrically heated catalyst to decease the time required for HC light-

off [12]. Finally, it has also been proposed [13] to take advantage of low temperature exothermic H_2 oxidation, which can occur at room temperature over precious metals. The H_2 can be generated in an on-board device by hydrolysis of water. However, this method is complex and expensive [14].

It is important to note that high HC or CO conversions, at high temperature, can be limited by mass transfer in the catalyst [6]. This is influenced by cell density, pore size, and dispersion of active sites.

There is no single HC exiting the engine, and therefore, there is the possibility of competing reactions. For the sake of simplicity, individual HCs and simple HC mixtures are always studied [2, 10,15-17]. If competing reactions exist, the measured conversions in tests with individual reactant species would always be higher than that in real application. In practice, engine exhaust contains many HC species, which react at different rates [18]. Some HC emission rates, in grams per mile, in diesel exhaust from two vehicles are shown in Table 2.1 [6]. Conversions of CO and HC would not necessarily be comparable with laboratory measured conversions, where pure HC or CO is usually used. Therefore, it is of great importance to study more representative HCs and mixtures of those HCs to have a better understanding of HC oxidation reaction rates and mechanisms.

As a simpler example, CO and H_2 react competitively and affect other reactions, either promoting or suppressing the light-off temperatures. In a recent study [19], self-inhibition of CO on Pt/Al_2O_3 occurred when CO was used, but the addition of H_2 to the mixture caused a reduction in the light-off temperature of CO. In the same study, the authors

found that H_2, without CO, would oxidize at room temperature, but when CO was added H_2 oxidation began only when 50% CO conversion was attained. Similar observations have been reported in other studies [20,21]. Recent evidence suggests that H_2 reduces the light-off temperature of CO by promoting CO desorption from Pt, while CO inhibits the H_2 oxidation due to competitive adsorption [22].

Table 2.1 Emission rates of some hydrocarbons in diesel engine exhaust

Compounds	Heavy duty diesel (HD)	Light duty diesel (LD)
	(g/mile)	
Total HC	3.65	0.23
Methane	NA	0.01
Ethylene	NA	0.04
Propylene	NA	0.01
n-decane	0.01	NA
n-dodecane	0.027	NA
Benzene	0.024	0.02
Toluene	0.01	0.006
Xylene	0.006	0.002
Ethyl benzene	0.005	0.001
Aldehyde	NA	0.03
Formaldehyde	NA	0.02

NA= data not available, therefore the sum of the individual amounts listed do not equal the total measured.

Although DOCs do little in terms of reducing total NO_X emissions, they do oxidize NO to NO_2. The NO_2 formed can be used in the downstream aftertreatment technologies. For example, NO_2 can be used to oxidize soot on particulate filters [1, 23]. Particulate filters,

as the name implies, filter soot. At some point however, the soot builds up and needs to be removed. This is done via oxidation. Oxidation of soot with O_2 occurs at temperatures greater than 500ºC, while with NO_2, oxidation can occur as low as 300ºC [7,24]. Therefore, if the amount of NO_2 is increased by using an upstream DOC, this will lower the required temperature for filter regeneration. SCR catalysts, as mentioned above, perform better with an equimolar mix of NO and NO_2, especially at low operating temperature (~200˚C) [25]. Engine out NO: NO_2 is on the order of 90:10. Therefore, if the amount of NO_2 can be increased upstream of the SCR catalyst, this will result in higher NO_X reduction efficiency. For NSR catalysts, as will be discussed in further detail below, NO_2 is more readily trapped relative to NO, and NO oxidation is therefore critical for NSR catalyst efficiency.

2.1.2 Diesel Oxidation Catalyst Formulation

DOCs are typically made of a catalyst coating a ceramic or metallic monolithic substrate. Monolith substrates are used as they do not result in a high pressure drop, and provide excellent high temperature and thermal shock resistance [26]. The monolith wall is then coated with a porous, high surface area washcoat such as alumina or zeolite. The precious metals are dispersed on the surface and within the pores of the washcoat [14, 26].

Platinum and palladium are the most active precious metals in the oxidation of CO and HCs from diesel exhaust [27, 28]. In a comparative study, the activities of Pt- and Pd-based DOC catalysts were tested for CO and HC oxidation [6], and both CO and HC emissions over the Pd catalyst were higher than that of Pt. Most literature demonstrates

that Pd activity is less than Pt for the oxidation reactions involved in diesel exhaust [29-31]. Rhodium has also been studied for HC, CO, and NO oxidation [28, 32, 33] but the order of activity was Pt >Pd >Rh [28].

A combination of Pt/Pd has also been investigated [15, 34, 35]. After thermal aging, CO and C_3H_6 light-off temperatures were always lower when using the Pt/Pd bimetallic catalyst compared to tests with a monometallic Pt or Pd catalyst [15]. The authors attributed the higher activity of the bimetallic catalyst to two reasons. First, when only Pd is used, the chemical state of the Pd will be metallic after thermal aging, and metallic Pd is inactive toward HC oxidation. When using a combination of Pt/Pd, Pd will exist in both metallic and oxide states after thermal aging. The second reason is that Pd stabilizes Pt against sintering. This could be due to oxygen exchange between Pt and Pd at high aging temperatures, keeping Pt in a metallic form, which is more stable [28] or possibly because of strong interactions between PdO and the oxide supports [36]. Similar observations were found when comparing monometallic Pt or Pd and bimetallic Pt/Pd supported on γ-Al_2O_3 for benzene oxidation [35].

The catalyst support can also have a substantial effect on DOC performance. The main function of the catalyst support is to provide high surface area for good dispersion of the precious metal catalytic sites. Inorganic base metal oxides such as Al_2O_3, SiO_2, TiO_2, V_2O_5, ZrO_2, and zeolites have been tested as catalyst supports for DOCs [6, 37]. Al_2O_3 and zeolite washcoats are the most commonly used in commercial DOCs. Al_2O_3 is often used due to its high surface area, high porosity, and thermal stability. The increased use of zeolites is due their ability to store HCs at low operating temperatures. Due to their

nanometer diameter pore size, they can selectivity adsorb HCs during engine start up and then desorb them at temperatures where HC oxidation starts [38]. Incorporating zeolites in DOC washcoats has shown success in decreasing HC emissions during cold start up [14, 9, 26].

Cerium dioxide (CeO_2) is commonly added to DOC formulations [26, 37]. Ceria has the ability to adsorb oxygen in oxidizing atmospheres, and liberate oxygen in reducing atmospheres:

$$\text{oxidizing: } Ce_2O_3 + {}^1/_2O_2 \rightarrow 2CeO_2 \tag{2-7}$$

$$\text{reducing: } 2CeO_2 + CO \rightarrow Ce_2O_3 + CO_2 \tag{2-8}$$

CeO_2 also enhances the water gas shift (WGS) reaction, $CO + H_2O \rightarrow H_2 + CO_2$, and steam reforming reaction in a reducing environment to generate H_2, which can then act as a reducing agent for NO_X to N_2 [26]. CeO_2 also stabilizes Pt against sintering [26] by maintaining the dispersion of Pt particles.

2.1.3 Hydrocarbon Steam Reforming

Some current diesel automobiles are equipped with a DOC as an upstream catalyst and downstream SCR and/or NSR catalysts. For example, the Dodge Ram, Humvee, and some Toyota models are already equipped with both DOC and NSR catalysts. While the Mercedes-Benz E320 and Vision GL 320 in Europe are equipped with both DOC and SCR catalysts.

For this project, the design assumed is a DOC placed upstream of a NSR catalyst. For NSR catalyst application, as will be discussed in more detail below, the engine operates in two cycles; lean and rich. The lean phase is typically the normal diesel engine operating condition, whereas in the rich phase, the flow composition is similar except no O_2 and less NO_X is present, and reductant species are present. H_2, the most efficient NO_X reductant as will be shown below, can be produced in this rich phase from HC steam reforming:

$$C_nH_m + 2nH_2O \rightarrow (2n + m/2) \ H_2 + nCO_2 \quad\quad\quad\quad (2\text{-}9)$$

HC steam reforming has been extensively studied over the last several decades. The main interest in this study, however, is HC steam reforming during cyclic operation, and specifically what occurs when cycling between lean and rich atmospheres during NSR catalyst application.

Several studies have investigated HC steam reforming over Pd and Pt. The temperatures investigated in those past studies match the temperature range NSR catalysts operate in and since DOCs contain Pt and Pd supported on either alumina or zeolites, steam reforming is likely to occur. The following is a summary of a few studies that evaluated catalysts with similar components and in temperature ranges of interest.

C_3H_8 steam reforming has been investigated over $Pd/CeO_2/Al_2O_3$ and $Pt\text{-}Rh/CeO_2/ Al_2O_3$ catalysts [39, 40]. Steam reforming started at about 350ºC. Steam did not need to be added to the inlet gases to initiate steam reforming if oxygen was present since water formed from oxidation of some of the C_3H_8. Steam reforming began after the oxygen was

completely consumed. Steam reforming of C_3H_6 and isopropanol ($CH_3CHOHCH_3$) was also investigated over a powder Pd–Cu/γ-Al$_2$O$_3$ catalyst [41]. Steam reforming of both C_3H_6 and $CH_3CHOHCH_3$ started as low as 327ºC and increased steadily until complete conversion at about 527ºC.

During the reductant-rich phase of NSR catalyst testing, CH_4 has been observed [42], and it is therefore important to also consider CH_4 reforming reactions. Steam reforming of CH_4 was investigated over Pd/Al$_2$O$_3$, Pd/CeO$_2$/Al$_2$O$_3$ [43] and Rh/α-Al$_2$O$_3$ catalysts [44]. Again, steam reforming began at 345-400ºC and increased with temperature. The catalyst including CeO_2 showed higher amounts of H_2 formed, indicating CeO_2 has the ability to enhance the steam reforming reaction.

2.2 NO$_X$ Storage and Reduction Technology

The NSR process cycles through two phases; a lean phase and a rich phase. In the lean phase, NO is oxidized to NO_2. NO_2 is then adsorbed by trapping materials, such as Ba, in the form of Ba(NO$_3$)$_2$ and/or Ba(NO$_2$)$_2$. In operation, the lean phase continues until NO$_X$ starts to slip. At some point after slip is observed, the second phase of the cycle is typically started. In the rich phase, reductants are introduced to reduce the NO$_X$ species to N_2.

The entire process takes approximately ½ to 2 minutes. Overall, the reduction of NO$_X$ to N_2 over an NSR catalyst can be described, as shown in Figure 2.1 [45], with five sequential reaction steps.
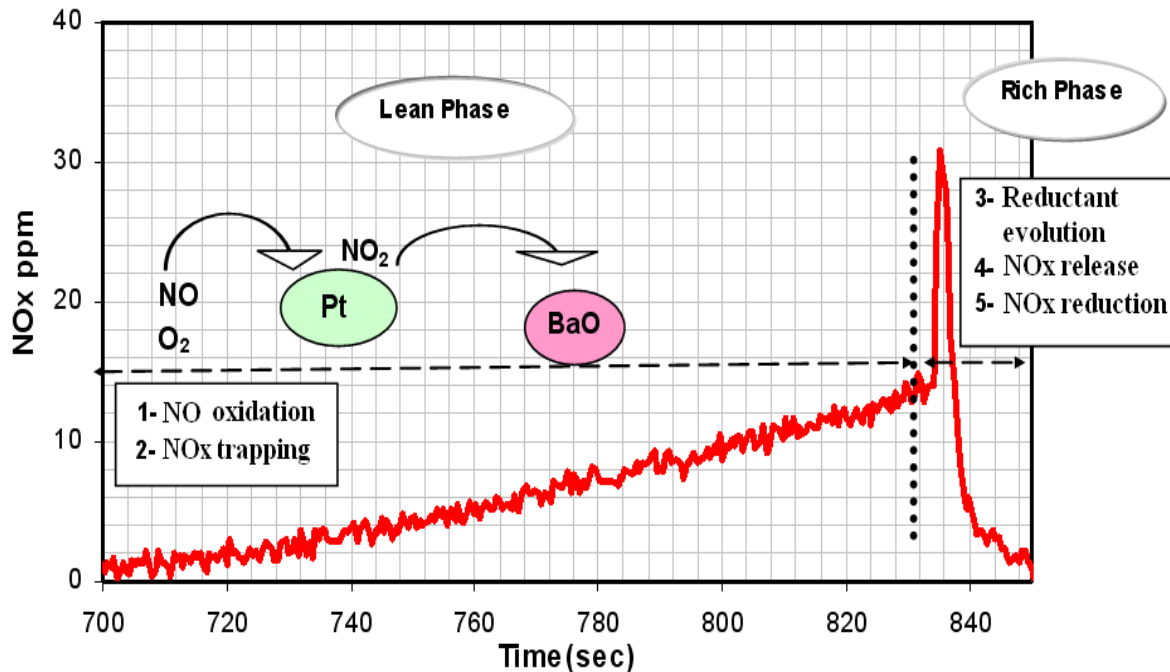
 Figure 2.1 Overall NSR cycle

2.2.1 NO Oxidation to NO_2 over the Noble Metal Component

The majority of NO_X emitted is NO, usually around 90%, with the rest NO_2. Since NO_2 is trapped more readily than NO, or may even be the required reactant for trapping, NO oxidation is a key step in the process. For this reason, DOCs are typically placed upstream of NSR catalysts, but NO oxidation can also occur on the NSR catalyst. Pt is the most commonly used catalyst component due to its high red-ox activity and results typically show that Pt is better than Pd for NO oxidation [29-31, 46]. Although Pd and Rh have less NO oxidation activity, they are key for NO_X reduction, thus their addition [47]. It has been demonstrated that Pt particle size affects NO oxidation rates; as the particle size of Pt increases, NO oxidation surprisingly increases, demonstrating structure dependence [48].
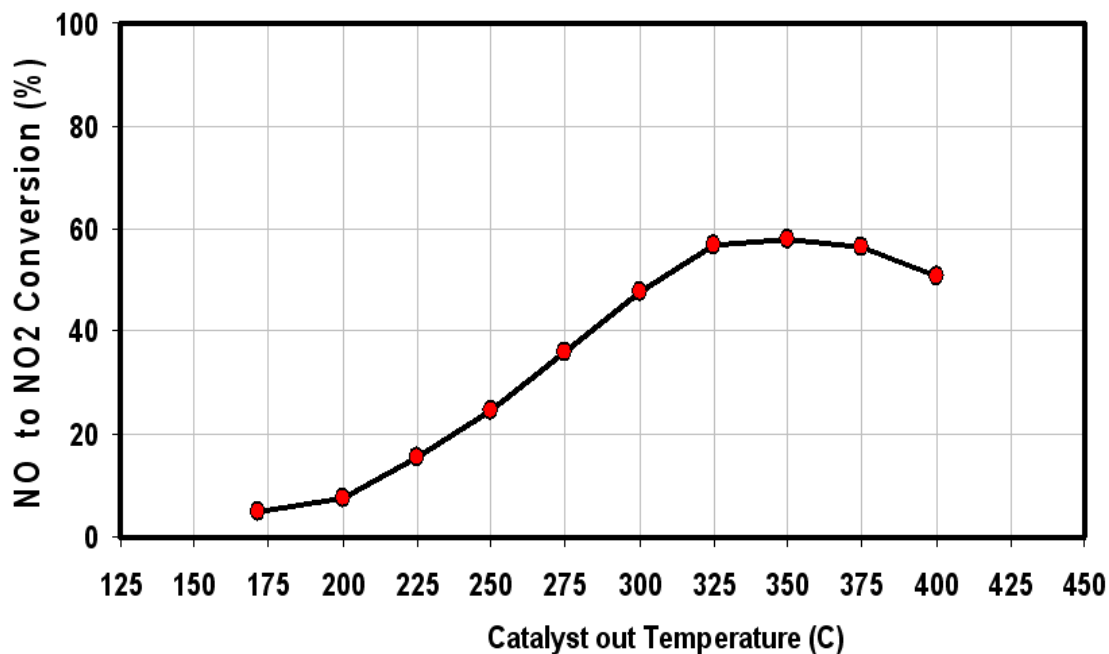
Figure 2.2 Effect of temperature on NO oxidation. The inlet gas contained 10% O_2, 330 ppm NO, 5% H_2O, 5% CO_2 and a balance of N_2 and the experiment was run with a commercial NSR sample at a space velocity of 30,000 hr^{-1}.

As shown in Figure 2.2 [45], NO oxidation is a function of temperature. At low temperature, the NO oxidation rate increases as the temperature increases and is kinetically limited. The conversion under the conditions of the test described reached its maximum at approximately 350°C and then started to decrease. The decrease at high temperature is due to thermodynamic limitations; the equilibrium conversion was reached.

The rate of NO oxidation has a positive dependency with respect to NO concentration and a negative dependency with respect to the product NO_2 concentration [49]. However,

the NSR catalyst traps NO_2 and therefore may minimize this inhibition when trapping sites are available, but will still result in less NO oxidation once those sites are full. This inhibition is due to the fact that Pt activity toward NO oxidation drops with oxygen chemisorption [50]. The oxygen may not only originate from gas-phase O_2, but also can come from product NO_2, and NO_2 is known as a strong oxidizer [51].

2.2.2 Adsorption of NO/NO₂ on the Trapping Sites

After NO is oxidized to NO_2, the NO_2 is adsorbed by the trapping components, which are usually alkali and alkaline earth components, the most typical studied being BaO. Numerous studies [52-54] have suggested that NO_2 is a precursor for adsorption and nitrate formation. However, there is some indication that NO might also be adsorbed by trapping materials in the presence of O_2, although to a lesser extent and at slower rates [55]. Overall, NO_X is adsorbed in the form of nitrate and/or nitrite species on the alkali and alkaline earth components. Nitrate species, for example, have been detected when introducing NO_2 to $Pt/Ba/Al_2O_3$ [54] while nitrites and nitrates have been detected when $NO + O_2$ was introduced at low temperature [56].

The selection of trapping materials is obviously an important factor and several have been tested, such as mixed oxides, perovskites, and inorganic oxides [55]. However, alkali and alkaline earth components show better trapping capacity due to their higher basicity [57]. Although NO_2 is adsorbed by trapping materials, it can also be adsorbed by the catalyst support, which is typically Al_2O_3. For example, NO_2 sorbed on Al_2O_3 when Pt/Al_2O_3, BaO/Al_2O_3, and $Pt/BaO/Al_2O_3$ catalysts were used [58], however, the amount of NO_2 adsorbed was small; approximately 1% of the NO_X trapped by Ba [55].

Temperature also impacts NO_X sorption. As shown in Figure 2.3 [45], sorption increases with temperature until the 300 to 400°C range and then decreases.
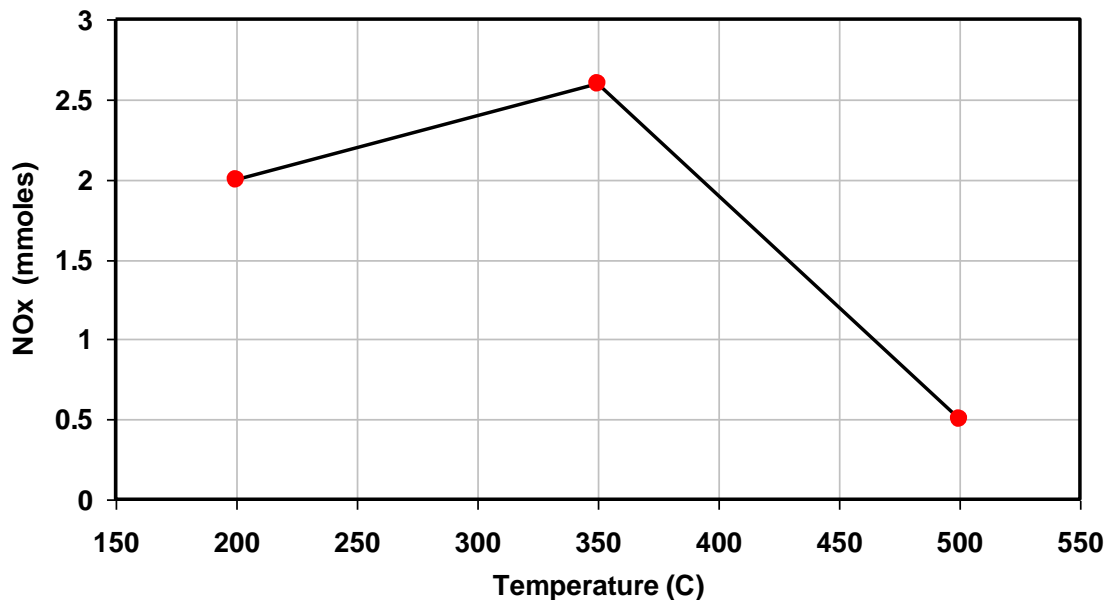
Figure 2.3 NO_X storage capacity. The reactant gas was composed of 10% O_2, 330 ppm NO, 5% H_2O, 5% CO_2 and a balance of N_2 at a space velocity of 30,000 hr^{-1} using a commercial NSR catalyst.

With increasing temperature, the thermal stability of nitrate and/or nitrite species decrease, and therefore, at temperatures greater than ~350°C, typically NO_X storage capacity decreases [59, 60]. One reason for the increase observed, when the temperature is increased from a relatively low temperature, is increasing NO oxidation. NO conversion to NO_2 typically reaches a maximum at around 350ºC, helping to increase storage rates up to this temperature as well. The increase in capacity as the temperature increases, at low test temperatures, is also due to improved regeneration with temperature as will be discussed below. Thus, at low temperatures, the amount of NO_X trapped is limited by NO oxidation and efficiency in removing nitrate or nitrite species during

regeneration. At high temperatures, the trapping capacity is limited by nitrate or nitrite stability.

Another factor that influences NO_X trapping capacity is the gas composition. A common assumption is that BaO is the easiest to form nitrates, relative to hydroxides or carbonates [48]. The presence of CO_2 in the gas stream results in $BaCO_3$ formation which is more stable than BaO. This increased stability can hinder nitrate and/or nitrite formation, which in turn will affect the trapping capacity. In one example, with a $Pt/K/Al_2O_3$ catalyst the trapping capacity decreased by 45% when CO_2 was added to the gas mixture [61].

Similarly, the presence of H_2O can cause decreased trapping capacity by $Ba(OH)_2$ formation. In the same study described above, the addition of 5% H_2O to a dry mixture caused a 16% loss in trapping capacity [61]. However, when both CO_2 and H_2O are added, the H_2O had a positive impact on NO_X storage capacity, via equilibrium between $BaCO_3$ and $Ba(OH)_2$. The carbonate is more stable than the hydroxide, so additional hydroxide relative to carbonate resulted in better trapping performance.

The presence of O_2 also can influence the trapping capacity via oxidation of NO to NO_2 as well as oxidation of surface NO_X to nitrates. It has been shown [62] that as O_2 concentration increases, the NO_X storage capacity increases.

Although the trends and mechanisms of NO_X storage have been investigated [51,55,63,64], due to the complexity of the catalyst, process and their sensitivity to experimental conditions, there is still debate regarding the mechanisms and the potential reactions involved in multiple catalytic steps [64]. Several mechanisms have been

suggested for NO_X adsorption. The more accepted are listed below, with Ba used as a representative alkali or alkaline earth components. Hydroxide and carbonates are also present, but the oxide is selected as an example.

- NO_2 reacts with BaO to form nitrate in the absence of O_2 via the disproportionation reaction [65]

$$BaO + 3NO_2 \rightarrow Ba(NO_3)_2 + NO \qquad\qquad (2\text{-}10)$$

- NO_2 reacts with BaO first and then with BaO_2 to form nitrate [51]

$$BaO + NO_2 \rightarrow BaO_2 + NO, \quad BaO_2 + 2NO_2 \rightarrow Ba(NO_3)_2 \qquad (2\text{-}11)$$

- NO_2 reacts with BaO to form nitrate in the presence of O_2

$$BaO + 2NO_2 + O \rightarrow Ba(NO_3)_2 \text{ [66]} \qquad\qquad (2\text{-}12)$$

- NO_2 reacts with BaO to form nitrate and nitrite species [67]

$$2BaO + 4NO_2 \rightarrow Ba(NO_2)_2 + Ba(NO_3)_2 \qquad\qquad (2\text{-}13)$$
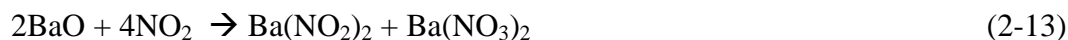
Several mechanisms have been proposed to explain the performance improvements observed when NO_2 is used instead of NO as the NO_X source. First, if trapping is a function of NO_2 partial pressure [68], then when NO_2 is used, the very inlet of the catalyst can participate in trapping [48] whereas with NO, oxidation to NO_2 must occur before efficient trapping can be seen. A second possibility invokes the presence of two types of trapping sites. One Ba site type is that near Pt and the other is distant from Pt. NO can only adsorb on the Ba sites which are in close proximity with Pt since it needs to be oxidized to NO_2 prior the adsorption event. While with NO_2, it can be adsorbed on both Ba site types.

2.2.3 Reductant Evolution

Trapping rates decrease with time as the trapping sites become saturated. Consequently, the catalyst needs to undergo periodic regeneration to remove the adsorbed NO_X, and hopefully reduce these to N_2. This can be achieved by introducing reductants and removing the O_2, resulting in a net-reducing environment. The reductants can be introduced in a few ways. One is via adjusting combustion so that they exit with the rest of the exhaust [69]. Thus, for the rich phase, more fuel is injected into the engine, which in turn increases the amount of reductant. Enough fuel must be added so that more reductant exits than O_2, thus the stream is reductant rich. The most widely used reductants in NSR catalyst testing are H_2, CO, and C_3H_6 [70-77] the former two observed in rich engine exhaust and the last representing hydrocarbon species, also observed. H_2 is superior for NO_X reduction with NSR catalysts at lower temperatures compared to CO and C_3H_6; however, they are all comparable at higher temperature [70-76]. CO can go through the water-gas-shift reaction to produce H_2, which can act as a reductant as well. It has been extensively demonstrated that the WGS reaction occurs over NSR catalysts [60,78]. But, the CO can poison Pt at lower temperatures ($< \sim200°C$), affecting NO oxidation and NO_X reduction reactions. For example, in a previous study with both commercial and model NSR catalysts [79], CO was found to decrease performance when present at $200°C$, due to Pt poisoning, primarily of the reduction and nitrate decomposition reactions.

Hydrogen can also be obtained from HC steam reforming during regeneration, either over an upstream DOC, as discussed in the previous section, or over the NSR catalyst since it

contains precious metal components as well. Ultimately, the formed H_2 can then act as a reductant to reduce NO_X species over the NSR catalyst.

Reductants are not only required to reduce the trapped NO_X, but they are also competitively consumed by oxygen stored on the catalyst surface. Consequently, the amount of reductant needed for regeneration and reduction is also dependent on surface oxygen; the more stored oxygen, the more reductant required.

2.2.4 Nitrate Decomposition and NO_X Release

Nitrate decomposition and the release of NO_X from the trapping site occurs due to (1) heat caused by the exothermic reaction between the entering reductant and any surface or residual gas-phase oxygen and (2) a change in gas composition with the switch from the lean to rich environment [48]. In terms of the temperature change, more heat will be generated with more reactant oxygen. Nitrate stability and therefore NO_X release is a function of temperature and therefore, the associated temperature rise may be enough to decrease the stability of the surface nitrate or nitrite species and result in NO_X release from the trapping site.

The NO_X observed in the catalyst outlet gas composition of course originates from NO_X release, but also lack of reduction of those released species. For reduction to occur, nitrates must first decompose. The NO_X can then be reduced on the surface, if in contact with a precious metal site, or is released into the gas-phase for re-adsorption onto a precious metal site. What is observed in the outlet gas during the rich phase is a portion of the latter. For example, at lower temperatures, the observed release of NO_X is strongly dependent on the degree that the catalyst can activate the reductants [48]. As the

temperature increases, the capability of reductants to reduce NO_X to N_2 should increase and the release of observed NO_X in the outlet gas should decrease. While, at higher temperatures, around 350°C and above, where the activation of reductant is not an issue, the weak stability of nitrate species, and therefore increased amounts released, is the main cause for observed NO_X release [48].

The absence of NO_X and O_2 in the regeneration phase leads to a decrease in the stability of nitrate and/or nitrite species. For example, by Liu and Anderson [76] demonstrated that oxygen enhances the stability of nitrate and/or nitrite species. Therefore, upon switching to the rich phase, where little or no oxygen is introduced, the nitrate and/or nitrite species become less stable, leading to nitrate and/or nitrite species decomposition and NO_X release. Via thermodynamic calculations, it has been predicted [80] that there is a direct correlation between the amount of CO_2 and the stability of NO_X species, with more CO_2 present resulting in more NO_X released; likely associated with carbonate/nitrate stability. The presence of H_2O in the gas stream decreased the amount of observed NO_X release [80, 81], possibly being related to displacement of carbonate groups by hydroxyl groups.

Pt catalyzes the decomposition of nitrate species [76], and therefore another contributing factor to nitrate decomposition and NO_X release is the proximity of Pt sites to the alkali and alkaline earth components [82].

2.2.5 Reduction of NO_X to N_2

Reduction of NO_X to N_2 is the last step in the overall NSR cycle. In this step, the NO_X stored during the lean phase and then released at the onset of the rich phase is reduced to

N_2 over the precious metals. Two main mechanisms have been proposed for reduction of NO_X to N_2 on the precious metal sites of NSR catalysts. The first mechanism postulates that the reductant reduces the precious metal site. Afterward, the reduced precious metal site participates in NO decomposition [73]. The second mechanism [83] proposes that the reductant is activated on the precious metal and reacts directly with NO_X. Propylene was taken as an example for the reductant source in the scheme presented below.

$$C_3H_6 \text{ (g)} + Pt \;\rightarrow\; Pt\text{-}C_3H_6 \tag{2-14}$$

$$Pt - C_3H_6 + 2Pt \;\rightarrow\; 3\,Pt\text{-}CH_2 \tag{2-15}$$

$$Pt\text{-}CH_2 + 3Pt\text{-}NO \rightarrow 4Pt + CO_2 \text{ (g)} + H_2O \text{ (g)} + 1.5\ N_2 \text{ (g)} \tag{2-16}$$
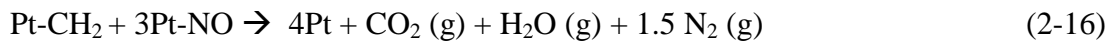
Reductant type and amount, temperature, and lean/rich time ratio are known to affect NO_X reduction.

Abdulhamid et al. [84] did a comparative study between H_2, CO, C_3H_6, and C_3H_8 for reduction of NO_X over BaO/Al_2O_3 samples containing Pt, Pd, or Rh. The results of this study showed that H_2 and CO were superior for NO_X reduction in comparison to C_3H_6 and C_3H_8 especially when $Pt/BaO/Al_2O_3$ was used. Another study compared H_2, CO, and a mixture of H_2 and CO as the reductant source over a $Pt/BaO/Al_2O_3$ catalyst [85]. The results showed that when mixtures of CO and H_2 were used at low temperature (~147°C), low NO_X reduction was achieved in comparison with using only H_2. The authors attributed the poor NO_X reduction when using the mixture to reductant competition for adsorption on Pt sites. With stronger CO bonding, the surface H_2 concentration would be lower in the presence of CO, and if conditions favor reduction with H_2 instead of CO, the

NO_X reduction rate would be lowered. They also showed that NO_X conversion was higher with mixtures of H_2 and CO in comparison to just CO as the reductant under otherwise identical conditions. With only CO as the reductant, NCO and CO_2 species were formed. And in the presence of H_2, the resultant H_2O hydrolyzed the NCO to form the intermediate that ultimately decomposed to N_2 and H_2O. In a separate study [79] the effect of CO and H_2 mixtures on overall reduction performance was studied. At 200ºC, the mixture of CO and H_2 was better than using only CO, but using only H_2 always resulted in better performance. At 300°C, the trapping and reduction of NO_X were comparable when either H_2, CO, or mixtures of the two for were used. At 400 and 500°C, mixtures of the two led to slightly improved performance relative to H_2 and CO. The authors found that the lower performance at 200°C when CO was present was due to CO poisoning the precious metal sites to not just reduction of released NO_X, but also toward the catalyzed decomposition of the nitrates.

The amount of reductant of course also has an impact on NO_X reduction. In one study [79] the performance of the catalyst improved with each incremental increase in H_2 or CO concentration, except at 200ºC, where the performance decreased with each increase in CO amount due to Pt poisoning. In another study, Bailey et al. [86] demonstrated that increasing the amount of CO during the regeneration phase at T > 300ºC resulted in improved overall NO_X reduction under the conditions tested.

NH_3 is a by-product that can be formed during the regeneration phase [75, 87-89]. NH_3 formation has been observed when H_2 was used as a reducing agent in the regeneration period over Pt/Ba-based catalysts [88, 89] as well as with mixtures of H_2 and CO [87],

and pure CO [75]. NH_3 can be formed in two ways; directly from reaction of H_2, added during regeneration, with NO on the catalyst or with the H_2 produced from the WGS reaction when CO and H_2O are available in the regeneration mixture [90]. NO can be easily dissociated to atomic nitrogen and oxygen over precious metals at higher temperatures [91]. Subsequently, the N atom would react with dissociated H_2 to form NH_3. It should also be pointed out that NH_3 has been labeled as a hydrogen carrier and a reductant participating in NO_X reduction via SCR reaction chemistry [88]. Cumaranatunge et. al. [92] have demonstrated equivalent reduction efficiency of H_2 and NH_3 in NSR catalysis, and facile formation of NH_3 from a feed of NO and H_2 over a Pt/Al_2O_3 catalyst.

Formation of N_2O during the regeneration phase is also common. In a proposed path, during the regeneration phase, the reductant can reduce the Pt site allowing NO to decompose and form N_2O via: 2Pt-NO $\rightarrow$ N_2O (g) + Pt + Pt-O [94]. Formation of N_2O demonstrates incomplete reduction of NO_X species.

2.2.6 Spatially Resolved Capillary Inlet Mass Spectrometry (SpaciMS)

A mass spectrometer (MS) can be used to spatially resolve concentration profiles within a reactor and has been used to measure the gas species concentrations at different locations in monolith-supported NSR catalysts. Such a technique has been developed at Oak Ridge National Laboratory and is called spatially-resolved capillary-inlet mass spectrometry (SpaciMS). Choi et al. [94, 95] have investigated NO_X and H_2 concentration profiles over a monolith $Pt/K/Al_2O_3$ catalyst. As an example, the NO_X concentrations at different axial

positions along the catalyst are shown in Figure 2.4. This initial study showed that the reaction chemistry in NSR catalysts is a function catalyst length, with some parts of the catalyst utilized more than others.
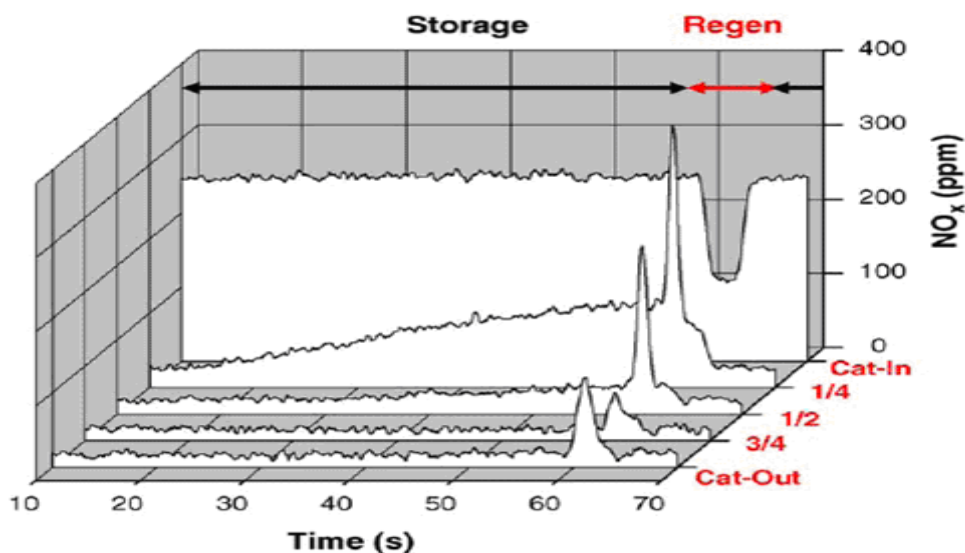
Figure 2.4 NO_X breakthrough profiles as a function of catalyst length at T = 430ºC. The lean gas composition was 250 ppm NO, 8% O_2, 5% H_2O and N_2 balance; and the regeneration gas consisted of 4% CO, 1% O_2, 5% H_2O and N_2 balance [94].

In a more recent study [96], SpaciMS was used to investigate the influence of sulfur and temperature on the spatiotemporal distributions of NSR reactions over a commercial NO_X trap. The authors divided the catalyst into two zones for discussion; namely a NO_X storage and reduction zone and an oxygen storage capacity (OSC) zone. The NSR zone was upstream, where both NO_X and oxygen storage occurred, while in the downstream zone only oxygen storage was relevant, as shown in Figure 2.5. At 200ºC, it was found that the NSR zone extended to more than half of the catalyst length, while less than half was used to store NO_X at 325ºC. At 325ºC, and after sulfur exposure, the catalyst could

be described with three zones, a sulfated zone with no NO_X or oxygen storage, then an NSR zone, and finally the OSC zone.
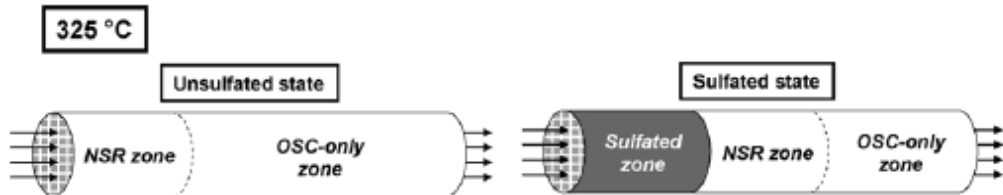
Figure 2.5 The reactions distribution inside a commercial NSR catalyst at 325ºC before and after sulfation. 40 ppm SO_2 was added into the feed for 1 hr at 400ºC. The lean phase composition was 300 ppm NO, 10% O_2, 5% H_2O, 5% CO_2 and N_2 balance; and the regeneration phase composition was 3.4% H_2, 5% H_2O, 5% CO_2, and N_2 balance. The space velocity was 30,000 h^{-1}.

Overall, those three studies showed that using SpaciMS can develop an improved understanding of dynamic spatiotemporal distribution reaction chemistry inside a monolithic NSR catalyst.

References

1. T. Nakane, M. Ikeda and M. Hori, O. Bailey, and L. Mussmann, SAE technical paper series 2005-01-1759.

2. Y. Banno, Y. Tanaka, T. Hihara, and M. Nagata, SAE technical paper series 2004-01-1430.

3. C. Kwon, J. Lee, S. Kim and G. Yeo, SAE technical paper series 2005-01-0672.

4. J. C. Fayard and T. Seguelong, SAE technical paper series 2004-01-1937.

5. Dieselnet website: http://www.dieselnet.com/tech/cat_doc.html

6. W. A. Majewski and M. K. Khair, Diesel emissions and their control, SAE International, 2006, pages 20, 90, and 150.

7. M. V. Twigg, Applied Catalysis B: Environmental 70(2007)2.

8. M. Shelef and R. W. McCabe, Catalysis Today 62(2000)35.

9. K. M. Adams, J. V. Cavataio, T. Sale, W. A. Rimkus, and R. H. Hammerle, SAE technical paper series 962049.

10. M. Kamijo, M. Kamikubo, H. Akama and K. Matsushita, JSAE Review 22(2001) 277.

11. Y. Lui, J. Dettling, O. Weldlich, R. Krohn, D. Neyer, W. Engeler, and G. Kahman, P. Dore, SAE technical paper series 962048.

12. Y. Shimasaki, H. Kato, F. Abe, S. Hashimoto, and T. Kaneko, SAE technical paper series 971031.

13. Y. Kanada, M. Hayasi, M. Akaki, S. Tsuchikawa, and A. Isomura, SAE technical paper series 960346.

14. R. M. Heck and R. J. Farrauto, Applied Catalysis A: General 221(2001)443.

15. A. Morlang, U. Neuhausen, K.V. Klementiev, F.W. Schutze, G. Miehe, H. Fuess, and E. S. Lox, Applied Catalysis B: Environmental 60(2005)191.

16. D. Schmitt, H. Fuess, H. Klein, U. Neuhausen and E. S. Lox, Topics in Catalysis 16/17(2001)355.

17. P. R. Phillips, G. R. Chandler, D. M. Jollie, A. J. J. Wilkins and M. V. Twigg, SAE technical paper series 1999-01-3075.

18. M. J. Patterson, D. E. Angove, and N. W. Cant, Applied Catalysis B: Environmental 26(2000)47.

19. S. Salomons, M. Votsmeier, R.E. Hayes , A. Drochner , H. Vogel, and J. Gieshof Catalysis Today 117(2006)491.

20. N. D. Hoyle, P. Kumarasamy, V. A. Self, P. A. Sermon, and M. S.W. Vong, Catalysis Today 47(1999)45.

21. M. Sun, E. Croiset, R. R. Hudgins, P. L. Silveston, and M. Menzinger, Industrial Engineering Chemical Research 42(2003) 37.

22. S. Salomons, R. E. Hayes, and M. Votsmeier, Applied Catalysis A: General 352 (2009)27.

23. A. Setiabudi, M. Makkee, and J. A. Moulijn, Applied Catalysis B: Environmental 50(2004)185.

24. M. Pfeifer, M. Votsmeier, M. Kögel, P. C. Spurk, E. S. Lox, and J. F. Knoth, SAE technical paper series 2005-01-1756.

25. C. S. Sluder, J. M Storey, S. A. Lewis and L. A. Lewis, SAE technical paper series 2005-01-1858.

26. R. J. Farrauto and R. M. Heck, Catalysis Today 51(1999)351.

27. N. Harayama, K. Niimura, and Y. Watanabe, SAE technical paper series 920852.

28. A. Kalantar, F. Klingstedt, T. Salmi, and D. Y. Murzin, Fuel 83(2004)395.

29. H. J. Stein, Applied Catalysis B: Environmental 10(1996)69.

30. M. Kawanami, M. Horiuchi, H. Klein, and M. Jenkins, SAE technical paper series 981196.

31. W. A. Majewski, J. L. Ambs, and K. Bickel, SAE technical paper series 950374.

32. E. A. Efthimiadis, G. D. Lionta, S. C. Christoforou, and I. A. Vasalos, Catalysis Today 40(1998)15.

33. E. A. Efthimiadis, S. C. Christoforou, A. A. Nikolopoulos, and I. A. Vasalos, Applied Catalysis B: Environmental 22(1999)91.

34. A. Knafl, M. Han, S. V. Bohac, D. N. Assanis, and P. G. Szymkowicz, SAE technical paper series 2007-01-0231.

35. H. S. Kim, T. W. Kim, H. L. Koh , S. H. Lee , and B. R. Min, Applied Catalysis A: General 280(2005)125.

36. P. Forzatti and L. Lietti, Catalysis Today 52(1999)165.

37. R. J. Farrauto and K. E. Voss, Applied Catalysis B: Environmental 10(1996)29.

38. T. Kanazawa and K.Sakurai, SAE technical paper series 2001-01-0660.

39. W. Faria, L.C. Dieguez, and M. Schmal, Applied Catalysis B: Environmental 85(2008)77.

40. J. Barbier, and D. Duprez, Applied Catalysis A: General, 85(1992)89.

41. C. Resini, L. Arrighi, M. Delgado, M. Vargas, L. J. Alemany, P. Riani, S. Berardinelli, R. Marazza, and G. Busca, International Journal of Hydrogen Energy 31(2006)13.

42. C. C. Webb, P. A. Weber, and M. Thornton, SAE technical paper series 2004-01-0585.

43. F. Arosio, S. Colussi, G. Groppi, and A. Trovarelli, Catalysis Today 117(2006)56.

44. A. Donazzi, A. Beretta, G. Groppi, and P. Forzatti, Journal of Catalysis 255(2008) 241.

45. M. AL-Harbi, Environmental technology management (ETM): Performance and reaction activity changes of a NOx storage/reduction catalyst as a function of regeneration mixture and thermal degradation, Master's thesis, 2008.

46. S. Salasc, M. Skoglundh and E. Fridell, Applied Catalysis B: Environmental 36(2002)145.

47. H. Ohtsuka and T. Tabata, Applied Catalysis B: Environmental 29(2001)177.

48. W. S. Epling, L. E. Campbell, A. Yezerets, N. W.Currier, and J. E. Parks II, Catalysis Review 46(2004)163.

49. S. S. Mulla, N. Chen, L. Cumaranatunge, G. E. Blau, D. Y. Zemlyanov ,W. N. Delgass, W. S. Epling , and F. H. Ribeiro, Journal of Catalysis 241(2006)389.

50. L. Olsson, B. Westerberg, H. Persson, E. Fridell, M. Skoglundh, and B. Andersson, Journal of Physical Chemistry B 103(1999)10433.

51. E. Fridell, H. Persson, B. Westerberg, L. Olsson and M. Skoglundh, Catalysis Letters 66(2000)71.

52. F. Rodriquez, L. Juste, C. Potvin, J. Tempere, G. Blanchard, and G. Djegam, Catalysis Letters 72(2001)59.

53. S. Hodjati, K. Vaezzadeh, C. Petit, V. Pitchon, and A. Kiennemann, Applied Catalysis B: Environmental 26(2000)5.

54. S. Hodjati, P. Bernhardt, C. Petit, V. Pitchon, and A. Kiennemann, Applied Catalysis B: Environmental 19(1998)209.

55. H. Mahzoul, J. Brilhac, P. Gilot, Applied Catalysis B: Environmental 20(1999)47.

56. L. Liotta, A. Macaluso, G. Arena, M. Livi, G. Centi, G. Deganello, Catalysis Today 75(2002)439.

57. J. Choi, W. Partridge, and C. S. Daw, Applied Catalysis A: General 293(2005)24.

58. B. Westerberg and E. Fridell, Journal of Molecular Catalysis A: Chemical 165(2001)249.

59. W. S. Epling, J. E. Parks, G. C. Campbell, A. Yezerets, N. W. Currier, and L. E. Campbell, Catalysis Today 96(2004) 21.

60. M. AL-Harbi, W. S. Epling, A. Yezerets, N. W. Currier, H-Y Chen, and H. Hess, SAE technical paper series 2009-01-0631.

61. T. J. Toops, D. B. Smith, W. S. Epling, J. E. Parks, W. P. Partridge, Applied Catalysis B: Environmental 58(2005)255.

62. E. Fridell, M. Skoglundh, B. Westerberg, S. Johansson, and G. Smedler, Journal of catalysis 183(1999)196.

63. I. Nova, L. Lietti, and P. Forzatti, Catalysis Today 136(2008)128.

64. P. Schmitz and R. Baird, Journal of Physical Chemistry B 106(2002)4176.

65. N. W. Cant and M. J. Patterson, Catalysis Today 73(2002)271.

66. F. Rodrigues, L. Juste, C. Potvin, J.F Tempere. G. Blanchard, and G. Mariadassou, Catalysis Letters 72(2001)72.

67. I. Mochida, N. Shirahama, S. Kawano, Y.Korai, A. Yasutake, M. Tanoura, S. Fujii, M. Yoshikawa, Fuel 79(2000)1713.

68. J. Kwak, D. Kim, T. Szailer, C. Peden, and J. Szanyi, Catalysis Letters 111(2006)3.

69. K. C. Narula, R. S. Nakouzi, W. Ruowen, J. Goralski, and J. Allard, AIChE Journal 47(2001)3.

70. C. Narula, S. Nakouzi, C. R. Goralski, and L. Allard, AIChE 47(2001)744.

71. H. Abdulhamid, E. Fridell and M. Skoglundh, Topics in Catalysis 30/31(2004) 161.

72. P. Jozsa, E. Jobson, and M. Larsson, Topics in Catalysis 30/31(2004)177.

73. D. James, E. Fourré, M. Ishii, and M. Bowker, Applied Catalysis B: Environmental 45(2003)147.

74. S. Poulston and R. R. Rajaram, Catalysis Today 81(2003)603.

75. T. Lesage, C. Verrier, P. Bazin, J. Saussey, and M. Daturi, Physical Chemistry Chemical Physics 5(2003)4435.

76. Z. Liu and J. A. Anderson, Journal of Catalysis 224(2004)18.

77. Y. Li, S. Roth, J. Dettling and T. Beutel, Topics in Catalysis 16/17(2001)139.

78. W. S. Epling, A. Yezerets, and N. W. Currier, Applied Catalysis B: Environmental 74(2007)117.

79. M. AL-Harbi and W. S. Epling, Applied Catalysis B: Environmental 89(2009) 315.

80. A. Amberntsson, H. Persson, P. Engström.and B. Kasemo, Applied Catalysis B: Environmental 31(2001)27.

81. W. S. Epling, G. Campbell, and J. E. Parks, Catalysis Letters 90(2003)45.

82. J. M. Coronado and J. A. Anderson, Journal of Molecular Catalysis A: Chemical 138(1999)83.

83. L. Olsson, E. Fridell, M. Skoglundh, and B. Andersson, Catalysis Today 73(2002)263.

84. H. Abdulhamid, E. Fridell, and M. Skoglundh, Applied Catalysis B: Environmental 62(2006)319.

85. T. Szailer, J. H. Kwak, D.H. Kim, J. C. Hanson, C. H. F. Peden and J. Szanyi, Journal of Catalysis 239(2006)51.

86. O. Bailey, D. Dou, and G. Denison, SAE Technical Paper Series 972845.

87. T. Lesage, C. Verrier, P. Bazin, J. Saussey, S. Malo, C. Hedouin, G. Blanchard, and M. Daturi, Topics in Catalysis 30/31(2004)31.

88. A. Lindholm, N.W. Currier, E. Fridell, A. Yezerets and L. Olsson, Applied Catalysis B: Environmental 75(2007)78.

89. L. Castoldi, I. Nova, L. Lietti, and P. Forzatti, Catalysis Today 96(2004)43.

90. L. Limousy, H. Mahzoul, J.F. Brilhac, F. Garin, G. Maire, and P. Gilot, Applied Catalysis B: Environmental 45(2003)169.

91. M. Radojevic, Environmental Pollution 102(1998)685.

92. L. Cumaranatunge, S. S. Mulla, A. Yezerets, N. W. Currier, W. N. Delgass, and F. H. Ribeiro, Journal of Catalysis 246(2007)29.

93. V. Medhekar, V. Balakotaiah, and M. P. Harold, Catalysis Today 121(2007)226.

94. J. Choi, W. Partridge, and C. Daw, Applied Catalysis A: General 293(2005)24.

95. J. Choi, W. Partridge, W. S. Epling, N. W. Currier, and T. M. Yonushonis, Catalysis Today 114(2006)102.

96. J. Choi, W. Partridge, J. A. Pihl, and C. S. Daw, Catalysis Today 136(2008) 173.

Chapter 3

Competitive NO, CO and hydrocarbon oxidation reactions over a diesel oxidation catalyst

3.1 Abstract

The oxidation of NO, CO, and hydrocarbons individually, and in mixtures with NO_2, were investigated over a monolith-supported Pt/Al_2O_3 catalyst under oxidizing conditions. NO_2 was completely reduced by CO and C_3H_6, under NO_2 limited conditions, at temperatures as low as 110°C and at temperatures above 140°C with dodecane and m-xylene. NO_2 was then again observed once the extent of oxidation of the other species by oxygen was significant. Under the conditions tested, NO, CO, and hydrocarbon oxidation was inhibited by NO_2 in the feed gas mixture. Hydrocarbons were also found to inhibit the oxidation of NO and other hydrocarbon species due to site adsorption competition. For CO, hydrocarbons did not change the onset of oxidation, but did inhibit the extent after their light off began. At low temperatures, CO was found to initially inhibit NO oxidation, but at higher temperatures, once CO oxidation was significant, CO promoted NO conversion to NO_2. The observed inhibition effects of the different gases on hydrocarbon oxidation were not additive, indicating one species would cause inhibition, but once its inhibition ended, another species could still then cause inhibition. The combined effect of C_3H_6, NO and NO_2 on CO conversion was found to be additive unlike that observed for C_3H_6. This is because CO oxidation started prior C_3H_6.

3.2 Introduction

Relative to today's gasoline engine, which uses a stoichiometric amount of fuel and air for combustion, the diesel engine and lean-burn gasoline engines have better fuel economy, and emit less CO_2. However, NO_X emissions, and particulate matter (PM) for diesel engines, remain an issue. An oxidation catalyst, called a diesel oxidation catalyst (DOC) in diesel engine exhaust aftertreatment systems, is commonly used to reduce CO and hydrocarbon exhaust emissions. Pt and Pd are the most frequently used metals [1, 2] in DOC formulations, with Pd added for some activity, but also to stabilize the Pt [1-6].

In general, DOCs can achieve more than 90% reduction in CO and HC emissions at exhaust temperatures higher than ˜300°C [6]. At low operating temperatures however, as in the case of low-speed driving and engine start-up conditions, the catalytic oxidation of HC and CO remains a significant challenge [7, 8]. One solution to overcome the low operating temperature difficulty is incorporating zeolites into the catalyst formulation [9, 10]. Zeolites can adsorb and trap HCs at low operating temperatures. Then as the temperature rises, to about 250°C, which is above the light-off temperature (the temperature necessary to initiate the catalytic reaction) for most HCs over Pt [11], HCs desorb and are oxidized to H_2O and CO_2.

DOCs are now also used with NO_X and PM control systems. Their role in these systems is as a preheating device for the diesel particulate filters (DPFs), selective catalytic reduction (SCR) and NO_X storage and reduction (NSR) catalysts [12, 13], as well as for NO oxidation. The heat is generated from exothermic HC oxidation reactions, with HC amounts controlled either by directly injecting fuel into the exhaust stream or adjusting the combustion strategy in the engine [12, 14, 15]. Although DOCs have little

effect on reducing NO_X emissions, they do oxidize NO to NO_2. NO_2 is a key reactant for SCR, NSR and DPF aftertreatment technologies. For example, NO_2 can be used to oxidize soot on DPFs at lower temperatures than O_2 [7, 12, 16, 17]. In SCR, ammonia is used as a reducing agent and it has been shown that SCR catalysts perform better with an equimolar mix of NO and NO_2, especially at low operating temperature [18-20]. Furthermore, NO_2 is more readily trapped on NSR catalysts, relative to NO, and NO oxidation is therefore critical for low temperature NSR catalyst efficiency [21-24].

Although an increased amount of NO_2 is beneficial for the downstream SCR, NSR, and DPF catalysts, previous studies show that NO_2 can inhibit both NO and HC oxidation over Pt/Al_2O_3 catalysts. Mulla et al. [25] studied NO oxidation kinetics over a Pt/Al_2O_3 catalyst and found the rate is first order with respect to both NO and O_2 concentrations, but negative first order with respect to NO_2 concentration. The inhibition effect was attributed to the strong oxidizing character of NO_2, where on the Pt it dissociates to NO and elemental oxygen, the latter causing the inhibition. Further work has shown [26] that adsorbed oxygen can react with NO resulting in the restoration of the activity, but when Pt oxides formed as a result of NO_2 dissociation (forming elemental oxygen), the catalyst did not regain its initial oxidation activity. Other literature has attributed inhibition by NO_2 to its high sticking coefficient on Pt [25, 27].

In a recent study [28], C_3H_6 inhibition of NO oxidation was shown over a model $Pt-Pd/Al_2O_3$ catalyst. The apparent decrease in NO oxidation was due the preferential consumption of product NO_2 as an oxidant for C_3H_6 oxidation. In the same study, it was found that the addition of NO_2 inhibits C_3H_6 oxidation, after the onset of light-off, due to the decomposition of NO_2 to NO, which then competed with C_3H_6 for adsorption sites

[29]. Although inhibition of hydrocarbon oxidation by NO has been studied, there is little evidence of similar inhibition by NO_2 [25-27, 30].

Numerous studies have addressed the influence of hydrocarbons and CO on NO oxidation. In one study, the interaction of CO, NO_2 and NO in the presence of excess O_2 was studied over Pd/SiO_2 catalysts [31]. The authors found that CO was effective in reducing NO_2 at low temperature (below 180°C), but above 200°C reduction stopped because CO was consumed via oxidation by O_2. Additionally, the interaction between C_3H_6, NO and O_2 was also studied over a Pt supported on zeolite catalyst [32], where it was shown that O_2 promotes the reduction of NO by C_3H_6 between 200 and 300°C, by facilitating the activation of C_3H_6. In the same study, NO_2 was found to selectively react with C_3H_6, being reduced primarily to NO, although N_2O formation was also observed. Moreover, NO oxidation light-off is inhibited by hydrocarbons and CO over DOCs [33], which the authors attributed to competitive adsorption between NO, CO and hydrocarbons on oxidation sites. Several similar observations have also been reported [34-38].

The effect of hydrocarbon and/or CO addition on the oxidation of CO and hydrocarbons has also been investigated [39-41]. In these studies, the addition of a second HC species typically resulted in reaction inhibition relative to individual HC oxidation performance. In terms of CO effects, the oxidation of benzene, toluene and hexane individually and in the presence of a mixture of CO and isooctane over supported Pt, Pd, and Rh catalysts has been characterized [42]. The authors observed that inclusion of CO in the mixture considerably inhibited the oxidation of all the hydrocarbons. Such

inhibition was attributed to competitive adsorption between the hydrocarbons and CO for catalytic sites.

Diesel exhaust contains a variety of reactive species, with key regulated species including CO, hydrocarbons and NO. DOCs are used to oxidize all of these. Based on the above discussion, it is likely that each of these influences the catalyst's performance toward the other species. In the present study, reactions involving NO, NO_2, CO and different hydrocarbons (C_3H_6, dodecane, and xylene), all during lean conditions, were investigated to study the extent of inhibition between the species.

3.3 Experimental Methods

The monolith-supported sample was supplied by Umicore. The sample contains 95 g/ft^3 Pt supported on Al_2O_3. The sample was cut to 0.9" diameter with a length of 2.4" from a monolith block that had a cell density of 400 cpsi. The sample was placed into a horizontal quartz tube, which was placed inside a Lindberg Minimite temperature-controlled furnace. To ensure that no gas slipped around the sample, the catalyst was wrapped with 3M insulation material to seal the catalyst in the quartz tube. For temperature measurements, two thermocouples were used; one just inside the inlet face and one just inside the outlet face of the catalyst.

The gases and gas mixtures were supplied by Praxair and were metered with Bronkhorst mass flow controllers. Water was introduced using a Bronkhorst CEM system downstream, after the dry gas mixture had been heated. In experiments using dodecane and m-xylene, the hydrocarbons were again metered with a Bronkhorst CEM system and introduced after the wet gas mixture had been heated to >170°C to avoid condensation.

Experiments were performed between 100 and 400°C with a space velocity, at standard conditions, of 25,000 hr^{-1}. The outlet CO, CO_2, NO, NO_2, N_2O, H_2O, C_3H_6, $C_{12}H_{26}$ and C_8H_{10} gas concentrations were measured using a MKS MultiGas 2030 FT-IR analyzer.

In experiments investigating the effect of NO_2 concentration on NO oxidation activity in the absence of both hydrocarbons and CO, the catalyst was heated from 150°C to 400°C at a rate of ~3.5°C/min in a mixture containing 200 ppm NO, 0, 20, 100 or 200 ppm NO_2, 10% O_2, 5% H_2O, 5% CO_2, and balance N_2. In the second set of experiments, where hydrocarbons and CO were used, the catalyst was heated from 100°C to 350°C at a rate of ~5°C/min. The gas concentrations used were 1080 ppm C_3H_6, 270 ppm dodecane, 405 ppm xylene, 3240 ppm CO, 200 ppm NO, 0, 20, 100 or 200 ppm NO_2, 10% O_2, 5% H_2O, 5% CO_2, and balance N_2. Relatively high concentrations of CO and HC species were used due to lower flow limitations of the dodecane, and all others were kept on the same C1 basis.

3.4. Results and Discussion

This discussion is divided into four sub-sections, based on different trends observed in Figure 3.1. In section 3.1, discussion of the overall trends when NO, NO_2, O_2, hydrocarbons and CO are present in the inlet feed, is presented. In section 3.2, the effect of NO_2, hydrocarbons, and/or CO on NO to NO_2 conversion specifically, which takes place when most of the reductant species have been consumed, will be discussed, and is described in Figure 3.1 as part B. In sections 3.3 and 3.4, the effect of NO, NO_2, hydrocarbons, and/or CO on the oxidation of hydrocarbons and CO will be discussed,

which occurs in the temperature regime covered in the section labeled as "A" in Figure 3.1.
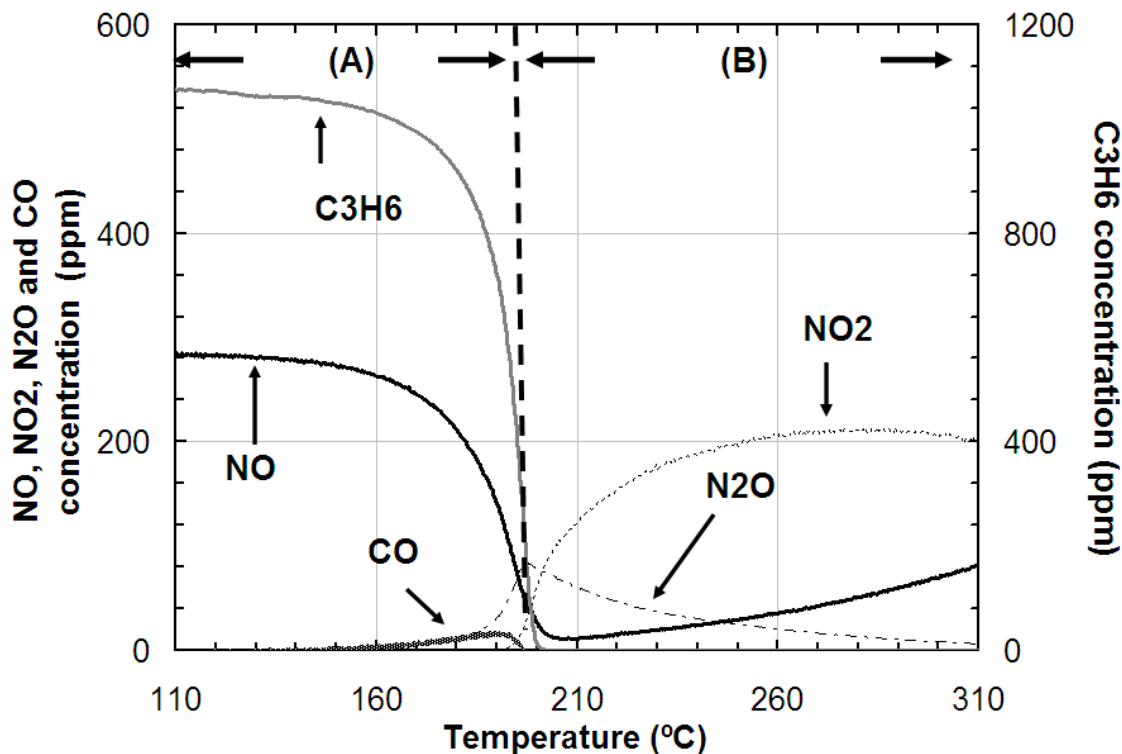
Figure 3.1 Outlet concentrations obtained during TPO with 1080 ppm C_3H_6, 200 ppm NO, 100 ppm NO_2, 10 % O_2, 5% CO_2, 5% H_2O, and balance N_2.

3.4.1 Overall trends

The effect of temperature on the various key gas species concentrations, with 200 ppm NO, 100 ppm NO_2, 1080 ppm C_3H_6, and 10% O_2 in the feed stream, is shown in Figure 3.1. NO_2 was not detected in the outlet stream below ~190°C, though 100 ppm was in the feed stream. The NO_2 is preferentially reduced by C_3H_6 in the presence of O_2 via selective catalytic reduction chemistry, even at low operating temperatures (~110°C was the starting temperature). The NO outlet concentration increased by approximately

83 ppm from its initial value (200 ppm) at the experiment onset. The increase in the NO concentration is due to incomplete NO_2 reduction.
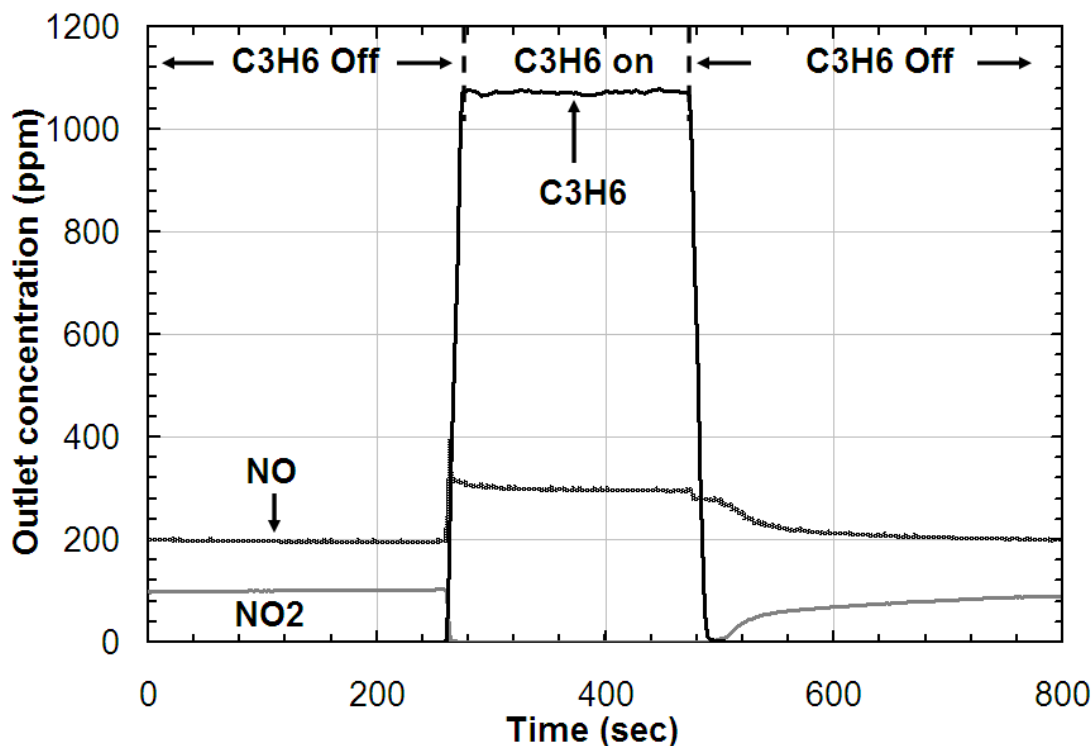
Figure 3.2 Outlet concentrations obtained at 100°C in the presence and absence of 1080 ppm C_3H_6, 200 ppm NO, 100 ppm NO_2, 10 % O_2, 5% CO_2, 5% H_2O, and balance N_2.

To further investigate the reduction of NO_2 by C_3H_6 below 200°C, an extra experiment was carried out at 100°C with 200 ppm NO, 100 ppm NO_2, 10% O_2, and in the presence and absence of C_3H_6, with the data shown in Figure 3.2. At the beginning of the experiment, NO, NO_2 and O_2 were introduced and both NO and NO_2 were detected, at their nominal inlet values. When C_3H_6 was introduced, the NO_2 concentration immediately decreased, reaching zero, and the NO concentration increased, again by

about ~83 ppm. When C_3H_6 was shut off, the NO_2 concentration increased and re-achieved its inlet value and NO decreased to its inlet value. According to Figures 3.1 and 2, 83% of NO_2 was converted to NO via reduction of NO_2 by C_3H_6 while the rest of NO_2 was reduced to N_2.

C_3H_6 and NO concentrations steadily decreased from 110 to ~160-170°C, after which, the decrease in both C_3H_6 and NO concentrations accelerated. Complete C_3H_6 conversion was reached by ~202°C. NO reached a minimum value (10 ppm) at 205°C and then slowly increased as temperature increased. NO_2 was observed at 192°C and reached a maximum at 275°C. The formation of N_2O and CO, presumably as a product of incomplete NO reduction and C_3H_6 oxidation, or the selective reduction between the two, was detected at approximately ~150°C. The maximum outlet CO detected was 17 ppm at 190°C and then decreased to zero by 197°C. N_2O formation reached a maximum value of 82 ppm at 198°C, and then slowly decreased and reached zero by 310°C. The N_2O data show that C_3H_6 is still reducing some NO and/or NO_2 at temperatures higher than when complete C_3H_6 conversion was observed.

Hydrocarbon SCR, or in this case the interaction between NO-C_3H_6-O_2, has been extensively investigated in the literature. In a previous study investigating the interactions of C_3H_6-NO-O_2 over Pt-based catalysts, at T < 250°C, high NO reduction efficiency was observed and the authors attributed this activity to O_2 facilitating the activation of C_3H_6, forming oxidized hydrocarbon intermediates on catalytic sites [43]. These intermediates are believed to preferentially react with adsorbed NO, forming N_2 and/or N_2O. However, at T > 250°C, NO reduction decreased due to combustion of C_3H_6 by O_2 becoming competitive/dominant [44]. NO_2-C_3H_6-O_2 interactions have also been

studied [23, 28, 34, 35, 45, 46]. Most agree that SCR of NO_2 is faster than NO [45, 46], especially over un-promoted oxides, such as Al_2O_3. Burch et al. reported that NO_2 is more reactive than NO, with NO_2 reacting rapidly with the surface of the catalyst to form ad-NO_X species (surface adsorbed NO_X species), including organo-nitro, organo-nitrite species, and hydroxynitropropane, considered intermediates in the reaction. The observations from Figures 3.1 and 3.2 are seemingly consistent with those previously made, in terms of NO_2 reduction by C_3H_6 being more favored compared to that with NO. Although the data cannot explicitly be used to show whether it is NO or NO_2 participating in the SCR reaction, no NO_2 is observed until the higher temperatures. According to the data shown in Figure 3.1, NO_2 is easily reduced, at least to NO at lower temperatures. And as will be shown below, NO oxidation occurs at temperatures lower than 150°C over this catalyst (> 60% conversion at 150°C). These results therefore suggest that NO_2 is selectively and preferentially consumed by C_3H_6 at low operating temperatures, either to primarily NO at lower temperatures and then to N_2O and N_2 with increasing temperature.

Similar experiments were performed but with 3240 ppm CO instead of C_3H_6. The outlet concentration of CO and NO_X species are shown in Figure 3.3, along with the equilibrium NO_2 levels for reference. Overall, trends were similar as those with C_3H_6 are observed with CO. Again, no NO_2 was detected at the onset of the experiment and not below 168°C. The NO concentration increased by only 65 ppm compared with 83 ppm with C_3H_6. A steep decrease in the NO concentration was observed starting at 170°C and reached a minimum value at 195°C, then NO slowly increased as the temperature increased. A sharp drop in the CO concentration was observed starting at 164°C, and

reached 0 ppm by 176°C (C_3H_6 reached zero at 201°C). NO_2 was observed starting at 168°C, at which point 40% of the CO was consumed, and is lower by 24°C compared to that with C_3H_6. The maximum NO_2 amount was attained at 215°C. The N_2O amounts were very small, indicating that CO suppressed the N_2O formation pathway compared with C_3H_6.
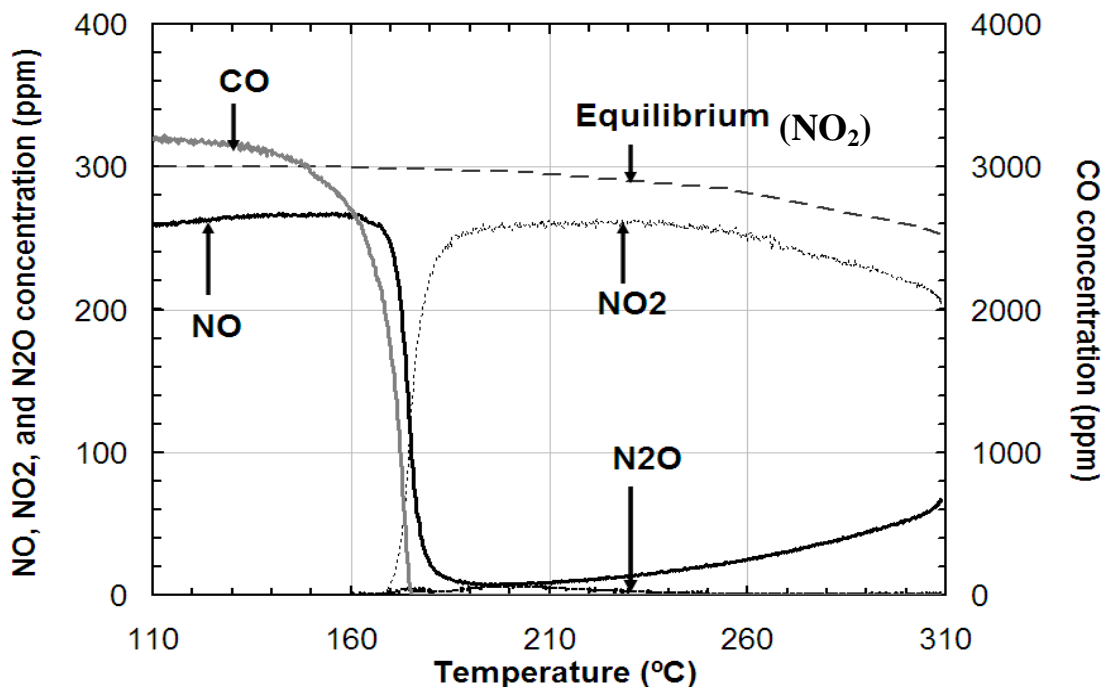
Figure 3.3 Outlet concentrations obtained during TPO with 3240 ppm CO, 200 ppm NO, 100 ppm NO_2, 10 % O_2, 5% CO_2, 5% H_2O, and balance N_2.

In a previous study with aged DOCs [32], the effect of hydrocarbons and CO on NO oxidation and NO_2 reduction was investigated. Like the data shown in Figures 3.1-3, the authors showed that both hydrocarbons and CO can completely reduce NO_2 to NO at low temperature, until around 250°C in their study, and then the NO was oxidized back to NO_2. Studies involving CO-NO-O_2 have shown similar trends [28, 31, 47].

The effects of dodecane and m-xylene were also investigated, with NO, NO_2, N_2O and the hydrocarbon concentrations shown in Figure 3.4. Unlike with CO and C_3H_6, NO_2 was observed at the onset of the experiment, i.e. at 110°C. This shows that neither dodecane nor xylene are as strong as the CO and C_3H_6 in reducing NO_2 to NO or N_2. The summation of NO_2 and NO at 110°C was equal to the inlet value of NO_X. The likely reason for the lower activity of dodecane and xylene at 110°C is related to the nature of hydrocarbon chains. First, long chain and cyclic hydrocarbons can partially block access of NO_2 to active sites, resulting in lower reduction activity. Also, their reactivity is lower in the sense that they are not activated at such low temperature. However, as the temperature increases, the activity of both dodecane and xylene to reduce NO_2 improved. With m-xylene, NO_2 was completely reduced by 145°C and by 165°C with dodecane. NO_2 was then again observed at 190°C with m-xylene, and reached a maximum value at about 295°C. With dodecane, NO_2 was observed starting at 170°C, and reached a plateau again at 295°C. NO_2 being observed at low dodecane conversion demonstrates that m-xylene is more reactive toward NO_2 reduction, which will be discussed further in section 3.3. No CO was observed in these two cases, indicating complete combustion once these hydrocarbons were activated. The combined data also show that NO reduction is coincident with reductant oxidation, suggesting that reduction is tied to the reductant activation as the limiting step at low temperature.

It should be noted that due to the presence of various types of hydrocarbons, CO, NO_X and excess O_2 in diesel exhaust, SCR chemistry over a DOC is inevitable. Figures 3.1 to 3.4 show this overall trend. With CO and C_3H_6, NO_2 is preferentially being reduced by either CO or C_3H_6 to NO and N_2. With larger hydrocarbons (dodecane and

xylene) reduction is still observed, but to a lesser extent. Once the temperature is high enough to oxidize most of the incoming CO and hydrocarbons, NO oxidation to NO_2 is observed. N_2O formation was very low when CO was used as a reductant, ~ 5 ppm, while more than 80 ppm was detected when hydrocarbons were used. Hydrocarbons require an intermediate to reduce NO_2 to NO and N_2, facilitating the formation of N_2O, as will be discussed below.
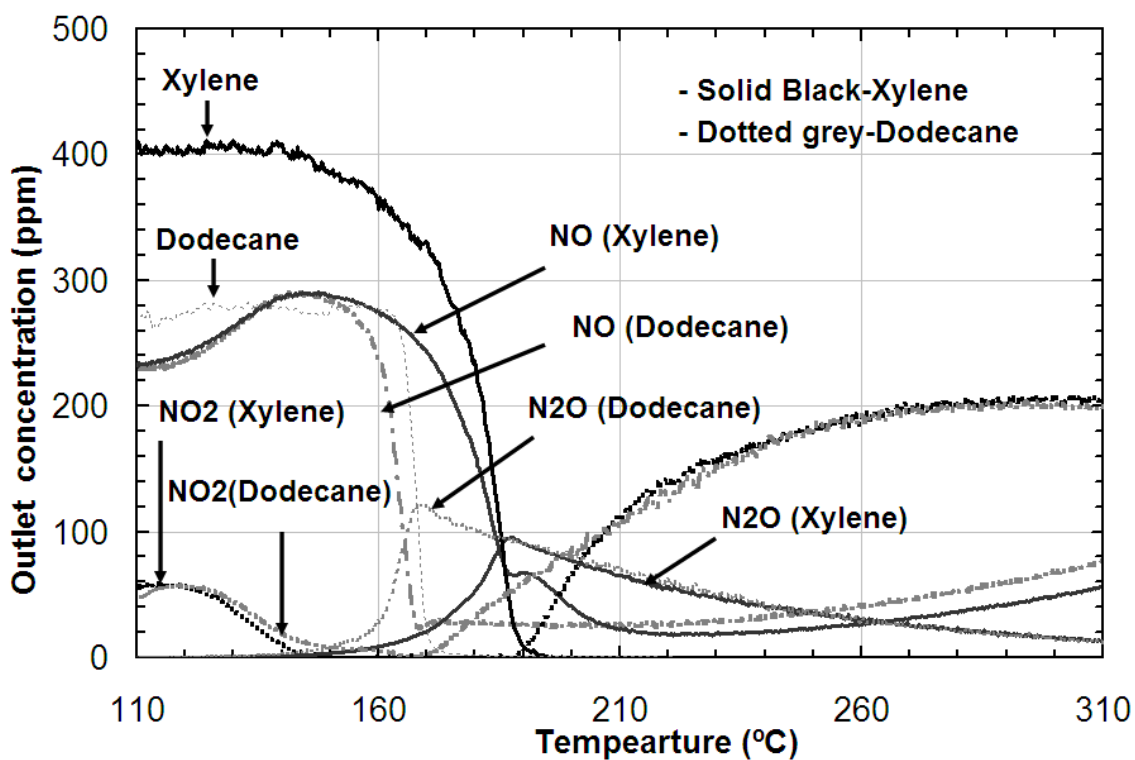
Figure 3.4 Outlet concentrations obtained during TPO with either 270 ppm dodecane or 405 ppm m-xylene, 200 ppm NO, 100 ppm NO_2, 10 % O_2, 5% CO_2, 5% H_2O, and balance N_2.

The interactions between HCs-NO_X-O_2 and CO-NO_X-O_2 over Pt/Al_2O_3-based catalysts have been widely discussed [23, 28, 31, 34, 35, 45-50]. Burch et al. [50] suggested the following NO_X reduction mechanism. CO and hydrocarbons first reduce

some Pt-O sites to metallic sites and subsequently NO dissociates on these reduced Pt sites, leading to N_2O formation at lower temperature and N_2 at higher temperature. Other research has provided an alternate explanation, with the path mentioned above possibly still occurring. For example, (1) NO oxidizes to NO_2 and subsequently reacts with the hydrocarbon over Pt [51-53], and (2) formation of an oxidized hydrocarbon or isocyanate as an intermediate [54-56]. The latter mechanism could explain the trend observed in our data, where reduction activity increased as the extent of NO oxidation to NO_2 increased or once inlet NO_2 increased. It has also been proposed that the ad-species originating from decomposition of CO and hydrocarbons could facilitate the decomposition of NO [57], which the data here also follow, since the activation of the reductant is critical for reduction to begin.

3.4.2 Effect of NO_2, hydrocarbons, and CO on NO oxidation

The NO oxidation conversion calculated and plotted is based on NO_2 made, not NO consumed. For the data after Figure 3.5, these calculations were made when most of the reductants have been consumed as illustrated in Figure 3.1, part B. Figure 3.5 shows data obtained during NO oxidation tests as a function of temperature, where 200 ppm NO were added with various NO_2 concentrations. A maximum conversion was reached between 240 and 270°C for all NO_2 concentrations. Below 240°C, the conversions increased as a function of temperature because the reaction is kinetically limited. At high temperature, the NO conversion to NO_2 is limited by thermodynamic equilibrium [58, 59]. The data clearly show that the conversion decreases with increasing concentrations of NO_2 in the feed, consistent with previous studies [25, 26, 60, 61]. The reason for the significant inhibition by NO_2 is the reduced activity of Pt when

substantially covered with chemisorbed oxygen species or if in a more fully oxidized state, and more extensive oxide formation or oxygen coverage is evident when Pt is exposed to NO_2 compared to O_2 [26, 61, 62]. For example, previous work has shown that with O_2, Pt [111] can have up to a 2/3 monolayer coverage by oxygen, whereas with NO_2 the coverage is 3/4 monolayer [62].
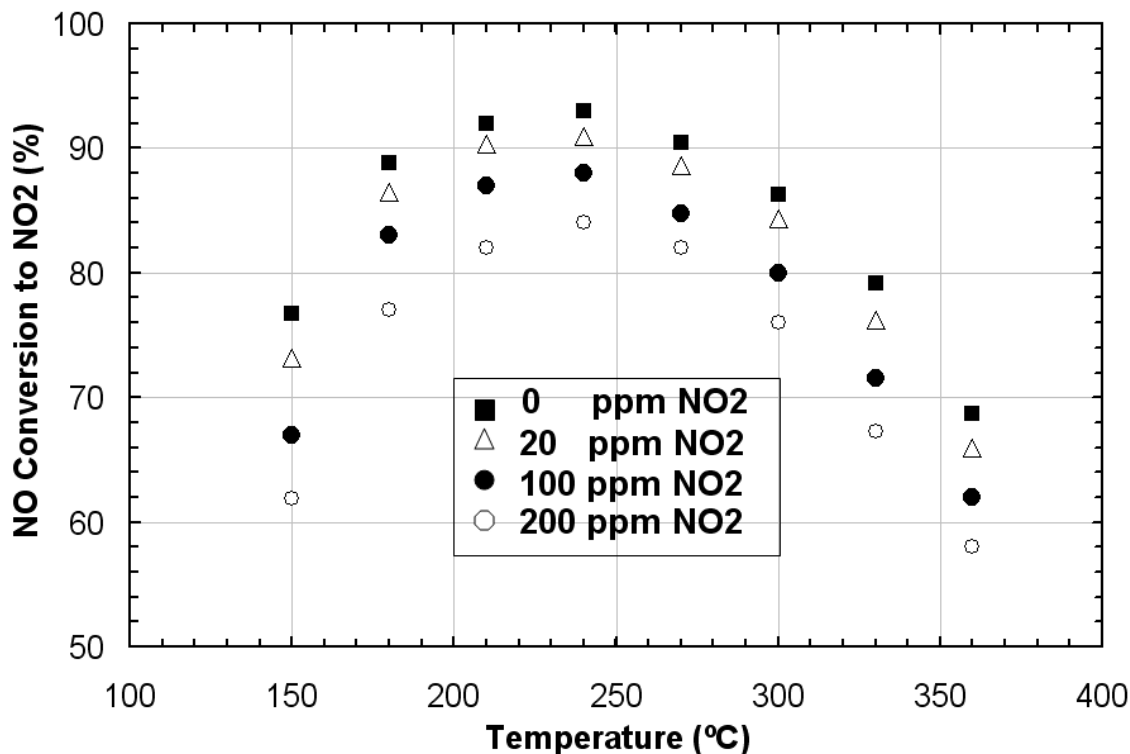
Figure 3.5   NO to NO_2 conversion obtained during TPO with 200 ppm NO, 0, 20,100, and 200 ppm NO_2, 10 % O_2, 5% CO_2, 5% H_2O, and balance N_2.

Olsson and Fridell [61] reported that NO_2 can readily oxidize Pt supported on Al_2O_3 and smaller Pt particles were more quickly oxidized, indicating larger particles are ultimately better for NO oxidation. Furthermore, previous experimental work has shown that there can be a slow decrease in oxidation kinetics with time-on-stream, which was specifically

attributed to oxidation of Pt particles by NO_2 with time [26]. The data presented here are all consistent with these previous studies; NO_2 inhibits NO oxidation through formation of Pt oxides or oxygen coverage of the Pt sites.

The results of the effect of C_3H_6 addition, combined with NO_2, on NO oxidation are shown in Figure 3.6. The conditions are otherwise the same as those in Figure 3.5. The NO conversion to NO_2, in terms of outlet NO_2 concentration, was zero at $T \leq 180°C$ for all NO_2 concentrations. This is not to say that NO oxidation did not occur, but that if it did, the NO_2 formed was immediately reduced via reaction with the C_3H_6 [28]. Evolution of NO_2 was observed at ~185°C with 0 ppm NO_2 while at 190, 195 and 200°C with 20, 100 and 200 ppm NO_2, respectively. Once NO oxidation was evident, there was decreased overall NO conversion with increasing inlet NO_2 amount. At $T < 215°C$, the negative impact of NO_2 was obvious and at higher temperatures less evident. This is due facile hydrocarbon oxidation at the elevated temperature, resulting in easy consumption of the oxygen associated with any Pt oxides and therefore a relative abundance of active metal sites. Thus, the hydrocarbon is able to reduce the negative impact of NO_2 that arises from NO_2 oxidizing the Pt. Also, at the higher temperatures, thermodynamic limitations become more significant, limiting kinetic effects.

However, in comparing the results in Figures 3.5 and 3.6, it is apparent that C_3H_6 has an overall detrimental effect on NO to NO_2 conversion. At $T \leq 180°C$, no NO_2 was observed due to the reduction of any formed NO_2 by C_3H_6, as discussed above. At $T \geq 180°C$, NO oxidation started, which is associated with the onset of C_3H_6 oxidation, discussed below, and therefore NO can adsorb and react on the active Pt sites. However, even at higher temperatures, the overall NO oxidation conversions are less than those

observed in the absence of C_3H_6. This is consistent with previous research that has shown hydrocarbons inhibit NO oxidation. At high temperature, site competition has been proposed to explain hydrocarbon inhibition of NO oxidation [29], with some impact of NO_2 being consumed by the hydrocarbon observed as well [28, 32]. Also contributing is competition between NO and C_3H_6 for surface oxygen.
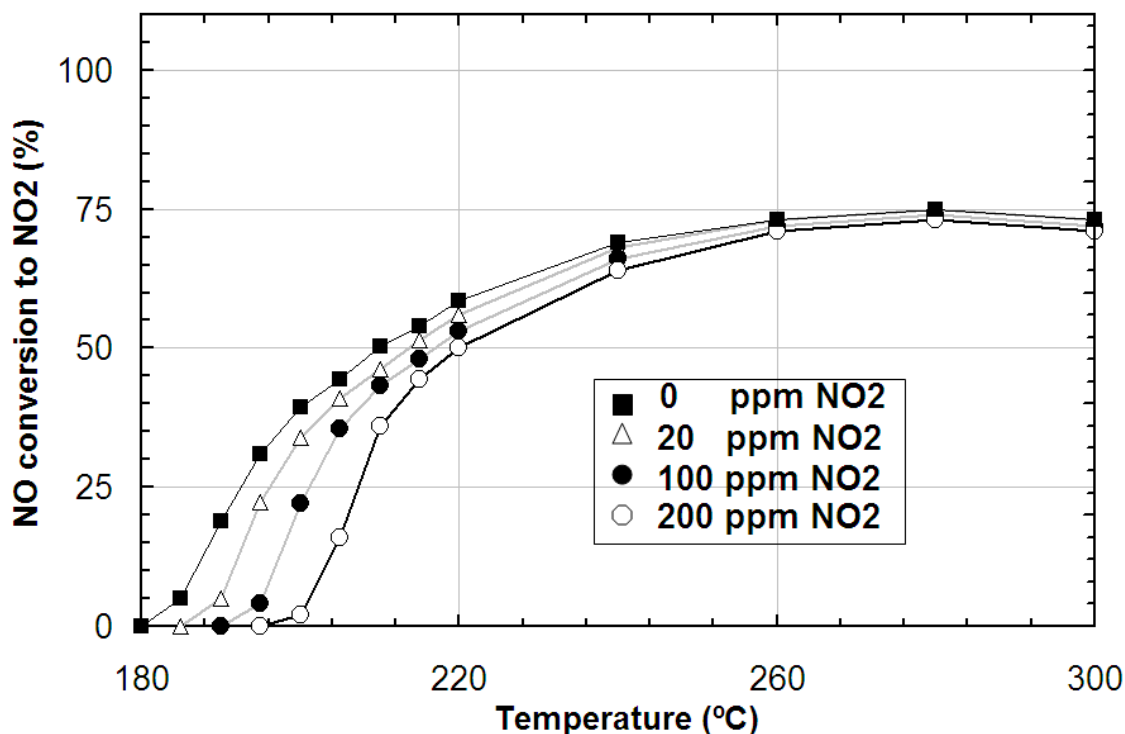
Figure 3.6   NO to NO_2 conversion obtained during TPO with 1080 ppm C_3H_6, 200 ppm NO, 0, 20,100, and 200 ppm NO_2, 10 % O_2, 5% CO_2, 5% H_2O, and balance N_2.

Experiments with dodecane or m-xylene were also performed and data are shown in Table 3.1. Overall there was a decrease in the NO conversion to NO_2, similar to that of C_3H_6. In terms of the effect of NO_2 concentration, the temperature changes to achieve the

same NO to NO_2 conversions were on the order of 1 to 5°C, indicating insignificant NO_2 inhibition with the larger hydrocarbon species being present.

Table 3.1 Temperatures (°C) required for 10 and 50% conversion of NO to NO_2

Feed Gas	NO	NO + 20 ppm NO_2	NO + 100 ppm NO_2	NO + 200 ppm NO_2
Temperature (°C) at 10% NO Conversion (T_{10})				
no HCs or CO	114	116	123	131
CO	162	165	171	177
C_3H_6	186	191	197	203
Dodecane	177	178	179	181
Xylene	191	191	193	196
C_3H_6 + CO	216	218	221	227
C_3H_6 + Dodecane	215	217	222	225
Temperature (°C) at 50% NO Conversion (T_{50})				
no HCs or CO	132	134	139	145
CO	165	168	174	181
C_3H_6	210	213	217	220
Dodecane	233	234	235	237
Xylene	225	225	227	229
C_3H_6 + CO	226	227	231	239
C_3H_6 + Dodecane	241	247	258	272

These results suggest that NO oxidation inhibition by the larger hydrocarbons is dominant relative to that of NO_2. The temperature differences to attain similar conversions are smaller than those observed with C_3H_6. As will be shown later (Figures 3.9 and 3.11), the light-off of dodecane is faster once oxidation begins (the temperature range from the onset to complete oxidation is narrower), relative to C_3H_6. This is in part due to the exothermicity of the reactions, with dodecane oxidation resulting in more heat

released. And although the same C1 basis was used, the larger hydrocarbon has more H compared with C_3H_6, therefore the larger hydrocarbons can consume more surface oxygen and, thereby again limit the negative effect of the NO_2.

The effect of mixtures of hydrocarbons and NO_2 on NO oxidation was also studied and summary data are listed in Table 3.1. With a mixture of C_3H_6 and dodecane, NO conversion to NO_2 was significantly decreased. For example, with only C_3H_6, 10 and 50% conversion of NO to NO_2, with 200 ppm NO_2 also added, was achieved at 204 and 225°C, respectively, while the same conversions were achieved with a mixture of C_3H_6 and dodecane at 220 and 272°C respectively. The maximum conversion in the presence of both hydrocarbons did not exceed 58%, which was reached at 275°C. In terms of NO_2 addition, there were decreases in the overall NO conversions to NO_2 with each increase in the amount of NO_2. The decreased performance with addition of dodecane to C_3H_6 is due to additional competitive adsorption between NO and C_3H_6, dodecane, and NO_2 for active sites. The effect of the addition of NO_2 to the mixed hydrocarbon system on the T_{50} values is more pronounced than when added to mixtures with just the individual species, while the T_{10} changes were similar. This is due to the decreased overall conversion nearing the 50% conversion and therefore exaggerating the effect relative to the simpler mixtures.

NO oxidation conversion as a function of NO_2 concentration and temperature, in the presence of 3240 ppm CO is shown in Figure 3.7. At low temperature, in the absence of CO, there was appreciable NO conversion at 150°C (Figure 3.5). But, in the presence of CO, no NO_2 was observed at 150°C with or without NO_2 added. Again, this is due to

the inlet and any formed NO_2 being reduced by CO. However, at $T > 170°C$ where NO_2 was observed, the addition of CO promoted NO conversion to NO_2.
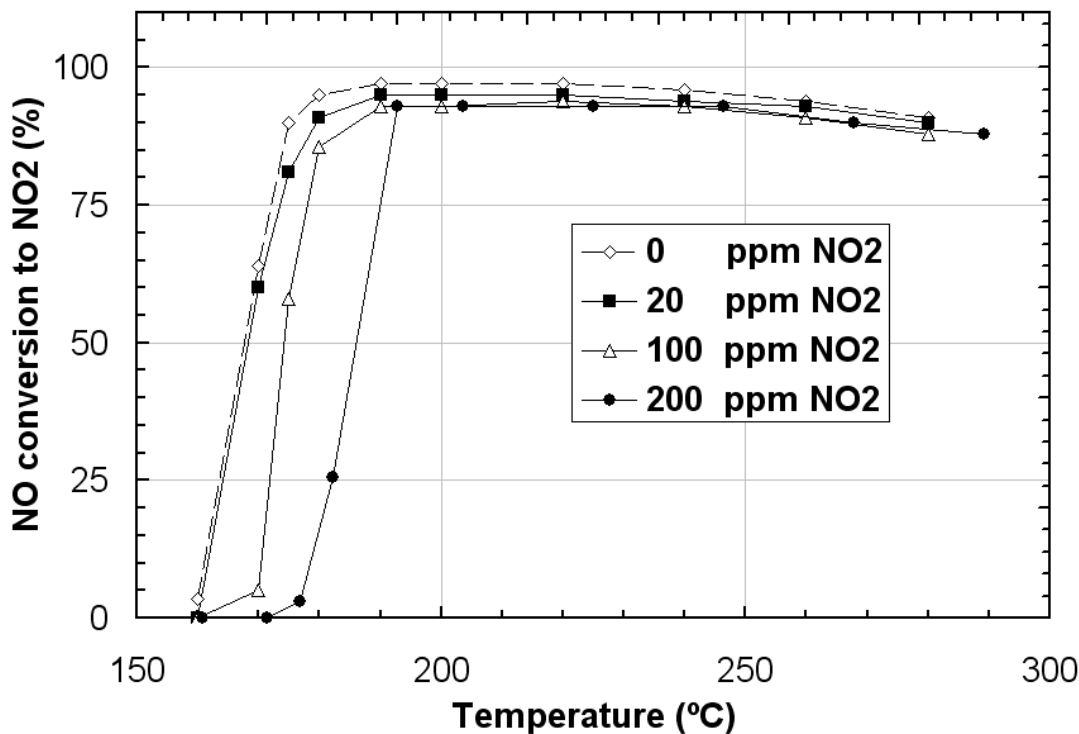
Figure 3.7 NO to NO_2 conversion obtained during TPO with 3240 ppm CO, 200 ppm NO, 0, 20,100, and 200 ppm NO_2, 10 % O_2, 5% CO_2, 5% H_2O, and balance N_2.

In terms of increasing NO_2, it is clear that catalyst performance decreased monotonically with each increase in NO_2 concentration at $T < 190°C$. Beyond that, NO conversion to NO_2 was relatively independent of NO_2 amount, for the same reasons discussed above; surface oxygen consumption by the reductant species and increased local temperatures from the exothermic CO oxidation reaction. NO oxidation to NO_2 reached $> 90\%$ conversions at the 190°C test point with all NO_2 concentrations, which is much higher than that observed in the presence of the individual hydrocarbons, or mixture of

hydrocarbons, and is also higher than the conversions observed in the absence of hydrocarbons and CO (Figure 3.5). Between 190 and 220°C, there were no changes observed in the NO conversion to NO_2 and at higher temperatures the conversions decreased with increasing temperature. One contributing factor to the higher NO_2 amounts made with CO compared to that with hydrocarbons is the absence of H, which could react with NO_2 resulting in NO. Another possibility is that since CO lit-off at a lower temperature than the hydrocarbons, as shown by comparing Figures 3.1, 3.3 and 3.4 for example, there is less reduction by CO as it's oxidation is likely limited to the very front portion of the catalyst. Consequently, hydrocarbons can reduce more NO or NO_2 to N_2 or N_2O. As shown in Figures 3.1, 3.3 and 3.4, significantly more N_2O formed with hydrocarbons, in the range of 82 to 121 ppm, compared with approximately ~ 6 ppm with CO. Therefore, since reduction of NO_X continues at higher temperatures with hydrocarbons relative to CO, less NO_2 formation would be observed with hydrocarbons compared with CO, which was observed.

Similar experiments were also performed but with a mixture of CO and C_3H_6. Summary results are also listed in Table 3.1. Overall, there was a decrease in NO conversion with increasing NO_2 amount in the feed stream. The NO conversions with a mixture of C_3H_6 and CO were lower than that with either just C_3H_6 or CO. The more significant inhibition on NO oxidation with the mixture of CO and C_3H_6 is surprising based on the data in Figure 3.7, where CO was shown to promote NO oxidation at temperatures above 180°C. However, CO inhibits C_3H_6 oxidation (with O_2), shifting the 50% conversation by 15°C when CO was added to the C_3H_6-containing feed, as will be shown below. This therefore extends the temperature range where C_3H_6 is reacting with

NO_X, either in reducing it to N_2, reducing any NO_2 made to NO, or in simple site competition. Otherwise, the effect of NO_2 is similar to that observed with just CO or C_3H_6.

3.4.3 Effect of NO, NO_2, CO and hydrocarbons on hydrocarbon oxidation

The effect of 200 ppm NO and different concentrations of NO_2 on the conversion of 1080 ppm C_3H_6 is shown in Figure 3.8. With the addition of 200 ppm NO and increasing amounts of NO_2, the light-off and complete conversions of C_3H_6 occurred at higher temperatures. For example, with the addition of 200 ppm NO and 200 ppm NO_2, the 50 and 90% C_3H_6 conversions were achieved at 198 and 203°C compared with 161 and 165°C without NO_X added. These data clearly show inhibition by NO, NO_2, or total NO_X on C_3H_6 conversion.

Further experiments were performed to investigate whether the inhibition in C_3H_6 conversion was due to NO, NO_2, or total NO_X (NO+NO_2). In one set of experiments, 300 and 400 ppm NO were used with 1080 ppm C_3H_6. While, in another set of experiments, a mixture of NO and NO_2 was used, with the same total NO_X used with NO alone (i.e total NOx was 300 or 400 ppm). The 50% C_3H_6 conversions with NO only as inlet NO_X were 189 and 196°C with 300 and 400 ppm NO, respectively, while they were 192 and 198°C with 300 and 400 ppm of a mixture of both NO and NO_2 as inlet NO_X, respectively. The 50% C_3H_6 conversions were very close, the differences in order of 3°C, with temperature error analysis in C_3H_6 oxidation being -/+ 1°C. Although attempts were made to more clearly determine whether it is NO, NO_2, or total NO_X inhibiting C_3H_6 conversion, these data indicate it is simply the total NO_X amount.
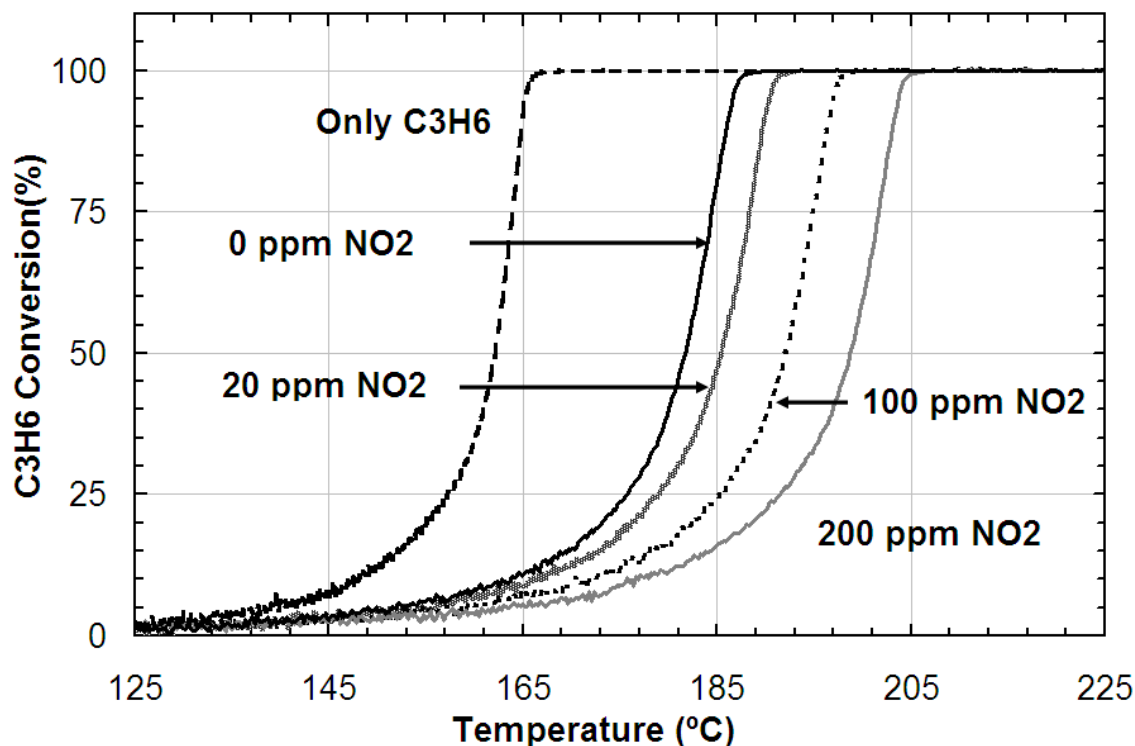
Figure 3.8 C_3H_6 conversion obtained during TPO with 1080 ppm C_3H_6, 200 ppm NO, 0, 20, 100, and 200 ppm NO_2, 10 % O_2, 5% CO_2, 5% H_2O, and balance N_2.

Dodecane and m-xylene conversions were also evaluated and data are listed in Table 3.2. In the absence of NO and NO_2, 25 and 90% dodecane conversions were attained at 131 and 136°C, respectively, while with m-xylene they were achieved at 161 and 165°C, respectively. Previous literature has shown that the ease of alkane oxidation increases with increasing chain length, [64, 65]. Conversely, the ease of alkene oxidation decreases with increasing hydrocarbon chain length from ethylene to hexene [64], but is less dependent at chain lengths for $7 < n < 10$ [65]. A general consensus is that light alkenes are more reactive than light alkanes, while heavier alkanes are more reactive than heavier alkenes [65]. Additionally, it has been shown that C_6-C_9 aromatics behave similarly to alkenes (C_2-C_6) in terms of oxidation [64], which coincides with the data

listed in Table 3.2, where C_3H_6 and m-xylene light off were similar. With the addition of 200 ppm NO and with 0, 20, 100, and 200 ppm NO_2, the conversions of both dodecane and m-xylene were shifted to higher temperatures. The reason for the lower hydrocarbon conversions is due to competition between NO and NO_2 and hydrocarbons for the same adsorption sites. This is consistent with previous literature [28] regarding the effect of NO on higher hydrocarbon oxidation, where evidence suggests that under oxidizing conditions, a Pt-based catalyst showed inhibition by NO.

Table 3. 2 Temperatures (°C) required for 25, 50, and 90% conversion of hydrocarbon species

Feed Gas	No NO$_X$	NO	NO + 20 ppm NO$_2$	NO + 100 ppm NO$_2$	NO + 200 ppm NO$_2$
25% HC Conversion (T$_{25}$)					
Dodecane	131	162	163	166	171
Xylene	156	166	169	173	184
C$_3$H$_6$	157	175	178	185	191
C$_3$H$_6$ + CO	174	208	209	215	223
50% HC Conversion (T$_{50}$)					
Dodecane	133	163	164	167	172
Xylene	161	175	176	181	190
C$_3$H$_6$	161	182	185	192	198
C$_3$H$_6$ + CO	176	211	212	218	226
90% HC Conversion (T$_{90}$)					
Dodecane	136	165	167	170	174
Xylene	165	181	182	187	195
C$_3$H$_6$	165	186	189	196	203
C$_3$H$_6$ + CO	179	215	216	222	229

Figures 3.9 - 11 compare the overall effect of individual species and a mixture of NO, NO_2, CO, C_3H_6, or dodecane on the C_3H_6 and dodecane conversions. As shown in Figure 3.9, with the addition of only dodecane, there was an insignificant shift in C_3H_6

conversion, the 50% conversion temperature shifted by 3°C. The lack of significant effect is due to surface coverages at the onset of the experiment. The C_3H_6 initially covers the surface, blocking dodecane adsorption, as also shown in Figure 3.9 where dodecane begins oxidizing after C_3H_6. Addition of CO to the C_3H_6-containing feed shifted the 50% C_3H_6 conversion temperature by 15°C. This coincides with literature evidence, where CO inhibition has been attributed to CO adsorbing more strongly than the hydrocarbons and consequently occupying Pt sites [42, 66].
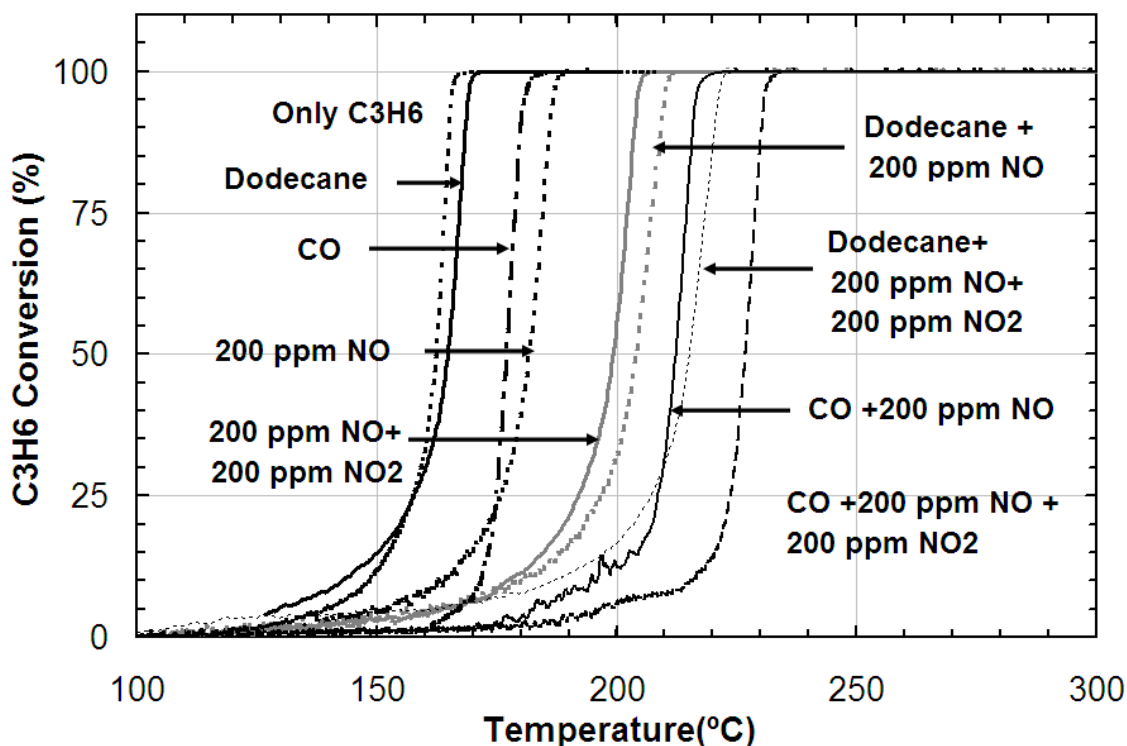
Figure 3.9 C_3H_6 conversion obtained during TPO with 1080 ppm C_3H_6, and either 3240 ppm CO, 270 ppm dodecane, and/or 200 ppm NO, 200 ppm NO_2, and 10 % O_2, 5% CO_2, 5% H_2O, and balance N_2.

With NO, or a mixture of NO and NO_2, the 50% conversion temperature was shifted to significantly higher temperatures, on the order of 20 to 40°C under our test conditions. The increase in 50% C_3H_6 conversion temperature was 53°C with a mixture

of dodecane and NO_X whereas it increased 65°C with a mixture of CO and NO_X. As with

only CO the shift was 15°C, with only dodecane it was negligible and with the NO/NO_2

mixture it was 37°C, this shift in 50% C_3H_6 oxidation temperature in the mixture of CO

and NO_X or dodecane and NO_X demonstrated that the combined effect is not additive; the

increased temperature is beyond that of the sum of the individual inhibitions.
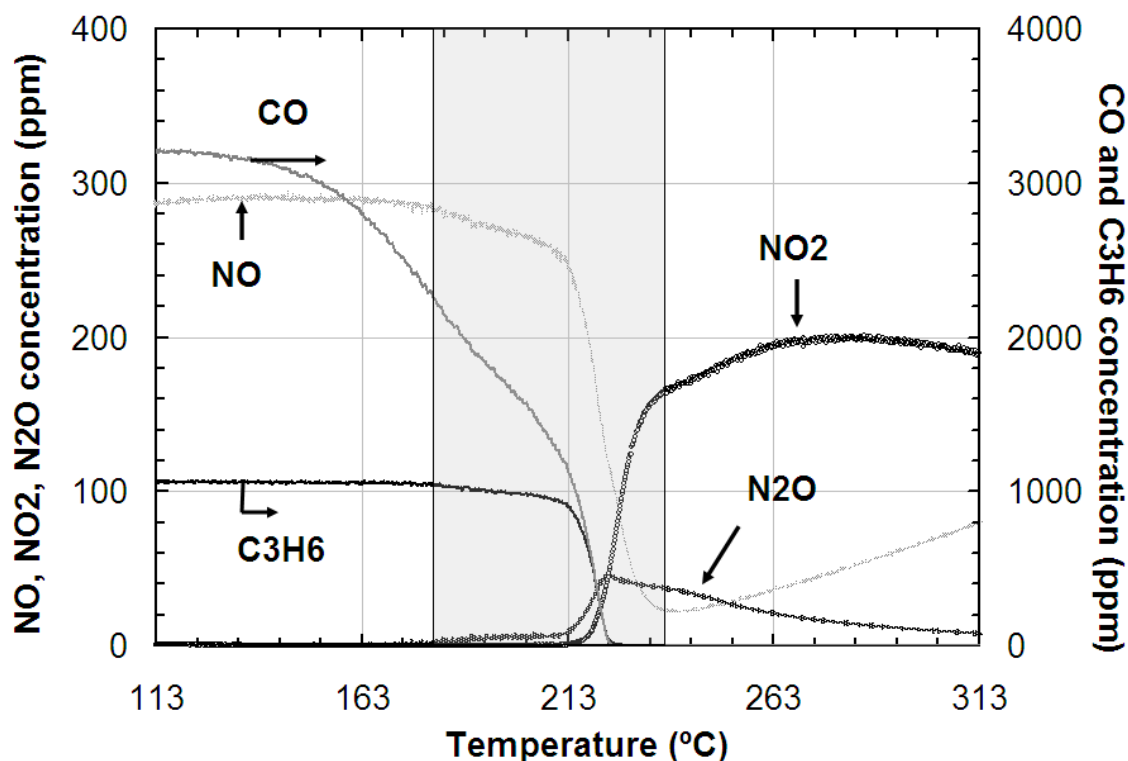
Figure 3.10 Outlet concentrations obtained during TPO with 3240 ppm CO, 1080 ppm
C_3H_6, 200 ppm NO, 100 ppm NO_2, 10 % O_2, 5% CO_2, 5% H_2O, and
balance N_2.

To further explain the combined effect with a mixture of CO, C_3H_6, and NO/NO_2, the

species concentration vs. temperature was plotted and data are shown in Figure 3.10. A

mixture of 200 ppm NO and 100 ppm NO_2 were used. As shown, the CO concentration

gradually decreased and no change was observed for both NO and C_3H_6 concentrations

up to 178°C, as shown in left of the shaded area, indicating that CO adsorbs more strongly on Pt and shifts both C_3H_6 and NO oxidation to higher temperature. Subsequently, when C_3H_6 oxidation started, after CO oxidation had begun, NO can co-adsorb and compete with C_3H_6 on Pt sites, causing the observed extra shift in C_3H_6 conversion.

It could be expected that the addition of CO to a mixture of hydrocarbons can reduce the hydrocarbon light-off temperatures due to the exotherm originating from CO oxidation. This however was not observed. Thus, an exotherm does not explain the observations in this study and the inhibition effects, instead of promoting effects, are relevant to the results obtained.

The dodecane data are shown in Figure 3.11. In the presence of only NO, the temperature required for 50% conversion was shifted by 31°C and with the addition of C_3H_6, the 50% dodecane conversion shifted by 36°C. So although dodecane had little influence on C_3H_6 conversion, C_3H_6 had a negative impact on dodecane conversion as discussed above. The reason is that the C_3H_6 covers the surface preferentially at low temperature relative to the dodecane. With a mixture of NO and NO_2, the temperature for 50% conversion of dodecane was increased by 40°C, and with inclusion of C_3H_6 to a mixture of NO and NO_2 the 50% conversion increased by 86°C, compared to the experiment with only dodecane. Again, the combined effect of the mixtures is more than additive.
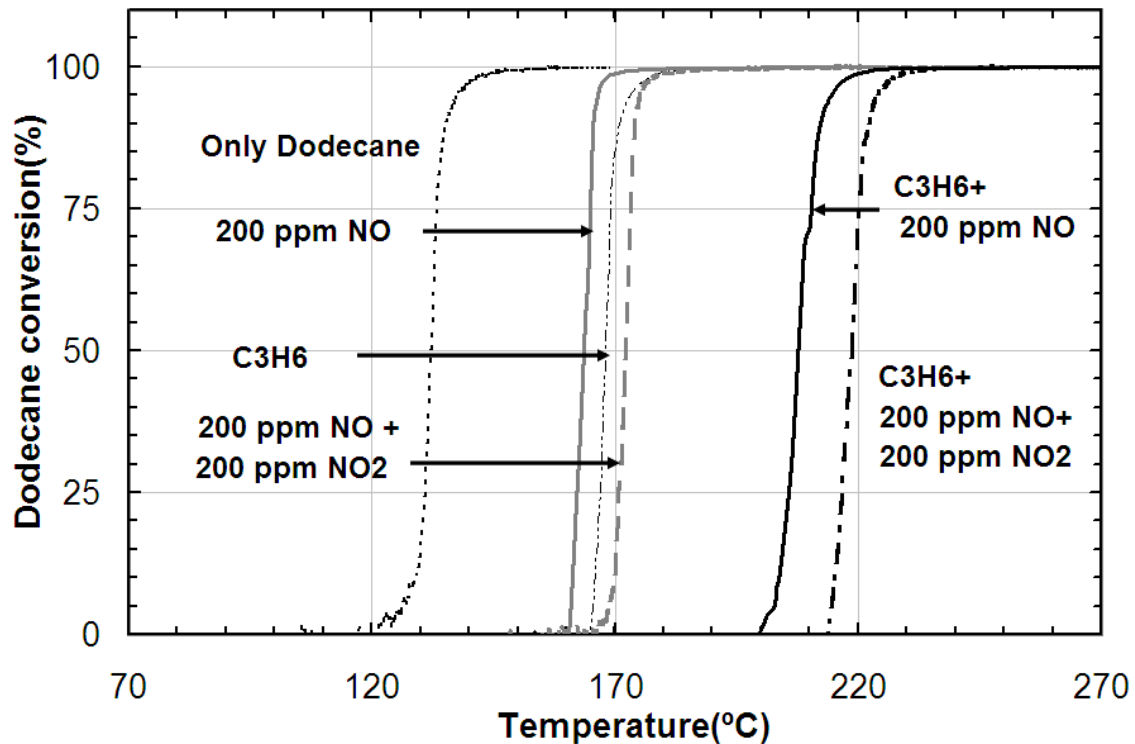
Figure 3.11 Dodecane conversion obtained during TPO with 270 ppm dodecane and either 1080 ppm C_3H_6, , and/or 200 ppm NO, 200 ppm NO_2, and 10 % O_2, 5% CO_2, 5% H_2O, and balance N_2.

3.4.4 Effect of NO, NO_2, and hydrocarbons on CO oxidation

The CO conversion data in the presence and absence of the other components are shown in Figure 3.12. Note: the associated error in the temperature was calculated was 2.3°C for CO conversions. With only CO, 50% conversion was achieved at 145°C and 90% at 153°C. In the presence of 200 ppm NO, the 50% CO conversion temperature increased by 17°C. The addition of 100 and 200 ppm NO_2, with 200 ppm NO, shifted the 50% conversions to 170 and 177°C, respectively, showing CO oxidation inhibition by NO_X, again likely through competitive adsorption with CO on the Pt sites [29, 47]. Adding C_3H_6 in with CO shifted the 50% conversion temperature to 172°C. Adding C_3H_6

to the mixtures of 200 ppm NO and NO_2, the 50% CO conversion temperatures increased to 187, 200, and 208°C with 0, 100, and 200 ppm NO_2 respectively. Although above it was pointed out that at low temperature CO preferentially adsorbs to the active sites relative to the C_3H_6, comparing the data in Figure 3.12 with those in Table 3.2, it is obvious that both C_3H_6 and CO result in mutual inhibition. An important observation is that the CO light-off curves are less steep in the presence of C_3H_6 and the NO/NO_2 mixture compared to those in the presence of only NO/NO_2. Furthermore, the inhibition by C_3H_6 and NO/NO_2 on CO oxidation, as shown in Figure 3.10, was minimal at low temperature (and as shown in the shaded are of Figure 3.12), however, as the temperature increased inhibition became apparent, i.e. the slope of the oxidation extent decreased relative to the absence of the other components. This is due to CO poisoning decreasing once oxidation began, freeing sites for both C_3H_6 and NO adsorption, resulting in the inhibition effect. This is consistent with the conclusions made by Voltz who investigated the effect of NO and C_3H_6 on CO oxidation over a Pt/Al_2O_3 catalyst [29] and inhibition by both NO and C_3H_6 was attributed to competitive adsorption on catalytic sites. These data indicate that CO adsorbs more strongly on Pt sites at lower temperature than either C_3H_6 and NO do, and therefore CO was inhibiting both NO and C_3H_6 oxidation. As shown in Figure 3.10, there was no change in the NO and C_3H_6 concentrations up to 178°C, while the CO concentration gradually decreased, as shown in the shaded area. Also as highlighted in the shaded area of Figure 3.12 the onset of CO light-off was not affected by NO_X and C_3H_6, further suggesting that CO oxidation inhibition, by C_3H_6 and NO_X, occurs only after CO oxidation begins.
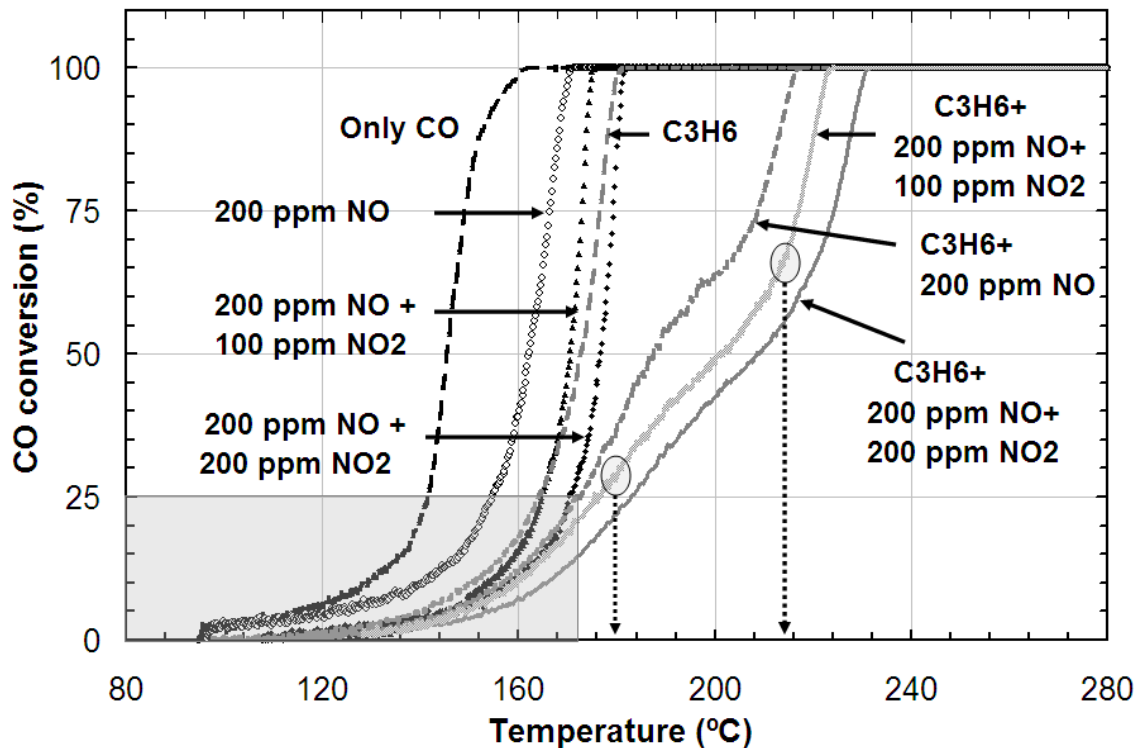
Figure 3.12 CO conversion obtained during TPO with 3240 ppm CO, and either 1080 ppm C_3H_6, and/or 200 ppm NO, 200 ppm NO_2, and 10 % O_2, 5% CO_2, 5% H_2O, and balance N_2.

Beyond 178°C, the NO concentration progressively decreased indicating enough sites are free of CO for it to adsorb and begin oxidation. The two circles in Figure 3.12 highlight the start and end of an inflection, the first being where C_3H_6 oxidation begins (~185°C), or where C_3H_6 can adsorb to Pt sites and compete with both CO and NO. At 213°C, there was a sharp decrease in CO concentration, as observed in Figure 3.10, and at this point the inflection ends as observed in Figure 3.12. Subsequently, steep decreases in both NO and C_3H_6 concentrations were observed. Inflections in the C_3H_6 oxidation curves (Figure 3.9) were not observed with a mixture of CO and NO and NO_2. This is because C_3H_6 adsorbs and oxidizes after CO.

Table 3.3 Summary of the temperatures at which the 50% conversion of CO was attained and the increase in temperature to achieve 50% CO conversion with the addition of other reactive species.

Gases	Temperature (°C) at 50% CO conversion	Increase in temperature
CO	145	-
NO	162	17
C_3H_6	172	27
C_3H_6 + NO	187	42
NO + 100 ppm NO_2	170	25
NO + 100 ppm NO_2 + C_3H_6	200	55
NO + 200 ppm NO_2	177	32
NO + 200 ppm NO_2 + C_3H_6	208	63

Table 3.3 summarizes the temperatures at which the 50% CO conversions were attained and the increase in 50% CO conversion temperatures with the addition of other reactive components. The 50% CO conversion temperature was shifted by 17°C with only NO, whereas it was shifted 27°C with only C_3H_6. With a mixture of both NO and C_3H_6, the 50% conversion of CO was shifted by 42°C, indicating the combined effect of NO and C_3H_6 is additive in this case. Also, the 50% CO conversion temperature increased 25°C with a mixture of 200 ppm NO and 100 ppm NO_2 and 55°C when C_3H_6 was added to a mixture of 200 ppm NO and 100 ppm NO_2. The 50% conversion of CO was increased by 30°C when C_3H_6 was added to a mixture of 200 ppm NO and 100 ppm NO_2, which is similar to the increase in temperature caused by only C_3H_6 (27°C). This again shows that the combined inhibition of C_3H_6 and NO/NO_2 on CO conversion is additive. It should be also mentioned that the effect of CO on C_3H_6, as shown in Figure 3.9, is far from additive. This additive effect on CO oxidation is due to the preferential low

temperature adsorption of CO on the active Pt sites, thus the effect on the onset of CO oxidation is absent and NO and C_3H_6 only adsorb once CO oxidation began.

3.5 Conclusions

The effect of reactant exhaust gas species on the oxidation of NO, hydrocarbons, and CO was investigated over a Pt/Al_2O_3 catalyst in the presence of excess O_2. CO and C_3H_6 were found to reduce NO_2 at temperatures as low as 110°C whereas higher hydrocarbons (dodecane and xylene) reduced NO_2 at temperatures above 140°C, indicating the reduction ability is related to the activation of the reductant species. Once oxidation of the CO or hydrocarbon species with oxygen began, NO_2 was observed in the outlet stream. The addition of NO_2 to the feed stream inhibited the oxidation of NO, CO, and hydrocarbons. Hydrocarbons were also found to inhibit NO oxidation, as well as the oxidation of other hydrocarbon species (i.e. C_3H_6 inhibited dodecane oxidation and vice versa) due to competition for adsorption sites. The influence of these species on hydrocarbon oxidation was not additive. CO was found to initially hinder the oxidation of NO to NO_2, but as the temperature increased, and CO oxidation via O_2 was favored, CO promoted NO conversion to NO_2. The onset of CO oxidation was not affected, but the extent of oxidation after was inhibited. The combined effect of C_3H_6 and NO and NO_2 on CO conversion was additive since C_3H_6 oxidation occurred after CO oxidation.

3.6 Acknowledgements

References

1. N. Harayama, K. Niimura, and Y. Watanabe, SAE technical paper series 920852.

2. A. Kalantar, F. Klingstedt, T. Salmi, and D.Y.Murzin, Fuel 83(2004)395.

3. H. J. Stein, Applied Catalysis B: Environmental 10(1996)69.

4. M. Kawanami, M. Horiuchi, H. Klein, and M. Jenkins, SAE technical paper series 981196.

5. A. Morlang , U. Neuhausen, K. V. Klementiev, F.W. Schutze, G. Miehe , H. Fuess, and E. S. Lox, Applied Catalysis B: Environmental 60(2005)191.

6. W. A. Majewski and M. K. Khair, Diesel emissions and their control, SAE International, 2006, pages 20, 90, and 150.

7. M. V. Twigg, Applied Catalysis B: Environmental 70(2007)2.

8. M. Shelef and R. W. McCabe, Catalysis Today 62(2000)35.

9. K. M. Adams, J. V. Cavataio, T. Sale, W. A. Rimkus, and R. H. Hammerle, SAE technical paper series 962049.

10. M. Kamijo, M. Kamikubo, H. Akama and K. Matsushita, JSAE Review 22(2001) 277.

11. Y. Lui, J. Dettling, O. Weldlich, R. Krohn, D. Neyer, W. Engeler, G. Kahman, and P. Dore, SAE technical paper series 962048.

12. T. Nakane, M. Ikeda and M. Hori, O. Bailey, and L. Mussmann, SAE technical paper series 2005-01-1759.

13. Y. Banno, Y. Tanaka, T. Hihara, and M. Nagata, SAE technical paper series 2004-01-1430.

14. C. Kwon, J. Lee, S. Kim and G. Yeo, SAE technical paper series 2005-01-0672.

15. J. C. Fayard and T. Seguelong, SAE technical paper series 2004-01-1937.

16. A. Setiabudi, M. Makkee, and J. A. Moulijn, Applied Catalysis B: Environmental 50(2004)185.

17. M. Pfeifer, M. Votsmeier, M. Kögel, P. C. Spurk, E. S. Lox, and J. F. Knoth, SAE technical paper series 2005-01-1756.

18. C. Ciardelli, I. Nova, E. Tronconi, D.Chatterjee, B. Bandl-Konrad, and M. Weibel, B. Krutzsch, Applied Catalysis B: Environmental 70(2007) 80.

19. C. S. Sluder, J. M Storey, S. A. Lewis and L. A. Lewis, SAE technical paper series 2005-01-1858.

20. M. Koebel, M. Elsener and G. Madia, SAE technical paper series 2001-1-3625.

21. W. S. Epling, J. E. Parks, G. C. Campbell, A. Yezerets, N. W. Currier, and L. E. Campbell, Catalysis Today 96(2004)21.

22. S. Hodjati, K. Vaezzadeh, C. Petit, V. Pitchon, and A. Kiennemann, Catalysis Today 59(2000)323.

23. S. Erkfeldt, E. Jobson, and M. Larsson, Topics in Catalysis 16/17(2001)1.

24. M. AL-Harbi, and W. S. Epling, Catalysis Letters 130(2009)121.

25. S. S. Mulla, N. Chen, W. N. Delgass, W. S. Epling, and F. H. Ribeiro, Catalysis Letters 100(2005)3.

26. D. Bhatia, R. W. McCabe, M. P. Harold, and V. Balakotaiah, Journal of Catalysis 266(2009)106.

27. K. Kabin, R. Muncrief, and M. Harold, Catalysis Today 96(2004)79.

28. K. Irani, W. S. Epling, and R. Blint, Applied Catalysis B: Environmental 92(2009)422.

29. S. E. Voltz, C. R. Morgan, D. Liederman, and S. M. Jacob, Industrial & Engineering Chemistry Product Research and Development 12(1973)294.

30. S. S. Mulla, N. Chen, L. Cumaranatunge, W. N. Delgass, W.S. Epling, and F.H. Ribeiro, Catalysis Today 114(2006)57.

31. M. Li, K. Seshan, and L. Lefferts, Applied Catalysis B: Environmental 50(2004)143.

32. M. D. Amiridisa, K. L. Robertsa, and C. J. Pereirab, Applied Catalysis B: Environmental 14(1997)203.

33. S. R. Katare, J.E. Patterson, and P. M. Laing, Industrial and Engineering Chemistry Research 46(2007)2445.

34. A. A. Konnova, J. N. Zhub, J. H. Bromlyb, and D. Zhangb, Proceedings of the Combustion Institute 30(2005)1093.

35. B. Grbic, N. Radic, and A. Terlecki-Baricevic, Applied Catalysis B: Environmental 50 (2004)161.

36. E. Joubert, X. Courtois, P. Marecot, and D. Duprez, Applied Catalysis B: Environmental 64(2006)103.

37. I. V. Yentekakis, V. Telloub, G. Botzolaki, and I. A. Rapakousios, Applied Catalysis B: Environmental 56(2005)229.

38. A. Kotsifa, D. I. Kondarides, and X. E. Verykios, Applied Catalysis B: Environmental 72(2007)136.

39. J. Hermia, and S. Vigneron, Catalysis Today 17(1993) 349.

40. S. K. Gangwal, M.E. Mullins, J. J. Spivey, P.R.Caffrey, and B. A. Tichenor, Applied Catalysis 36(1988)231.

41. P. Papaefthimiou, T. Ioannides, and X. Verykios, Applied Catalysis B: Environmental 13(1997)175.

42. M. J. Patterson, D. E. Angove, N. W. Cant, Applied Catalysis B: Environmental 26(2000)47.

43. S-C. Shen, and S. Kawi, Applied Catalysis B: Environmental 45(2003)63.

44. R. Burch, and D. Ottery, Applied Catalysis B: Environmental 9(1996)L19.

45. H. Hamada, Y. Kintaichi, M. Inaba, M. Tabata, T. Yoshinari, and H. Tsuchid, Catalysis Today 29(1996)53.

46. R. Burch, J. P. Breen, and F. C. Meunier, Applied Catalysis B: Environmental 39(2002)283.

47. D. T. Wickham and B. E. Koel, Journal of Catalysis 114(1988)207.

48. N. Macleod, and R. M. Lambert, Applied Catalysis B: Environmental 35(2002)269.

49. C. Yokoyama and M. Misono, Journal of Catalysis 150(1994)9.

50. R. Burch, P.J. Millmgton, and A. P. Walker, Applied Catalysis B: Environmental 4 (1994)65.

51. S. Naito, and M. Tanimoto, Chemistry Letters 22(1993)1935.

52. T. Tanaka, T. Okuhara, and M. Misono, Applied Catalysis B: Environmental 4(1994)L1.

53. A. Obuchi, A. Ogata, H. Takahashi, J. Oi, G.R. Bamwenda and K. Mizuno, Catalysis Today 29(1996)10.

54. A. Obuchi, A. Ohi, M. Nakamura, A. Ogata, K. Mizuno, and H. Ohuchi, Applied Catalysis B: Environmental 2(1993)71.

55. M. Sasaki, H. Hamada, Y.Kintaichi, and T. Ito, Catalysis Letters 15(1992)297.

56. G. R. Bamwenda, A. Obuchi, A. Ogata, and K. Mizuno, Chemistry Letters 23(1994)2109.

57. R. Burch and T.C. Watling, Catalysis Letters 37(1996)51.

58. L. Olsson, B. Westerberg, H. Persson, E. Fridell, M. Skoglundh, and B. Andersson, Journal of Physical Chemistry B 103(1999)10433.

59. W.S. Epling, L.E. Campbell, A. Yezerets, N.W. Currier and J.E. Parks, Catalysis Reviews 46(2004)163.

60. J. Després, M. Elsener, M. Koebel, O. Kröcher, B. Schnyder, and A. Wokaun, Applied Catalysis B: Environmental 50(2004)73.

61. L. Olsson, and E. Fridell, Journal of Catalysis 210(2002)340.

62. R. B. Getman, W. F. Schneider, A. D. Smeltz, W. N. Delgass, and F. H. Ribeiro, Physical Review Letters 102, 076101 (2009).

63. R. Burch, and D. Ottery, Applied Catalysis B: Environmental 13(1997)105.

64. I. Amon-Mézière, F. Castagna, M. Prigent, and A. Pentenero, SAE technical paper series 950932.

65. F. Diehl, J. Barbier Jr., D. Duprez, I. Guibard, and G. Mabilon, Applied Catalysis B: Environmental 95(2010)217.

66. D. H. Kim, M.C. Kung, A. Kozlova, S.D. Yuan, and H.H. Kung, Catalysis Letters 98(2004)11.

Chapter 4

Hydrogen generation and coke formation over a diesel oxidation catalyst under fuel rich conditions

4.1 Abstract

Hydrogen production via hydrocarbon steam reforming and water gas shift reactions was investigated over a monolith-supported Pt-based diesel oxidation catalyst. The evaluation included comparison between constantly rich gas composition conditions and cycling between rich gas conditions and an inert stream. Analysis was performed along the catalyst length at temperatures ranging from 200 to 500°C. During the constant inlet composition experiments, C_3H_6 steam reforming started at 375°C, while dodecane steam reforming began at 450°C, and resulted in less hydrogen produced. With a mixture of C_3H_6 and dodecane, hydrogen production originated solely from C_3H_6 steam reforming and, under otherwise identical conditions, was less than that observed with only C_3H_6, but higher than that with only dodecane. Hydrogen production from the water gas shift reaction was higher than that observed with hydrocarbon steam reforming, and started at 225°C. During cycling experiments, hydrogen production via hydrocarbon steam reforming was higher than that observed during the constant inlet composition experiments. This improvement was observed at all temperatures. Temperature programmed oxidation experiments performed after steam reforming indicate coke formed on the catalyst surface during steam reforming, and that the coke deposits were primarily toward the upstream portion of the catalyst. The data also show that the reason for better performance during cyclic operation is that less coke was deposited compared to that during non-cyclic experiments.

86

4.2 Introduction

Diesel oxidation catalysts (DOC) are used in a variety of lean-burn engine aftertreatment systems. They are typically installed upstream of selective catalytic reduction (SCR) and NO_X storage/reduction (NSR) catalysts. Their function in such systems is to oxidize engine-out NO to NO_2, as NO_2 is trapped more readily than NO on NSR catalysts [1-2] and a 1:1 $NO:NO_2$ ratio promotes the "fast" SCR reaction over SCR catalysts [3]. DOCs are also installed upstream of diesel particulate filters, again to oxidize NO to NO_2. NO_2 is more reactive towards soot than O_2, lowering the soot oxidation temperature by approximately 200°C [4]. Literature evidence shows that the temperature range in which DOCs operate overlaps the temperature range in which steam reforming reactions are possible. Both water and hydrocarbons are present in diesel exhaust, providing reforming reactant species. And since DOCs contain Pt and Pd supported on either alumina or zeolites, steam reforming reactions are likely, especially during the reductant-rich phase of a NSR cycle.

Hydrogen can be produced via numerous catalytic methods, including catalytic partial oxidation, autothermal reforming, or steam reforming of hydrocarbons, alcohols, and biomass [5-9]. Hydrocarbon steam reforming is typically the preferred process for industrial-scale hydrogen production, because it does not require oxygen, operates at relatively low temperature, and maintains a higher product H_2/CO ratio than that of autothermal reforming and catalytic partial oxidation [10]. The CO produced during steam reforming can also be used in the water gas shift (WGS) reaction to drive the production of extra hydrogen.

Several studies have shown that the metal type [11-13] as well as the support type can influence the extent of steam reforming. Alumina is a typical support in catalysts, but tends to induce coke formation during steam reforming due to its surface acidity [14], with coke formation a primary steam reforming deactivation process [15-16]. However, the presence of precious metals, zirconium, or other alkaline components in the catalyst formulation can minimize coke formation [17] or facilitate its removal [18]. Hydrocarbon steam reforming over Pd and Pt has been extensively investigated. Previous results relevant to the current study include C_3H_8 steam reforming over $Pd/CeO_2/Al_2O_3$ and Pt-$Rh/CeO_2/Al_2O_3$ catalysts [19-20], with the reaction starting at about 350°C. Steam reforming of C_3H_6 and isopropanol was also investigated over a powder $Pd–Cu/\gamma-Al_2O_3$ catalyst [21], with both reactions starting at 327°C and increasing steadily until complete conversion was attained, which under the conditions of the test, was at 527°C.

For NSR catalysts, hydrogen has repeatedly been reported to be better than other reductant species (CO and hydrocarbons) in reducing surface NO_X species to N_2 [22-26]. Therefore, if the amount of hydrogen can be increased via steam reforming or WGS in the upstream DOC during the regeneration phase, which is reductant-rich relative to oxygen, the NO_X conversion to N_2 over the downstream NSR catalyst could be improved. The main interest in this study, is comparing and quantifying the amount of hydrogen formed during steady-state and cyclic operation over a diesel oxidation catalyst. Coke formation and regeneration was also investigated after these experiments to explain the observed differences.

4.3 Experimental Methods

In this study, a commercial monolith diesel oxidation catalyst supplied by Umicore AG was used. The sample contains 95 g/ft^3 Pt supported on Al_2O_3. The monolith block that the sample was removed from had a cell density of 400 cpsi. The sample was 2.3 cm in diameter with a length of 6 cm. The sample was wrapped in 3M insulation material and placed into a horizontal quartz tube reactor, which was in turn placed inside a Lindberg Minimite temperature-controlled furnace. The matting was used to seal the gap between the catalyst and reactor wall. Two K-type thermocouples were placed at the radial centres of the catalyst; one at the inlet face and one at outlet edge of the catalyst. A third was placed ~ 2.5 cm upstream of the sample. During the experiments, the monolith remained nearly isothermal, with only ~2°C temperature differences observed between the inlet and outlet face.

All gases except balance N_2 were supplied by Praxair. The N_2 was produced using an On-Site nitrogen generator system. Bronkhorst mass flow controllers were used to meter gases to the reactor system. The dry gas mixture was then heated to > 120°C and water was then introduced using a Bronkhorst CEM system. In experiments that included dodecane or m-xylene, they were also metered with a Bronkhorst CEM system and introduced downstream of the water injection location, closer to the reactor, thereby eliminating any reactions with the steel tubing walls. Small quartz tubes, 3 mm OD and 2 mm ID, were placed in the front portion of the furnace and before the catalyst to help in heat transfer and limit fully developed flow.

In the constant gas composition steam reforming and WGS experiments, 5% H_2O, 0.27% hydrocarbon on a C1 basis or 0.27% CO and a balance of N_2 were used. In cycling

experiments, 60 s inert and 10 s reductant-containing phases were used (labeled rich below, matching that of an NSR cycle). In the inert phase, 5% H_2O and a balance of N_2 were used while in the rich phase, 5% H_2O, 0.27% CO or hydrocarbon on a C1 basis, and a balance of N_2 were used. In cycling experiments, the rich and inert gas mixtures were made in separate manifolds. A fourway, fast-acting solenoid valve was used to switch between the two. Experiments were also performed to investigate coke formation during cycling and non-cycling experiments. C_3H_6 steam reforming experiments were performed between 300 and 500°C, which typically took about 3 hours in total to complete, or at one temperature depending on the experiment. Upon completion of a steam reforming experiment, the reactor was cooled to 50°C in N_2 and then 10% O_2 was added to the feed and the reactor was ramped to 500°C at rate of 7°C/min. Catalyst regeneration from deposited coke by O_2, H_2O, H_2, and a mixture of H_2O and H_2 after C_3H_6 steam reforming experiments were evaluated, using the same TPO protocol, but substituting in the other regeneration species for the O_2.

Experiments were performed with a 25,000 h^{-1} space velocity at standard conditions. The gas compositions were measured using a MKS MultiGas 2030 FTIR analyzer. Spatially resolved capillary-inlet mass spectrometry (SpaciMS) was also used to measure H_2, H_2O and hydrocarbons along a radially-centred monolith channel. In these studies, He was added and used as a tracer for calibration purposes. To resolve the gas concentrations spatially, a silica capillary, connected to the sampling end of a capillary from a Hiden Analytical mass spectrometer, was placed within one of the radially-centred catalyst channels. The capillary dimensions were 0.3 mm I.D. and 0.43 mm O.D. Gases

were collected at different positions by moving the silica capillary tip to different positions within the channel.

4.4 Results and Discussion

4.4.1 H_2 generation during non-cyclic conditions

Hydrogen generation via steam reforming was investigated between 300 and 500°C. In the steam reforming experiments, C_3H_6, $C_{12}H_{26}$, m-C_8H_{10} and mixtures of these were selected to represent different hydrocarbon species in diesel exhaust. In this series of experiments, 5% H_2O, 0.27% hydrocarbon on a C1 basis, and a balance of N_2 were used. Also in these experiments, spatially resolved capillary-inlet mass spectrometry (SpaciMS) was used to quantify the amounts of the species and study their axial concentration distribution. In m-C_8H_{10} steam reforming experiments, no hydrogen was detected in the outlet stream at temperatures as high as 500°C and therefore data associated with m- C_8H_{10} are not shown.

Figure 4.1 shows the amount of hydrogen formed at different catalyst positions during the C_3H_6 steam reforming experiments. Note, the position labeled zero is just inside the inlet face of the catalyst (really about 1 mm). C_3H_6 steam reforming began at 375°C, though to a very small extent. As the temperature was increased stepwise to 500°C, hydrogen formation monotonically increased. It is also clear from Figure 4.1 that hydrogen production increased as a function of catalyst length. In a recent study [27], C_3H_6 steam reforming was investigated over a model Pt/BaO/Al$_2$O$_3$ NSR catalyst. Hydrogen formation started at a similar temperature (375°C), but to a higher extent than that observed in this study due to the presence of Ba. Alkaline materials are known to

suppress the acidity of the alumina support [28] and thus to reduce coke formation, which leads to higher hydrogen formation.

Figure 4.1 H_2 concentrations obtained at different temperatures and lengths of the catalyst during steam reforming experiments. The inlet gas composition was 900 ppm C_3H_6, 5% H_2O, and balance N_2.

Hydrogen generation via dodecane steam reforming was also investigated and the outlet hydrogen concentration data are shown in Figure 4.2. Below 450°C, no steam reforming occurred and beyond that hydrogen production was observed, starting at a higher temperature than that observed with C_3H_6, and increased at 475 and 500°C. Also, the amount of hydrogen formed at 500°C with dodecane was 10, 100, and 209 ppm at 0, 3, and 6 cm from the catalyst face, respectively, whereas the amount of H_2 formed with

C_3H_6 at the same temperatures and locations were 15, 210, and 488 ppm, or about 2 times more by the outlet with C_3H_6. These results demonstrate that the extent of steam reforming over a diesel oxidation catalyst depends on the type of hydrocarbon used. In previous studies [13, 29-32], alkane steam reforming was investigated over Pt, Pd, Rh, Ru, and Pt/Rh catalysts. According to these studies, alkane steam reforming occurs at higher temperatures than those observed with alkenes, consistent with our data, although different hydrocarbon chain lengths were used in the present study.

Figure 4.2   Outlet H_2 concentrations obtained at different temperatures and with different hydrocarbon feed mixtures during steam reforming experiments. The inlet gas composition was 900 ppm C_3H_6, 225 ppm $C_{12}H_{26}$, or 900 ppm C_3H_6 and 225 ppm $C_{12}H_{26}$, 5% H_2O, and balance N_2.

Similar experiments were also carried out with a mixture of C_3H_6 and dodecane. The quantified outlet hydrogen amounts are shown in Figure 4.2. During these experiments, no change in the dodecane amount was observed, indicating that dodecane steam reforming did not occur. The C_3H_6 amount monotonically decreased as a function of temperature and catalyst length (data not shown); consequently, the hydrogen measured during these experiments originated exclusively from C_3H_6 steam reforming. It should be noted that hydrogen production started at 400°C, slightly higher than that observed with only C_3H_6 (375°C). This decreased hydrogen production in the presence vs. absence of dodecane was observed at all temperatures tested. For example, at 500°C and in the absence of dodecane, the outlet hydrogen measured was 488 ppm while in the presence of dodecane it was 285 ppm. These results demonstrate that there was mutual inhibition between C_3H_6 and dodecane, resulting in lower hydrogen production. Maillet et al. [34] investigated hydrocarbon steam reforming over Rh, Pt and Pd supported on Al_2O_3 catalysts. The authors divided the steam reforming process into three main steps. The first step involves dissociative adsorption of the hydrocarbon on the metal sites, the second includes dissociative adsorption of water on the support, and finally, OH groups from the support migrate to the metal particles to react with a CHx fragment originating from the dissociative adsorption to yield CO_2 and H_2. This mechanism explains the mutual inhibition between dodecane and propylene observed. C_3H_6 adsorbs strongly on the Pt sites, relative to dodecane, possibly dissociating to a CHx fragment and blocking access of dodecane to the Pt. Adsorption on the support is less selective, and some of the dodecane adsorbs on the catalyst support, which in turn inhibits water dissociation, or inhibits migration of OH groups to the metal site, ultimately inhibiting the reaction

between OH groups and the CHx fragment. TPD of adsorbed dodecane (data not shown) further supports that dodecane is adsorbed on the catalyst surface, as it was observed desorbing up to ~400°C.

Hydrogen production via the water gas shift (WGS) reaction was also investigated, between 200 and 500°C. In this series of experiments, 5% H_2O, 2700 ppm CO, and a balance of N_2 were used. The results are shown in Figure 4.3, along with equilibrium H_2 concentrations for the conditions tested. It is clear that the WGS reaction started at a lower temperature (~225°C) than steam reforming for the hydrocarbons tested. SpaciMS data show that hydrogen concentrations increased as a function of catalyst length and temperature, although the rate of increase slowed at higher temperature with the approach to equilibrium. The amount of hydrogen formed by the outler via the WGS reaction at 500°C was 3.5 times higher than that observed with C_3H_6 steam reforming and 6 times higher than that observed with dodecane steam reforming. In the WGS reaction, for every mole of CO reacted, 1 mole of hydrogen will form and therefore at 500°C approximately 60% of the CO was consumed in the formation of hydrogen. No methanation was observed, and CO conversion was only associated with H_2 and CO_2 production. This finding is in contrast to previous studies [35, 36], where methane formation started at temperatures > 375°C with a Pt/CeO_2 catalyst during WGS experiments. However, methanation depends on numerous factors such as inlet gas composition, metal loading, and the inclusion of promoters such as alkali and cerium oxide components. In the previous studies [35,36], significantly larger amounts of both CO and H_2O were used in the feed mixtures (e.g. 11.4% CO and 45.7% H_2O) coincident with including H_2, while in this study CO and H_2O concentrations were 0.27% and 10%,

respectively, with no H_2 added. Furthermore, in the present study the catalyst does not contain cerium oxides or other promoters while in the previous studies, the catalyst included cerium oxide, and as stated by the authors, this would provide extra adsorption sites for water rather than CO blocking all surface sites. Therefore, using an excess amount of CO and H_2O with a catalyst containing cerium oxide would lead to high C/H ratios at the catalyst surface, driving the reactions toward methanation.
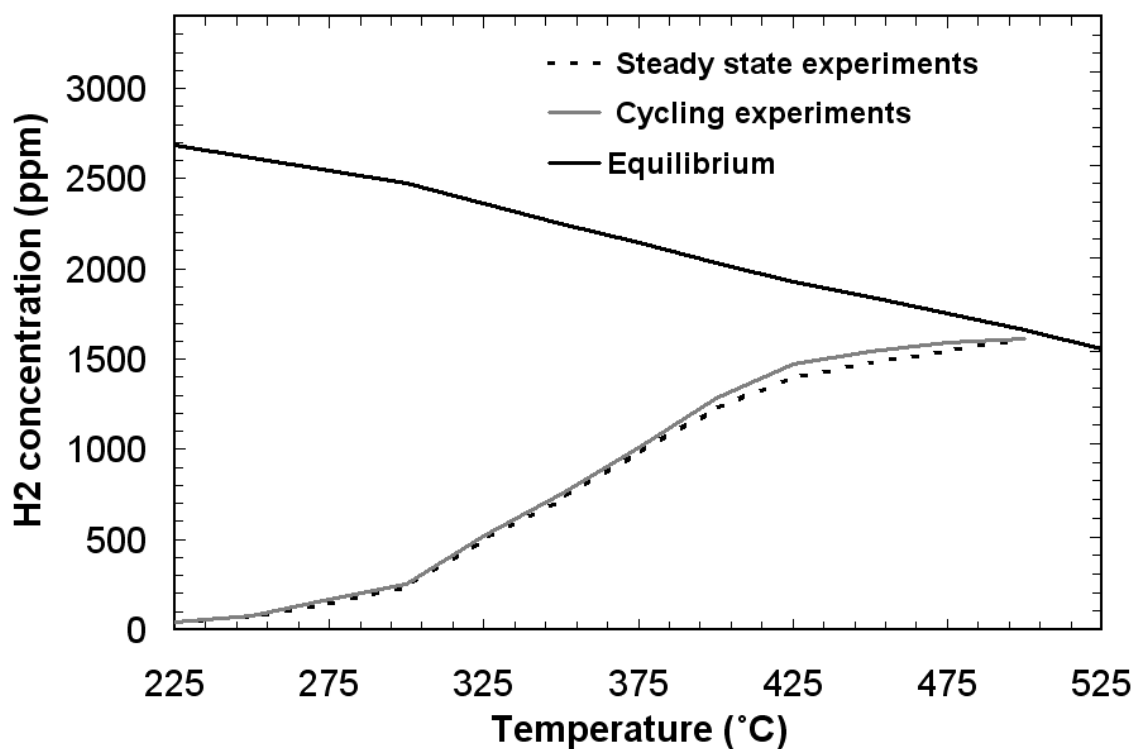
Figure 4.3 Outlet H_2 concentrations obtained at different temperatures during non-cycling and cycling water gas shift reactions experiments. The inlet gas composition was 2700 ppm CO, 5% H_2O, and balance N_2.

4.4.2 H$_2$ generation during cycling conditions

Hydrogen production via the steam reforming and WGS reactions during cycling experiments was also investigated at different temperatures. Steam reforming is typically carried out under steady-state inlet conditions, however, for diesel aftertreatment NSR applications, the feed is cycled between those of normal engine exhaust and those of the rich phase, where significant steam reforming is possible. In the "inert" phase, which lasted 60 seconds, 5% H$_2$O and a balance of N$_2$ were used, while in the rich phase, which lasted 10 seconds, 5% H$_2$O, 0.27% CO or hydrocarbon on a C1 basis, and a balance of N$_2$ were used. An inert phase rather than a true lean phase was used to better understand the phenomena occurring along the catalyst during the rich phase. In both steam reforming and WGS experiments, SPACiMS was used to quantify gas-phase concentrations and study their axial distribution at three different catalyst positions. In the plotted data, the front position is at the inlet of the sample (~1mm in).

Propylene steam reforming during cycling was performed between 300 and 500°C. The measured amounts of hydrogen produced are shown in Figure 4.4. C$_3$H$_6$ steam reforming again started at 375°C, the same as that for the non-cyclic experiments. The hydrogen formed increased as a function of catalyst length and temperature. Two primary differences were observed in these experiments when compared with non-cyclic C$_3$H$_6$ steam reforming. The first is that a significantly higher amount of hydrogen formed at the front of the catalyst during cycling compared with non-cyclic experiments, where the maximum amounts of hydrogen with all temperatures tested did not exceed 15 ppm. For example, at 500°C, the hydrogen production at the front of catalyst during cycling experiment was ~10 times higher than that observed under steady inlet conditions.

97

Another observation is that the amounts of hydrogen formed at the middle and outlet positions in the catalyst during cylcing were also higher, but to a lesser extent, being about 2 times higher than that observed during steady-state experiments. These differences are likely due to more coke being deposited along the catalyst during non-cyclic tests, especially at the upstream portion, which will be discussed in the following section.
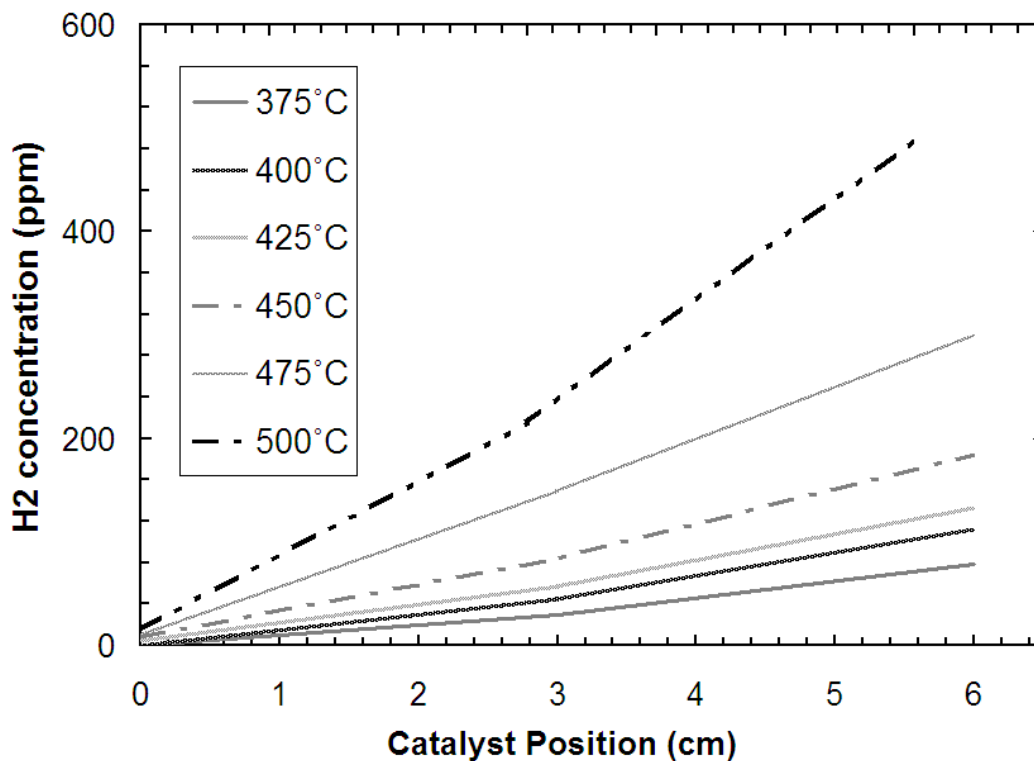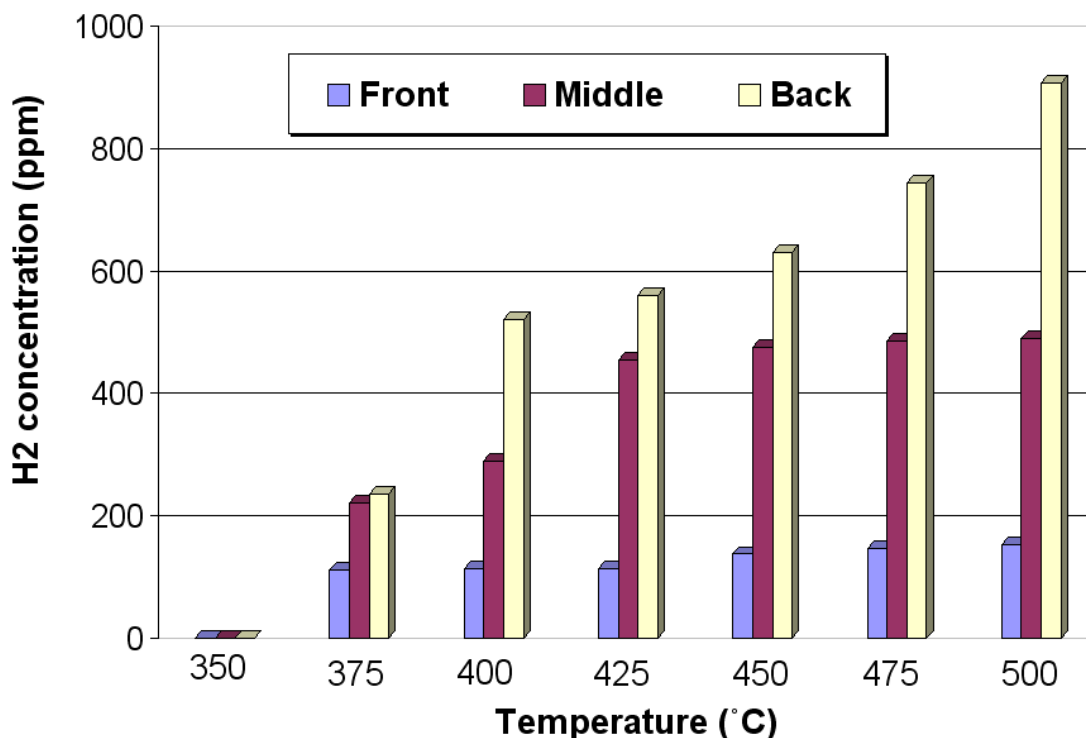

Figure 4.4 H_2 concentrations obtained at different temperatures and lengths of the catalyst during cycling steam reforming experiments. The inert phase gas composition was 5% H_2O and balance N_2. The rich phase gas composition was 900 ppm C_3H_6, 5% H_2O, and balance N_2. The inert phase was 60 sec and the rich phase was 10 sec. The front position represents the inlet of sample (~1mm in).

Similar experiments were carried out, but with dodecane, and the H_2 generation results shown in Figure 4.5. Again, dodecane steam reforming started at 450°C and the hydrogen amount progressively increased with catalyst length. Although there were differences in the amounts of hydrogen formed during cycling and non-cycling experiments, they were not as significant as those observed with C_3H_6. For example, at 500°C, the hydrogen formed in the middle and outlet of the catalyst was 100 ppm and 210 ppm during non-cycling experiments, while 130 and 300 ppm were formed during cycling experiments. Again, however, more significant differences were observed at the front of the catalyst, where again the hydrogen amount was higher with cycling experiments. The smaller differences between dodecane cycling and non-cycling steam reforming experiments compared with those observed with C_3H_6 is related to the hydrocarbons type, where C_3H_6 is activated faster and more easily than dodecane, and therefore steam reforming and associated coke formation occur at lower temperatures. The positive effect of cycling is less evident for dodecane due to the higher temperatures required for the onset of reaction, and at these higher temperatures, as will be shown below, coke can be reacted from the surface.

Hydrogen production with a mixture of C_3H_6 and dodecane was also investigated and the quantified amounts of hydrogen are shown in Figure 4.5. The conditions are otherwise similar to those experiments with either C_3H_6 or dodecane. Again, no change in the dodecane amount was observed while the C_3H_6 concentration steadily decreased along the length and with increasing temperature. This indicates that the hydrogen formed was again solely due to C_3H_6 steam reforming. The hydrogen amounts formed were also again lower than those observed in the absence of dodecane.
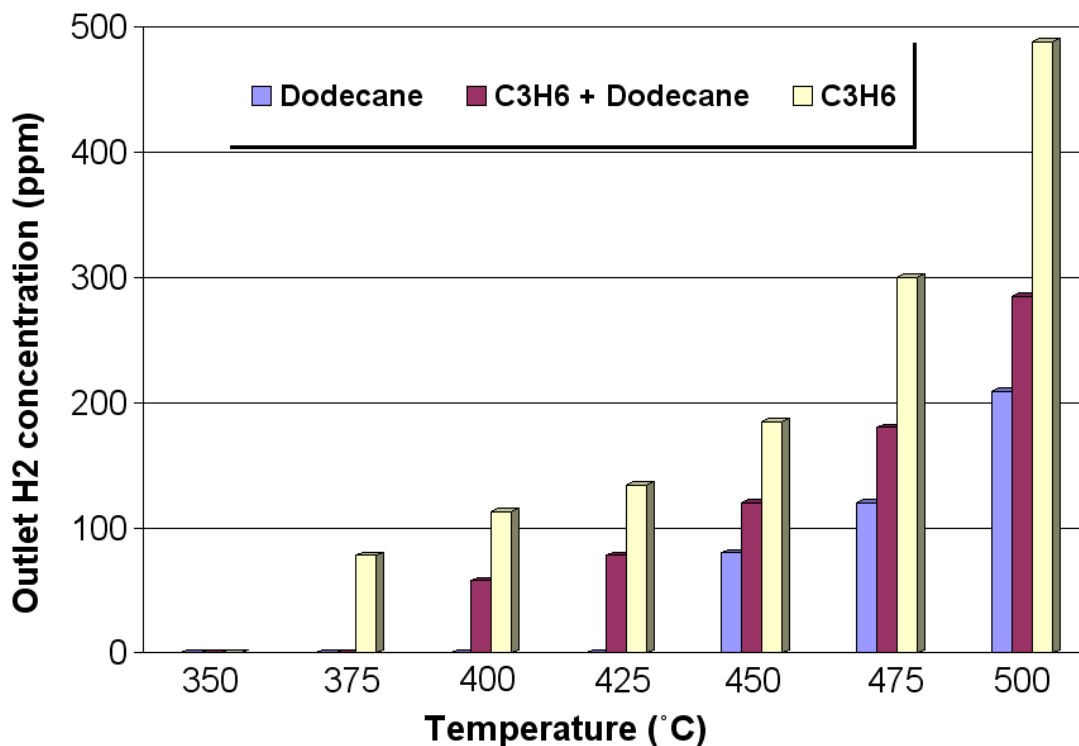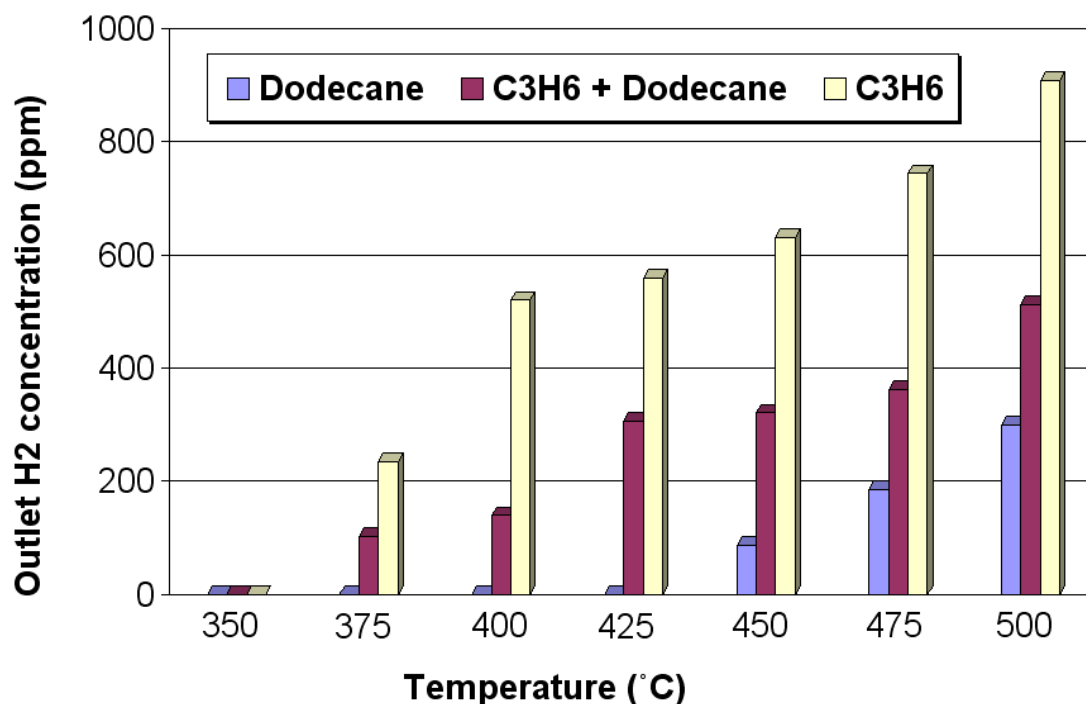
Figure 4.5 Outlet H_2 concentrations obtained at different temperatures and with different hydrocarbon feed mixtures during cycling steam reforming experiments. The inert phase gas composition was 5% H_2O and balance N_2. The rich phase gas composition was 900 ppm C_3H_6, 225 ppm $C_{12}H_{26}$, or 900 ppm C_3H_6 and 225 ppm $C_{12}H_{26}$, 5% H_2O, and balance N_2. The inert phase was 60 sec and the rich phase was 10 sec.

The reason as stated earlier is because of the mutual inhibition between C_3H_6 and dodecane. It should also be pointed out that hydrogen production was observed at 375°C, which is 25°C lower than those observed during non-cyclic experiments (Figure 4.2). This suggests that dodecane inhibition was mitigated by the cycling conditions, likely by desorption from the surface during the inert phase. Additionally, the amount of hydrogen formed during cycling experiments was about twice the amount formed during non-

100

cycling experiments. The lower coke build-up on the catalyst during the 10 s rich phase of the cycle followed by the inert phase, as will be shown in the next section, explains the higher hydrogen production and lower temperature during cycling.

The extent of hydrogen formed via the WGS reaction during cycling was also investigated at different temperatures and different catalyst positions. The hydrogen formed during the 10 sec rich phase was measured and the results are shown in Figure 4.3. Again, hydrogen production started at 225°C and the hydrogen amount increased as a function of catalyst position and temperature. In previous studies [37, 38], the WGS reaction was investigated during cyclic operation over a commercial NSR catalyst. The extent of the WGS reaction was 10% at 200°C and 81% at 500°C, which is higher than those observed in this study. The higher WGS reaction extent in the previous studies is due to the presence of excess O_2 (10%) in the lean phase, thereby removing any residual CO adsorbed during the previous rich phase, and the presence of Ce and alkali and/or alkaline earth elements (e.g Ba), which are known to enhance the WGS reaction [39-41] and suppress coke formation [31, 32]. During cycling experiments with the DOC in this study, the trends were relatively similar to those observed during the non-cycling WGS experiments, except at the front of catalyst, where a higher amount of hydrogen was observed with cycling. Compared with hydrocarbon steam reforming during cycling, the hydrogen formed during cycling for the WGS reaction was still higher along all catalyst positions and all temperatures. Takahashi et al. [42] studied C_3H_6 steam reforming and WGS reactions over a NSR catalyst between 200 and 400°C under cycling conditions. They also showed that the amount of H_2 formed during the WGS reaction was higher than that formed during C_3H_6 steam reforming, consistent with our data. But, it should be

mentioned that the amount of H_2 formed via the C_3H_6 steam reforming and WGS reactions was higher than those observed in our experiments and attained at lower temperatures. In Takahashi's study, 7% O_2 was used in the lean phase and the catalyst contained alkali and alkaline earth elements (Ba and K) and ceria-zirconia-based oxygen storage components. Therefore, during the rich pulse, the stored or residual oxygen would lead to combustion of some CO and C_3H_6, possibly resulting in a temperature increase within the catalyst bed. Thus, the measured temperatures for hydrogen production in the previous study would be lower than those observed in our study and hence might explain the observed differences. Another contributing factor is that the O_2 in the lean phase removes coke deposited during the previous rich phase, or adsorbed CO, which should not affect the reaction onset temperature, but will the amounts of H_2 or conversions observed.

4.4.3 Coke formation during steady-state and cycling experiments

As discussed above, there were no significant differences in outlet hydrogen formed for the WGS reaction between cycling and non-cycling conditions. However, hydrogen generation was higher during steam reforming under cycling conditions compared to that observed under constant inlet feed steam reforming conditions. To determine if coke formation is the reason for this latter difference, coke formation during steam reforming experiments was investigated. Ethylene was observed during catalyst outlet measurements, and since ethylene is considered a coke precursor during steam reforming, coke formation is likely. And although coke formation is a product of complete hydrocarbon decomposition, CO is the standard reforming product, and at the reforming temperatures, CO is not considered a catalyst poison, while coke deposition

does lead to deactivation because it reduces the effective surface area [43]. It is likely that the amount of coke deposited on the catalyst during non-cyclic steam reforming experiments was ultimately higher than that during the cycling steam reforming experiments. Further evidence includes the time-resolved H_2 concentration profiles, with an example shown in Figure 4.6, where the H_2 measured by mass spectrometry dropped over time during the non-cyclic C_3H_6 steam reforming experiment. C_3H_6 steam reforming was selected for these tests.
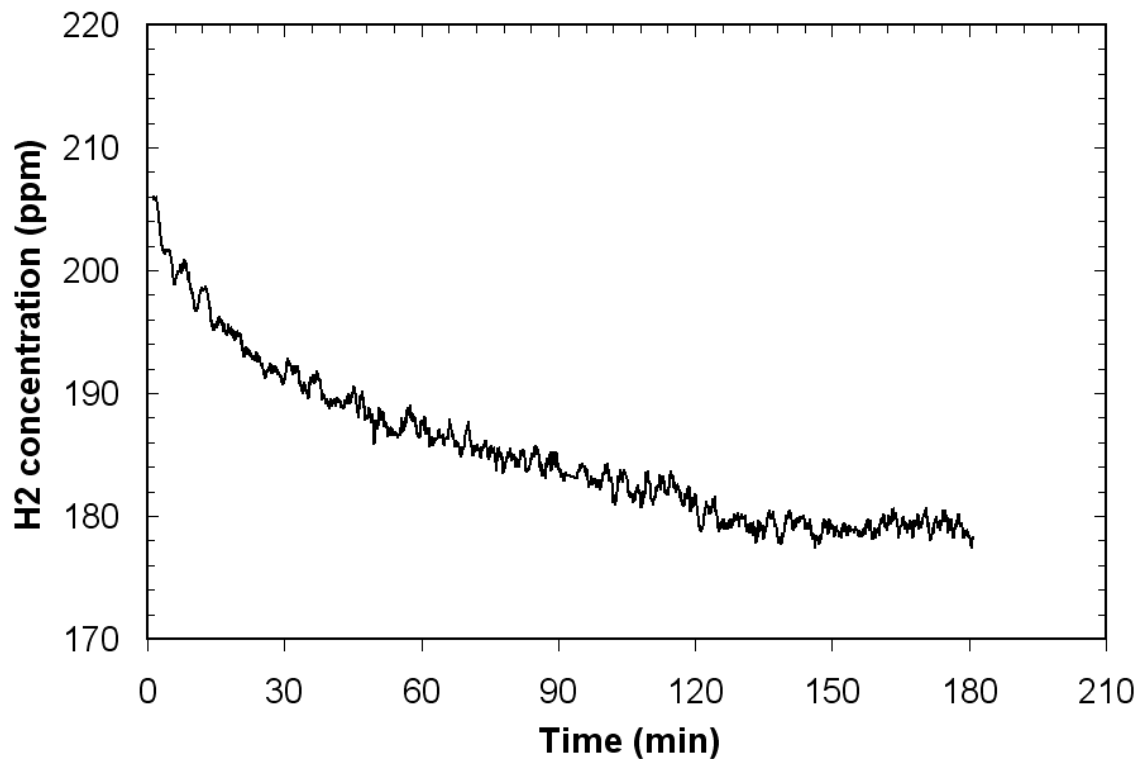
Figure 4.6 Outlet H_2 concentrations obtained during C_3H_6 steam reforming experiments at 450°C. The inlet gas composition was 900 ppm C_3H_6, 5% H_2O, and balance N_2.

In the first set of experiments, non-cyclic C_3H_6 steam reforming experiments were performed between 300 and 500°C under conditions identical to those in Figure 4.1. Upon completion of the steam reforming experiments at 500°C, the reactor was cooled to 50°C in N_2 and then 10% O_2 was added to the inlet gas feed and the reactor was ramped to 500°C at 7°C/min. The capillary for SpaciMS readings was placed at two locations; 2 and 4 cm from the inlet face, to investigate the amount of coke deposited during the test (two experiments were performed, with measurements taken at 2 cm during the first and 4 cm during the second). The amount of evolved CO_2 during these TPO experiments was measured and the results are shown in Figure 4.7; no CO was observed. The amounts of C deposited on the catalyst were quantified based on the CO_2 evolved and were 394 and 395 μmoles upstream of 2 and 4 cm, respectively. As shown, oxygen begins to remove the coke from the catalyst as low as 190°C. Coke removal reached a maximum at 230°C and coke was completely removed by 250°C. Such data suggest that during normal NSR cycling, less inhibition would be observed, at least above 230°C, from coke build-up because O_2 will be available during the lean phase to remove any built-up coke from the previous rich phase of the cycle.

The data shown in Figure 4.7 also show that the amount of formed CO_2 is quite similar at the 2 and 4 cm positions, indicating that the deposited coke was only in the front 2 cm of the catalyst. Based on the data shown in Figure 4.1, reaction is still occurring downstream, and is a combination of steam reforming and WGS, with the WGS originating from CO formed during steam reforming. The constantly higher hydrocarbon concentrations at the front of the catalyst lead to larger coke deposits there, and a drop in formation down the length as the hydrocarbon is consumed.

104
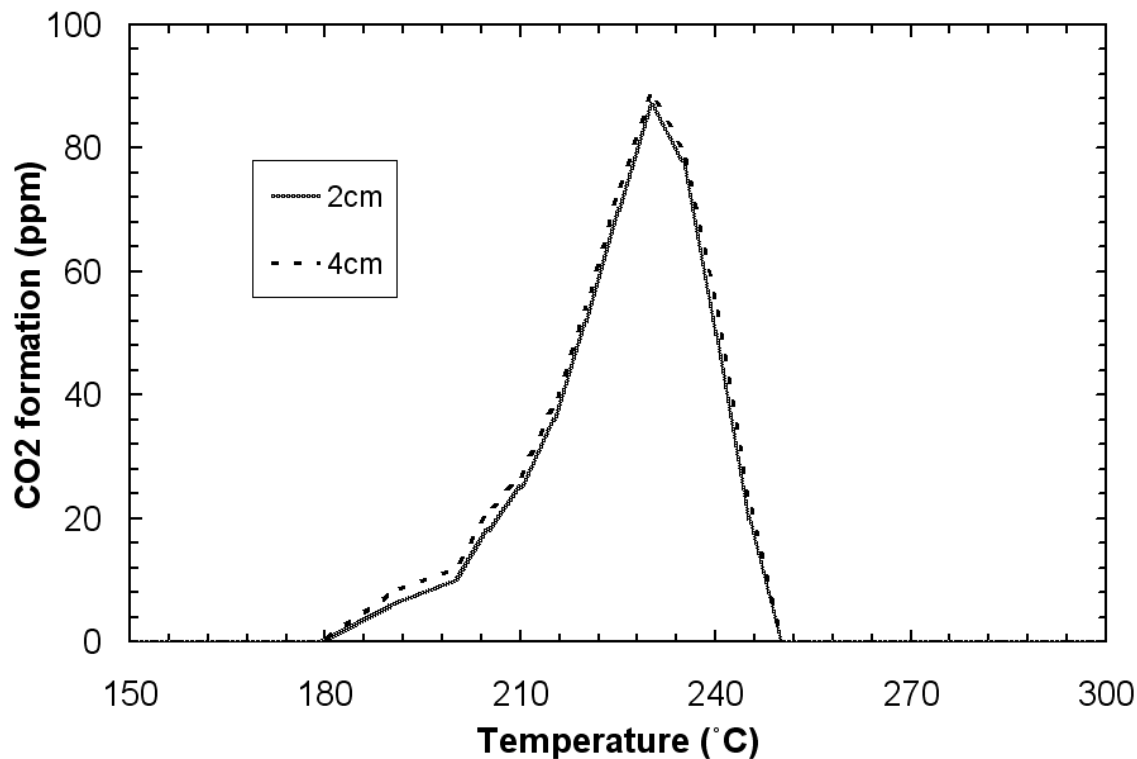
Figure 4.7 CO_2 formation obtained during temperature programmed oxidation experiments at 2 and 4 cm from the front of the catalyst. After C_3H_6 steam reforming experiments, the reactor was cooled down to 50°C with only N_2 and then 10% O_2 was added to feed and the reactor was ramped to 500°C at rate of 7°C/min.

Furthermore, hydrogen is known to suppress coke formation during steam reforming [44], and thus the product hydrogen leads to decreasing amounts of coke observed down the length of catalyst. With the test ending at 500°C, these effects are even more pronounced due to the higher reaction rates and therefore more reaction at the inlet.

To isolate the effect of the temperature and further investigate coke deposition along the catalyst length, non-cyclic C_3H_6 steam reforming experiments were performed

at 450°C and for different reaction times; 4, 60 and 180 min. The reactor was subsequently cooled to 50°C in N_2, 10% O_2 was then added, and the reactor was ramped to 500°C at 7°C/min. The capillary for SpaciMS was placed at 4 cm from the catalyst front. As expected, coke formation increased as the reaction time increased. These results indicate that coke deposition builds as a function of reaction time, at least to 180 min, which is consistent with the data shown in Figure 4.6. The formed CO_2 during TPO was measured to quantify the amount of C on the catalyst surface. The amounts of C deposited on catalyst surface were 269, 422, and 887 µmoles at 4, 60 and 180 min, respectively. CO_2 measurements during TPO after non-cyclic C_3H_6 steam reforming experiments performed at 450°C for 180 minutes were obtained at two different locations; 2 and 4 cm. The amounts of C deposited on catalyst surface were 354 and 887 µmoles at 2 and 4 cm, respectively. The amount of coke at 4 cm was almost 2.5 times that at 2 cm. Due to the integral nature of the monolith, coke will be deposited first at the front of the catalyst and further verifies that coke deposition was spread along the catalyst length with this longer reaction time.

Similar experiments were also performed after the cycling C_3H_6 steam reforming experiments, run at 375°C and under conditions otherwise identical to those described for Figure 4.4. During cycling experiments, no CO_2 was observed evolving during the inert phase, up to ~500°C. After the cycling experiment, the reactor was cooled to 50°C and then ramped at 7°C/min to 500°C with 10% O_2 and balance N_2. The capillary was placed at three different locations (thus steam reforming was repeated at 375°C three times); 1, 2, and 4 cm from the catalyst front. The detected CO_2 during TPO was measured and the results are shown in Figure 4.8.

106
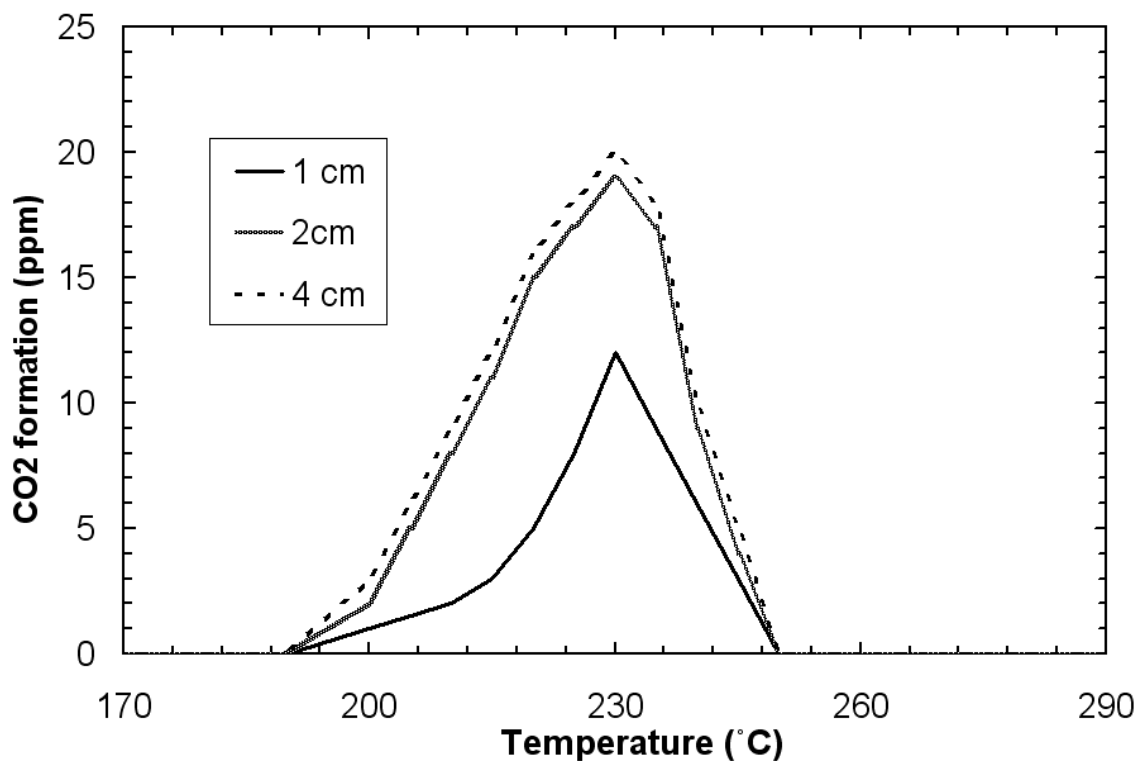
Figure 4.8 CO_2 formation obtained during a temperature programmed oxidation experiments at 1, 2 and 4 cm from the front of catalyst. After cycling C_3H_6 steam reforming experiments at 375°C, the reactor was cooled down to 50°C with only N_2 and then 10% O_2 was added to the feed and the reactor was ramped to 500°C at rate of 7°C/min.

At 1 cm, the maximum amount of CO_2 measured was about 12 ppm whereas 19 and 20 ppm were detected at 2 and 4 cm, and the amounts of C deposited on the catalyst surface were 31, 91 and 102 μmoles at 1, 2 and 4 cm, respectively. Again, these data demonstrate that coke deposition occurred more at the front portion with small reaction times, here over the front 2 cm of the catalyst during the 10 sec of C_3H_6 steam reforming. Coke deposition was also primarily observed in the front 2 cm with longer times in the

non-cyclic runs mentioned above, but in those experiments the temperature was higher, resulting in increased rates at the front as well. For the sake of a more direct comparison, cycling and non-cycling C_3H_6 steam reforming experiments were performed at 400ºC. The non-cyclic experiment was held for 50 min, and three 10 sec rich cycles for the cycling experiment. This admittedly leads to significantly less exposure during the cycling experiments, but based on the TPO data presented above, any built-up coke could be oxidized at these temperatures in any case. The reactor was cooled to 50°C and then ramped at 7°C/min to 500°C with 10% O_2 and balance N_2. The capillary was placed 4 cm from the catalyst front. The C amount was measured during TPO after 50 min was 385 µmoles, while 137 µmoles was measured after the 10 sec cycling experiment. It is apparent that significantly less total carbon was deposited during the briefer cycling experiments, although definitely non-linear with respect to time, which ultimately leads to the increased H_2 production observed.

4.4.4 Regenerating the catalyst from deposited coke

Numerous regeneration methods have been proposed in the literature to remove coke deposited on catalysts. Oxygen, H_2O, CO_2, and H_2 are the most commonly used gases for removing coke [45]. In this study, catalyst regeneration from deposited coke by O_2, H_2O, H_2, and a mixture of H_2O and H_2 was investigated after non-cyclic C_3H_6 steam reforming experiments. Although the TPO data show coke removal at relatively low temperatures, it is necessary to determine if the other gas components play a critical role in coke removal as well, in order to understand and model such phenomena. The steam reforming conditions prior to the regeneration tests are similar to those described in

108

Figure 4.1. In all of these experiments, the mass spectrometer capillary was placed at 4 cm from the catalyst front. In one experiment, C_3H_6 steam reforming was performed during a temperature programmed ramp from 300 to 490°C at a rate of 1°C/min. Subsequently, the reactor was cooled in N_2 to 50°C. The reactor was then ramped up at a rate of 7°C/min to 525°C with a feed containing 5% H_2O and the balance N_2. The CO_2 measured during the ramp is shown in Figure 4.9.
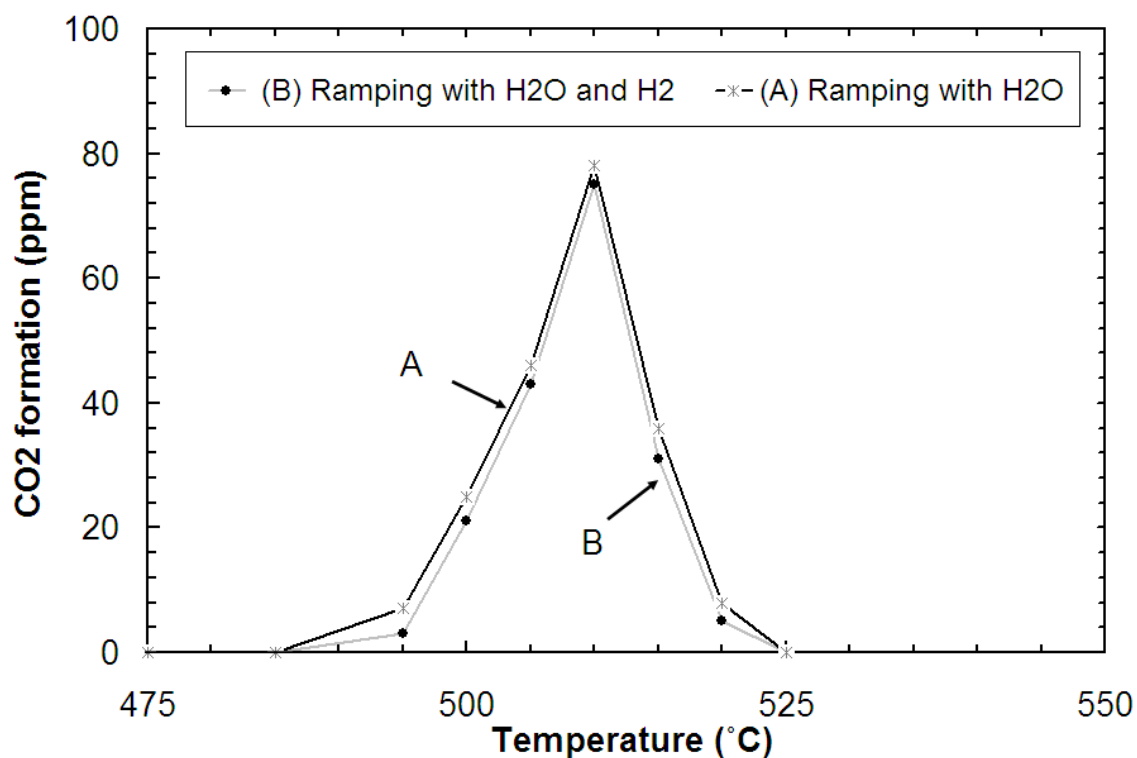
Figure 4.9 CO_2 formation data obtained during temperature programmed reduction experiments at 4 cm from the front of catalyst. After non-cyclic C_3H_6 steam reforming experiments during a temperature programmed ramp from 300 to 490°C at 1°C/min, the reactor was cooled down to 50°C with only N_2 and then (A) 5% H_2O was added to the feed, or (B) 1000 ppm H_2 and 5% H_2O were added to feed, and the reactor was ramped to 525°C at a rate of 7°C/min.

Water began to remove coke at 495°C and the catalyst was completely "cleaned" at 525°C. Similar experiments were also performed, but the regeneration mixture during the temperature ramp portion of the experiment contained 1000 ppm H_2 and 5% H_2O (a H_2 value similar to those observed during steam reforming experiments). No CH_4 or CO was detected in the product stream. The CO_2 was observed at the same temperature when regenerating with only H_2O, as shown in Figure 4.9. This indicates the 1000 ppm of H_2 had little, if any, impact on regeneration although it suppresses coke formation [44]. Further experiments were also carried out to investigate the ability of just H_2 to remove coke.

C_3H_6 steam reforming was carried out at 400°C, to eliminate the effect of H_2O on coke removal, since H_2O begins to react with the coke at ~495°C as was shown in Figure 4.9. C_3H_6 was turned off after 50 min of steam reforming and then 500 ppm of H_2 was introduced for 20 min. If the H_2 was able to remove the deposited coke, CH_4 should be detected in the outlet stream via the following reaction: $C + 2H_2 \rightarrow CH_4$. However, no CH_4 was observed in the outlet stream. One possible reason is that the formed CH_4 could be reformed in the presence of H_2O to H_2 and CO or CO_2 via the following reactions:

$$CH_4 + H_2O \rightarrow CO + 3H_2;$$
$$CH_4 + 2H_2O \rightarrow CO_2 + 4H_2.$$
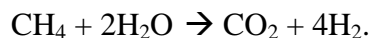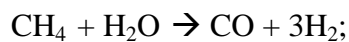
But, neither CO nor CO_2 was observed in the outlet stream, indicating that CH_4 steam reforming also did not occur. To verify that the coke was not removed from the catalyst, the reactor was cooled to 50°C in N_2, 10% O_2 was then added, and the reactor was ramped to 500°C at 7°C/min. CO_2 was detected in the outlet stream (data not shown),

peaking at 75 ppm at about 225°C, indicating that the H_2 did not clean the catalyst from deposited coke in the presence of H_2O. As further evidence for the lack of H_2 reaction with surface coke, a TPR experiment was performed after C_3H_6 steam reforming during a temperature ramp from 300 to 480°C. The reactor was cooled afterwards in N_2 to 50°C and then ramped at 7°C/min to 525°C with a feed containing 1000 ppm H_2 and a balance N_2. No CH_4, CO, or CO_2 were detected in the outlet stream, again indicating that H_2 did not remove the deposited coke from the catalyst. The reactor was subsequently cooled in N_2 to 50°C and then 10% O_2 was introduced and the reactor was ramped to 500°C at 7°C/min. Again, CO_2 was detected in the outlet stream. Overall, these data demonstrate that H_2 does not react with deposited coke on this DOC at temperatures as high as 525°C. H_2 could be able to regenerate the catalyst at T > 525°C, but this was not investigated to avoid catalyst aging. Furthermore, these data support previous conclusions regarding the effect of H_2 in suppressing coke formation, such that as H_2 is produced via steam reforming, less coke forms, consistent with the observed axial gradient in surface C along the length of catalyst.

4.5 Conclusions

Hydrocarbon steam reforming and water gas shift reactions were investigated as a function of catalyst length and temperature over a monolith supported diesel oxidation catalyst. Hydrogen production was measured during both cycling and non-cycling (constant steam reforming and water gas shift reaction conditions) experiments using spatially resolved capillary-inlet mass spectrometry (SpaciMS). The data demonstrate that hydrogen production with C_3H_6 steam reforming started at 375°C, while dodecane steam reforming occurred at 450°C and with less hydrogen produced. When C_3H_6 and

dodecane were present together, mutual inhibition was observed and the hydrogen formed only originated from C_3H_6 steam reforming. The amount of hydrogen formed via the WGS reaction was higher, and started at a lower temperature (~225°C) than that observed with hydrocarbon steam reforming. The amount of hydrogen formed during cycling hydrocarbon steam reforming experiments was consistently higher than that obtained from the non-cycling experiments. Coke deposition was investigated during both types of experiments and the results show that higher amounts of coke were deposited during the non-cycling experiments, compared to cycling experiments, providing the reason for the observed differences in hydrogen formed. Coke deposition was found to start at the front of the catalyst and spread downstream as the reaction time increased.

4.6 Acknowledgments

References

1. W. S. Epling, L. E. Campbell, A. Yezerets, N. W. Currier and J. E. Parks, Catalysis Reviews 46(2004)163.

2. M. AL-Harbi and W. S. Epling, Catalysis Today 130(2009)121.

3. A. Grossale, I. Nova, E. Tronconi, D. Chatterjee and M. Weibel, Journal of Catalysis 256(2008)312.

4. S. A. Setiabudi, M. Makkee and J. A. Moulijn, Applied Catalysis B: Environmental 50(2004)185.

5. J. Wei and E. Iglesia, Journal of Physical Chemistry B 188(2004)4094.

6. R. M. Navarro, M. C. Alvarez-Galvan, M. C. Sanchez-Sanchez, F. Rosa and J .L. G. Fierro, Applied Catalysis B: Environmental 55(2004)223.

7. R. M. Navarro, M. A. Peňa and J. L.G. Fierro,Chemical Reviews 107(2007)3952.

8. S.M. de Lima, I.O. da Cruz, G. Jacobs, B.H. Davis, L.V. Mattos and F.B. Noronha, Journal of Catalysis 257(2008)356.

9. H. F. Abbas, and W. M Daud, International Journal of Hydrogen Energy 35(2010)1160.

10. J. D. Holladay, J. Hu, D. L. King and Y. Wang, Catalysis Today 139(2009)244.

11. J. R. Rostrup-Nielsen, Journal of Catalysis 31(1973)173.

12. J. R. Rostrup-Nielsen and I. Alstrup, Catalysis Today 53(1999)311.

13. G. Kolb, R. Zapf, V. Hessel and H. Löwe, Applied Catalysis A: General 277(2004)155.

14. M. C. Sanchez-Sanchez, R. M. N. Yerga, D. I. Kondarides, X. E. Verykios and J. L. G. Fierro, Journal of Physical Chemistry A 114(2010)3873.

15. C. H. Bartholomew, Applied Catalysis A: General 212(2001)17.

16. D. L. Trimm and Z. Ilsen Önsan, Catalysis Reviews 43(2001)31.

17. R. H. Ross, M. W. Roberts and J. M. Thomas, Chemical Society, London, 4(1974)34.

18. T. Montini, L. De Rogatis, V. Gombac, P. Fornasiero and M. Graziani, Applied Catalysis B: Environmental 71(2007)125.

19. W. Faria, L. C. Dieguez and M. Schmal, Applied Catalysis B: Environmental 85(2008)77.

20. J. Barbier and D. Duprez, Applied Catalysis A: General 85(1992)89.

21. C. Resini, L. Arrighi, M. Delgado, M. Vargas, L. J. Alemany, P. Riani, S. Berardinelli, R. Marazza and G. Busca, International Journal of Hydrogen Energy 31(2006)13.

22. P. Jozsa, E. Jobson and M. Larsson, Topics in Catalysis 30–31(2004)177.

23. D. James, E. Fourre´, M. Ishii and M. Bowker, Applied Catalysis B: Environmental 45(2003)147.

24. S. Poulston and R.R. Rajaram, Catalysis Today 81(2003)603.

25. T. Lesage, C. Verrier, P. Bazin, J. Saussey and M. Daturi, Physical Chemistry Chemical Physics 5(2003)4435.

26. Z. Liu and J. A. Anderson, Journal of Catalysis 224(2004)18.

27. M. AL-Harbi, W. S. Epling and D. Radtke, Applied Catalysis B: Environmental 96(2010)524.

28. V. Bolis, G. Magnacca, and C. Morterra, Research on Chemical Intermediates 25(1999)25.

29. A. Igarashi , T. Ohtaka and S. Motoki, Catalysis Letters 13(1991)189.

30. Y. Lia, X. Wanga, C. Xiea and C. Songa, Applied Catalysis A: General 357(2009)213.

31. S. Wang and G.Q. Lu, Applied Catalysis B: Environmental 19(1998)267.

32. R. S. Monteiro, L. C. Dieguez and M. Schmal, Catalysis Today 65(2001)77.

33. Y-F. Y. Yao, Journal of Catalysis 87(1984)152.

34. T. Maillet, J. Barbier, D. Duprez, Applied Catalysis B: Environmental 9(1996)251.

35. A. Ghenciu, Current Opinion in Solid State and Material Science 6(2002)395.

36. C. Wheeler, A. Jhalani, E. J. Klein, S. Tummala and L. D. Schmidt, Journal of Catalysis 223(2004)191.

37. M. AL-Harbi, W. S. Epling, A. Yezerets, N. W. Currier, H.-Y Chen and H. Hess, SAE technical paper series 2009-01-0631.

38. M. AL-Harbi and W. S. Epling, Applied Catalysis B: Environmental 89(2009) 315.

39. A. M. Venezia, G. Pantaleo, A. Longo and G. D. Carlo, Journal of Physical Chemistry B: 109(2005)2821.

40. S. Letichevsky, C. A. Tellez, R.R. Avillez, M. I. P. Silva, M. A. Fraga and L. G. Appel, Applied Catalysis B: Environmental 58(2005)203.

41. Q. Fu, A. Weber and M. Flytzani-Stephanopoulos, Catalysis Letters 77(2001)87.

42. N. Takahashi, K. Yamazaki, H. Sobukawa and H. Shinjoh, Applied Catalysis B: Environmental 70(2007)198.

43. S. Adhikari, S. Fernando and A. Haryanto, Energy & Fuels 21(2007)2306.

44. C. Kern and A. Jess, Chemical Engineering Science 60(2005)4249.

45. P. Forzatti and L. Lietti, Catalysis Today 52(1999)165.

Chapter 5

Investigating the Effect of NO Versus NO_2 on the Performance of a Model NO_X Storage/Reduction Catalyst [*]

5.1 Abstract

The effects of using NO or NO_2 as the NO_X source on the performance of a NO_X storage/reduction catalyst were investigated from 200 to 500°C. The evaluation included comparison with constant cycling times and trapping the same amount of NO_X during the lean phase. With NO_2 as the NO_X source, better trapping and reduction performance was attained in comparison to NO, at all operating temperatures except 300°C. This exception, under the conditions tested, was likely due to high NO oxidation activity and rapid trapping of NO_2, although it is expected that extending the trapping time would lead to consistent differences. Several reasons for the observed improvements at 200, 400 and 500°C with NO_2 relative to NO are discussed. One that can explain the data, for both trapping and release improvement, is treating the monolith as an integral reactor. With NO_2, more NO_X is trapped at the very inlet of the catalyst, whereas with NO, the maximum in trapping during cycling occurs slightly downstream. Thus more of the catalyst can be used for trapping with NO_2 as the NO_X source. The decreased release during catalyst regeneration is similarly explained; with more being released at the very inlet, there is more residence time and therefore contact with downstream Pt sites, but more importantly more interaction between reductant and stored NO_X. NH_3 and N_2O measurements support this conclusion.

---

[*] See the permission from Springer Science+Business Media in appendix A

5.2 Introduction

Concern over fluctuating fuel prices and depleting fuel reserves has led to increased interest in more fuel-efficient engines, such as lean-burn gasoline and diesel engines. However, the excess oxygen present in lean-burn engine exhaust significantly decreases the reduction of NO_X to N_2 over today's three way catalytic converter (TWC), which was designed to operate efficiently in stoichiometric-burn, near-zero oxygen, engine exhaust. An alternative, emerging catalyst technology for NO_X clean-up from lean-burn engine exhaust is NO_X storage and reduction (NSR). NSR catalysts are typically composed of a high surface area substrate such as γ–alumina, alkali and alkaline metal earth components that trap NO_X in the form of nitrites and nitrates, and precious metals such as Pt, Pd, and Rh for the redox reactions [1-4]. This technology operates in two modes: lean and rich. In the lean mode, which is where the engine normally operates, NO is oxidized to NO_2 over precious metal sites and the NO and/or NO_2 is then stored on the trapping material as a nitrate and/or nitrite [4-8]. When some portion of these trapping materials becomes saturated, the engine exhaust is switched to a reductant-rich mode where reductants such as H_2, CO, and HC are introduced to induce the reduction of the stored NO_X to N_2 [9-11].

Although the trends and mechanisms of NO_X storage, release, and reduction have been investigated [12-15], due to the complexity of the catalyst, process and their sensitivity to experimental conditions, there is still debate regarding the mechanisms and the potential reactions involved in the multiple catalytic steps [15]. However, there is consensus in the literature that improved NO oxidation to NO_2 results in improved NSR catalyst performance. Previous work [16] has demonstrated that over a wide range of

117

operating temperatures, NO can not be adsorbed over barium aluminates and barium stannate, even in the presence of O_2, whereas NO_2 is readily absorbed. In a study that investigated the storage of NO and NO_2 over a Pt-containing commercial NSR catalyst [17], no storage occurred when NO was used as the NO_X source below 150°C, while significant storage was observed when NO_2 was used. However, at 380ºC with a Pt/Rh/Ba/Al$_2$O$_3$ sample [18], no significant difference was observed in storage capacity when either NO or NO_2 was used. This improvement with NO at higher temperature is likely attributed to one, or all of, three reasons. First, NO oxidation activity in this higher temperature range is significant [19-21]. Second, NO_2 is known to inhibit the NO oxidation reaction [22], and with NO_2 being trapped more rapidly as the temperature is increased, at least until approximately 300 to 400°C [13,23], less is present to inhibit the reaction, thus allowing even more NO oxidation. Finally, thermodynamic equilibrium between NO and NO_2 within this temperature range [18] imposes a constraint on the NO_2 concentration, which is easily achieved over a typical NSR catalyst [19]. Therefore at downstream positions, the same amounts of NO and NO_2 are present, resulting in similar performance no matter the NO_X source. The interaction of NO, NO/O$_2$, and NO_2 mixtures was also investigated at even higher temperature, 500°C, over Pt-Ba/Al$_2$O$_3$, Ba/Al$_2$O$_3$, and Pt/Al$_2$O$_3$ [7]. The trapping efficiency followed the order NO < NO + O$_2$ < NO_2. Similar findings were also observed over a commercial NSR catalyst at 400ºC [24]. These results indicate that it must be more than just NO oxidation efficiency that dictates performance, otherwise there would be a consistently decreasing difference as the temperature is increased. Overall, NSR catalysts are more efficient with NO_2 as the NO_X source, or NO_2 may even be a necessary intermediate for NO_X storage.

Several mechanisms have been proposed for NO_X storage when either NO or NO_2 is present in the inlet gas feed. Previous work has proposed that nitrites and nitrates can form, either individually [7,12,13,18,25-27], or both form simultaneously via $2BaO + 4NO_2 \rightarrow Ba(NO_3)_2 + Ba (NO_2)_2$ [15,18]. NO_X release mechanisms have also been investigated, with the research indicating that nitrate species decompose releasing NO or NO_2 [7,13,18].

There are several reasons that might explain the performance improvements observed when NO_2 is used instead of NO as the NO_X source. First, if trapping is a function of NO_2 partial pressure [6], then when NO_2 is used, the very inlet of the catalyst can participate in trapping whereas with NO, oxidation to NO_2 must occur before efficient trapping is realized. A second possibility involves the presence of multiple types of trapping sites [28-30]. As an example, if one Ba site type is near Pt and another is distant from Pt, NO might only adsorb on the Ba sites which are in close proximity with Pt since it needs to be oxidized to NO_2 prior the adsorption event. While with NO_2, it can be adsorbed on both Ba site types.

Although NO_2 improves NSR catalyst efficiency, increasing NO_2 amounts to the NSR catalyst or within the NSR catalyst requires the addition of more oxidation catalyst. Diesel oxidation catalysts have been added upstream of NSR catalysts to provide higher inlet NO_2, as well as for other functions. These are currently precious metal-based catalysts. To improve NO oxidation within the NSR catalyst, more precious metal can also be added. These obviously come at a cost and therefore it is important to understand the effects of NO_2 and optimize the amount of NO_2 in the inlet. In the present work, we have investigated the performance of a model NSR catalyst as a function of NO_X source

at operating temperatures between 200 and 500ºC. Although there are studies that have investigated the influence of NO versus NO_2, as shown above, the NO_X trapping, release, and reduction characteristics as well as N_2O and NH_3 formation when the two are used has not been systematically investigated. Furthermore, a comparison was made between the two when the same amount of NO_X is trapped so that the effects during the regeneration phase could be observed.

5.3 Experimental Methods

The model $Pt/BaO/Al_2O_3$ sample used in this study was supplied by Johnson Matthey in monolithic form. The model sample contains 2.0 g/in^3 Al_2O_3, 1.45% Pt and 20% BaO relative to the Al_2O_3. The sample was removed from a monolith block that had a cell density of 300 cpsi. The sample used was 0.83" in diameter with a length of 3". The sample was inserted into a horizontal quartz tube reactor, which was placed inside a Lindberg temperature-controlled furnace. The catalyst was wrapped with 3M matting material to cover the gap between the catalyst and the wall of the reactor to ensure that no gas slipped around the sample. Two K-type thermocouples were placed at the radial center of the catalyst; one just inside the inlet face of the catalyst and one just inside the outlet face of the catalyst. A third was placed ~ 1" upstream of the sample.

The gases and gas mixtures were supplied by Praxair and were metered with Bronkhorst mass flow controllers. A four-way, fast-acting solenoid valve was used to switch between the lean and rich mixtures, which were made in separate manifolds. After the dry gas mixture had been heated to >120°C, water was introduced downstream of this valve. Table 5.1 lists the gas compositions used in the cycling experiments. The gas mixture then passed through a high-capacity furnace, achieving the target test

temperature prior to entering the furnace holding the sample. This set-up minimized any artificial axial and radial temperature gradients during the experiments.

Before each experiment, the sample temperature was ramped to 500°C with 5% H_2O, 5% CO_2, and a balance of N_2 and then the catalyst was cleaned/conditioned with a gas mixture consisting of 5% H_2O, 5% CO_2, 1% H_2, and a balance of N_2 for 15 min. The reactor was then cooled to the target test temperature. Experiments were performed at 200, 300, 400 and 500°C with a space velocity, at standard conditions, of 25,000 hr^{-1}. The gases exiting the reactor were maintained at >190°C to avoid condensation and NH_3 hold-up. The gas compositions were measured using a MKS MultiGas 2030 FT-IR analyzer at approximately a 2 Hz collection rate. CO, CO_2, NO, NO_2, N_2O, NH_3, and H_2O concentrations were measured.

Table 5.1 Details of flow conditions used in the experiments

Flow Conditions	Trapping (lean) phase	Regeneration (rich) phase
Space velocity	25,000 hr^{-1}	25,000 hr^{-1}
Concentrations		
NO_2 or NO	330 ppm	0
O_2	10%	0
CO_2	5%	5%
H_2O	5%	5%
H_2	0	3%
N_2	Balance	Balance

5.4 Results

5.4.1 Effect of inlet NO versus NO_2, with identical cycling times

The outlet NO_X concentrations when either NO or NO_2 was used as the NO_X source at 200°C are shown in Figure 5.1. For this set of experiments, the lean, or

121

trapping, time was 40 seconds, the rich, or regeneration, time was 4 seconds and 3% H_2 was used as the reductant in the regeneration phase. The conversions and amounts of NO_X trapped and released for these experiments are listed in Table 5.2. All reported values and plotted data were obtained after steady cycle-to-cycle performance was observed. The data plotted in Figure 5.1 show that the trapping performance for both cases, when either NO or NO_2 was used, is similar during the first 11 seconds of the lean phase. Beyond the first 11 seconds, however, differences in the outlet concentrations were observed. The outlet NO_X concentrations at the end of the lean phase were 63 and 178 ppm with NO_2 and NO, respectively, and the amounts of NO_X trapped were 101 and 85 μmoles. The amounts released as unreduced NO or NO_2 during the rich period were relatively small, but slightly more was actually released with NO as the feed NO_X source although less NO was trapped in the prior lean phase. This is somewhat surprising since the same amount of reductant was added in both cases.
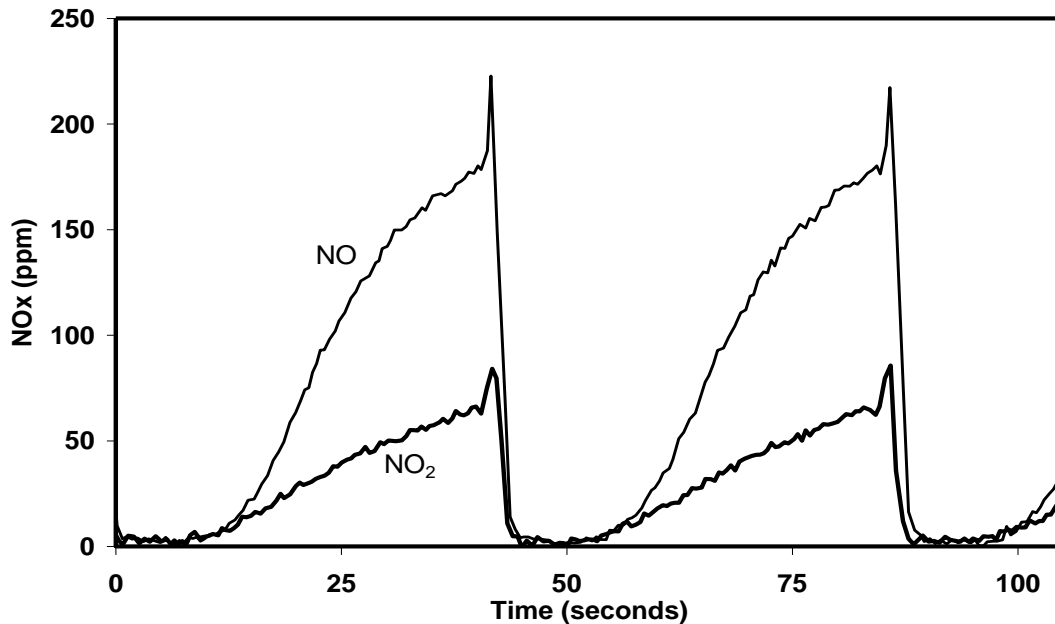
Figure 5.1 NO_X outlet concentrations obtained when testing the sample at 200°C.

122

Similar experiments were carried out at 300, 400 and 500°C, with data shown in Figures 5.2-4. At 300ºC, 100 seconds of storage and 4 seconds of regeneration were used for cycling. A summary of the results for all temperatures is also listed in Table 5.2.

Table 5.2 Calculated performance characteristics as a function of temperature, NO_X source, and lean phase time over a $Pt/BaO/Al_2O_3$ catalyst

Temperature (°C)	NO_X source	Time (sec)		NO_X Trapped (μmoles)	NO_X Released (μmoles)	NO_X Conversion (%)	N_2O Released (μmoles)	NH_3 Released (μmoles)
		Lean	Rich					
200	NO	40	4	85	3.5	73	5.2	47
	NO_2	40	4	101	1.5	90	4.1	50.5
	NO_2	35	4	92	1.3	94	3.5	45.6
	NO_2	30	4	80	0.9	95	3.4	39.6
300	NO	100	4	264	1.8	94	0.57	58
	NO_2	100	4	268	1.6	96	0.55	79
	NO_2	95	4	256	1.6	96	0.51	73
400	NO	120	4	278	8	81	0.27	0
	NO_2	120	4	312	6.4	92	0.07	0.80
	NO_2	100	4	277	3	98	0.01	24
500	NO	80	4	163	31	59	0.26	11
	NO_2	80	4	189	23	75	0.19	26.5
	NO_2	62	4	162	19	83	0.11	24

At 300ºC, with NO_2, the calculated NO_X conversion was 96%, while with NO, it was 94%. It is apparent from Figure 5.2 that the differences in the breakthrough profiles are less than those observed at 200ºC, but with some difference in trapping performance

noted after 34 seconds into the lean phase. However, even at end of the 100-second lean phase, the difference in the breakthrough was only about 10 ppm. The amounts trapped were 268 and 264 μmoles with NO_2 and NO, respectively, and the amounts released were 1.8 μmoles with NO to 1.6 μmoles with NO_2. Overall, using either NO_2 or NO at 300°C led to similar performance for these cycling conditions.
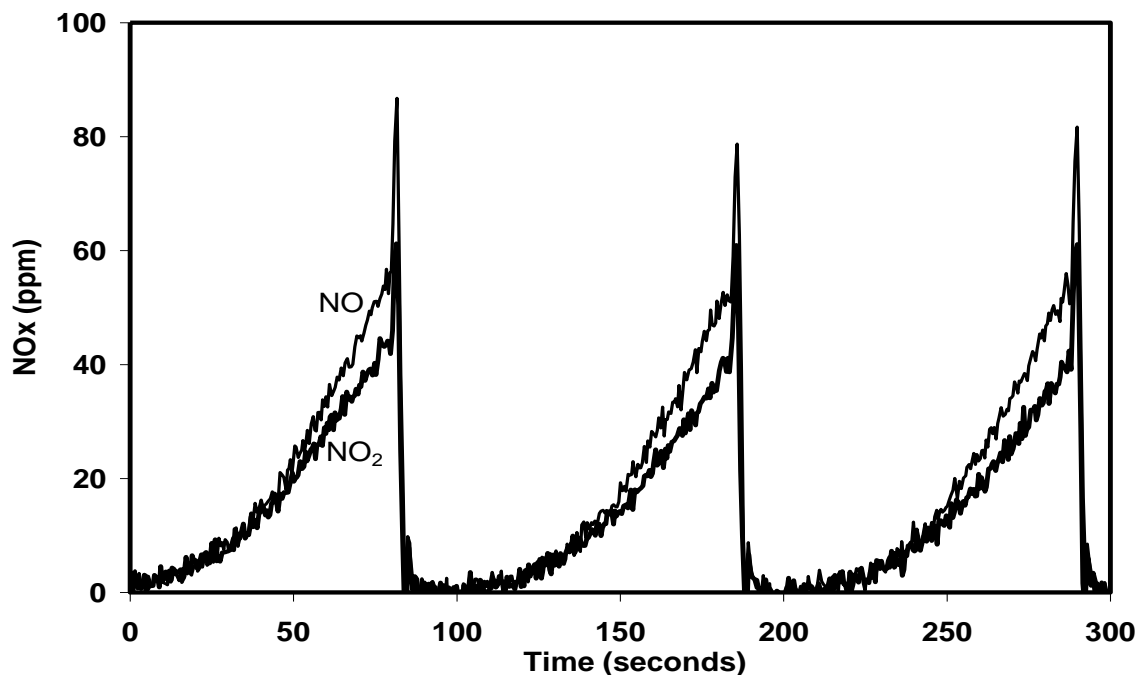
Figure 5. 2 NO_X outlet concentrations obtained when testing the sample at 300°C

The outlet NO_X concentration data obtained at 400°C are shown in Figure 5.3. For this set of experiments, the trapping time was 120 seconds and the regeneration time was 4 seconds. With NO as the NO_X source, the calculated NO_X conversion was 81%, while with NO_2 the NO_X conversion was 92%. The NO_X released decreased from 8 μmoles

with NO to 6.4 μmoles with NO_2, while the trapping performance increased from 278 to 312 μmoles.
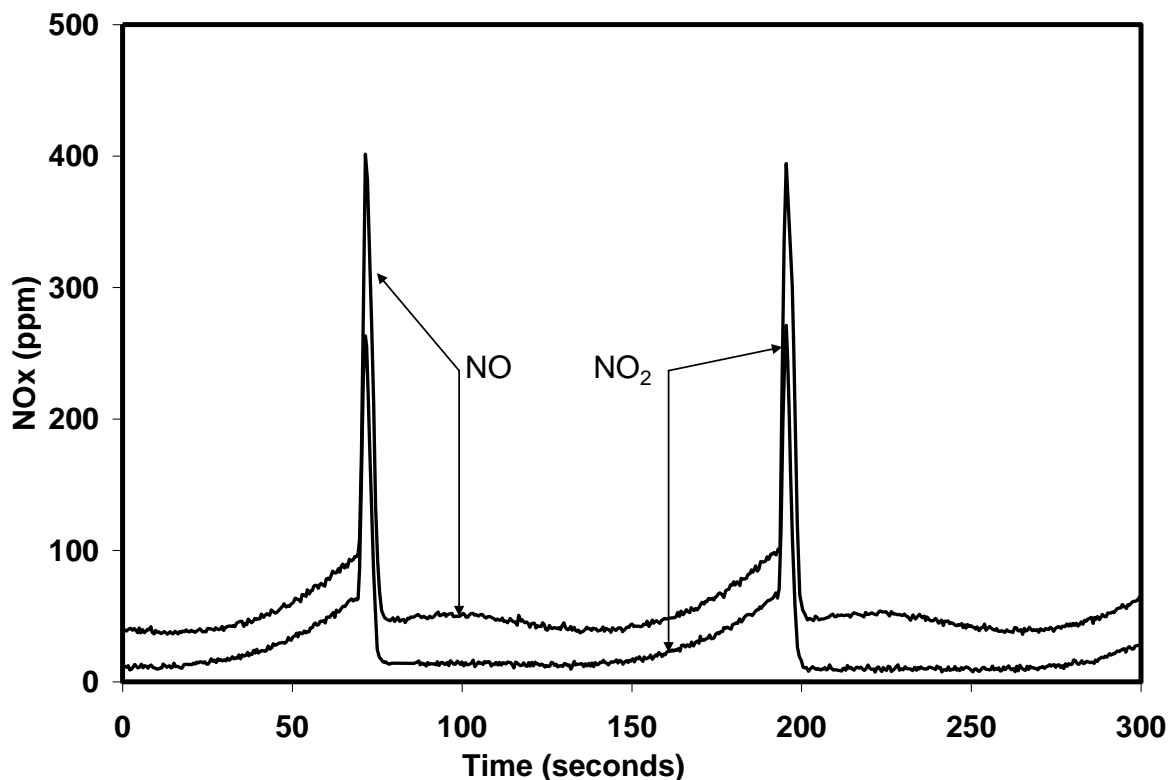
Figure 5. 3 NO_X outlet concentrations obtained when testing the sample at 400°C.

The data obtained at 500°C are shown in Figure 5.4. The cycle time was 80 seconds for storage and 4 seconds for regeneration. The NO_X trapped with NO_2 as the NO_X source was 189 μmoles and 23 μmoles were released during the regeneration phase. When NO was used, 163 μmoles were trapped and 31 μmoles released. From the data shown in Figure 5.4, the NO_X breakthrough was similar for the first 38 seconds of the lean phase and beyond that, differences were observed. At the end of lean phase, the difference in the concentrations exiting the reactor was about 63 ppm.
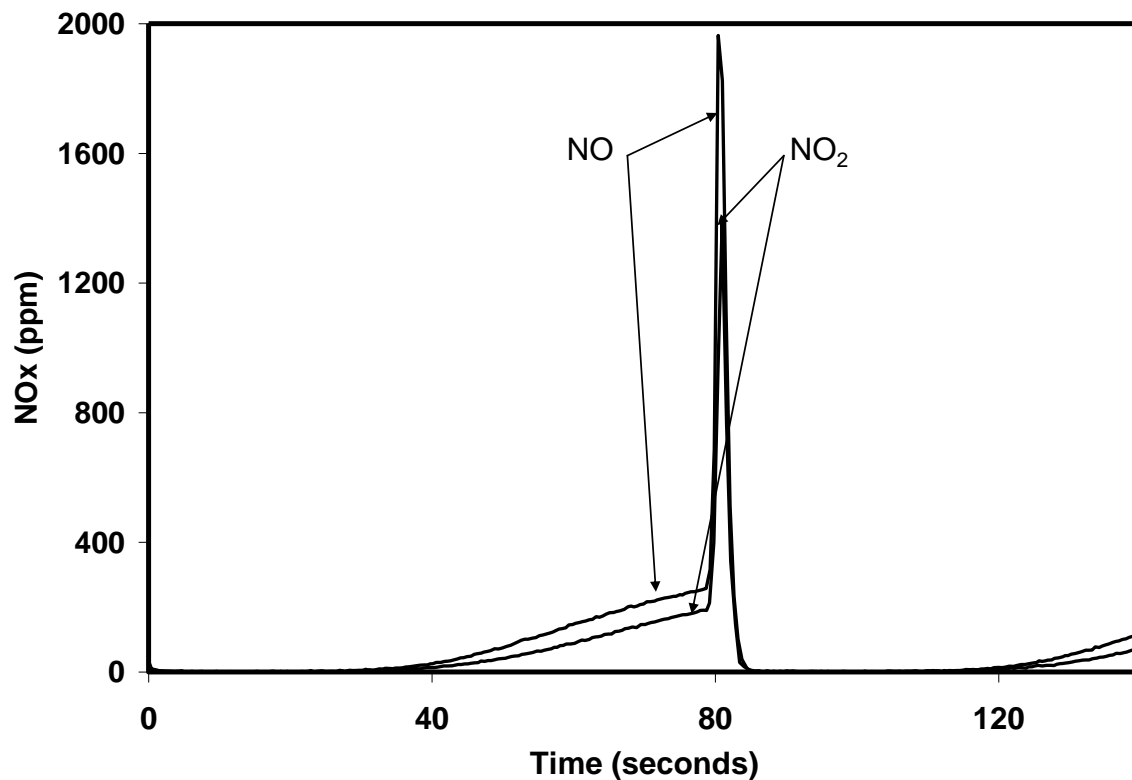
Figure 5. 4 NO_X outlet concentrations obtained when testing the sample at 500°C.

5.4.2 Effect of inlet NO versus NO_2 with the same amount trapped

In this set of experiments, the catalyst performance when trapping the same, or similar, amount of NO_X, using either NO or NO_2, was monitored. The same reductant amounts during the regeneration phase were delivered, resulting in a constant surface NO_X species-to-reductant amount in the cycles. The conversions and amounts of NO_X trapped and released for these experiments are also listed in Table 5.2. In this case, although listed for completeness and to demonstrate the more dramatic effects, the conversions are not directly comparable since the lean times for the experiments differ. For example, at 200°C, when a similar amount is trapped with NO and NO_2, the lean-phase times were 40 seconds and 30 or 35, respectively. The amount of NO_X in during 30

126

seconds is 75% of that in over 40 seconds, and thus when calculating the conversion, the basis or inlet amount is not the same. At 200ºC, with NO as the NO_X source, the NO_X trapped was 85 μmoles. To achieve a similar trapped amount of NO_X with NO_2 as NO_X source, the lean phase was decreased to 30 and 35 seconds. For these two times, the NO_X trapped was 80 and 92 μmoles, respectively. For all three experiments, 3% H_2 was used in the 4-second regeneration phase. One would think that since a similar amount of NO_X was trapped with both NO and NO_2 for these experiments, and the same amount of reductant was introduced during the regeneration phase, a similar amount of release might be expected. This was not the case at 200, 400 and 500°C. For the four experiments run at 200°C, the NO_X released was 3.5 μmoles with NO (85 μmoles trapped) and 1.5, 1.3 and 0.8 μmoles with NO_2 (101, 92 and 80 μmoles trapped).

At 300ºC, performance was comparable with the same cycling times, therefore extra experiments were not run. At 400ºC, the lean time was reduced to 100 seconds when testing with NO_2 so that a similar amount was trapped as that with NO for 120 seconds. When NO was used in the lean phase, the NO_X trapped was 278 μmoles and the NO_X released was 8 μmoles, while with NO_2, the NO_X trapped was 277 μmoles and the NO_X released was 3 μmoles. At 500ºC, when NO was used, 163 μmoles were trapped and 31 μmoles released and with NO_2, the lean phase was shortened to 62 seconds resulting in 162 μmoles of NO_X trapped and 19 μmoles released. The above results demonstrate that the use of NO_2 as the NO_X source is not merely better for trapping, but also less release occurred.

5.5 Discussion

In comparing the results obtained at 200 and 500°C when testing with either NO or NO_2, similar trapping profiles were observed at the onset of the trapping phase. Low initial NO_X out values indicate that active trapping sites were regenerated during the prior rich phase. It has been suggested that there are sites with different relative activities and the more active sites for $Pt/Ba/Al_2O_3$ samples are associated with the outermost layers of Ba particles or are in close proximity to the precious metal sites [28-30]. If the reduction equation is assumed as follows; $Ba(NO_3)_2 + 5H_2 \rightarrow N_2 + BaO + 5H_2O$, for 2 moles of NO_X trapped, 5 moles of H_2 are required for reduction to N_2. At 200°C, the amount of NO_X that enters the reactor during a 40-second lean phase is 0.11 mmoles, so the H_2 required to reduce all of the entering NO_X to N_2 if it all were trapped is 0.28 mmoles. Therefore, 3% H_2, or 1.01 mmoles input during the 4 seconds of rich, is in large excess. Since the catalyst does not contain any oxygen storage components, such as ceria, this amount will be in excess even if including that needed to consume the very small amount of oxygen stored on the catalyst surface. Hence, excess reductant was delivered during the regeneration phase and therefore similar cleaning might be expected with either NO or NO_2. However, except at 300°C, the data demonstrate that trapping is significantly more efficient if NO_2 is the NO_X source. Such improvements in overall performance have been repeatedly observed when comparing NO_2 to NO [7,12,13,15,31-34]. In this study, the differences between the two are especially apparent at the temperature extremes. There are several possible reasons for this trend in trapping.

First, monolith-supported catalysts are integral devices, and introducing NO_2 can increase use of sites at the very inlet of the catalyst if trapping depends on NO_2, or is

enhanced via NO_2. With NO, NO_2 becomes available via NO oxidation, and therefore the NO_2 concentration will be relatively low at the very inlet, but increase downstream, meaning that for some distance within the sample, the amount of NO_2 will be significantly less than when introducing NO_2 as the NO_X source. For example, applying previously derived NO oxidation kinetics [22], demonstrates that at steady-state conditions, in other words after the Ba is saturated and no trapping occurs, the conversions of NO to NO_2 at 200°C and at positions 0", 1", 2" and 3" from the inlet are 0, 11, 16 and 21%, respectively. This build-up in NO_2 would result in higher nitrate concentrations downstream of the inlet, which has indeed been observed [35]. Note that with trapping, NO_2 would be adsorbed from the gas phase, resulting in higher local NO oxidation rates compared to the absence of trapping. Also, using NO_2 as the NO_X source can result in good trapping performance even in the absence of oxygen in the inlet feed [31]. Thus activation of the O_2 molecule is not required with NO_2, possibly helping reaction at low temperature. Another possible contribution is from different trapping sites having different adsorption affinities for NO_2 and NO. Multiple Ba sites or adsorbing types have been proposed [28-30]. In one example, there are two Ba site types, one proximal to Pt sites and the other further away. With such a scheme, only the sites close to Pt might participate in trapping when NO is the inlet NO_X source, as the Pt would oxidize the NO to NO_2, which would then "spill-over" to an adjacent Ba site. Otherwise, the NO_2 would have to desorb from the precious metal site and re-adsorb to Ba downstream, but as described above, the overall NO oxidation rate is fairly limited at the lower temperatures. NO_2 can be adsorbed on both types of Ba sites, the one proximal to Pt and the one far away from Pt via direct nitrite formation, or via the disproportionation

129

mechanism to nitrates. This of course increases the available amount of trapping sites when NO_2 is introduced, therefore increased trapping will occur and overall higher NO_X reduction performance would be expected. Again, however, this would contribute to more being trapped at upstream sites as well as throughout the catalyst. Another possibility, along the same concept, is that nitrate species and not nitrite species are always, or at least preferentially, formed when NO_2 was used, while a mixture of the two species are formed with NO. The thermal stability of nitrate species is higher than nitrite species [4,7], and therefore they are less likely to decompose during the lean phase (via an adsorption/desorption like equilibrium) leading to more NO_X trapped. Most evidence, however, suggests that at temperatures below 300°C, a mixture of nitrites and nitrates form when NO is used, but at higher temperatures, although a mixture may initially form, the nitrites are quickly oxidized to nitrates and have therefore not been observed [6,7]. This is therefore unlikely to significantly influence higher temperature performance and therefore cannot explain the differences observed at 400 and 500°C.

At 300ºC, the trapping performance of the catalyst appears only slightly dependent on the NO_X source under the conditions of these tests. NO oxidation initially increases with temperature [36] and most NSR catalyst types attain their maximum oxidation activity between 300 and 400°C, resulting in high NO_2 amounts, thus leading to more favorable trapping and comparable performance. Again, using previously derived kinetics [22], at 300°C and in the absence of trapping, 50% NO conversion is predicted. However, the generated NO_2 over a NSR catalyst can be immediately trapped, leading to maintained, higher overall NO oxidation rates due to lesser NO_2 product inhibition, especially in this 300 to 400°C range. Additionally, in this temperature range, some

130

thermodynamic equilibrium between NO and NO_2 is being established [18], with a calculated maximum 87% conversion allowed at 300°C, indicating the kinetics are still responsible for the lower conversion. Even so, based on the data shown in Figure 5.2, it is expected that with longer lean time, more difference would be observed, with NO_2 still resulting in improved NO_X trapping at 300°C. At 400 and 500°C, more significant differences were observed. It should also be noted that NO_2 was observed in the outlet gas composition at 400 and 500°C, with NO and NO_2 as the NO_X source, indicating it is not an absence of NO_2 limiting trapping at these high temperatures.

At all temperatures, with NO_2 used, there was also noticeable improvement in the regeneration phase, i.e. less unreduced NO and NO_2 was released. This is based on the data obtained from the experiments where the same amount of NO_X was trapped during the prior lean phase, presented in Table 5.2, resulting in a constant reductant-to-trapped NO_X ratio for comparison purposes. A likely reason that explains this trend as well, is the integral nature of the NSR catalyst system. As mentioned above, if NO_2 is introduced as the NO_X source, more sites at the front of the catalyst will participate in trapping. Trapping with NO will be limited at the very inlet due to low NO_2 partial pressures, until the extent of NO oxidation is significant enough. Therefore, upon switching from the lean to rich phase, in the case of NO_2, more NO_X is released at the very front of the catalyst giving it more chance to be reduced by downstream Pt sites before exiting the monolith. While with NO, more is released slightly further downstream, and has less time spent in the monolith or chance to contact the reducing Pt sites. This is compounded by the local reductant-to-NO_X ratio as will be discussed below.

Another impact, still in conjunction with the integral reactor explanation, is the oxygen stored on the catalyst surface affecting the amount of reductant available for NO_X reduction. Previous research [37,38] has shown that reductant can be used up in reducing the stored oxygen on the catalyst and hence influences the amount of reductant available for regeneration and reduction of NO_X. With NO_2, more NO_X is trapped at the very inlet and upon switching from lean to rich, the reductant will simultaneously be depleted to reduce both oxygen and NO_X stored on the catalyst. Although competitive, this still results in the opportunity for reductant to be consumed in the reduction of NO_X. However, when NO is used, more is trapped slightly downstream and the incoming reductant is first used to deplete the oxygen stored at the very inlet, thereby delaying reductant delivery to downstream Pt and Ba sites where the higher concentrations of stored, or released, NO_X species are. This will likely play an increasing role as the nitrate decomposition reaction becomes more significant, i.e. with increasing temperature. Also, with the catalyst studied in these experiments, although present, little OSC was measured due to the absence of standard OSC components. Therefore, the effect described may be minor with this system, but more significant with commercial formulations that contain ceria and other OSC components.

Further evidence supporting the increased reduction being related to where the NO_X was trapped is the formation of N_2O and NH_3 byproducts during the regeneration event. As shown in Table 5.2, the formation of N_2O was always higher when NO was used. With more NO_X trapped at the front of the catalyst when NO_2 is used, during regeneration there is more opportunity for complete reduction downstream, leading to decreased selectivity toward N_2O formation, where N_2O can be considered an incomplete

reduction product. While with NO, the distribution of trapped NO_X is shifted downstream, and there is therefore less chance for released NO_X to be completely reduced. This is again related to residence time, since for any NO_X released further upstream, there is more chance for reduction at downstream sites, but can also be related to the reductant-to-NO_X ratio. As the reductant enters, it is consumed by surface oxygen and in reducing the nitrites and nitrates. Therefore, reductant delivery to downstream active sites lags the lean/rich gas transition, and as time increases, or the lean/rich transition front distance into the catalyst increases, this lag increases as well. With NO_2 as the NO_X source, more was trapped at the very upstream Ba sites, and a relatively higher reductant-to-NO_X ratio is achieved, leading to more complete reduction overall. As a matter of fact, NH_3 formation was always higher when NO_2 was used instead of NO (Table 5.2). NH_3 is formed from the trapped nitrite/nitrate species and the H_2 input during regeneration and leads to selective catalytic reduction of NO_X over the NSR catalyst [39,40]. Following the same concept discussed above, if NO_2 is trapped at the very inlet of the catalyst, more NH_3 can be formed due to longer residence time of the released NO_X in the channel with the reductant, as well as a higher reductant-to-NO_X ratio, a key parameter in NH_3 formation on NSR catalysts [41]. Furthermore, with NO_2 leading to more upstream trapping, NH_3 that does form will have less trapped NO_X downstream to react with, contributing to the greater amounts observed with NO_2 as the feed. In the case of NO, the NO_X is trapped slightly downstream relative to the NO_2 case, and therefore less NH_3 is formed, due to the decreased reductant-to-NO_X ratio and decreased residence time. It should be noted that the amount of N_2O, overall, decreased with increasing temperature, while NH_3 did not show a consistent trend. Typically, observed NH_3

decreases with increasing temperature, but this was not the case when comparing the data at 400 and 500°C. But, different lean times were used and less NO_X was trapped at 500°C, and with the same amount of reductant added, more NH_3 was therefore formed at 500°C. With the trapped NO_X being different between the temperatures, a direct correlation of NH_3 as a function of temperature cannot be made.

Other than the axial distribution of trapped NO_X explaining the trends, another possibility is the nature of the stored NO_X during the lean phase. Several complex compounds, (e.g., barium aluminates) could be present, which may have different NO and NO_2 dependencies on trapping [18]. Similarly, the decomposition trends of the nitrates or surface NO_X compounds formed might be different. However, these types of sites are typically formed via high temperature treatments [42], which were not done with this sample, making this an unlikely path.

There are other factors that can contribute to the observed trends differentiating NO and NO_2, but these have different extents of significance in different temperature ranges, and therefore do not explain the consistently observed trends ranging from 200 to 500°C. These possible contributing factors are discussed here. The possibility of nitrates forming at sites near and far from the precious metal sites when using NO_2 was discussed in conjunction with the trapping results. Previous studies [7,33,43] have also addressed the influence of Pt on the thermal stability and decomposition of nitrate and/or nitrite species. If with NO, more NO_X is trapped at Ba sites that are near Pt, then there may be higher release associated with NO as the inlet NO_X source as Pt could induce the decomposition of the Ba nitrite/nitrate during the regeneration phase. With a catalyzed release, or simply higher than that compared to sites that are not necessarily near Pt, more

will escape unreduced. Along the same concept, nitrates are more thermally stable than nitrites. More nitrates form with NO_2 introduced as compared to NO, which at low temperatures is trapped as a nitrite or nitrite/nitrate pair [5,6,15,44]. Therefore at low temperature, nitrite decomposition could lead to a higher amount of unreduced NO_X, while the nitrates formed with NO_2 as the inlet NO_X source would lead to less. This however, just as with the trends in trapping, does not explain the differences observed at higher temperatures, as above 300°C, nitrites are rapidly oxidized to nitrates during the lean phase [4,7,19]. Another possibility is that NO is released as the decomposition product when NO is used and NO_2 is released when NO_2 is used, for example from $Ba(NO_3)_2$ decomposition, which is more prevalent with NO_2 as the NO_X source. In the absence of gas-phase O_2, NO_2 still has some affinity for downstream adsorption, whether it be on Pt or Ba [14]. Therefore, if NO_2 can indeed stick to downstream sites during the regeneration phase, it will have more opportunity for reduction as the reductant propagates along the catalyst length. Again, however, this should only be expected at low temperature where nitrites might still exist with the switch to the regeneration phase.

A last consideration was the associated temperature rise with the switch from the trapping to regeneration phase. This is caused by reaction of the entering reductant with surface oxygen species, nitrate reduction and possibly mixing phenomena between the two phases. Measured temperature rises at the very inlet and outlet of the sample were on the order of 5°C during all tests. These are significantly smaller than those observed with commercial sample [37], due to the lack of a purposefully added oxygen storage component, such as ceria, in the sample used in this study. This small temperature increase, and it being observed at both the front and back of the sample, suggests that

135

temperature change is not a significant factor for the trends seen. Furthermore, previous work with $Pt/Ba/Al_2O_3$ model samples at 350°C has also indicated that with little or no temperature rise at the onset of regeneration, regeneration is associated with a surface-catalyzed reaction, as mentioned above, and not via thermal decomposition of nitrate species [45]. Again, however, at higher temperatures thermal decomposition of the nitrates is expected and therefore this effect distinguishing NO from NO_2 less significant.

Overall, of the possibilities proposed, only the integral nature of the NSR catalyst can explain the observations at all temperatures and amounts of NO_X trapped used in this study. The different surface species and their relative rates of decomposition can contribute to the observations at low temperature, but not to the differences still observed at 400 and 500°C. At low temperature, NO_2 is readily trapped at the very inlet, while NO is oxidized and then trapped. At higher temperature, NO_2 will decompose to establish NO/NO_2 equilibrium, but this still leaves higher NO_2 amounts at the very inlet. Therefore, with NO, there is a distribution of trapped NO_X as a function of axial position along the catalyst length during cycling that has a maximum, rather than a monotonic decrease with NO_2 as the NO_X source. This leads to the better performance consistently observed with NO_2 as the NO_X source and when upstream oxidation catalysts are used.

5.6 Conclusions

In this study, the performance of a model monolith-supported NSR catalyst when using NO or NO_2 as the inlet NO_X source at temperatures between 200 and 500°C was investigated. The evaluation was based on two different types of experiments; one with the same lean cycle times and the other with same amount of NO_X trapped. The results clearly demonstrated that performance was better when using NO_2 at all operating

136

temperatures. At 300ºC, similar performance between the two was observed, due to high NO oxidation activity, rapid trapping of formed NO_2 and therefore no inhibition effect on NO oxidation, but differences were becoming apparent at the end of the lean phase.

The improved performance with NO_2 relative to NO at the other temperatures can be explained by NO_2 being more reactive towards trapping than NO, or even being an intermediate in the trapping process. This NO_2 dependency leads to more NO_X trapped at the catalyst inlet when NO_2 was used, while with NO there was less since oxidation to NO_2 prior to trapping is required or leads to more appreciable trapping. A distribution of stored NO_X along the length of catalyst forms, where with NO_2 it monotonically decreases and with NO there is a maximum downstream of the very inlet. Thus more NO_X is stored with NO_2 as the NO_X source since the very front of the catalyst can be used and there are no NO_2/reactant concentration limitations. Also, less released NO_X during regeneration was observed when NO_2 was used. Again, if with NO_2 more is trapped at the very inlet, upon switching from lean to rich, the reductant is used to simultaneously reduce both surface oxygen and stored NO_X. While in the case of NO, the reductant will be consumed first to deplete the surface oxygen and lesser quantities of stored NO_X at the catalyst inlet, resulting in less reductant available to reduce NO_X at downstream positions where it is being released in higher concentrations. Analysis of byproduct N_2O and NH_3 formation during the regeneration phase support this conclusion, as more N_2O was observed with NO as the inlet NO_X source, and more NH_3 with NO_2. Possible contributions to improved performance with NO_2 at lower temperatures were also discussed, and included nitrate versus nitrite stability and trapping at sites near or far from the Pt sites.

5.7 Acknowledgment

References

1. W. Bogner, M. Kramer, B. Krutzsch, S. Pischinger, D. Voigtlander, G. Wenninger, F. Wirbeleit, M. Brogan, R. Brisley, and D. Webster, Applied Catalysis B: Environmental 7(1995) 153.

2. N. Takahashi, H. Shinjoh, T. Iijima, T. Suzuki, K. Yamazaki, K. Yokota, H. Suzuki, N. Miyoshi, S. Matsumoto, T. Tanizawa, T. Tanaka, S. Tateishi, and K. Kasahara, Catalysis Today 27(1996)63.

3. I. Hachisuka, H. Hirata, Y. Ikeda, and S. Matsumoto, SAE Technical Paper Series 1999-08-0571.

4. W.S. Epling, L.E. Campbell, A. Yezerets, N.W. Currier and J.E. Parks, Catalysis Reviews 46(2004)163.

5. B. Westerberg and E. Fridell, Journal of Molecular Catalysis A: Chemical 165(2001)249.

6. J. Kwak, D. Kim, T. Szailer, C. Peden, and J. Szanyi, Catalysis Letters 111(2006)3.

7. F. Prinetto, G. Ghiotti, I. Nova, L. Lietti, E. Tronconi, and P. Forzatti, Journal of Physical Chemistry B 105(2001)12732.

8. T. Toops, D. Smith, W.S. Epling, J. Parks and W. Partridge, Applied Catalysis B: Environmental 58(2005) 255.

9. P. Jozsa, E. Jobson, and M. Larsson, Topics in Catalysis 30/31(2004)177.

10. D. James, E. Fourré, M. Ishii and M. Bowker, Applied Catalysis B: Environmental 45(2003)147.

11. S. Poulston and R.R. Rajaram, Catalysis Today 81(2003)603.

12. E. Fridell, H. Persson, B. Westerberg, L. Olsson, and M. Skoglundh, Catalysis Letters 66(2000)71.

13. H. Mahzoul, J.F. Brilhac, and P. Gilot, Applied Catalysis B: Environmental 20(1999)47.

14. I. Nova, L. Lietti, and P. Forzatti, Catalysis Today 136(2008)128.

15. P. Schmitz and R. Baird, Journal of Physical Chemistry B 106(2002)4176.

16. S. Hodjati, K. Vaezzadeh, C. Petit, V. Pitchon, and A. Kiennemann, Catalysis Today 59 (2000) 323.

17. S. Erkfeldt, E. Jobson, and M. Larsson, Topics in Catalysis 16/17(2001)1.

18. E. Fridell, M. Skoglundh, B. Westerberg, S. Johansson and G. Smedler, Journal of Catalysis 183(1999)196.

19. L. Olsson and E. Fridell, Journal of Catalysis 210(2002)340.

20. M. Crocoll, S. Kureti, and W. Weisweiler, Journal of Catalysis 229(2005)480.

21. S.S. Mulla, N. Chen, L. Cumaranatunge, W.N. Delgass, W.S. Epling, and F.H. Ribeiro, Catalysis Today 114(2006)57.

22. S.S. Mulla, N. Chen, W.N. Delgass, W.S. Epling, and F.H. Ribeiro, Catalysis Letters 100(2005)3.

23. K. Kabin, R. Muncrief, and M. Harold, Catalysis Today 96(2004)79.

24. F. Rodrigues , L. Juste, C. Potvin, J.F. Tempère, G. Blanchard, and G. Djéga-Mariadassou, Catalysis Letters 7(2001)1.

25. L. Meng, M. Lin, Y. Fu, T. Hu, Y. Xie, and J. Zhang, Topics in Catalysis 22(2003)111.

26. L. Lietti, P. Forzatti, I. Nova, and E. Tronconi, Journal of Catalysis 204(2001)175.

27. N. W. Cant and M. J. Patterson, Catalysis Today 73(2002)271.

28. W. S. Epling , J. E. Parks , G. C. Campbell , A. Yezerets, N.W. Currier , and L. Campbell, Catalysis Today 96 (2004) 21.

29. M. Piacentini, M. Maciejewski, and A. Baiker, Applied Catalysis B: Environmental 60 (2005) 265.

30. V. Medhekar, V. Balakotaiah, and M. Harold, Catalysis Today 121(2007) 226.

31. S. Salasc, M. Skoglundh, and E. Fridell, Applied Catalysis B: Environmental 36(2002)145.

32. T. Kobayashi, T. Yamada, and K. Kayano, SAE Technical Paper Series 970745.

33. S. Kikuyama, I. Matsukuma, R. Kikuchi, K. Sasaki, and K. Eguchi, Applied Catalysis A: General 226(2002)23.

34. F. Laurent, C. Pope, H. Mahzoul, L. Delfosse, and P. Gilot, Chemical Engineering Science 58(2003)1793.

35. K. Aftab, J. Mandur, H. Budman, N.W. Currier, A. Yezerets, and W. S. Epling, Catalysis Letters 125(2008)229.

36. L. Olsson, B. Westerberg, H. Persson, E. Fridell, M. Skoglundh, and B. Andersson, Journal of Physical Chemistry B 103(1999)10433.

37. W. S. Epling, A. Yezerets and N. W. Currier, Catalysis Letters 110(2006)143.

38. J. Choi, W. P. Partridge, W. S. Epling, N. W. Currier, and T. Yonushonis, Catalysis Today 114(2006)102.

39. A. Lindholm, N.W. Currier, E. Fridell, A. Yezerets and L. Olsson, Applied Catalysis B: Environmental 75(2007)78.

40. L. Cumaranatunge, S.S. Mulla, A. Yezerets, N.W. Currier, W.N. Delgass, and F.H. Ribeiro, Journal of Catalysis 246(2007)29.

41. J.A. Pihl, J.E. Parks II, C.S. Daw, and T.W. Root, SAE Technical Paper Series 2006-01-3441.

42. D.H. Kim, Y.-H. Chin, J.H. Kwak, J. Szanyi, and C.H.F. Peden, Catalysis Letters 105(2005)259.

43. L. Zhaoqiong and J.A. Anderson, Journal of Catalysis 224(2004)18.

44. F. Frola, F. Prinetto, G. Ghiotti, L. Castoldi, I. Nova, L. Lietti, and P. Forzatti, Catalysis Today 126 (2007) 81.

45. I. Nova, L. Lietti, L. Castoldi, E. Tronconi and P. Forzatti, Journal of Catalysis 239(2006)244.

Chapter 6

Effects of Different Regeneration Timing Protocols on the Performance of a Model NO$_X$ Storage/Reduction Catalyst[*]

6.1 Abstract

The effects of different regeneration times, but with a constant total amount of reductant delivered, were investigated over a model NO$_X$ storage and reduction (NSR) catalyst. The different regeneration times were 4, 8 and 16 seconds with 4, 2, and 1% H$_2$ as the reductant amounts, respectively. The lean time was kept the same during these experiments, resulting in a constant inlet NO$_X$-to-reductant amount in the cycles. Overall, the results show clear improvements with longer regeneration times in both NO$_X$ trapping and overall reduction performance at all temperatures except 500°C. At 500°C, there was still an increase in trapping performance with longer regeneration time, but a more significant increased NO$_X$ release coincident with a small increase in the trapping performance resulted in an overall decrease in NO$_X$ conversion with increasing regeneration time. The data demonstrate that the different concentrations of H$_2$ did not lead to different regeneration extents, but that the main factor for the improved performance was the regeneration time itself. With longer regeneration times, more nitrate/nitrite decomposition occurred, thereby leading to more extensive surface cleaning.

---

* See the permission from Elsevier in appendix A

6.2 Introduction

With growing concern and public awareness about the environmental, ecological and health impacts of air pollution and global warming, environmental agencies have been setting increasingly stringent regulations to mitigate and control vehicle emissions. This is made more difficult by a coincident demand for higher fuel economy. One solution is a shift from stoichiometric burn engines, such as today's standard gasoline engine, to lean-burn gasoline or diesel engines. Such a transition could result in a reduction in both fuel consumption and CO_2 emissions. A significant challenge that still remains is NO_X emissions. NO_X storage and reduction (NSR) catalysis is one of the currently accepted and implemented technologies for lean-burn engine NO_X emissions control. NSR catalysts are typically composed of precious metals such as Pt, Pd, and Rh for the redox reactions, alkali and alkaline metal earth components that trap NO_X in the form of nitrites and nitrates, all supported on a high surface area substrate such as γ–alumina [1-4]. This technology cycles through two phases; a lean and a rich phase. In the lean phase NO is oxidized to NO_2 on the precious metal sites and then NO_2 is adsorbed by the trapping materials, such as Ba in the form of $Ba(NO_3)_2$ and/or $Ba(NO_2)_2$ [5-7]. In operation, the lean phase continues until some level of NO_X slips past the catalyst. At this stage, the rich phase of the cycle is started, where reductants such as CO, H_2, and hydrocarbons are introduced to reduce the surface NO_X species to N_2 thereby regenerating the trapping sites for the next lean phase, with reduction occurring also via participation of the precious metals sites [8-10].

Numerous studies have investigated regeneration phenomena, including the effect of reductant type, reductant amount, and different lean and rich times [10-16]. In terms of

143

reductant type [11], the reduction efficiencies of H_2, CO, C_3H_6 and C_3H_8 at different temperatures were investigated over a $Pt/BaO/Al_2O_3$ model catalyst. The results showed that H_2 was a superior reductant at low temperatures (T≤250°C), while at high temperatures H_2 and CO were similar and showed higher reduction efficiency than C_3H_6. C_3H_8 was inefficient at all temperatures tested. Similar observations were also reported over a commercial NSR catalyst [10]. The effect of H_2 and CO amounts on the overall performance of a commercial NSR catalyst was also investigated [14]. The performance of the catalyst improved with each incremental increase in H_2 concentration, with 5% H_2 the highest level evaluated. At high temperature, the performance also increased with increasing CO amounts, however at 200°C, increasing CO was found to decrease performance due to precious metal site poisoning.

The effect of the lean and rich times on the performance of a model NSR catalyst was also investigated, using H_2, CO, and C_3H_6 as reducing agents [15]. As an example of the results, at 300°C, when the lean time was increased from 45 to 135 sec while maintaining a constant rich time (1.5 sec), the overall conversion decreased from 93 to 40%. This was attributed to a lack of sufficient reductant during the 1.5 sec rich phase as the lean time was increased. In the same study, the rich time was increased from 1.5 to 4.5 sec with a constant reductant concentration (3%) and lean phase time (135 sec), and the NO_X conversion increased from 41 to 98%. This was due to the Ba sites being more extensively regenerated with the longer regeneration time and therefore able to participate in trapping during the following lean phase. At lower operating temperatures (T≤250°C), the authors found that NO_X conversion was less dependent on the lean/rich ratio. In another study, the effect of rich time vs. reductant amount on the overall NO_X

conversion performance of a powder $Pt/Ba/Al_2O_3$ catalyst was investigated [16]. With a fixed reductant-to-inlet NO_X ratio at 400°C, the authors concluded that using longer regeneration times with lower reductant concentrations was more efficient compared to short regeneration times with higher reductant concentrations, which they attributed to two effects. The first was consumption of reductant by the oxygen at the lean/rich interface and the second was that the reduction process with the shorter regeneration time was not as efficient as that with longer regeneration.

The overall reduction of NO_X and regeneration of trapping sites during the rich phase depends not only on the amount and type of reductant, but also on the amount of NO_X released via decomposition of the surface nitrite and nitrate species. Primary causes of nitrate/nitrite decomposition and NO_X release are changes is the gas phase composition, such as the absence of oxygen and NO and the presence of CO_2, H_2O and reductant during the rich phase, as well as heat generated from the exothermic reaction between reductants and oxygen stored on the catalyst surface. For the latter, in a previous study [17] the temperature patterns during cyclic operation of a commercial NSR catalyst were investigated. Just after the onset of the rich phase, the measured temperature rise observed within the first few millimeters of the catalyst surpassed 30°C. As the nitrite/nitrate species stability is a decreasing function of temperature, the increased temperature can lead to decomposition. Such large temperature rises are not typically observed over model $Pt/Ba/Al_2O_3$ samples due to a lack of significant oxygen stored on the surface, and therefore this exotherm driven decomposition could be insignificant on these model systems.

Nova and coworkers [18] clearly demonstrated the relative unimportance of a purely thermally driven decomposition versus reductant-induced decomposition on a model $Pt/Ba/Al_2O_3$ system. In their study little NO_X desorption/nitrate decomposition was observed during temperature-programmed desorption experiments up to the temperature where NO_X adsorption was performed. However, in the presence of H_2, decomposition could begin at temperatures 200°C lower than the adsorption temperature. Beyond the reductants, other gas-phase constituents influence nitrate stability as well. The presence of oxygen increases nitrate stability [19] and in its absence, the nitrates/nitrites become less stable and decompose. Similarly, it has been shown that CO_2 and H_2O can influence the stability of surface nitrate species, with CO_2 negatively impacting performance [20] via a reduction in nitrates formed, while H_2O has been observed to both decrease [21] and increase [5] NO_X conversion performance. The effect of Pt on the thermal stability of nitrate and/or nitrite species has also been addressed [22-24, 18]. Results show that Pt induces decomposition of the Ba nitrite/nitrate during the regeneration phase and therefore NO_X trapped close to Pt might be released faster. Along the same concept, two types of Ba nitrate have been observed; surface and bulk [25-27]. Previous studies have concluded that surface Ba nitrate species are not as thermally stable as a bulk nitrate species.

In this study, the effect of regeneration time, while keeping the total amount of reductant introduced during the regeneration phase the same, was investigated. The analysis includes experiments with and without reductant to monitor time dependent surface NO_X species decomposition and reductant-induced decomposition. The trapping performance, NO_X release and formation of NH_3 were measured.

146

6.3 Experimental Methods

The model $Pt/BaO/Al_2O_3$ sample used in this study was supplied by Johnson Matthey in monolithic form. The sample contains 0.12 g/cm^3 Al_2O_3, 1.45% Pt and 20% BaO relative to the Al_2O_3. The sample was cut to 2.1 cm diameter with a length of 6.4 cm from a monolith block that had a cell density of 300 cpsi. The sample was inserted into a horizontal quartz tube, which was placed inside a Lindberg Minimite temperature-controlled furnace. The catalyst was wrapped with 3M insulation material to seal the catalyst in the quartz tube, to ensure that no gas slipped around the sample. For temperature measurements, two K-type thermocouples were placed at the radial center of the catalyst; one just inside the inlet face of the catalyst and one just inside the outlet face of the catalyst. A third was placed ~ 2.5 cm upstream of the sample.

The gases and gas mixtures were supplied by Praxair and were metered with Bronkhorst mass flow controllers. A four-way, fast-acting solenoid valve was used to switch between the lean and rich mixtures, which were made in separate manifolds. After the dry gas mixture had been heated to >120°C, water was introduced downstream of this valve. Table 6.1 lists the gas compositions used in the cycling experiments. Small quartz tubes were inserted into the main quartz reactor tube to provide better heat transfer to the gas, such that at the catalyst position, temperature gradients were minimized along the length of catalyst.

Before each experiment, the sample temperature was ramped to 500°C with 5% H_2O, 5% CO_2, and a balance of N_2 and then the catalyst was cleaned with a gas mixture consisting of 5% H_2O, 5% CO_2, 1% H_2, and a balance of N_2 for 15 min at 500°C. The

reactor was then cooled to the target test temperature. Experiments were performed at 200, 300, 400 and 500°C with a space velocity, at standard conditions, of 25,000 hr^{-1}. Different lean times were used at the different temperatures to reflect the different efficiencies at those temperatures, for example performance at 200°C is worse than at 300°C, so longer lean times were used at 300°C, which also matches application trends better. The gases exiting the reactor were maintained at >190°C to avoid condensation and NH_3 hold-up. The gas compositions were measured using a MKS MultiGas 2030 FT-IR analyzer at approximately a 2 Hz collection rate. CO, CO_2, NO, NO_2, N_2O, NH_3, and H_2O concentrations were measured.

Table 6.1 Details of flow conditions used in the experiments

Flow Conditions	Trapping (lean) phase	Regeneration (rich) phase
Space velocity	25,000 hr^{-1}	25,000 hr^{-1}
Concentrations		
NO	330 ppm	0
O_2	10%	0
CO_2	5%	5%
H_2O	5%	5%
H_2	0	1-4%
N_2	balance	Balance
Temperature (°C)		
200	40 seconds	4, 8, 16 seconds
300	80 seconds	4, 8, 16 seconds
400	120 seconds	4, 8, 16 seconds
500	80 seconds	4, 8, 16 seconds

6.4 Results and Discussion

In the first set of experiments, 4, 8 and 16 second regeneration times were used, with 4, 2, and 1% H_2 as the reductant amounts, respectively. Thus the same amount of

reductant was introduced during each experiment. As previously shown [14], at low temperature CO as a reductant has a severe negative impact on NSR catalyst performance relative to H_2. However, the same study also demonstrated that if H_2 is added to the reductant stream, some performance can be maintained, and more H_2 led to better performance and less CO poisoning. So although CO was not added to the regeneration mixture in this study, the trends observed with H_2 will still be viable if H_2 is present in any amount in the regeneration gas mixture. The lean phase times at each temperature were maintained during these experiments, resulting in a constant inlet NO_X-to-reductant amount in the cycles. However, different lean times were used at the different temperatures to avoid saturation and 0 ppm NO_X slip at the performance extremes, better reflecting times and saturation levels used in practice. The performance of the catalyst was evaluated at different test temperatures, as listed in Table 6.2. The outlet NO_X (the sum of NO + NO_2) concentrations as a function of time obtained during one of the cycles at an inlet temperature of 200°C are shown in Figure 6.1. The lean, or trapping, time was 40 seconds. The conversions and amounts of NO_X trapped and the amount of un-reduced, released NO_X during the rich phase, are listed in Table 6.2. The amount of unreduced NO_X release is obtained by integrating the quantity of NO_X released during the rich phase, which is defined by the trigger sent to switch the valve controlling which gas phase enters the reactor. All reported values and plotted data were obtained after steady cycle-to-cycle performance was attained.

Table 6.2 Calculated performance characteristics as a function of temperature, amount of H$_2$, and regeneration time.

Temperature (°C)	H$_2$ (%)	Time (sec) Rich	Lean	NO$_X$ Conversion (%)	NO$_X$ Trapped (µmoles)	NO$_X$ Released (µmoles)	NH$_3$ Released (µmoles)	CO Formed (µmoles)
	4	4	40	42	44	4.9	23	0.1
200	2	8	40	49	51	5.5	28	0.4
	1	16	40	57	60	6.4	31	0.5
	4	4	80	79	150	2.8	51	4
300	2	8	80	86	163	3.6	89	9
	1	16	80	92	175	4.4	99	15
	4	4	120	78	226	10	37	18
400	2	8	120	80	237	16	38	33
	1	16	120	80	247	25	35	55
	4	4	80	37	84	15	19	110
500	2	8	80	35	88	23	15	157
	1	16	80	30	91	34	10	198

The data plotted in Figure 6.1 show that the trapping performance was similar during the first few seconds of the lean phase, no matter the regeneration time, but differed after. The amounts of NO$_X$ trapped were 60, 51, and 44 µmoles for the 16, 8, and 4 second regeneration times, respectively. The amounts released as unreduced NO or NO$_2$ during the rich period were relatively small, but steadily increased as the regeneration time increased. This increase was expected since the amount of NO$_X$ released is a function of NO$_X$ trapped during the previous lean phase, and the amount of NO$_X$ trapped was larger with increasing regeneration time. The total inlet NO$_X$ during the 40 second lean time

was 93 µmoles. During the regeneration period, with 1, 2, and 4% H_2, 1124 µmoles of H_2 were introduced. If the reduction reaction is assumed to be $Ba(NO_3)_2 + 5H_2 \rightarrow N_2 + BaO + 5H_2O$, then for 2 moles of NO_X trapped, 5 moles of H_2 are required for reduction to N_2, or 232 µmoles to reduce all the entering NO_X. The catalyst used in these experiments does not contain any oxygen storage components, such as ceria, so the amount of H_2 input was in large excess even if including that needed to consume the very small amount of oxygen stored on the catalyst surface (i.e. Pt oxides and possibly Ba peroxides at low temperatures).
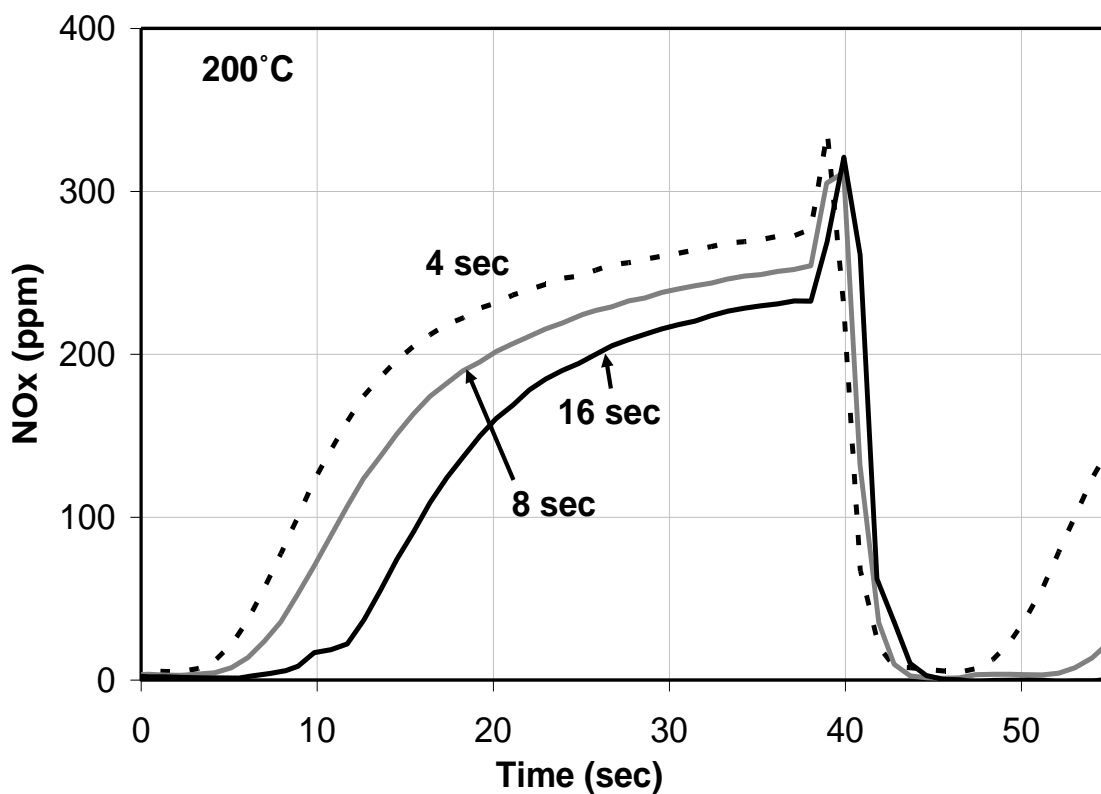
Figure 6.1 NO_X outlet concentrations obtained at 200°C with 1% H_2 and 16 sec, 2% H_2 and 8 sec, and 4% H_2 and 4 sec regeneration phases.

Similar experiments were carried out at 300, 400, and 500°C to investigate the effect of operating temperature on the storage, release, and reduction of NO_X with the different regeneration protocols. The outlet NO_X concentrations as a function of time at 300°C are shown in Figure 6.2. A summary of the results are also listed in Table 6.2. Again, there was initially little difference in the performance of the catalyst at the beginning of the lean phase with differences appearing as the lean time progressed. The trapping trends were similar to those observed at 200°C, where increased regeneration time led to increased amounts trapped. This increase in the amount trapped, with little impact on the amount released, led to higher overall conversions.
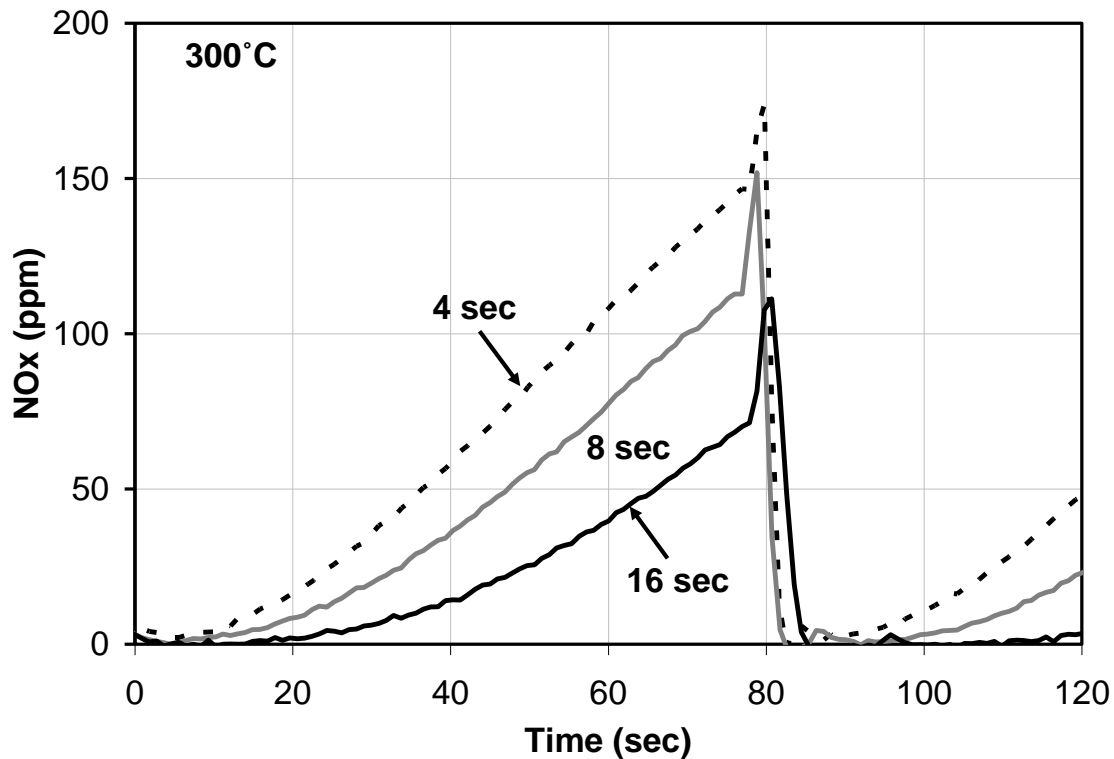
Figure 6.2 NO_X outlet concentrations obtained at 300°C with 1% H_2 and 16 sec, 2% H_2 and 8 sec, and 4% H_2 and 4 sec regeneration phases.

The total inlet NO_X during the 80 second lean phase was 186 μmoles and the amount of H_2 required to reduce this NO_X, if all was trapped, is 464 μmoles. The inlet H_2 during regeneration was 1120 μmoles, still in significant excess.

Figure 6.3 compares the outlet NO_X concentrations at 400°C, with a lean phase duration of 120 seconds. At this temperature, the performances for all three regeneration times were similar for a larger portion of the lean phase, relative to that observed at the lower temperatures. Differences were still observed, just much later, and again trapping performance was improved with increasing regeneration time. The observed NO_X release was higher than that observed during the 200 and 300°C tests, but this increase had little impact on the overall NO_X conversions. The improved trapping performance at 400°C relative to 200 and 300°C is related to two main factors. First, at low operating temperature, NO oxidation is kinetically limited [5] [28] and most NSR catalyst types attain their maximum oxidation activity between 300 and 400°C. This would therefore result in higher NO_2 amounts and subsequently more rapid and extensive trapping of NO_X as NO_2 is preferred relative to NO for trapping and nitrate formation [29]. Second, not only does the oxidation activity increase as the temperature increases, but also the extent of regeneration increases. As mentioned, with increasing temperature, nitrates become less stable and in the absence of O_2 and NO_X in the gas stream, a more significant amount decomposes at 400°C relative to the lower temperatures. Furthermore, at high operating temperature, activation of reductants is not an issue [5], and hence the reductant can easily reduce decomposing nitrate species to N_2. With more extensive regeneration, there is more trapping site availability expected in the subsequent lean phase portion of the cycle.

153
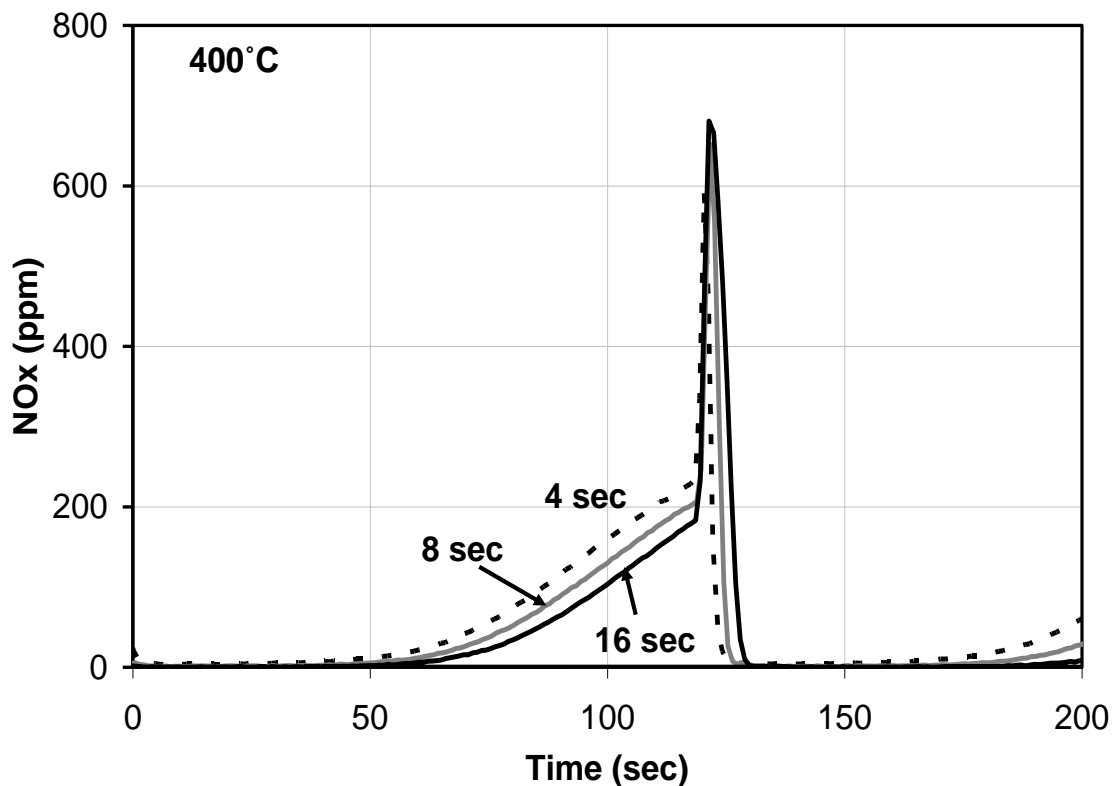
Figure 6.3 NO$_X$ outlet concentrations obtained at 400°C with 1% H$_2$ and 16 sec, 2% H$_2$ and 8 sec, and 4% H$_2$ and 4 sec regeneration phases.

The data obtained at 500°C and an 80-second lean phase are shown in Figure 6.4. Again, improved trapping was observed with longer regeneration times coincident with increased release during the regeneration phase. At this high temperature, however, the NO$_X$ release increased significantly with each increase in regeneration time; 15, 23, and 34 μmoles with 4, 8, and 16 seconds of regeneration time, respectively. This increase in NO$_X$ release coincident with the relatively smaller increase in the trapping performance with longer regeneration times resulted in an overall decrease in NO$_X$ conversion as the regeneration time was increased. Although the reduction rate increases with temperature, the too rapid decomposition rate of the Ba nitrate species combined with decreasing

reductant concentration and its rapid consumption at the onset of the regeneration phase led to the increased significance of released and unconverted NO_X.
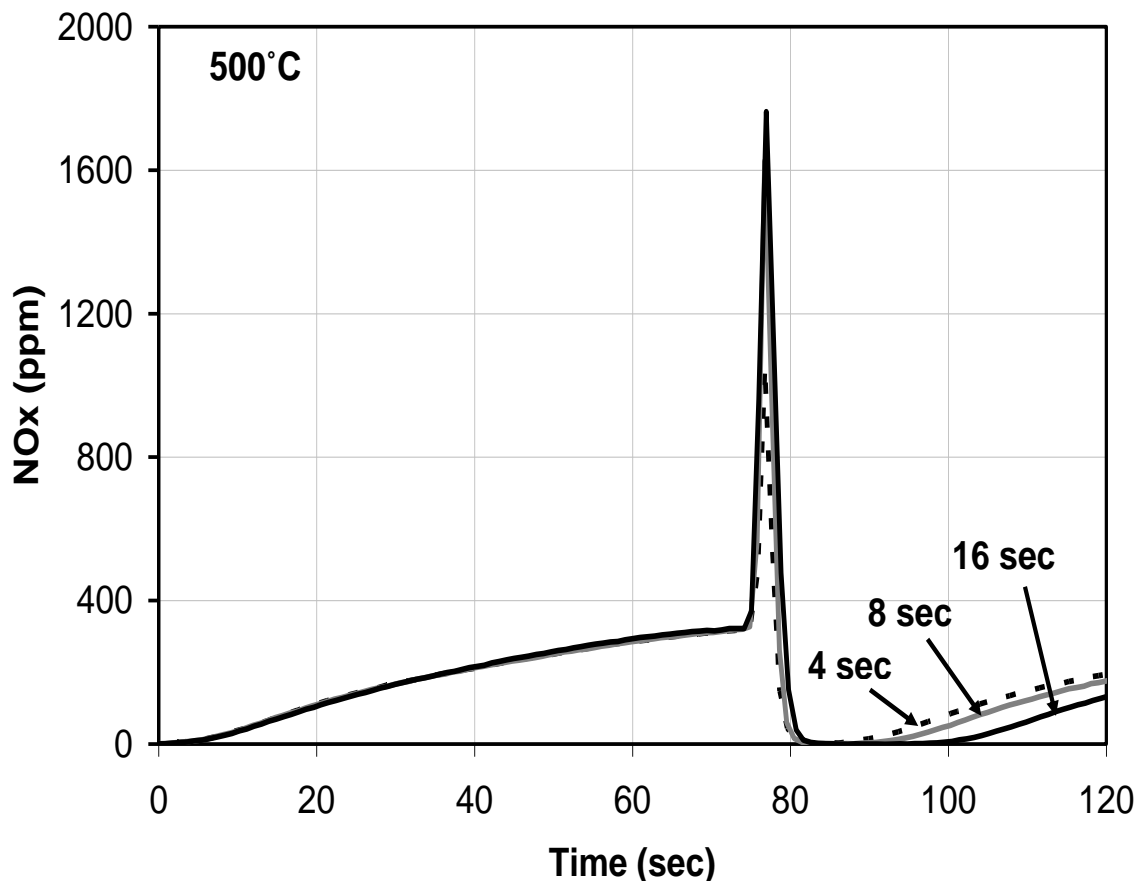
Figure 6.4 NO_X outlet concentrations obtained at 500°C with 1% H_2 and 16 sec, 2% H_2 and 8 sec, and 4% H_2 and 4 sec regeneration phases.

In further detail, at the beginning of the trapping phase, NO_X is trapped at sites located at upstream positions. These sites become saturated with time and then stop taking part in the trapping process, so downstream sites begin to participate. If the trapping phase is long enough, both upstream and downstream trapping sites will have participated in NO_X trapping. At 500°C, nitrate decomposition is rapid and upon switching to the rich phase,

155

the reductant interacts with NO_X species trapped at the upstream sites to reduce NO_X and regenerate the surface. The evolved NO_X species originating from the downstream trapping sites move through the catalyst without being reduced, as the reductant is being used to regenerate the upstream sites. This would in turn lead to the observed lower conversion of trapped NO_X to N_2. The amount released was higher with longer regeneration times at 500°C due to the lower local concentration of reductant throughout the catalyst at the onset of the rich phase, with the reduction reaction therefore more reductant limited during the rapid nitrate decomposition and NO_X release. However, the amount trapped was still higher with longer regeneration time. At the lower test temperatures, the increased NO_X release is at least partially due to the increase in the amount trapped, combined with lesser local reductant concentrations when nitrate decomposition begins as well.

The results show a marked increase in the trapping performance coincident with slight increases in NO_X release and therefore overall performance improvement at all temperatures, except 500°C, with longer regeneration times even though the delivered reductant amounts were identical. The improvement in catalyst performance when using longer regeneration times can be primarily attributed to two effects. First, there will be an impact from gas mixing at the lean-to-rich transition interface, which will briefly lead to some reductant consumption. As mentioned in the Introduction, a previous study [16] investigated the effect of a longer regeneration pulse with a lower concentration of reductant vs. a shorter regeneration pulse with a higher concentration of reductant. The authors found that a better regeneration of the catalyst was achieved with the longer regeneration pulse and lower reductant concentration. One explanation proposed was the

consumption of reductants via combustion with oxygen at the interface between the lean and rich phase. With higher reductant concentrations, and the high level of O_2 used in the lean phases, more reductant can be lost compared to the lower reductant concentration case. Therefore, if indeed a significant amount of reductant was consumed at the interface when high concentrations (and a shorter rich pulse) were used in their study, the total amount of reductants delivered to the catalyst beyond the very upstream portion (where the oxidation will occur) will be lower than that when longer regenerations where less reductant concentration was used. Thus, a better regeneration could be expected with longer regeneration. If this mixing effect is significant, then in these experiments, as the rich time increased from 4 to 8 sec and 8 to 16 sec with decreasing reductant concentrations, the effect should have become less. But the difference between the 8 second, 2% H_2 experiment and the 16 second, 1% H_2 experiment was more significant than the difference between the 4 second, 4% H_2 experiment and the 8 second, 2% H_2 experiment. This indicates that this mixing impact on the observed trends is likely minimal, and there must at least be another factor. Furthermore, the temperature rises were relatively small, on the order of 2 to 6°C, and the temperature rise at the front of the catalyst was slightly higher during the shorter regeneration time experiments, relative to the longer regeneration times, in our study, indicating a higher combustion rate. This exotherm impact should, if a significant effect, have led to better regeneration with higher reductant concentrations, which was not observed.

The second effect is related specifically to the regeneration time and nitrate decomposition rate. The two reactions shown below, decomposition of the nitrate species,

as well as reduction of the nitrate species, describe an overall sense what occurs during the regeneration phase.

$$Ba(NO_3)_2 \rightarrow BaO + 2NO + 1.5O_2 \qquad\qquad (6\text{-}1)$$

$$Ba(NO_3)_2 + 5H_2 \rightarrow N_2 + BaO + 5H_2O \qquad\qquad (6\text{-}2)$$

Nitrate decomposition and NO_X release, reaction (6-1), depend on several factors including temperature, the presence or absence of O_2, H_2O, CO_2 and NO_X, and the inclusion of oxygen storage components such as Ce in the catalyst washcoat. There was little temperature rise during the rich phase of individual experiments, indicating little effect of changing temperature on NO_X release, although this effect might play a more significant role in commercial catalysts [17]. Reaction 1 is the reverse of the trapping reaction, and the absence of oxygen during the regeneration phase can drive the decomposition of Ba nitrate as shown. An oxygen source is required for stabilization and formation of Ba nitrate and if oxygen is not introduced during the regeneration event, the decomposition reaction will be favored. The presence of CO_2 and H_2O coincident with the absence of oxygen during regeneration event also induces the decomposition of Ba nitrate [30-34]. However, in each of these experiments, the inlet CO_2, H_2O and O_2 conditions were identical and therefore should not directly cause the observed changes in performance.

To clarify the effect of the rich-phase duration, a second set of cycling experiments at 200°C, where the most significant difference in overall performance was observed, was performed. The cycling experiments were identical to the previous experiments, but in the last cycle after steady cycle-to-cycle performance reached, the

reductant was not included during the regeneration phase. The NO_X concentration data as a function of time for these experiments are not plotted, but the NO_X ppm data from each experiment were identical for each incremental time frame. During this phase, the amounts of NO_X trapped in the previous part of the cycle and that released without reductant present are shown in Table 6.3.

Table 6.3 Calculated amount of NO_X (μmoles) trapped and unreduced NO_X released during regeneration at 200°C with and without reductant in the regeneration portion of the cycle.

Regeneration Protocols	NO_X Trapped	NO_X Released	Difference
4 sec - 4% H_2	45	7	38
8 sec - 2% H_2	49	10	39
16 sec - 1% H_2	57	16	41

The differences between the amount trapped with reductant used in the previous rich phase, and the amount released in the absence of H_2 in the regeneration phase are also listed. The amount of NO_X released in the absence of reductant of course increased as the regeneration time increased. The difference represents the amount of NO_X associated with trapping sites being regenerated during a rich phase when reductant is present, since steady cycle-to-cycle performance had been obtained. The values are quite similar with the three different regeneration times, indicating a similarity in the amount of regenerated trapping sites between the three experiments with three different regeneration times. This indicates that, in terms of a reductant dependency, the amount regenerated is a function of total reductant delivered, and not the concentration. Furthermore, this indicates that the

reduction process was not simply slower with short regeneration time or higher reductant levels. Finally, this also demonstrates that the extra regeneration observed with the longer regeneration time is solely due to the extra time for reaction 1 to continue.

Beyond just the amount of nitrate or nitrite species that decompose with time, there are other routes, still a function of the regeneration time, which might contribute to the improved performance with long regeneration times. The release/desorption and re-adsorption of the NO_X species from trapping sites to adjacent or downstream Ba sites during regeneration events is one such possibility. At low operating temperatures, the desorption rate of NO_X is slower than the reduction rate [5]. Therefore, extending the regeneration event could allow more released NO_X to spillover to adjacent Pt sites for reduction, or be re-adsorbed at downstream Ba sites and then eventually reduced to N_2 as the reductant propagates from the front to back portion of the catalyst. Another scenario, along the same concept, but also related to the time effect related to reaction 1 and discussed above, is that NO_X species can be trapped on two types of Ba sites; as proposed in the literature [35-37], one in close proximity to Pt sites, the other more remote from Pt sites. In previous studies [24], it was shown that Pt can catalyze the decomposition of nitrate species during the regeneration event. The nitrate species trapped on "distant" Ba sites can also be released, but at a slower rate than those proximal to Pt sites [5, 24]. Therefore, if the regeneration time is prolonged, it could lead to more NO_X release from both Ba site types. With more NO_X release, there are more sites available in the next trapping phase.
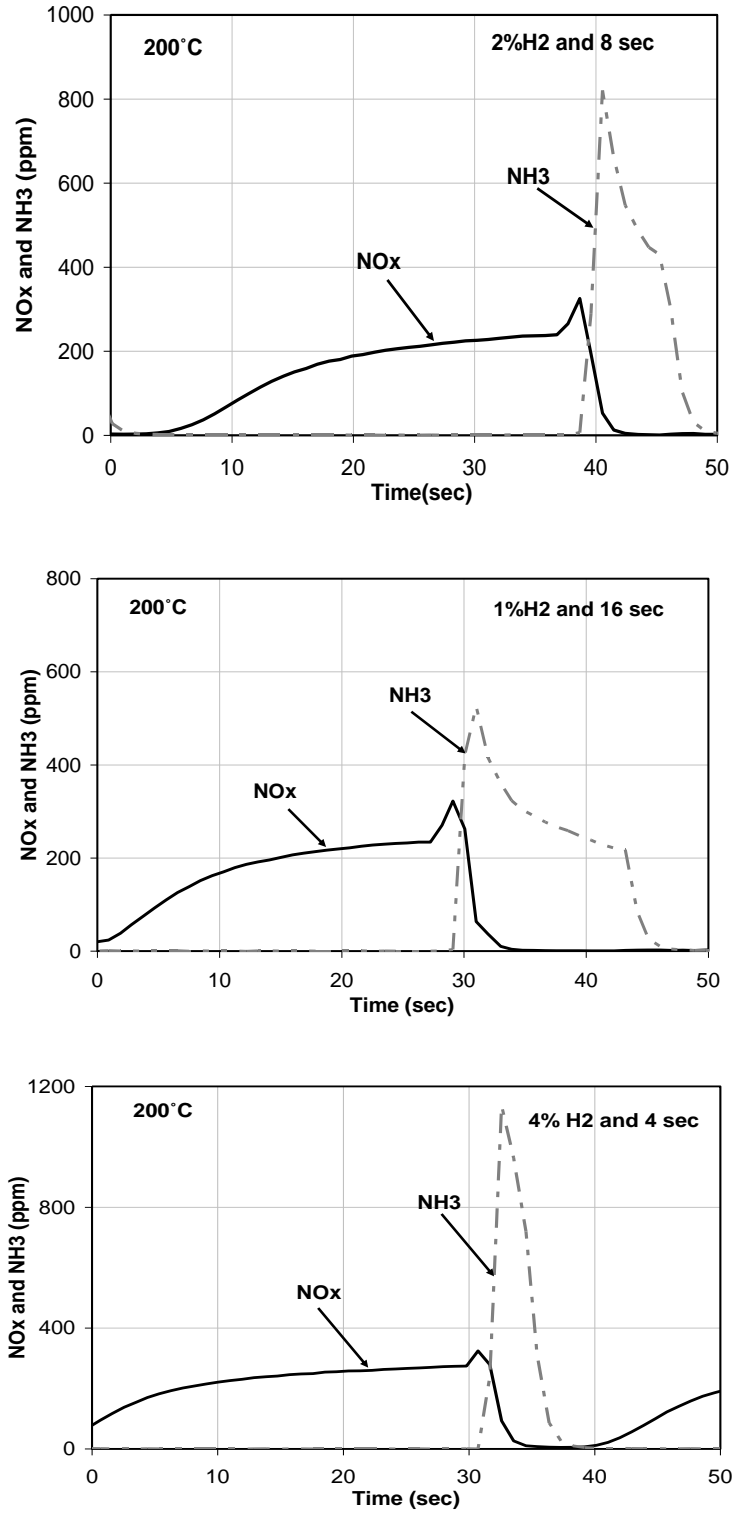
Figure 6.5 NH$_3$ and NO$_X$ outlet concentration data obtained at 200°C during different regeneration protocols.

Although no differences in catalyst performance would be expected when either H_2 or NH_3 is used as the reductant source [38], the following brief discussion is only to relate the NH_3 formation trends with different regeneration protocols. The NH_3 concentrations as a function of time at 200°C and for the three different regeneration protocols are shown in Figure 6.5. Ammonia formation upon NO_X reduction with H_2 over NSR catalysts has been widely reported [39-41]. Ammonia was consistently observed in our experiments shortly after the onset of the regeneration phase (about 1 to 2.5 sec after the onset) and reached a maximum when the released NO_X concentration decreased to close to the baseline level, as shown in Figure 6.5. This result is consistent with NH_3 formed along the catalyst participating in the reduction of NO_X following the selective catalytic reduction (SCR) mechanism. Ammonia formed at the front of the catalyst is used in the SCR mechanism to reduce downstream nitrate species. As the amounts of nitrates decrease and therefore the amount of NO_X release begins to decrease, less NH_3 formed upstream reacts downstream and more is then observed. The amounts of NH_3 formed during the cycling experiments were calculated as a function of temperature and regeneration time and are listed in Table 6.2. At 200 and 300°C, total NH_3 formation was always higher when longer regeneration times were used. However, as shown in Figure 6.5, peak NH_3 concentrations were observed with the higher reductant levels, or shorter regeneration times. These trends can be related back to local reductant-to-NO_X ratios, with the higher the ratio leading to more NH_3 formed [42-43], as well as nitrate exposure time to reductant. As shown in Figure 6.5, NO_X release occurs at the onset of the regeneration phase. As the regeneration time progresses, less NO_X is being released while reductant is still being delivered, and this results in NH_3 formation accelerating when the

observed NO_X release was decreasing. Nitrates were still decomposing, as is evident by the NH_3 formation. Therefore, at later regeneration times, the local reductant-to-NO_X ratio is higher thus the increase in NH_3 as NO_X decreases. With the shorter regeneration time, but higher reductant level, the increased reductant-to-NO_X ratio led to increased peak NH_3 formation values, while for the longer regeneration time experiments, the longer time led to a larger integral amount of NH_3 formed. At 400°C, there was not a significant change in the amount of NH_3 formed as a function of regeneration time, likely due to a balance in the more rapid release and reductant-to-NO_X ratio. At 200 and 300°C, the reductant-to-NO_X ratio was relatively higher due to the higher thermal stability of nitrate species. Therefore, more NH_3 was formed with longer regeneration time due to the increased total amount of NO_X release. However, at 500°C, the weak stability of nitrate species, and the higher reductant concentration during the shorter regeneration protocol, resulted in higher NH_3 formation since both reactants for NH_3 formation were present in abundant quantities. Overall, at low operating temperatures, the longer regeneration time is a key factor controlling the total release of trapped NO_X and to some extent the formation of NH_3 while at higher operating temperatures, where the thermal stability of nitrate species is weak, the higher reductant concentration is the more important parameter for NH_3 formation.

6.5 Conclusions

In this study, the effects of three different regeneration protocols between 200 and 500°C were investigated over a model NSR catalyst. The regeneration conditions were 4, 8 and 16 seconds with 4, 2, and 1% H_2 as the reductant amounts, respectively. The data showed an obvious improvement in the catalyst performance with increasing regeneration

time at 200, 300 and 400°C, with the effect related to improved NO_X trapping. At 500°C, the weaker stability of nitrate species resulted in an overall lower conversion due to a more significant amount of NO_X released with decreasing reductant concentrations, although the trapping performance was still better with longer regeneration time. The improved trapping performance with longer regeneration times was primarily due to prolonged regeneration conditions leading to more extensive nitrate decomposition, allowing more NO_X to be trapped in the subsequent trapping phase. Total NH_3 formation at 200 and 300°C was also higher with longer regeneration time, while at 500°C, the trend was reversed, and was related to the local reductant-to-NO_X ratios.

6.6 Acknowledgements

References

1. W. Bogner, M. Kramer, B. Krutzsch, S. Pischinger, D. Voigtlander, G. Wenninger, F. Wirbeleit, M. Brogan, R. Brisley and D. Webster, Applied Catalysis B: Environmental 7(1995)153.

2. N. Miyoshi, S. Matsumoto, K. Katoh, T. Tanaka, J. Harada, N. Takahashi, K. Yokota, M. Sugiura and K. Kasahara, SAE Technical Paper Series 950809.

3. S. Matsumoto, Catalysis Today 29(1996)43.

4. N. Takahashi, H. Shinjoh, T. Iijima, T. Suzuki, K. Yamazaki, K. Yokota, H. Suzuki, N. Miyoshi, S. Matsumoto, T. Tanizawa, T. Tanaka, S. Tateishi and K. Kasahara, Catalysis Today 27(1996)63.

5. W. S. Epling, L.E. Campbell, A. Yezerets, N. W. Currier and J. E. Parks, Catalysis Reviews 46(2004)163.

6. B. Westerberg and E. Fridell, Journal of Molecular Catalysis A: Chemical 165(2001)249.

7. J. Kwak, D. Kim, T. Szailer, C. H. F. Peden and J. Szanyi, Catalysis Letters 111(2006)3.

8. S. Poulston and R.R. Rajaram, Catalysis Today 81(2003)603.

9. D. James, E. Fourré, M. Ishii and M. Bowker, Applied Catalysis B: Environmental 45(2003)147.

10. P. Jozsa, E. Jobson and M. Larsson, Topics in Catalysis 30/31(2004)177.

11. H. Abdulhamid, E. Fridell and M. Skoglundh, Topics in Catalysis 30/31(2004)161.

12. T. Lesage, C. Verrier, P. Bazin, J. Saussey and M. Daturi, Physical Chemistry Chemical Physics 5(2003)4435.

13. Z. Liu and J.A. Anderson, Journal of Catalysis 224(2004)18.

14. M. AL-Harbi and W. S. Epling, Applied Catalysis B: Environmental 89(2009)315.

15. Y. Li, S. Roth, J. Dettling and T. Beutel, Topics in Catalysis 16/17(2001)1.

16. J. P. Breen, C. Rioche, R. Burch, C. Hardacre and F. C. Meunier, Applied Catalysis B: Environmental 72(2007)178.

17. W. S. Epling, A. Yezerets and N.W. Currier, Catalysis Letters 110(2006)143.

18. I. Nova, L. Lietti, L. Castoldi, E. Tronconi, and P. Forzatti, Journal of Catalysis 239(2006)244.

19. A. Amberntsson, H. Persson, P. Engstrom and B. Kasemo, Applied Catalysis B: Environmental 31(2001)27.

20. T. J. Toops, D. B. Smith, W. S. Epling, J. E. Parks, and W. P. Partridge, Applied Catalysis B: Environmental 58(2005)255.

21. W. S. Epling, L. E. Campbell, and J. E. Parks, Catalysis Letters 90(2003)45.

22. S. Hodjati, K. Vaezzadeh, C. Petit, V. Pitchon and A. Kiennemann, Catalysis Today 59(2000)323.

23. P. Schmitz and R. Baird, Journal of Physical Chemistry B 106(2002)4172.

24. J. M. Coronado and J. A. Anderson, Journal of Molecular Catalysis A: Chemical 138(1999)83.

25. J. Despres, M. Koebel, O. Krocher, M. Elsener and A. Wokaun, Applied Catalysis B: Environmental 43(2003)389.

26. D. James, E. Fourré, M. Ishii and M. Bowker, Applied Catalysis B: Environmental 45(2003)147.

27. H. Fang, J. Wang, R. Yu, C. Wan and K. Howden, SAE Technical Paper Series 2002-01-2889.

28. L. Olsson, B. Westerberg, H. Persson, E. Fridell, M. Skoglundh and B. Andersson, Journal of Physical Chemistry B 103(1999)10433.

29. S. Erkfeldt, E. Jobson, and M. Larsson, Topics in Catalysis 16–17 (2001) 127.

30. W. S. Epling, D. Kisinger and C. Everest, Catalysis Today 136(2008)156.

31. L. Lietti, P. Forzatti, I. Nova and E. Tronconi, Journal of Catalysis 204(2001)175.

32. S. Hodjati, P. Bernhardt, C. Petit, V. Pitchon, and A. Kiennemann, Applied Catalysis B: Environmental 19(1998)209.

33. N. W. Cant and M. J. Patterson, Catalysis Today 73(2002)271.

34. F. Rodrigues , L. Juste, C. Potvin, J. F. Tempère, G. Blanchard and G. Djéga-Mariadassou, Catalysis Letters 72(2001)59.

35. W. S. Epling, J. E. Parks, G. C. Campbell, A. Yezerets, N. W. Currier and L. Campbell, Catalysis Today 96(2004)21.

36. M. Piacentini, M. Maciejewski and A. Baiker, Applied Catalysis B: Environmental 60(2005)265.

37. V. Medhekar, V. Balakotaiah and M. Harold, Catalysis Today 121(2007)226.

38. L. Cumaranatunge, S. S. Mulla, A. Yezerets, N. W. Currier, W. N. Delgass and F. H. Ribeiro, Journal of Catalysis 246(2007)29.

39. A. Lindholm, N. W. Currier, E. Fridell, A. Yezerets and L. Olsson, Applied Catalysis B: Environmental 75(2007)78.

40. L. Castoldi, I. Nova, L. Lietti and P. Forzatti, Catalysis Today 96(2004)43.

41. T. Lesage, C. Verrier, P. Bazin, J. Saussey, S. Malo, C. Hedouin, G. Blanchard and M. Daturi, Topics in Catalysis 30/31(2004)31.

42. J. A. Pihl, J.E. Parks, C. S. Daw and T.W. Root, SAE Technical Paper Series 2006-01-3441.

43. M. AL-Harbi and W. S. Epling, Catalysis Letters 130(2009)121.

Chapter 7

Regeneration of a Model NO$_X$ Storage/Reduction Catalyst Using Hydrocarbons as the Reductant

7.1 Abstract

Regeneration of a model NSR catalyst using hydrocarbons, H_2, or CO as reducing agents was investigated. As previously shown, at low temperature, 200°C, H_2 proved best, while both CO and hydrocarbons were found to poison Pt sites. At 250°C, again H_2 was better but the decreased performance with CO and hydrocarbons was also due to slow kinetics and not solely as a result of Pt site poisoning. At $T \geq 300$°C, hydrocarbons were found to regenerate the catalyst as efficiently as CO and H_2. Hydrocarbon steam reforming experiments were performed to investigate the improved performance at $T \geq 300$°C. Steam reforming did not occur with either dodecane or m-xylene below 450°C. Additionally, although propylene steam reforming occurred at 375°C, the small amount of H_2 formed was insufficient for steam reforming to be the sole reason for improved regeneration. TPR experiments show that propylene was activated on the catalyst at $T \geq 217$°C and, under the conditions examined, the complete reduction of NO by propylene was achieved at 287°C. Furthermore, propylene was observed to reduce surface chemisorbed NO$_X$ species at $T > 200$°C, with high rates by 264°C, with this activity ultimately resulting in the comparable performance with either CO or H_2 at similar temperatures during NO$_X$ cycling experiments.

7.2 Introduction

With increasing environmental regulation pressure, reducing vehicle emissions has become a significant challenge facing automobile manufactures. This includes NO_X, CO and hydrocarbons, and there is increasing concern over vehicle CO_2 emissions as CO_2 is also considered a significant contributor to the greenhouse gas effect. One way to reduce vehicle CO_2 emissions and increase fuel economy is using lean-burn gasoline or diesel engines. However, lean-burn engine exhaust contains excess oxygen which makes NO_X reduction challenging. One technology to reduce NO_X emissions from lean-burn engines is NO_X storage and reduction (NSR) catalysis. A NSR catalyst contains precious metals, such as Pt, Pd and Rh for the redox reactions, and alkali or alkaline metal earth components, such as Ba, that trap or store NO_X as nitrite or nitrate species [1-4]. Overall, NO_X is reduced to N_2 over NSR catalysts in five steps, two of which occur in the normal lean-burn exhaust environment, and the latter three in a reductant-rich mode, relative to oxygen [5-7]. These are called the lean and rich, or trapping and regeneration, phases of the cycle. The 5 steps are NO oxidation, NO_2 trapping, reductant evolution, nitrate decomposition and finally NO_X reduction. In the lean phase, NO is oxidized to NO_2 and subsequently trapped by Ba in the form of a nitrate and/or nitrite. Upon saturation of some portion of the trapping material, the rich phase is required to regenerate the surface for further trapping capacity. In the rich phase, reductants, such as H_2, CO, and hydrocarbons (HCs), are introduced to induce nitrate/nitrite decomposition and reduce the trapped or released NO_X to N_2.

Numerous approaches have been explored to achieve the net reducing environment in the rich phase to regenerate the catalyst and reduce the NO_X. These

approaches include spraying diesel fuel into the exhaust (in-pipe injection) [8-10], using on-board fuel reformers to provide CO and H_2 [11-12], and in-cylinder injection of excess fuel (high F/A ratio) [13-14]. During this rich phase, it has been reported that diesel exhaust can, as an example, contain 2-6% CO, 1-2% H_2, 0.3- 0.92% hydrocarbons and less than 0.5% O_2 [15-17]. In previous studies [17-18], different hydrocarbons species were detected in the diesel exhaust including formaldehyde, propylene, ethylene, acetylene, methane and dodecane. These hydrocarbons will be partially consumed by an upstream diesel oxidation catalyst (DOC) during the rich phase either via steam reforming or reacting with the small amount of oxygen in the gas or stored on the catalyst surface. However, some of these hydrocarbons will pass through the DOC to the downstream NSR catalyst. Researchers at Oak Ridge National Laboratory [18] have investigated the amount of reductant (CO, H_2, and HC) prior to and after the DOC and NSR catalysts, with the DOC placed upstream of the NSR catalyst. They found only a small change in reductant level across the DOC during the regeneration event, but a major decrease in the reductant levels across the NSR catalyst.

The hydrocarbons that pass through the DOC can be also be reformed during the rich phase over the NSR catalyst. Furthermore, several previous studies reported that the WGS reaction occurs on precious-metal based catalysts and on three way catalysts (TWCs) [19-23]. In one study, the WGS reaction over a commercial NSR catalyst [23] was investigated and the extent of the WGS reaction ranged from only 10% at 200°C to 91% at 400°C. This reductant amount change makes it difficult to determine whether the CO or H_2 is consistently the active reductant species. Previous work has demonstrated however, that isocyanate species form when CO is present, and these are hydrolyzed to

form N_2 product [24, 25]. This of course complicates the impact of CO, as it can react via the isocyanate route, or via the WGS reaction to form H_2. In terms of the hydrocarbon species, steam reforming can occur to produce H_2. Again, the H_2 produced can ultimately be used as the reductant source for NO_X reduction. The proposed likelihood of steam reforming over NSR catalysts is based on the ease of hydrocarbon steam reforming over precious metal based catalysts [26-31]. For example, previous studies have shown that steam reforming of CH_4, C_3H_8 and C_3H_6 begins at approximately 325 to 350C over Pd and Pt/Rh-based catalysts [30,31]. Such data indicate that if H_2 is a necessary reductant, then NSR catalyst regeneration using such hydrocarbon species may be limited at temperatures below ~350°C, which is in the range that some authors have seen equivalent performance between HCs and H_2.

Regeneration of NSR catalysts using different reductants, such as H_2, CO, and hydrocarbons, and mixture of these reductants, at different operating temperatures has been investigated [32-43]. At low temperatures, there is a consensus that H_2 is better in comparison to CO and HC, possibly due to precious metal site poisoning [40-41] or Ba site poisoning by residual isocyanates [38, 42]. At higher temperatures (T $\geq$ 300°C), H_2, CO, and HC are to some extent comparable in their regeneration and reduction efficiencies [41,43], therefore leaving the active reductant, whether it is H_2 or hydrocarbon, ambiguous.

Although NSR regeneration phenomena have been investigated, to the best of our knowledge, the effects of HCs as the reducing agent on performance and trends in performance have not been systematically studied. In the present study, the regeneration of a NSR catalyst using representative HCs, propylene for short chain, dodecane for long

171

chain and m-xylene for cyclic species, was evaluated. Hydrogen and CO were also used for comparison with the HCs. Hydrocarbon steam reforming and temperature programmed reduction (TPR) experiments were also performed to characterize the performance changes observed as a function of temperature.

7.3 Experimental Methods

A model $Pt/BaO/Al_2O_3$ monolith-supported sample, supplied by Johnson Matthey, was used in this study. The sample is composed of 2.0 g/in3 Al_2O_3, 1.45% Pt and 20% BaO relative to the Al_2O_3. Via H_2 chemisorption, the Pt dispersion was found to be 12%. The sample had a cell density of 300 cpsi and was 2.1 cm in diameter and 6 cm in length. The catalyst was wrapped with 3M catalytic converter matting material and inserted into a horizontal quartz tube reactor, which was placed inside a Lindberg temperature-controlled furnace. Two K-type thermocouples were placed at the radial center of the catalyst. One was just inside the inlet face of the catalyst and one just inside the outlet face of the catalyst. A third was placed approximately 1" upstream of the sample. Small quartz tubes, 3 mm OD and 2 mm ID, were placed upstream of the catalyst to prevent fully developed flow patterns and to assist in heat transfer from the furnace to the gas phase. Preliminary experiments with just an inert phase demonstrated that the temperature difference between the front and back of the catalyst was less than 5°C for all flowrates and temperatures studied.

The gases and gas mixtures were supplied by Praxair. Bronkhorst mass flow controllers were used to meter the gases. For NSR cycling tests, a four-way, fast-acting solenoid valve was used to switch between the lean and rich mixtures, which were made

in separate manifolds. Water was introduced downstream of this valve after the dry gas mixture had been heated. In experiments using dodecane and xylene, the HCs were again metered with Bronkhorst mass flow controllers and introduced after the wet gas mixture had been heated to >170°C to avoid condensation, and at the reactor inlet to avoid reactions on the steel tubing upstream of the quartz tube.

To start each cycling experiment with a consistent surface, before each experiment, the sample temperature was ramped to 500°C and then cleaned, or conditioned, with a gas mixture consisting of 5% H_2O, 5% CO_2, 1% H_2, and a balance of N_2 for 15 min. The reactor was then cooled to the target test temperature. Cycling experiments were performed at 170, 200, 250, 300, 400 and 500°C. Table 7.1 lists the gas compositions used in the cycling experiments. The gas compositions were measured using a MKS MultiGas 2030 FT-IR analyzer at approximately a 2 Hz collection rate. CO, CO_2, NO, NO_2, N_2O, NH_3, H_2O, C_3H_6, C_8H_{10}, and $C_{12}H_{26}$ concentrations were measured. In steam reforming experiments, spatially resolved capillary-inlet mass spectrometry (SpaciMS) was also used. The gases measured by the mass spectrometer were H_2, H_2O, C_3H_6, C_8H_{10}, $C_{12}H_{26}$ and Ar. Ar was used as a tracer in the mass spectrometer for calibration purposes. Spatial resolution was achieved by placing a silica capillary, connected to the sampling end of a 6' capillary from a Hiden Analytical mass spectrometer via a zero dead volume steel union fitting, within one of the radially centered catalyst channels. The capillary dimensions were 0.3 mm I.D. and 0.43 mm O.D. Gases were collected at different positions by moving the silica capillary tip to different positions within the channel.

Two types of TPR experiments were performed; one evaluating the reaction chemistry when C_3H_6 and NO were both introduced together in the gas phase, and one a surface reaction experiment where NO_X species were formed on the catalyst surface and C_3H_6 input after. In the former experiments, the catalyst was cleaned under the conditions described above and then cooled to 109°C. The catalyst was then heated from 109°C to 500°C at a rate of about 3°C/min in a mixture containing 1017 ppm C_3H_6, 257 ppm NO, 5% H_2O, and a N_2 balance. In the latter experiment, the catalyst was heated to 300°C and saturated with NO_X using a mixture containing 350 ppm NO, 10% O_2, 5% CO_2, 5% H_2O, and balance N_2. Then the reactor was cooled to 115°C. The sample was then heated at about 2°C/min to 500°C in a mixture containing 55 ppm C_3H_6 and a N_2 balance. The products from the TPR experiments were monitored using the MKS MultiGas 2030 FT-IR analyzer.

Table 7.1 Details of flow conditions used in the cycling experiments

Flow Conditions	Trapping (lean) phase	Regeneration (rich) phase
Space velocity	$30,000 \text{ hr}^{-1}$	$30,000 \text{ hr}^{-1}$
Concentrations		
NO	350 ppm	0
O_2	10%	0
CO_2	5%	5%
H_2O	5%	5%
H_2	0	1%
CO	0	1%
Hydrocarbons	0	1% relative to C1
N_2	Balance	Balance

7.4 Results and Discussion

7.4.1 NO_X Cycling Experiments

Catalyst NO_X trapping and reduction performance results using different reductants at different temperatures are characterized in this section. This includes evaluating different HCs at the different temperatures to determine when they become efficient as reductants in the regeneration phase. The data shown in Figure 7.1 were obtained at 170°C. The lean, or trapping, time was 40 seconds and the rich, or regeneration, time was 10 seconds. The amounts of reductants used were 1% H_2, 1% CO, or 0.33% C_3H_6 (1% on a C1 basis). Although the amount of C_3H_6 is greater than that of the CO or H_2 on a total reductant basis (in terms of the amount of O species that can be consumed via inclusion of H_2 and CO), an equivalent C1 basis was chosen for these experiments. The conversions and amounts of NO_X (the sum of NO and NO_2) trapped and released during these experiments are listed in Table 7.2. All reported values and plotted data were obtained after steady cycle-to-cycle performance was attained. The data shown in the figure and table demonstrate that H_2 resulted in better trapping performance, consistent with previous work [33,41, 44]. Furthermore, at the onset of the lean phase, the outlet NO_X value reached 0 ppm for many seconds when H_2 was used, but not with CO and C_3H_6. With CO and C_3H_6, saturation of the available trapping sites occurred during the lean phase, whereas with H_2, the outlet NO_X level was still increasing at the end of the lean phase, not having reached the inlet value. The calculated NO_X conversions were 55, 7 and 6%, respectively, with differences primarily due to the significantly lower amounts trapped when using CO and C_3H_6. The total inlet NO_X during the 40-second lean time

175

was 118 µmoles. With H_2 and CO, 841 µmoles were introduced during each regeneration period. Although fewer C_3H_6 moles were input, more was entered based on a C and H basis. The catalyst used in these experiments does not contain any oxygen storage components, such as ceria, so these reductant levels were in large excess relative to the amount required for complete reduction even if all the NO_X was trapped. Therefore, it is inactivity of the CO and C_3H_6 toward regeneration, thus leaving the catalyst surface covered with nitrates, which caused their poorer performance.
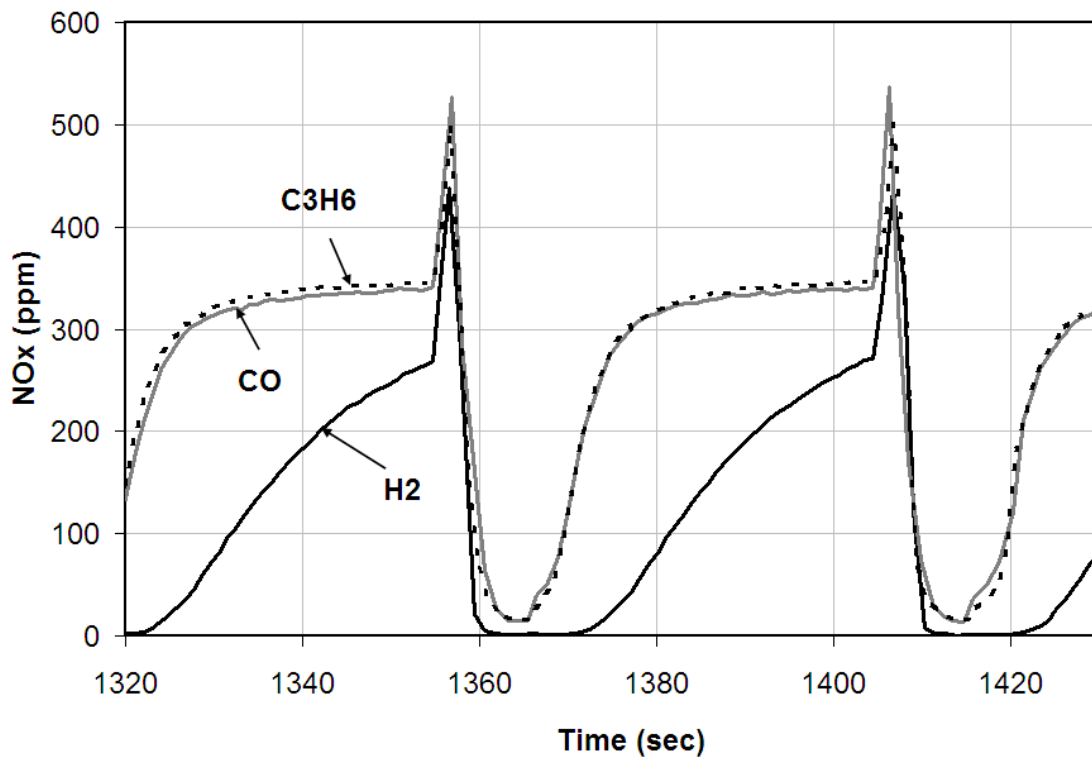
Figure 7.1 NO_X outlet concentrations obtained at 170°C with 1% H_2, 1% CO, or 3333 ppm C_3H_6.

Table 7.2 Calculated performance characteristics as a function of temperature and reducing agent type. The calculated errors associated with these measurements was less than 1% for trapping conditions and less than 2% for regeneration conditions.

Temperature (°C)	Reductant	Time (sec)		NO_X Trapped (µmoles)	NO_X Released (µmoles)	NO_X Conversion (%)
		Lean	Rich			
170	H_2	40	10	74	9.4	55
	CO	40	10	23	14	7.2
	C_3H_6	40	10	21	13	6.4
250	H_2	60	10	81	7.3	42
	CO	60	10	56	25	18
	C_3H_6	60	10	60	24	20
	C_8H_{10}	60	10	52	27	14
	$C_{12}H_{26}$	60	10	63	18	25
300	H_2	80	10	156	6.4	64
	CO	80	10	140	10	55
	C_3H_6	80	10	135	14	51
	C_8H_{10}	80	10	114	33	34
	$C_{12}H_{26}$	80	10	135	15	51
400	H_2	120	10	259	24	67
	CO	120	10	237	31	58
	C_3H_6	120	10	270	16	72
	C_8H_{10}	120	10	250	17	66
	$C_{12}H_{26}$	120	10	251	15	67
500	H_2	80	10	115	38	32
	CO	80	10	117	55	26
	C_3H_6	80	10	118	31	37
	C_8H_{10}	80	10	100	22	33
	$C_{12}H_{26}$	80	10	101	21	34

Experiments were carried out at higher temperatures to further investigate the effect of temperature on the storage, release, and reduction of NO_X with the different reductants. The outlet NO_X concentrations as a function of time at 250°C are shown in Figure 7.2. Dodecane and m-xylene were also tested as reductants at this temperature,

again with 1% on a C1 basis as their inlet concentrations. The summary of the results is also listed in Table 7.2. For this set of experiments, the trapping time was 60 seconds and the regeneration time was 10 seconds. With CO, C_3H_6, C_8H_{10}, and $C_{12}H_{26}$, the NO_X breakthrough profiles during the lean phase were comparable. It should be mentioned that the catalyst performance improved, with CO and C_3H_6, compared to the performance observed at 170°C. It is apparent that both hydrocarbons and CO have some activity toward regenerating the catalyst, albeit significantly less than the H_2. For H_2, the NO_X conversion was actually less than that observed at 170°C.
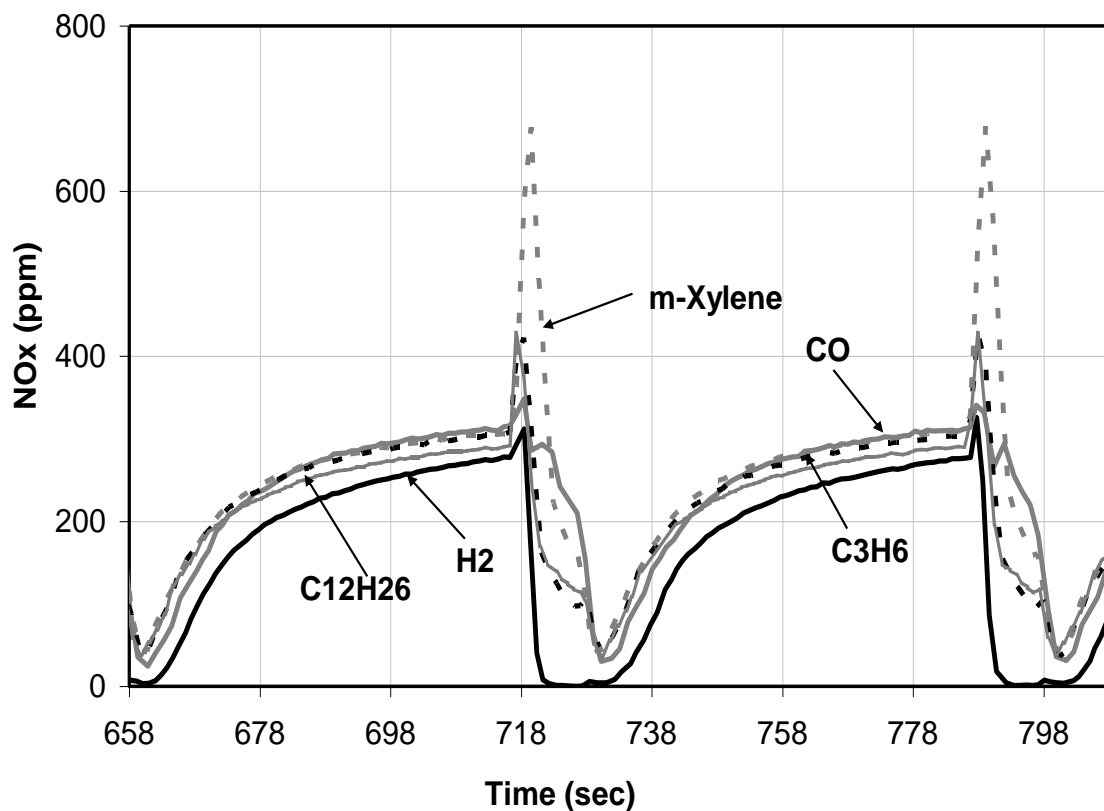
Figure 7.2 NO_X outlet concentrations obtained at 250°C with 1% H_2, 1% CO, 3333 ppm C_3H_6, 833 ppm $C_{12}H_{26}$, or 1250 ppm C_8H_{10}.

This can occur for two reasons. One is simply the longer lean time at 250°C, which will lead to lesser performance. Secondly, a similar trend has been noted before, where performance at temperatures as low as 100°C were as high as those at 200, 250 and 300°C. This trend was related to enhanced regeneration with H_2 when there are substantial hydroxyl amounts on the support surface and their promotion of the reductant spillover to the trapping sites [45].

To decouple the effect of poisoning and slow kinetics, a second set of cycling experiments was performed, at 200 and 250°C, where the rich-phase time was varied. The data obtained from experiments with CO and C_3H_6 at 200°C are shown in Figure 7.3. The lean phase was again 40 seconds but the regeneration times were 5, 10, and 20 seconds. No differences in trapping performance were observed when the regeneration time was increased from 5 to 20 seconds, using either reductant.
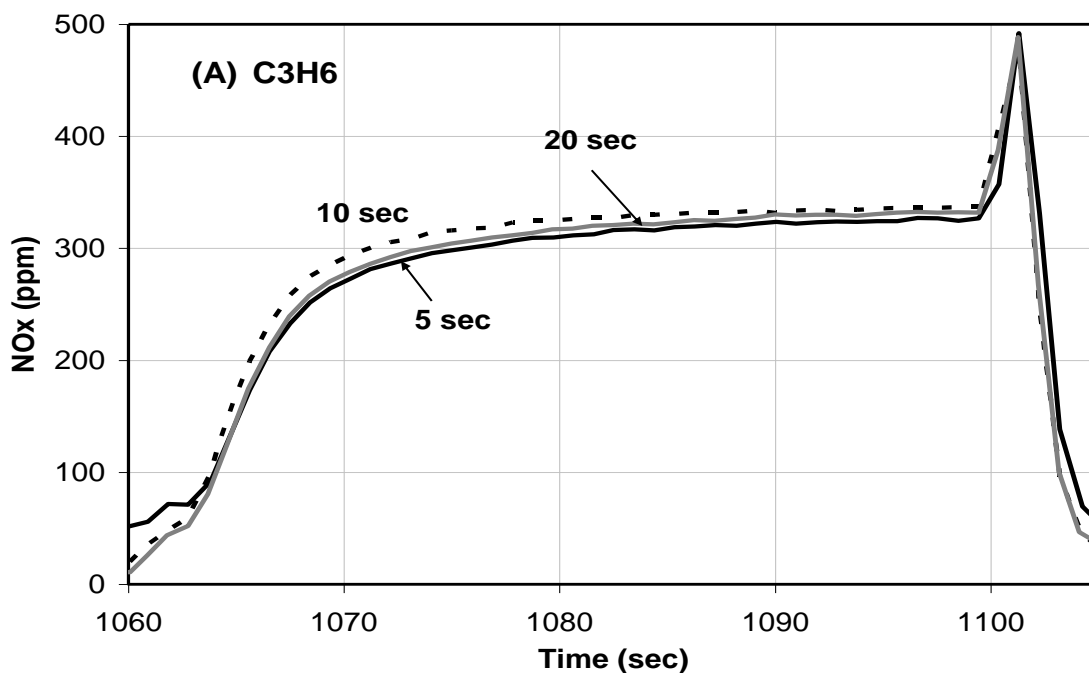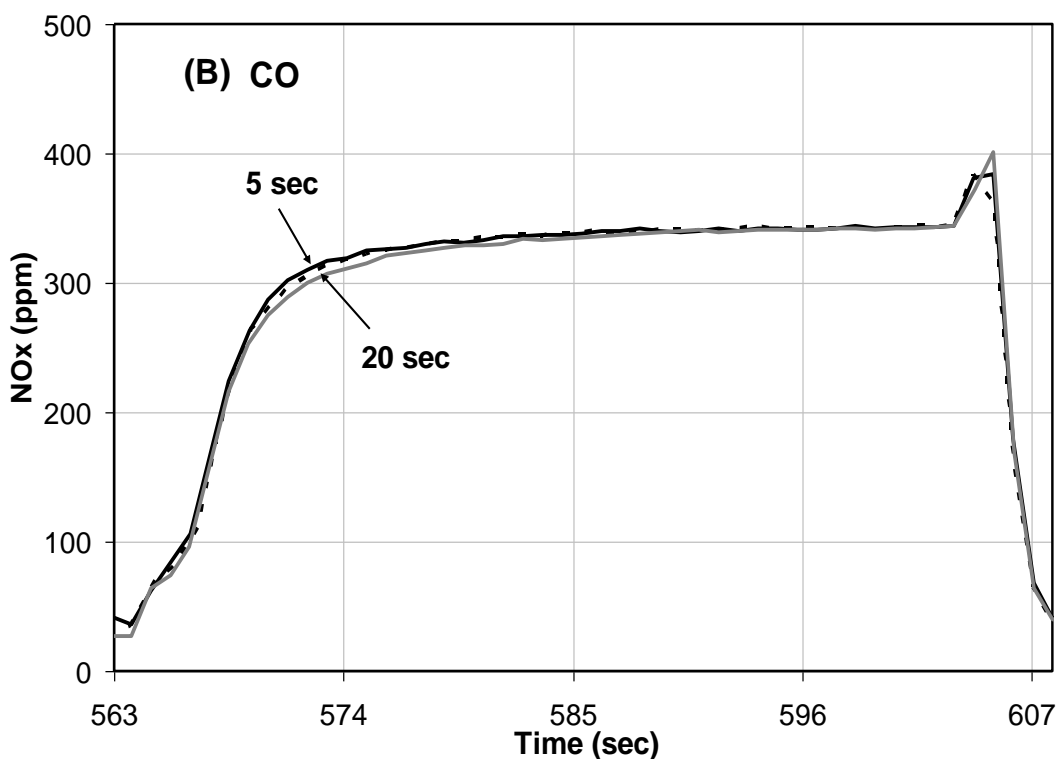
Figure 7.3 NO_X outlet concentrations obtained at 200°C with different regeneration times; 5, 10, and 20 sec. (A) 3333 ppm C_3H_6 and (B) 1% CO.

Data obtained at 250°C are shown in Table 7.3 and Figure 7.4. The lean phase was 60 seconds and again the rich-phase duration was changed between 5, 10, and 20 seconds, with CO, C_3H_6, as well H_2. With all three reductants, increasing rich time resulted in increased performance, for example with CO, the amount trapped increased from 37 to 78 μmoles with the increase from 5 to 20 seconds in rich time. The results shown in Figure 7.4 also suggest that if the rich time was prolonged further, further regeneration might still occur.
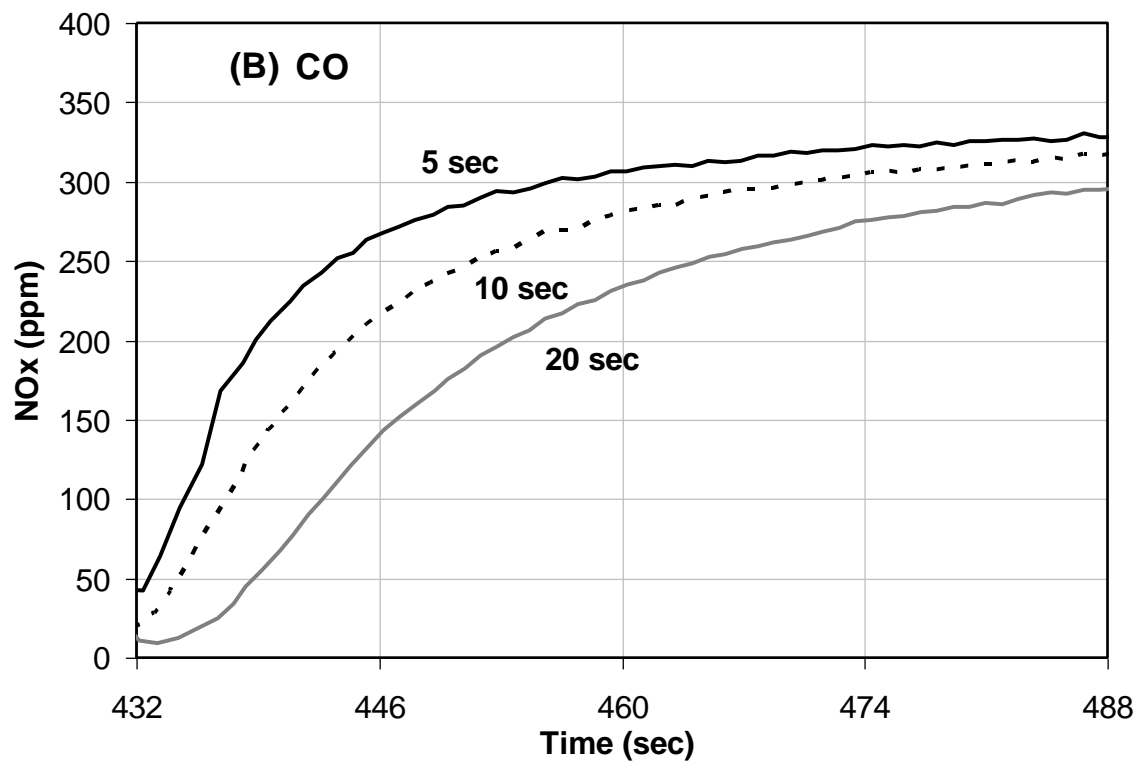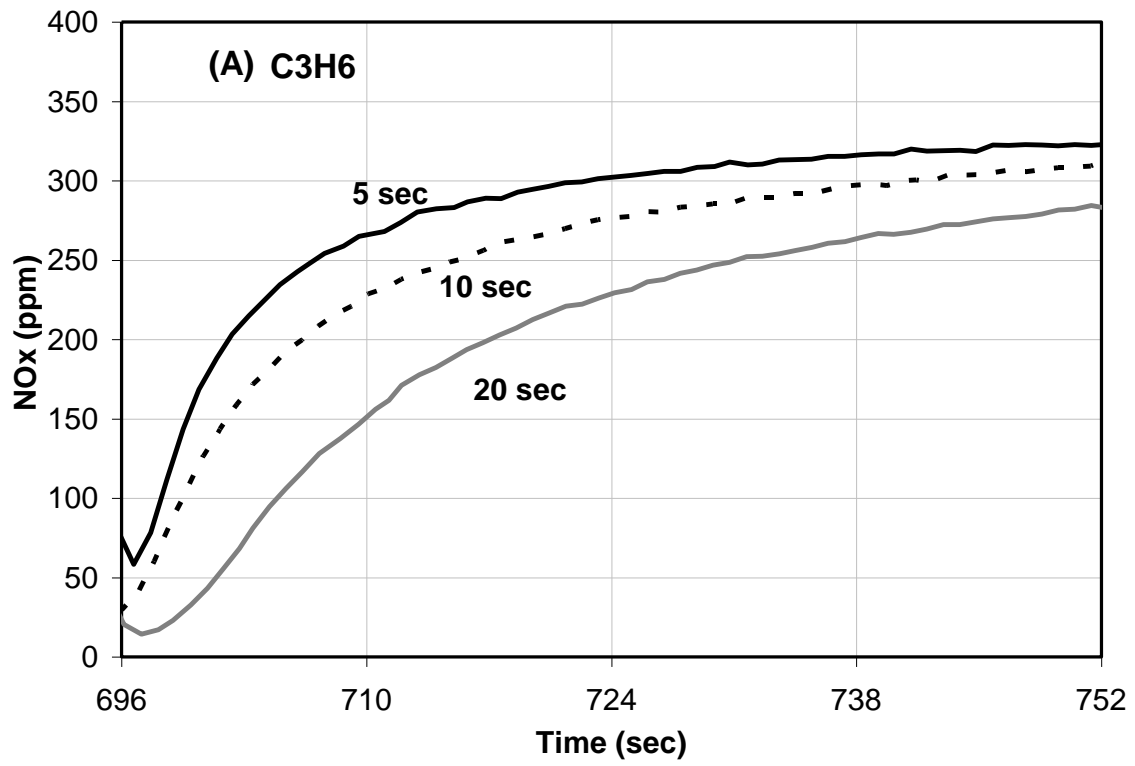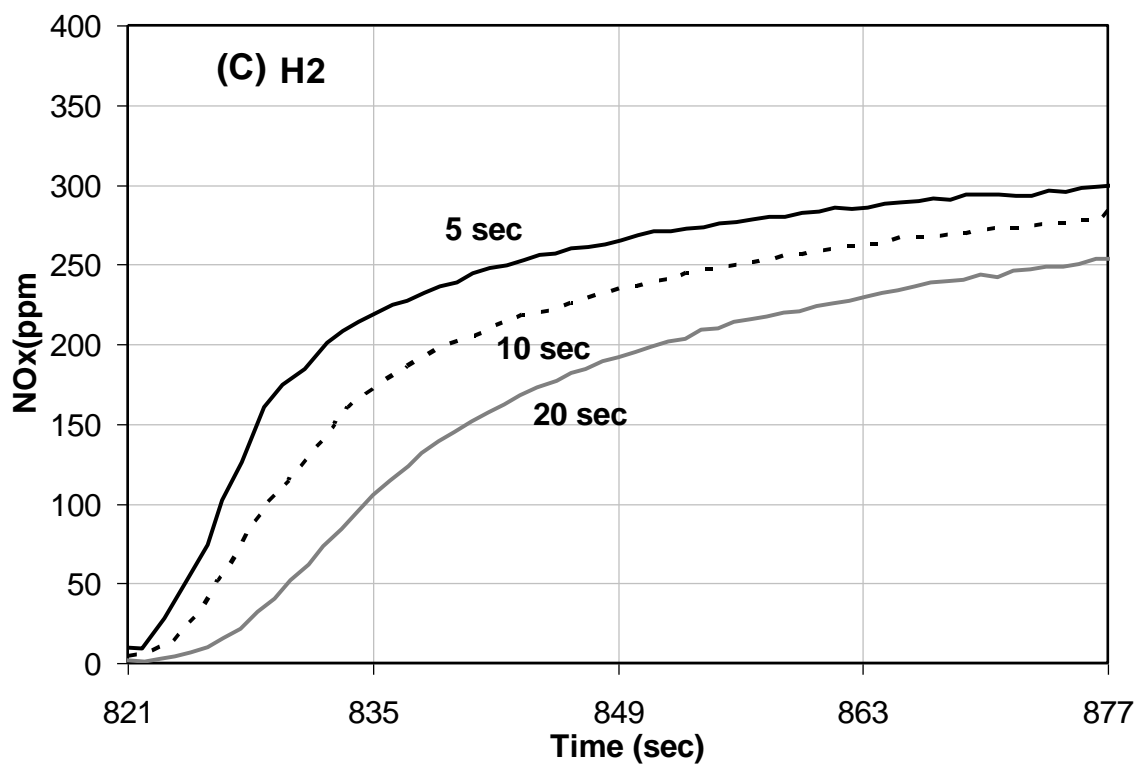
Figure 7.4 NO$_X$ outlet concentrations obtained at 250°C with regeneration times; 5, 10, and 20 sec. (A) 3333 ppm C$_3$H$_6$, (B) 1% CO and (C) 1% H$_2$.

Table 7.3 Calculated performance characteristics as a function of reductant type and regeneration time at 250°C

Reductant Type	Time(sec)		NO$_X$ Trapped (µmoles)	NO$_X$ Released (µmoles)	NO$_X$ Conversion (%)
	Rich	Lean			
CO	5	60	37	15	13
	10	60	54	22	18
	20	60	78	31	27
C$_3$H$_6$	5	60	37	15	13
	10	60	55	17	21
	20	60	80	19	34
H$_2$	5	60	63	8	31
	10	60	81	6.8	42
	20	60	98	6	52

182

The data obtained at 200°C indicate that it is not simply slow kinetics during the rich phase limiting the extent of regeneration, since increasing the rich-phase time had no effect. It is also not a lack of reductant activation as some regeneration does occur, nor is it diffusional resistance differences between the reductants as increased time had no effect for the CO and C_3H_6 species. The poor performance is due to Pt site poisoning by CO and C_3H_6, thereby inhibiting the release and reduction reactions. This is in line with previous NSR catalyst studies using CO and C_3H_6 at low temperature. Abdulhamid et al. [41] investigated the regeneration of a $Pt/BaO/Al_2O_3$ catalyst using CO at 150, 250, and 350°C and attributed the decrease in performance at low temperature to CO poisoning the Pt sites. In another study [46], surface IR results showed adsorbed CO and carbonate species when using CO or C_3H_6 at 200°C as reductants, which also resulted in a lower NO_X storage rate after the switch from the rich phase to the lean phase. However, the results at 250°C indicate that the performance is limited by slow kinetics, although still possibly in combination with some residual Pt site poisoning. If poisoning was stronger/dominant, the performance would not have improved with each increase in the rich time, as was the case at 200°C. Surface diffusion limitations may play a role, but this would be coupled with poisoning. Previous work has shown isocyanate formation when CO was used as a reductant [42] and the authors concluded that these formed around the Pt sites, which could cause blocking of further surface transport. Such results also demonstrate that reductant spillover from the precious metal sites to the Ba trapping sites occurs, suggesting spillover direction.

The data obtained at 300°C are shown in Figure 7.5, with summary data listed in Table 7.2. There was an improvement in the catalyst performance with CO and

hydrocarbons, relative to 250°C, but H_2 still showed better activity in both trapping and reduction performance. With H_2, the calculated NO_X conversion was 64%, while with CO it was 55%. Propylene and $C_{12}H_{26}$ led to slightly lower but similar conversions, indicating persistent kinetic limitations related to regeneration and reduction. With C_8H_{10}, the catalyst performance was significantly poorer, with the measured conversion being 34%. The poor performance with C_8H_{10} compared to C_3H_6 or $C_{12}H_{26}$ is likely related to its cyclic nature, where it is assumed that activation of cyclic hydrocarbons is more difficult than the straight chain hydrocarbons [47].
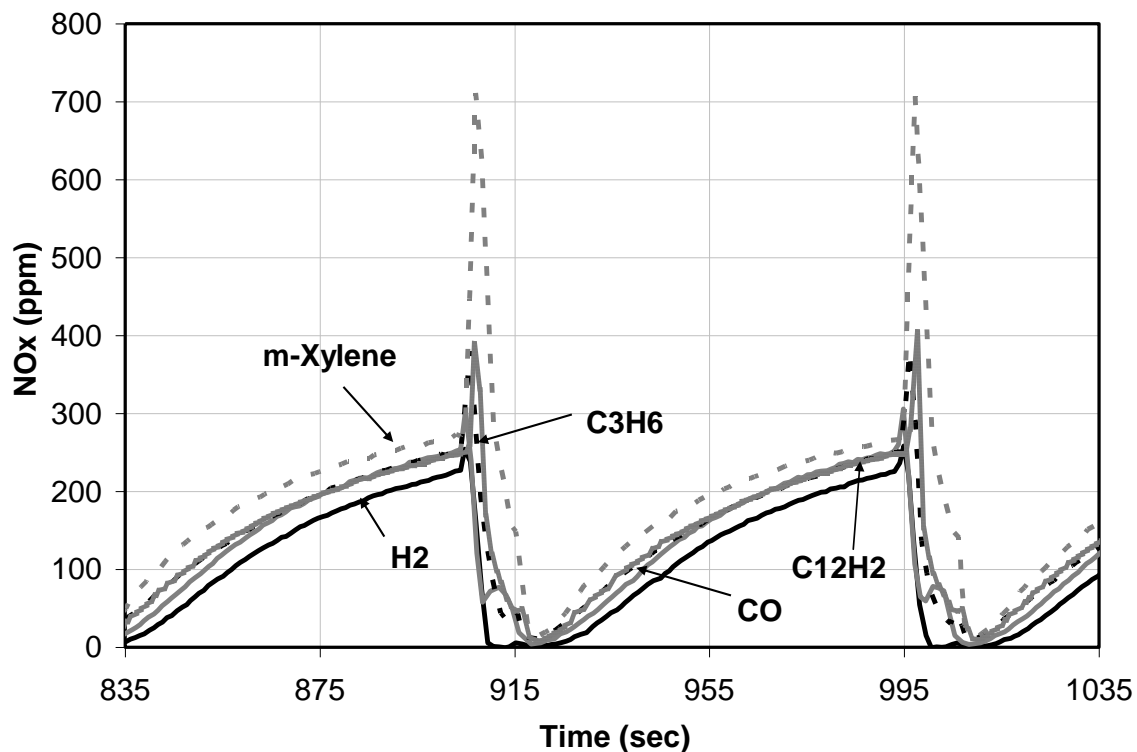
Figure 7.5 NO_X outlet concentrations obtained at 300°C with 1% H_2, 1% CO, 3333 ppm C_3H_6, 833 ppm $C_{12}H_{26}$, or 1250 ppm C_8H_{10}.

At 300°C, NO_X trapping and conversion performance was better with H_2 compared to CO and hydrocarbons and CO was better than the hydrocarbons. The reasons for the improved performance with CO as the temperature was increased has been previously studied and is explained by decreased CO poisoning and increased hydrolysis of cyanates, which form from direct reduction of the nitrate species by CO [40,48]. In general, the increased performance at 300°C when using the hydrocarbon reductants has been attributed to reductant activation vs. temperature [41]. Thus, as the temperature increased from 170 to 300°C, the activation of hydrocarbons on the Pt sites became easier and faster, and poisoning effects decreased, resulting in the higher reduction activity. This is in line with previous work that has shown similar trends and concluded that once C-H bond activation occurred, HCs could act as reductants [49]. In terms of improved performance for all the reductants, there is an increased surface diffusion rate with temperature [50-52], higher NO oxidation rates [53-54], and higher nitrate/nitrite decomposition rates during regeneration [5,54], all of which typically lead to improved NSR catalyst performance at test temperatures below 400°C.

Experiments at 400 and 500°C were also performed with summary data listed in Table 7.2. At 400°C, the amount of NO_X released was actually higher with H_2 relative to m-xylene and dodecane, leading to overall similar conversions. With C_3H_6, the catalyst performance was better than that observed with the other reductants, due to the higher overall reductant level introduced when counting both the H and C components as reductants. Similarly, there is more when using the m-xylene and dodecane, and with their similar performance to H_2, suggests that there is still some limitation with their use. At 500°C, catalyst performance was lower than that observed at 300, 350, and 400°C,

with all reductants. The amounts of NO_X trapped with H_2, CO and C_3H_6 were comparable, but there were differences in the amounts of NO_X released, with CO leading to higher release. Although the trapping performance was lower with C_8H_{10} and $C_{12}H_{26}$ compared to that observed with H_2, CO, and C_3H_6, the lower NO_X release during the rich phase led to comparable conversions. The reason for the decreased performance relative to 300 and 400°C is due to nitrate stability. The nitrate species decompose rapidly at the onset of regeneration due to their low thermal stability at high operating temperatures [55-56]. As the reductant is being used to regenerate NO_X species trapped at the upstream sites, NO_X species are rapidly decomposing at downstream sites and will travel through the catalyst without being reduced, leading to a lower ratio of rate of reduction to rate of NO_X release [57-58]. Also, due to their lower stability at higher temperature, less nitrates form during the trapping phase as well.

Two mechanisms have been proposed for reduction of NO_X to N_2 by hydrocarbons over the precious metal sites of NSR catalysts. The first mechanism [59] postulates that the reductant reduces the precious metal site, which then participates in NO decomposition. In the second mechanism [60], the reductant, C_3H_6 was selected as an example, is first adsorbed on the precious metal site and then breaks down to various types of reactive hydrocarbon sub-species [5]. The reactions pathways listed in reference [60] are shown below:

$$C_3H_6 \, (g) + Pt \rightarrow Pt\text{-}C_3H_6 \tag{7-1}$$

$$Pt\text{-}C_3H_6 + 2Pt \rightarrow 3 \, Pt\text{-}CH_2 \tag{7-2}$$

$$Pt\text{-}CH_2 + 3Pt\text{-}NO \rightarrow 4 \, Pt + CO_2 \, (g) + H_2O \, (g) + 1.5 \, N_2 \, (g) \tag{7-3}$$

For the sake of simplicity, the authors suggested CH_2 as the hydrocarbon sub-species formed from propylene decomposition. They proposed that the bound intermediate CH_2 group reacts with the sorbed NO_X species to form the reduction reaction products. In several IR characterization studies [49,61-64] nitro, organic nitro, nitrite and isocyanate surface species were observed on Ce-ZSM-5 and Pt/SiO_2 surfaces during lean- NO_X reduction tests and were suggested intermediates in this reaction process, supporting the CH_2-based mechanism shown above. However, a third possibility, due to the reaction mixtures imposed, is that hydrocarbons undergo steam reforming, producing CO and H_2, which act as the actual reductant species. This is discussed in the following section.

7.4.2 Hydrocarbon Steam Reforming

In cycling experiments, decreased catalyst performance at low temperatures using CO or hydrocarbons was related to Pt site poisoning, or slow kinetics as the temperature increased to 250°C. However, at higher operating temperatures (T ≥ 300°C), there was a significant improvement in the catalyst performance using hydrocarbons. A similar improvement was observed with CO as the reductant as well, which has been well explained in recent literature [40,48], thus the focus of this discussion will be on the hydrocarbons. In the rich phase, hydrocarbons and H_2O are both present and therefore steam reforming could occur, leading to H_2 which could then act as the reductant. To investigate this possibility, hydrocarbon steam reforming was evaluated at different temperatures.

In this series of experiments, steam reforming of C_3H_6, $C_{12}H_{16}$, and C_8H_{10}, and mixtures of these, were investigated. The reaction gas mixtures used in these experiments

187

contain 5% H_2O, 1% hydrocarbon on a C1 basis, and a balance of N_2. Experiments were carried out at different test temperatures, ranging between 250 and 525°C with no reaction observed at less than 375°C. Spatially resolved capillary-inlet mass spectrometry (SpaciMS) was used to quantify the amount of hydrocarbons, CO_2, H_2O, and H_2 at different catalyst positions. The capillary tip was moved to seven different positions within the channel to study the axial distribution of the species. In the plotted data, the zero position represents the inlet of sample and 6 cm represents the end of sample.

Figure 7.6 H_2 concentrations obtained at different temperatures and lengths of the catalyst during steam reforming experiments. The inlet gas composition was 3333 ppm C_3H_6, 5% H_2O, and balance N_2.

Propylene steam reforming results, obtained along the catalyst length at different temperatures, are shown in Figure 7.6. At 375°C, C_3H_6 steam reforming occurs, but with

very low conversions. As the temperature was increased to 525°C, H_2 production monotonically increased, with more significant increases after 475°C. H_2 production steadily increased as a function of catalyst length.

Similar experiments were also carried out, but with dodecane or m-xylene as the hydrocarbons. The H_2 production data as a function of temperature and axial length of the catalyst are shown in Figures 7.7 and 7.8.

Figure 7.7 H_2 concentrations obtained at different temperatures and lengths of the catalyst during steam reforming experiments. The inlet gas composition was 833 ppm $C_{12}H_{26}$, 5% H_2O, and balance N_2.

Dodecane steam reforming started slightly below 450°C, higher than that observed with C_3H_6 (375°C). At 525°C, H_2 production was 91, 690, and 1195 ppm at 0, 3, and 6 cm respectively, while the amount of H_2 formed with C_3H_6 at 525°C was 172, 6551 and 7973

ppm. The outlet level with C_3H_6 was approximately 6.6 times higher than that observed with dodecane at the same temperature. M-xylene steam reforming started at just below 475°C and the amounts of H_2 formed were significantly lower than those with the other hydrocarbons. Again, H_2 formation increased with temperature, but even at 525°C, only 20, 238, and 507 ppm were formed at 0, 3, and 6 cm inside of the sample, respectively, much lower than those observed with C_3H_6 and $C_{12}H_{26}$.
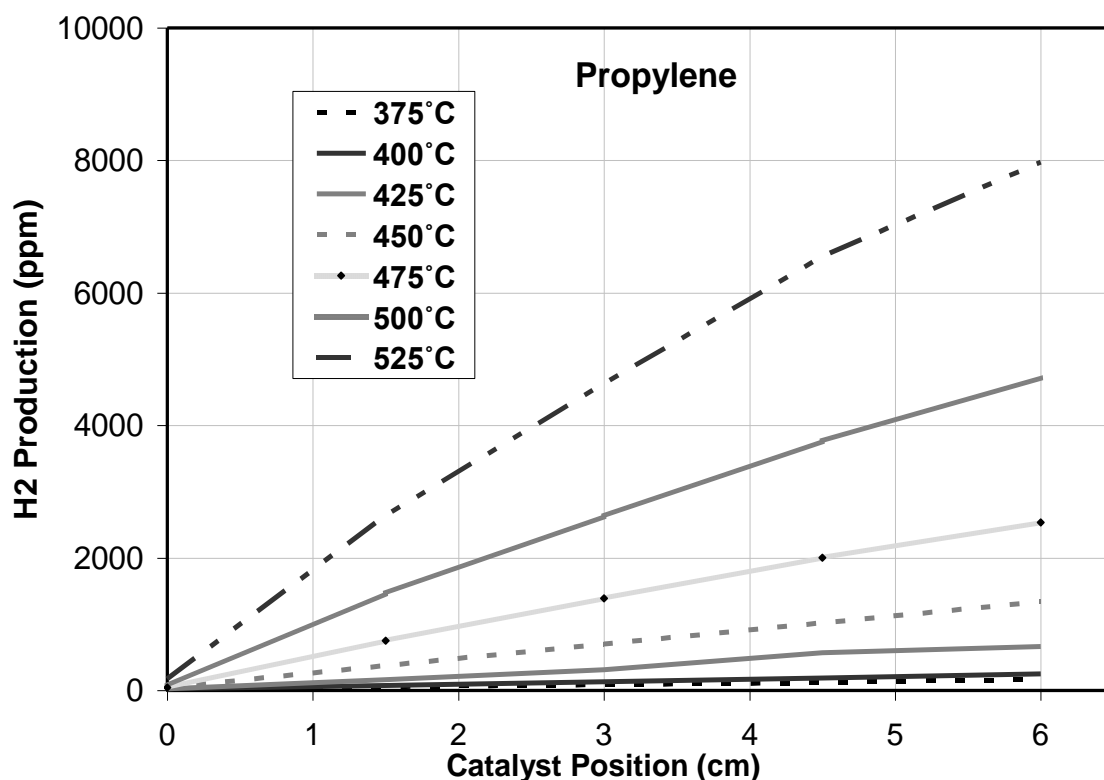

Figure 7.8 H_2 concentrations obtained at different temperatures and lengths of the catalyst during steam reforming experiments. The inlet gas composition was 1250 ppm C_8H_{10}, 5% H_2O, and balance N_2.

These results, as expected, show that different hydrocarbon types undergo steam reforming at different temperatures and with different rates on the NSR catalyst. It should

be noted that there is some measured conversion at the front of the catalyst. The capillary tip is positioned at the very edge of the sample, so will probe conversion that could occur at the face. Also, dodecane and m-xylene will homogeneously decompose in the reactor at temperatures above 320-330°C (based on empty reactor baseline experiments) and thus could lead to byproducts that are more easily reformed to H_2, even at or on the catalyst face.

H_2 production rates via steam reforming with a mixture of C_3H_6 and $C_{12}H_{26}$ were also investigated, with the data shown in Figure 7.9. According to the results obtained, there was no change in the amount of dodecane in any of these tests demonstrating that no dodecane steam reforming occurred. C_3H_6 steadily decreased along the catalyst length; therefore, the amount of H_2 measured originated solely as a result of C_3H_6 steam reforming. There were only slight differences in the amount of H_2 formed via C_3H_6 steam reforming in the absence and presence of dodecane at both 375 and 400°C. However, at the higher temperatures, significantly less H_2 was formed in the presence of dodecane. For example, at 525°C and in the absence of dodecane, the amount of H_2 formed was 7973 ppm whereas in presence of dodecane, the amount of H_2 produced was 3738 ppm. This indicates that dodecane inhibited C_3H_6 steam reforming, but at the same time C_3H_6 inhibited dodecane steam reforming. The latter is likely due to the higher reactivity of the C_3H_6 while the former is possibly due to the coverage of some metallic sites by the longer chain hydrocarbons, resulting in lower availability of metallic sites for adsorption of reactants.

These results show that steam reforming over a NSR catalyst can occur when hydrocarbons and water are present in the gas stream. Different hydrocarbon types have

different reactivities towards steam reforming. This could be related the extent of which the hydrocarbons can be activated on the surface of precious metals. Since steam reforming did not occur below 375°C for C_3H_6 and 450°C for $C_{12}H_{26}$ and C_8H_{10}, steam reforming cannot explain the improved performance in the cycling experiments at 300 to 400°C described above. Furthermore, even at 375 and 450°C, the amounts of H_2 produced were quite small, and built through the catalyst, such that at the catalyst front little H_2 was present until the higher temperatures.
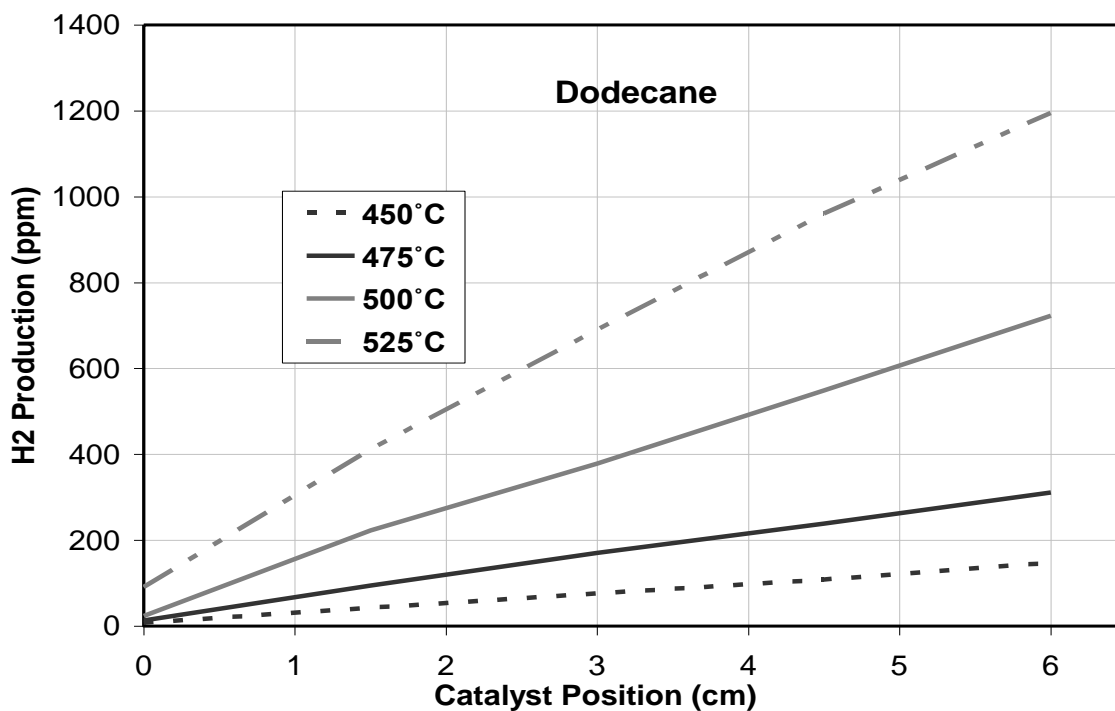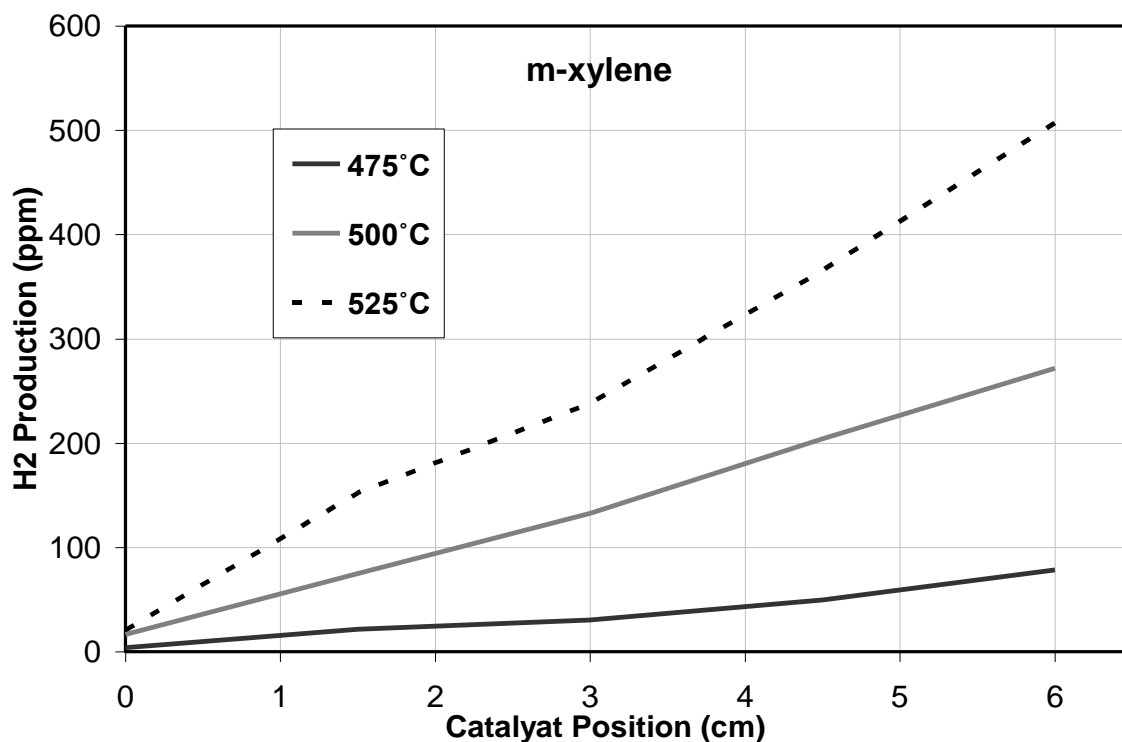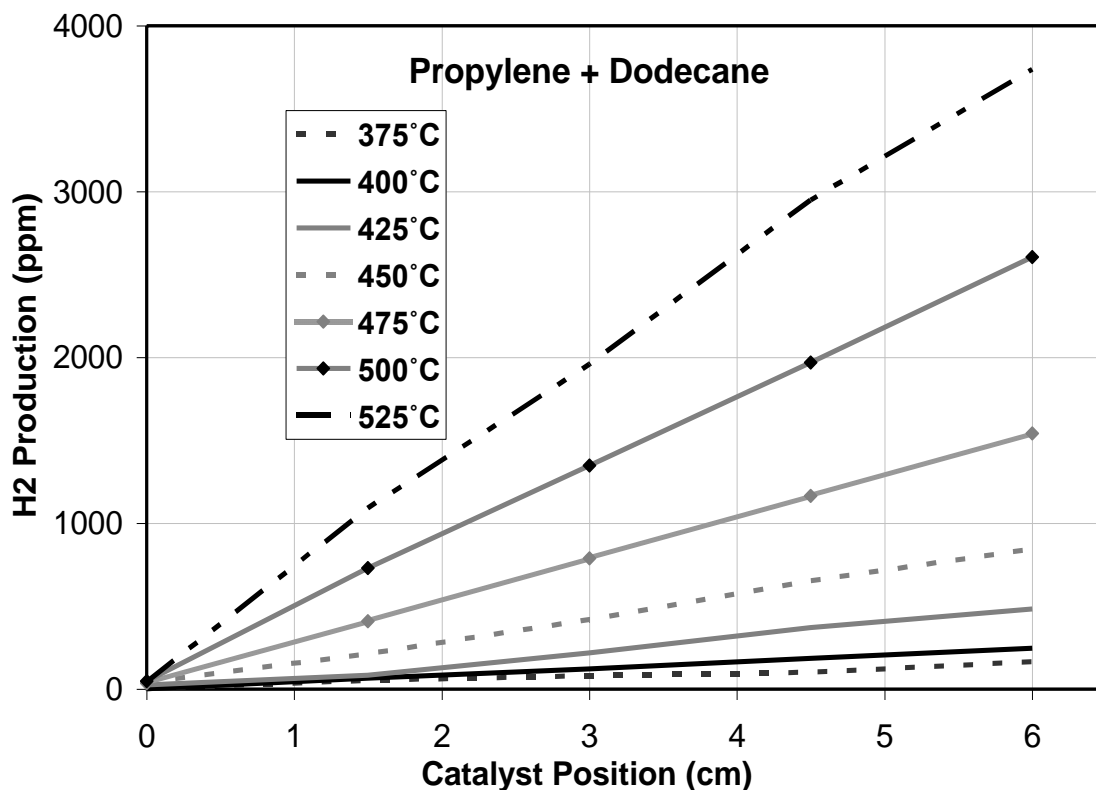

Figure 7.9 H_2 concentrations obtained at different temperatures and lengths of the catalyst during steam reforming experiments. The inlet gas composition was 3333 ppm C_3H_6, 833 ppm $C_{12}H_{26}$, 5% H_2O, and balance N_2.

These data therefore demonstrate that steam reforming does not play a critical role in NSR regeneration below 450°C. This is not to say that reforming is unimportant for NSR activity in general, as desulfation occurs at much higher temperatures, where steam reforming can have a more significant contribution.

7.4.3 TPR Experiments

In the previous section, hydrocarbon steam reforming was investigated and the data show that reforming to H_2 is not significant enough to explain the improved performance observed above 300°C when using hydrocarbons as reductants. To further investigate this issue, TPR experiments were performed with propylene selected as the reductant. Two types of experiments were performed; one where both the NO and C_3H_6 were simultaneously present in the gas phase and one where NO was first trapped on the catalyst and then C_3H_6 was input for the TPR.

In the first set of experiments, the catalyst was first cleaned with a gas mixture consisting of 5% H_2O, 5% CO_2, 1% H_2, and a balance of N_2 for 15 min at 500°C. The reactor was then cooled to down to 109°C. The catalyst was heated from 109°C to 500°C at approximately 3.3°C/min in a mixture containing 1017 ppm C_3H_6, 257 ppm NO, 5% H_2O, and a N_2 balance. The profiles of C_3H_6 and NO consumption as a function of temperature are shown in Figure 7.10. The reaction between C_3H_6 and NO started at approximately 200°C, but at low rates and lit-off beginning at 217°C. Full conversion of NO was observed by 287°C. In terms of a mass balance, if the reduction equation is assumed as follows, $9NO + C_3H_6 \rightarrow 4.5\ N_2 + 3CO_2 + 3\ H_2O$, then for 9 moles of NO, 1 mole of C_3H_6 is required for reduction to N_2. At 287°C, all inlet NO, 257 ppm, was

consumed and therefore ~29 ppm of C_3H_6 should be consumed as well for the reduction. But, as shown in Figure 7.10, approximately 41 ppm of C_3H_6 was consumed at 287°C. The excess amount of C_3H_6 reacted went toward production of CO and other short chain hydrocarbons via partial oxidation and reaction, as both CO and ethylene were detected by FT-IR.
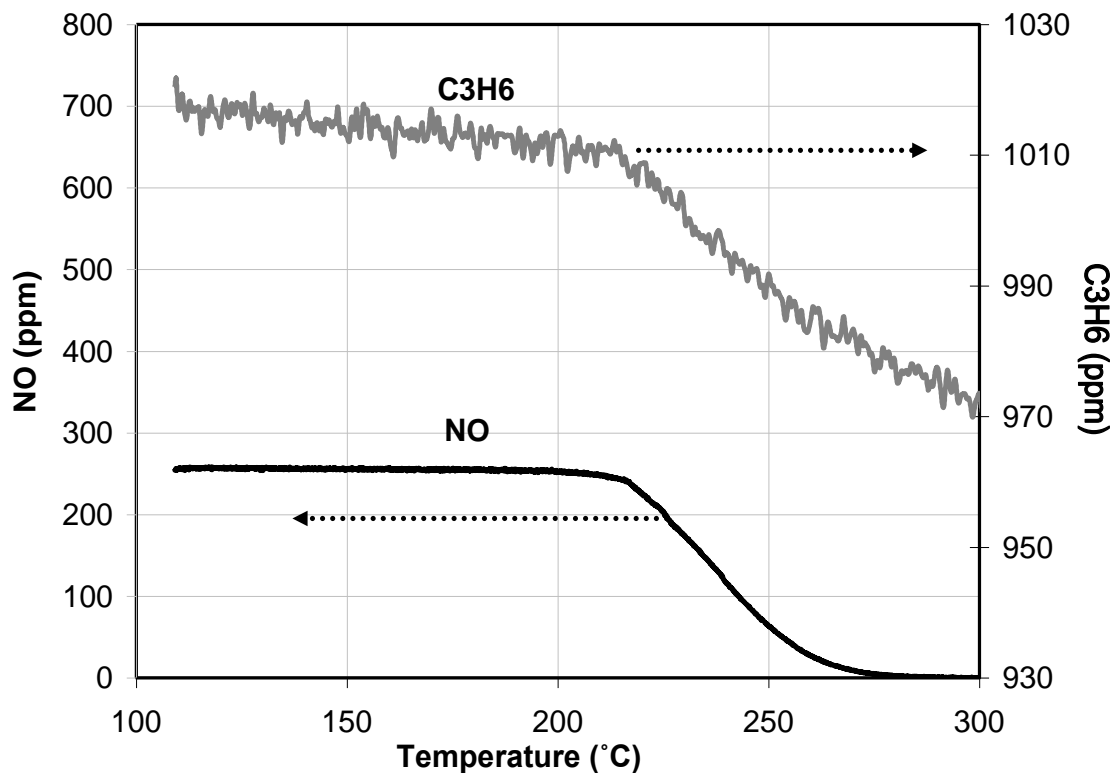
Figure 7.10   NO and C_3H_6 outlet concentrations obtained during a temperature programmed reduction experiment; the ramp rate was 3.3°C/ min. The inlet gas composition was 1017 ppm C_3H_6, 257 ppm NO, 5% H_2O, and balance N_2.

There have of course been several studies focused on NO_X reduction by hydrocarbons, but in the presence of O_2 (HC-SCR) [65-67]. Results from each of these studies indicate a similar temperature range in which C_3H_6 begins to reduce NO_X, even in the presence of

O_2, again suggesting the activation of C_3H_6, or the HC species in general, as a determining factor for regeneration temperature dependency. Furthermore, and as discussed earlier, with a $Pt/Ba/Al_2O_3$ catalyst [68], a mixture containing C_3H_6 and O_2 reacted with surface NO_X species at approximately 230°C, again in the same range as that observed here.

In the second experiment, the catalyst was heated to 300°C and saturated with NO_X using a mixture containing 350 ppm NO, 10% O_2, 5% CO_2, 5% H_2O, and a N_2 balance. Then the reactor was cooled to 115°C. The sample was then heated at 2.1°C/min to 500°C in a mixture containing 55 ppm C_3H_6 and a N_2 balance. Propylene consumption as a function of temperature is shown in Figure 7.11. Little to no change in the C_3H_6 concentration was observed before 175°C. Beyond that, there was a steady decrease in the C_3H_6 concentration until 264°C, where the maximum consumption of C_3H_6 was observed. The C_3H_6 consumption rate then decreased beyond 272°C as the surface NO_X species, thus reaction reactant, were depleted. Anderson et al. performed TPR experiments on a $Pt/Ba/Al_2O_3$ catalyst with a stoichiometric C_3H_6/air mixture and observed maxima in NO_X release just above 200°C [69]. This being done in an air-containing mixture resulted in some temperature increase due to the exotherm that would evolve from C_3H_6 combustion, thus their measured temperatures for NO_X release would be lower than those observed in our study. Furthermore, NO_X was not observed as a product with just C_3H_6 entering, indicating more complete reduction of the surface species. Jozsa et al. [33] also carried out TPR experiments, but on a commercial NSR catalyst, with C_3H_6, H_2, and CO. When the C_3H_6/N_2 mixture was used, NO_X release reached a plateau at 250°C, slightly lower than that observed in our experiments. This is

likely attributed to the trapping conditions, where NO_2 was stored between 60 and 100°C. Saturating the catalyst at 300°C, as in our study, would lead to states with higher stability than those formed with exposure at lower temperatures.
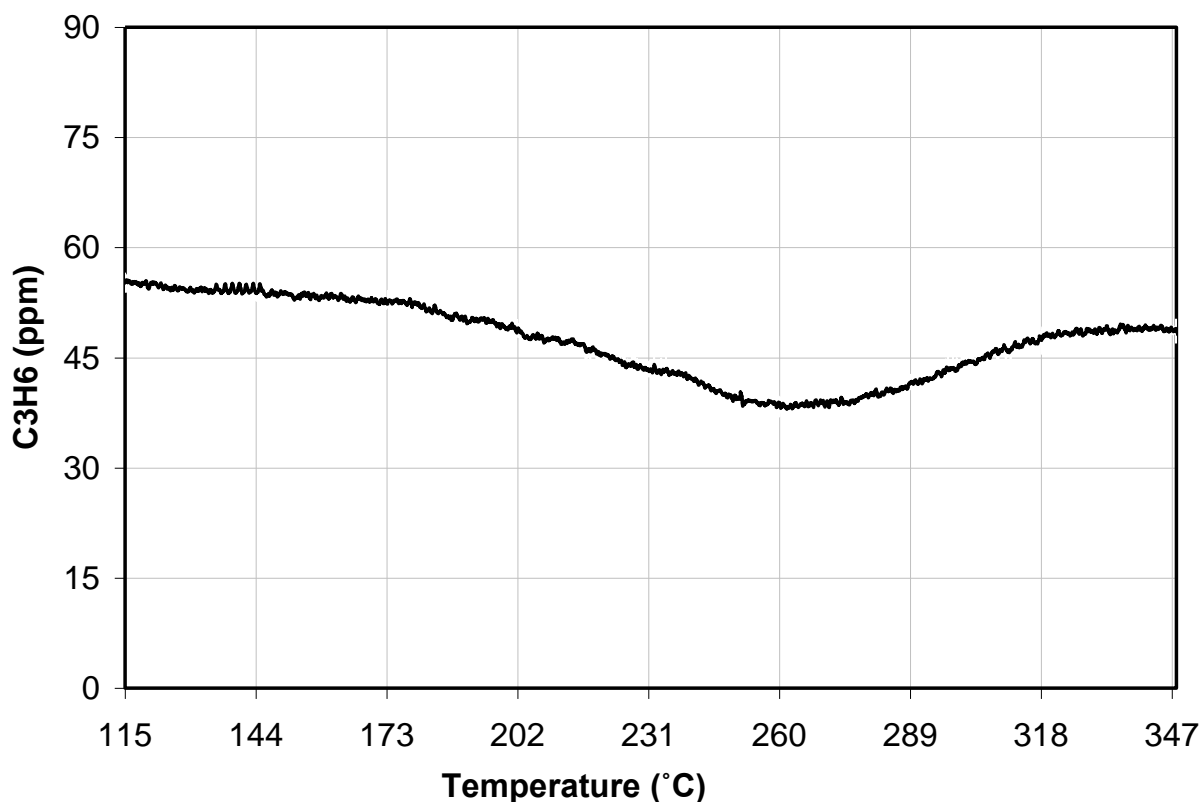
Figure 7.11 C_3H_6 outlet concentrations obtained during a temperature programmed reduction experiment; the ramp rate was 2.1°C/ min. The catalyst was first heated to 300°C and saturated with NO_X using a mixture containing 350 ppm NO, 10% O_2, 5% CO_2, 5% H_2O, and a N_2 balance. The reactor was then cooled to 115°C to start the TPR experiment. The TPR gas composition contained 55 ppm C_3H_6 and a N_2 balance.

At 200°C, as shown in Figure 7.2, C_3H_6 and CO poisoning of Pt sites was evident by the lack of improvement with increased regeneration times. The TPR data in Figure

7.10 show that NO reduction with C_3H_6 begins at temperatures slightly above 200°C, with little activity at 200°C, in-line with the cycling experiment data. At T ≥ 217°C, the C_3H_6 and NO reaction is evident over the catalyst with complete reduction observed at 287°C. Similarly, when reducing the previously trapped NO_X species (Figure 7.11), some reaction extent is observed ~200°C, with increasing reactivity as the temperature was increased. Thus at 250°C (Figure 7.4), where extending the regeneration time did have a positive effect, it is related to slower kinetics, not complete poisoning by, or inactivity, of the hydrocarbon, nor to steam reforming of the hydrocarbon species. At T ≥ 287°C, based on the TPR and cycling experiments, the activation of C_3H_6 is not an issue and therefore a more comparable performance with H_2 would be expected.

7.5 Conclusions

In this study, the effects of different reducing agents (hydrocarbons, CO and H_2) on the performance of a model NSR catalyst were investigated. In cycling experiments, H_2 was the best reductant for catalyst regeneration at 170°C and the poor performance with hydrocarbons and CO was due to Pt site poisoning. At 250°C, H_2 was still superior and the poorer catalyst performance with hydrocarbons and CO was due to their slow reactivity and not solely because of poisoning effects. At T ≥ 300°C, hydrocarbons and CO were comparable with H_2. Hydrocarbon steam reforming experiment results show that steam reforming alone cannot explain the improved performance since steam reforming of dodecane and m-xylene occurred at T ≥ 450°C. With propylene, steam reforming occurred at 375°C, but the small amount of H_2 formed was not enough to result in comparable performance to CO and H_2 in regenerating the NSR catalyst. TPR

experiments were also performed and the results show that the reduction of NO by C_3H_6 can start at 217°C. Moreover, propylene can also induce nitrate decomposition and reduction at ~ 200°C. Thus as the reaction temperature exceeds 200°C, the hydrocarbons become directly active over the NSR catalyst, but are kinetically limited. At T > 300°C, the regeneration-phase reaction rates with hydrocarbons become appreciable enough to make the extent of regeneration comparable to that with H_2.

7.6 Acknowledgements

References

1. N. Takahashi, H. Shinjoh, T. Iijima, T. Suzuki, K. Yamazaki, K. Yokota, H. Suzuki, N. Miyoshi, S. Matsumoto, T. Tanizawa, T. Tanaka, S. Tateishi, and K. Kasahara, Catalysis Today 27(1996)63.

2. W. Bogner, M. Kramer, B. Krutzsch, S. Pischinger, D. Voigtlander,G.Wenninger, F. Wirbeleit, M. Brogan, R. Brisley, and D. Webster, Applied Catalysis B: Environmental 7(1995)153.

3. S. Matsumoto, Catalysis Today 29(1996)43.

4. N. Miyoshi, S. Matsumoto, K. Katoh, T. Tanaka, J. Harada, N. Takahashi, K. Yokota, M. Sugiura, and K. Kasahara, SAE Technical Paper Series 950809.

5. W. S. Epling, L.E. Campbell, A. Yezerets, N. W. Currier and J. E. Parks, Catalysis Reviews 46(2004)163.

6. B. Westerberg and E. Fridell, Journal of Molecular Catalysis A: Chemical 165 (2001)249.

7. S. Poulston and R.R. Rajaram, Catalysis Today 81(2003)603.

8. J.E. Parks, A. Watson, G.C. Campbell, and W. S. Epling, SAE Technical Paper Series 2002-01-2880.

9. J. H. Stang, D. E. Koeberlein, and M. J. Ruth, SAE Technical Paper Series 2001-01-2065.

10. Y. Takahashi, Y. Takeda, N. Kondo, and M. Murata, SAE Technical Paper Series 2004-01-0580.

11. Y. Kong, S. Crane, P. Patel, and B. Taylor, SAE Technical Paper Series 2004-01-0582.

12. N. Khadiya, S. Crane, C. Huffmeyer, and B. Taylor, SAE Technical Paper Series 2004-01-2648.

13. D. Tomazic, M. M. Tatur, and M. J. Thornton, SAE Technical Paper Series 2004-01-0581.

14. K. Nakatani, S. Hirota, S. Takeshima, K. Itoh, and T. Tanaka, SAE Technical Paper Series 2002-01-0957.

15. S. Huff, B. H. West, J. Parks, M. Swartz, J. Green and R. Graves, SAE Technical Paper Series 2006-01-1416.

16. H. Mahzoul, P. Gilot, J.-F. Brilhac and B.R. Stanmore, Topics in Catalysis 16/17(2001) 293.

17. M. Swartz, S. Huff, J. Parks and B. H. West, SAE Technical Paper Series 2006-01-3423.

18. B. H. West, S. Huff, J. Parks, S. Lewis, J.-S. Choi, W. Partridge, and J. Storey, SAE Technical Paper Series 2004-01-3023.

19. C. Serre, F. Garin, G. Belot, and G. Marie, Journal of Catalysis, 141(1993)1.

20. J. Barbier and D. Duprez, Applied Catalysis B: Environmental 3(1993)61.

21. J. Kaspar, P. Fornasiero, and N. Hickey, Catalysis Today 77(2003)419.

22. J. Botas, M. Gutierrez-Ortiz, M. Gonzalez-Marcos, J. Gonzalez-Marcos, and J. Gonzalez-Velasco, Applied Catalysis B: Environmental 32(2001)243.

23. M. AL-Harbi, W. S. Epling, A. Yezerets, N. W. Currier, H.-Y Chen and H. Hess, SAE Technical Paper Series 2009-01-0631.

24. T. Szailer, J. H. Kwak, D. H. Kim, J.C. Hanson, C. H. F. Peden, and J. Szanyi, Journal of Catalysis 239(2006)51.

25. J.P. Breen, R. Burch, C. Fontaine-Gautrelet, C. Hardacre, and C. Rioche, Applied Catalysis B: Environmental 81(2008)150.

26. T. Maillet, C. Solleau, J. Barbier J, and D. Duprez, Applied Catalysis B: Environmental 14(1997)85.

27. A. Donazzi, A. Beretta, G. Groppi, and P. Forzatti, Journal of Catalysis 255(2008)241.

28. S. Lima, I. Cruz, G. Jacobs, B. H. Davis, L. V. Mattos, and F. B. Noronha, Journal of Catalysis 257(2008)356.

29. X. Wang, R. J. Gorte, and J. P. Wagner, Journal of Catalysis 212(2002)225.

30. F. Arosio, S. Colussi, A. Trovarelli, and G. Groppi, Applied Catalysis B: Environmental 80 (2008)335.

31. J. Barbier and D. Duprez, Applied Catalysis A: General 85(1992)89.

32. M. Konsolakis, and I. V. Yentekakis, Applied Catalysis B: Environmental 29(2001)103.

33. P. Jozsa, E. Jobson, and M. Larsson, Topics in Catalysis 30–31(2004)177.

34. D. James, E. Fourre´, M. Ishii, and M. Bowker, Applied Catalysis B: Environmental 45(2003)147.

35. S. Poulston, and R. R. Rajaram, Catalysis Today 81(2003)603.

36. T. Lesage, C. Verrier, P. Bazin, J. Saussey, and M. Daturi, Physical Chemistry Chemical Physics 5(2003)4435.

37. Z. Liu, and J.A. Anderson, Journal of Catalysis 224(2004)18.

38. C. M. L. Scholz, B. H. W. Maes, M. H. J. M. de Croon, and J. C. Schouten, Applied Catalysis A: General 332(2007)1.

39. C. M. L. Scholz, K. M. Nauta, M.H.J.M. de Croon, and J.C. Schouten, Chemical Engineering Science 63(2008)2843

40. M. AL-Harbi, and W. S. Epling, Applied Catalysis B: Environmental 89(2009) 315.

41. H. Abdulhamid, E. Fridell and M. Skoglundh, Topics in Catalysis 30/31(2004) 161.

42. I. Nova, L. Lietti, P. Forzatti, F. Frola, F. Prinetto, and G. Ghiotti, Topics in Catalysis 52(2009)1757.

43. C. Narula, S. Nakouzi, R. Wu, C. Goralski, and L. Allard, Journal of AIChE 47(2001)744.

44. J.-S. Choi, W. P. Partridge, and C. S. Daw, Applied Catalysis A: General 293(2005)24.

45. L. Lietti, I. Nova and P. Forzatti, Journal of Catalysis 257(2008)270.

46. P-H. Han, Y-K. Lee, S-M. Han and H-K. Rhee, Topics in Catalysis 16/17(2001)165.

47. R. Burch, and P. J. Millington, Catalysis Today 26(1995)185.

48. W. S. Epling, J. Parks, N. Currier, and A. Yezerets, Catalysis Today 96(2004)21.

49. Y. Li, S. Roth, J. Dettling, and T. Buetel, Topics in Catalysis 16–17(2001)139.

50. B. Westerberg, and E. Fridell, Journal of Molecular Catalysis A: Chemical 165(2001)249.

51. L. Liotta, G. Pantaleo, A. Macaluso, G. DiCarlo, and G. Deganello, Applied Catalysis A: General 245(2003)167.

52. J. Despres, M. Elsener, M. Koebel, O. Krocher, B. Schnyder, and A. Wokaun, Applied Catalysis B: Environmental 50(2004)73.

53. L. Olsson, B. Westerberg, H. Persson, E. Fridell, M. Skoglundh, and B. Andersson, Journal of Physical Chemistry B 103(1999)10433.

54. J.M. Coronado, and J.A. Anderson, Journal of Molecular Catalysis A: Chemical 138(1999) 83.

55. W. S. Epling, A. Yezerets, and N. W. Currier, Catalysis Letters 110(2006)143.

56. E. Fridell, M. Skoglundh, B. Westerberg, S. Johansson, and G. Smedler, Journal of Catalysis 183(1999)196.

57. E. Fridell, H. Persson, B. Westerberg, L. Olsson, and M. Skoglundh, Catalysis Letters 66(2000)71.

58. A. Obuchi, A. Ohi, M. Nakamura, A. Ogata, K. Mizuno, and H. Ohuchi, Applied Catalysis B: Environmental 2(1993)71.

59. R. Burch, J. Breen and F. Meunier, Applied Catalysis B: Environmental 39(2002)283.

60. L. Olsson, E. Fridell, M. Skoglundh, and B. Andersson, Catalysis Today 73 (2002)263.

61. C. Yokoyama, and M. Misono, Journal of Catalysis 150(1994)9.

62. H. Hamada, Y. Kintaichi, M. Inaba, M. Tabata, T. Yoshinari, and H. Tsuchida, Catalysis Today 29(1996)53.

63. T. Okuhara, Y. Hasada, and M. Misono, Catalysis Today 35(1997)83.

64. T. Maunula, J. Ahola, and H. Hamada, Applied Catalysis B: Environmental 26(2000)173.

65. J. M. García-Cortés, J. Pérez-Ramírez, M. J. Illán-Gómez, F. Kapteijn, J. A. Moulijn, and C. Lecea, Applied Catalysis B: Environmental 30(2001)399.

66. E. Joubert, X. Courtois, P. Marecot, and D. Duprez, Applied Catalysis B: Environmental 64(2006)103.

67. R. Burch, and D. Ottery, Applied Catalysis B: Environmental 13(1997)105.

68. Z. Liu and J. A. Anderson, Journal of Catalysis 224(2004)18.

69. J. A. Anderson, B. Bachiller-Baezaa and M. Fernández-García, Physical Chemistry Chemical Physics 5(2003)4418

Chapter 8

DeNO$_X$ Performance in Different Hybrid DOC+NSR Systems

8.1 Abstract

A combined, in series, DOC/NSR system was evaluated in terms of NO$_X$ trapping, release, and reduction. The evaluation included comparison between two configurations. In the fist configuration, a DOC upstream of a NSR catalyst was tested in series. In the other configuration, the original DOC and NSR catalyst were divided into two equal volumes and placed in alternating series, i.e. DOC + NSR + DOC + NSR. Overall, the data show an improvement in NO$_X$ trapping, release, and reduction when the catalysts were split. At 200°C, these differences were slight due to poisoning effects by CO and hydrocarbons, though the performance with the second configuration was better for the first 10 cycles, before steady cycle-to-cycle performance was reached. At higher temperatures, the improved performance with the second configuration is related to NO$_2$ dose. "Extra" NO oxidation occurred over the 2nd DOC, increasing the inlet amount of NO$_2$ to the 2nd NSR catalyst. NH$_3$ formed from the 1st NSR catalyst during the regeneration period is oxidized over the 2nd DOC resulting in a negative impact, but this was overcome by the improved trapping due to the extra NO$_2$ formed. Also, the extents of the WGS reaction and/or C$_3$H$_6$ steam reforming increased, resulting ultimately in more H$_2$ delivered to the downstream NSR catalyst.

8.2 Introduction

Minimizing fuel consumption has increased the interest in lean-burn engines, such as diesel engines. NO_X and particulate matter emissions, however, are still considered a challenging issue in diesel engines [1-3]. Diesel particulate filters (DPFs) are being used to filter diesel particulate matter, and NO_2 and/or O_2 are used as an oxidant to oxidize the particulates on the filter [4-6]. For NO_X emissions, two different technologies, selective catalytic reduction (SCR) and NO_X storage and reduction (NSR), are being used.

NSR catalysts typically contain alkali and alkaline metal earth components that trap NO_X in the form of nitrites and nitrates and precious metals, such as Pt, Pd and Rh for the redox reactions. Both are supported on a high surface area substrate such as γ–alumina [7-11]. A NSR catalyst operates in a cyclic mode; lean and rich. In the lean phase, or normal engine operation and exhaust, NO is oxidized to NO_2 over precious metal sites and the NO and/or NO_2 is subsequently stored on the trapping material as a nitrate and/or nitrite [12, 13]. When these trapping materials reach a certain level of saturation, the exhaust is switched to a fuel-rich mode [14, 15]. In the rich mode, reductants, such as H_2, CO, and hydrocarbons (HCs) are introduced to induce the reduction of the stored NO_X to N_2 [16]. It has been reported that diesel exhaust during this rich phase can contain 2-6% CO, 1-2% H_2, and 0.3-0.92% HCs [17-19]. Numerous studies [20-31] have investigated the regeneration of NSR catalysts using different reductants. The general conclusion is that H_2 is the best reductant at low temperature, likely because CO and HCs poison Pt sites [20, 21] or Ba sites by residual isocyanates [31]. At high temperature (T $\geq$ 300°C), H_2, CO, and HCs all have comparable efficiencies in reducing NO_X to N_2 [20,22].

Diesel oxidation catalysts (DOCs) are commonly used in current diesel vehicles to reduce CO and HC exhaust emissions. DOCs can also oxidize NO to NO_2, which plays an important role in SCR, NSR and DPF aftertreatment technologies. In DPFs, NO_2 can oxidize soot at lower temperatures than O_2 [4-6]. In ammonia-SCR, it was found that the rate of SCR can be significantly increased if a portion of the NO contained in the exhaust is converted to NO_2, with an equimolar mix of NO and NO_2 being optimal [33]. Moreover, NO_2 can be readily stored, relative to NO, on NSR catalysts, especially at low operating temperatures [16, 34].

Both water and HCs are present in diesel exhaust, which possibly leads to steam reforming, producing more H_2. Hydrocarbon steam reforming has been extensively investigated over Pt, Pd, Rh, Ru, and Pt/Rd supported catalysts [35-43]. In one study [43], C_3H_6 and dodecane steam reforming was investigated over a Pt/Al_2O_3 catalyst during both steady-state and cycling experiments. C_3H_6 steam reforming started at 375°C while dodecane steam reforming began at 450°C. In another study, C_3H_8 steam reforming was investigated over $Pd/CeO_2/Al_2O_3$ and $Pt-Rh/CeO_2/Al_2O_3$ catalysts [40, 41] and reforming started at about 350°C. It should be noted that CO inherent to diesel exhaust or formed during steam reforming can also be consumed in the water gas shift (WGS) reaction to produce extra H_2. In a previous study [43], it was found that H_2 production from the water gas shift reaction over Pt/Al_2O_3 started at 225°C during both steady-state and cycling experiments.

In NSR catalysts, NO oxidation to NO_2 is an important step for overall performance. Additionally, H_2 has repeatedly been reported to be better than other reductant species (CO and HCs) in reducing surface NO_X species to N_2 [20, 22]. Engine

out NO:NO$_2$ during the lean phase is on the order of 90:10 [16, 44] and H$_2$ concentrations are about 1-2% during the rich phase [17-19]. Therefore, if the amount of NO$_2$ during the lean phase and H$_2$ delivered to the NSR catalyst during the rich phase can be increased over the upstream DOC catalyst, the NO$_X$ reduction to N$_2$ performance over the downstream NSR catalyst could be improved.

The aim of this study is to evaluate overall NO$_X$ reduction performance when the DOC and NSR catalyst are placed in series, which represents the actual configuration in NSR-equipped diesel automobiles. Furthermore, performance was also evaluated with different configurations of the DOC and NSR catalyst, by splitting the samples and alternating the series, while keeping the overall catalyst volumes the same. The latter design was tested, under the hypothesis that any NO escaping the first NSR catalyst could be re-oxidized by the second DOC and then adsorbed on the fourth piece, another piece of NSR catalyst. Furthermore, at high temperatures where the WGS reaction could be thermodynamically limited, this arrangement could result in extra H$_2$ formed by eliminating hydrocarbon inhibition and again, with H$_2$ consumed in the first NSR catalyst, more could be made in the second DOC.

8.3 Experimental Methods

A commercial DOC supplied by Umicore AG and a model Pt/BaO/Al$_2$O$_3$ catalyst supplied by Johnson Matthey were used in this study. Both samples were in monolith form. The DOC contains 95 g/ft^3 Pt supported on Al$_2$O$_3$. The monolith block that the sample was removed from had a cell density of 400 cpsi. The samples were 2.25 cm in diameter with lengths of 1, 2 and 4 cm depending on the test. The model Pt/BaO/Al$_2$O$_3$ sample contains 2.0 g/in^3 Al$_2$O$_3$, 49.9 g/ft^3 Pt and 20% BaO relative to the Al$_2$O$_3$. The

sample was removed from a monolith block that had a cell density of 300 cpsi. The samples used were 2.23 cm in diameter with lengths of 2 and 4 cm. The samples were inserted into a horizontal quartz tube reactor, which was placed inside a Lindberg temperature-controlled furnace. The catalysts were wrapped with 3M matting material to cover the gap between the catalyst and the wall of the reactor to ensure that no gas slipped around the sample. K-type thermocouples were placed at the radial center of each catalyst; one just inside the inlet face of the catalyst and one just inside the outlet face of the catalyst.

The gases and gas mixtures, except N_2, were supplied by Praxair and were metered with Bronkhorst mass flow controllers. The N_2 was produced using an On-Site nitrogen generator system. The dry gas mixture was then heated to $> 120°C$ and water was then introduced using a Bronkhorst CEM system.

In these experiments, 250 ppm NO, 50 ppm NO_2, 10% O2, 5% CO_2, 5% H_2O, and a balance of N_2 were used in the lean phase while in the rich phase 1% H_2, 3% CO, 0.5% C_3H_6, 5% CO_2, 5% H_2O, and a balance of N_2 were used. The rich time was 6 seconds and the lean times were 40, 100, and 80 seconds with 200, 350, and 500ºC respectively. The lean and rich gas mixtures were made in separate manifolds. A fourway, fast-acting solenoid valve was used to switch between the two. The calculated errors associated with these experiments were less than 1% for trapping conditions and less than 2% for regeneration conditions.

Before each experiment, the sample temperature was ramped to 500ºC with 5% H_2O, 5% CO_2, and a balance of N_2 and then the catalyst was cleaned/conditioned with a

gas mixture consisting of 5% H_2O, 5% CO_2, 1% H_2, and a balance of N_2 for 15 min. The reactor was then cooled to the target test temperature.

Experiments were performed at 200, 350 and 500°C with a space velocity, at standard conditions, of 25,000 h^{-1}. The gases exiting the reactor were maintained at > 190°C to avoid condensation and NH_3 hold-up.

The gas compositions were measured using a MKS MultiGas 2030 FTIR analyzer. Spatially resolved capillary-inlet mass spectrometry (SpaciMS) was also used to measure outlet H_2 amounts from each sample.
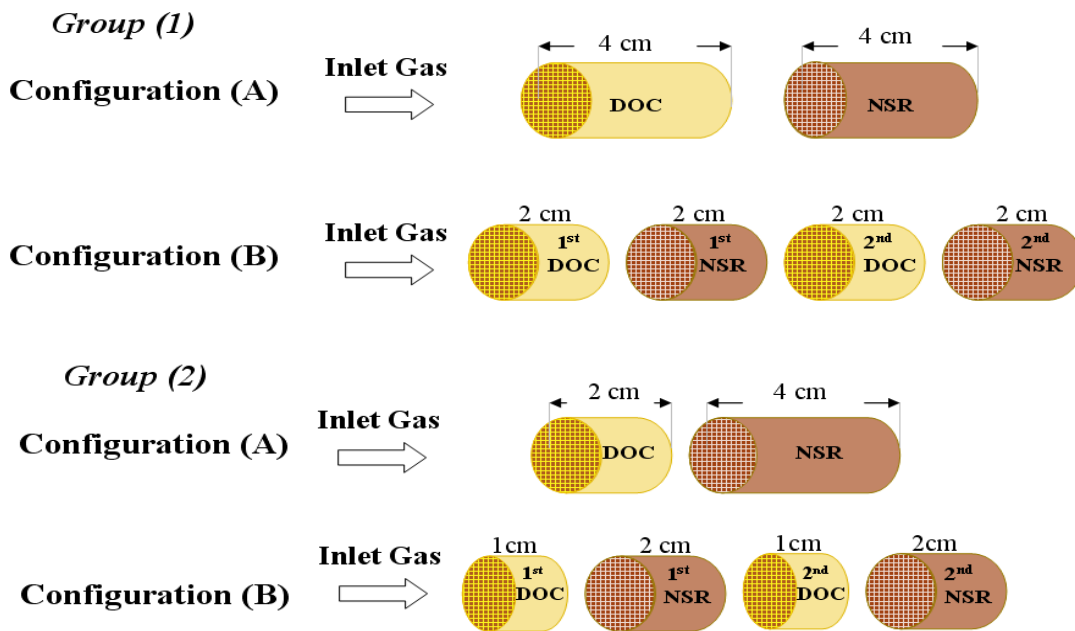
Figure 8.1 Catalyst configurations used in this study.

8.4 Results and Discussion

In this study, the DOC and NSR catalyst outlet concentrations of key reactant and product species were measured with different DOC/NSR configurations. In the first configuration, a 4 cm DOC and a 4 cm NSR catalyst were placed in series. In the second

configuration, the original DOC and NSR catalyst were divided into two equal volumes and then placed in series, so that the order of samples was: 2 cm DOC → 2 cm NSR → 2 cm DOC → 2 cm NSR. These two configurations are shown as group 1 in Figure 8.1.

8.4.1 Performance at 500°C

In the first set of experiments, the NO_X performance obtained with configuration A of group 1 were compared to configuration B. The outlet NO_X (the sum of $NO + NO_2$) concentrations obtained using 1% H_2, 3% CO, and 0.5% C_3H_6 as the reductant mixture in the regeneration phase, and at an inlet temperature of 500°C are shown in Figure 8.2.
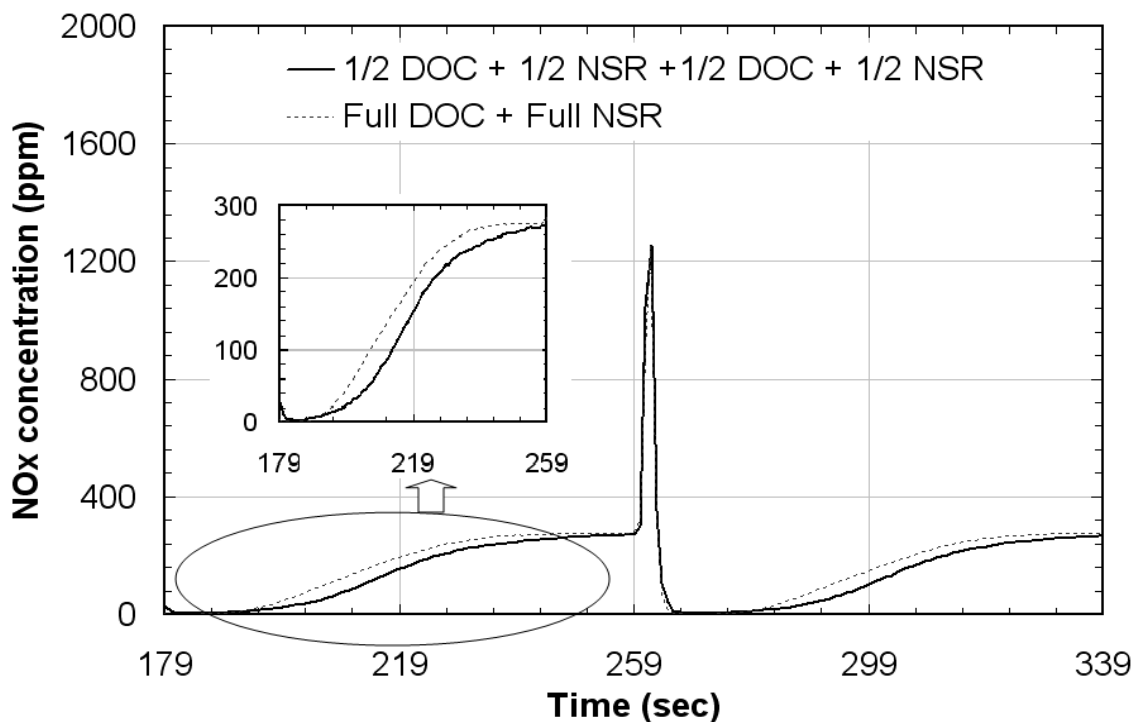
Figure 8.2 NO_X outlet concentrations obtained at 500°C with group 1 configurations. The lean gas mixtures were 250 ppm NO, 50 ppm NO_2, 10% O_2, 5% CO_2, 5% H_2O, and a balance of N_2. The rich gas mixtures were 1% H_2, 3% CO, and 0.5% C_3H_6, 5% CO_2, 5% H_2O, and a balance of N_2.

For this set of experiments, the lean, or trapping, time was 80 seconds and the rich, or regeneration, time was 6 seconds. The conversions and amounts of NO_X trapped and released for these experiments are listed in Table 8.1. All reported values and plotted data were obtained once steady cycle-to-cycle performance was observed. The data plotted in Figure 8.2 show that complete trapping was achieved over both sets for similar times, about 16 seconds. Both sets also reached trapping saturation by the end of the 80-second lean period. The amounts of NO_X trapped were 101 and 115 μmoles, and the amounts released as unreduced NO or NO_2 during the rich period were 25 and 26 μmoles for configurations A and B, respectively. It should be noted that overall catalyst performance at 500°C is low because of the weak stability of nitrate species at 500°C [45].

There are several reasons for the improved performance with the "split" configuration (configuration B). First, in the split configuration, the NSR catalyst is ultimately exposed to higher NO_2 amounts. NO_2 concentrations at the outlet of each catalyst are plotted in Figure 8.3. In both configurations, the upstream DOC oxidizes the same amount of NO, hitting thermodynamic equilibrium. As would be expected, NO_X breakthrough from the 1st NSR catalyst in the "split" configuration occurs earlier. Then some of the NO passing through the 1st NSR catalyst is oxidized to NO_2 over the 2nd DOC, which is more readily trapped on the 2nd, most downstream NSR catalyst. This is consistent with a previous study [46], where the performance of a NSR catalyst was improved when NO_2 was used instead of NO. With NO_2 being a precursor or an intermediate in the trapping process, more NO_X was trapped along the catalyst length and in conjunction with no NO_2/reactant concentration limitations, led to the improved performance. The data in Figure 8.3 demonstrate that ultimately the sum of the NSR

catalysts are exposed to a higher NO_2 flux during the trapping period compared to configuration A, where the single full size DOC and NSR samples are in series. Comparing the NO_X profiles in Figure 8.3 for the final outlet amounts, it is apparent that the bigger difference is in the amount of NO, indicating that similar NO_2 conversions are attained, and since more NO_2 was generated in configuration B, more extensive trapping was attained.

Table 8.1 Calculated performance characteristics as a function of temperature and catalyst configurations for group 1 in Figure 8.1.

| Temperature (ºC)	Group (1)	Time(sec)		NO_X Trapped (μmoles)	NO_X Released (μmoles)	NO_X Conversion (%)	NH_3 Released (μmoles)
		Lean	Rich				
200	Configuration A	40	6	44	14	27.5	0.52
	Configuration B (2nd NSR)	40	6	47	15	29.4	0.55
	Configuration B (1st NSR)	40	6	23	9	13.4	0.36
350	Configuration A	100	6	261	3.6	93	118
	Configuration B (2nd NSR)	100	6	267	3.3	95	105
	Configuration B (1st NSR)	100	6	172	22.6	54	66
500	Configuration A	80	6	101	25	34	12
	Configuration B (2nd NSR)	80	6	115	26	40	15.5
	Configuration B (1st NSR)	80	6	62	9	24	12
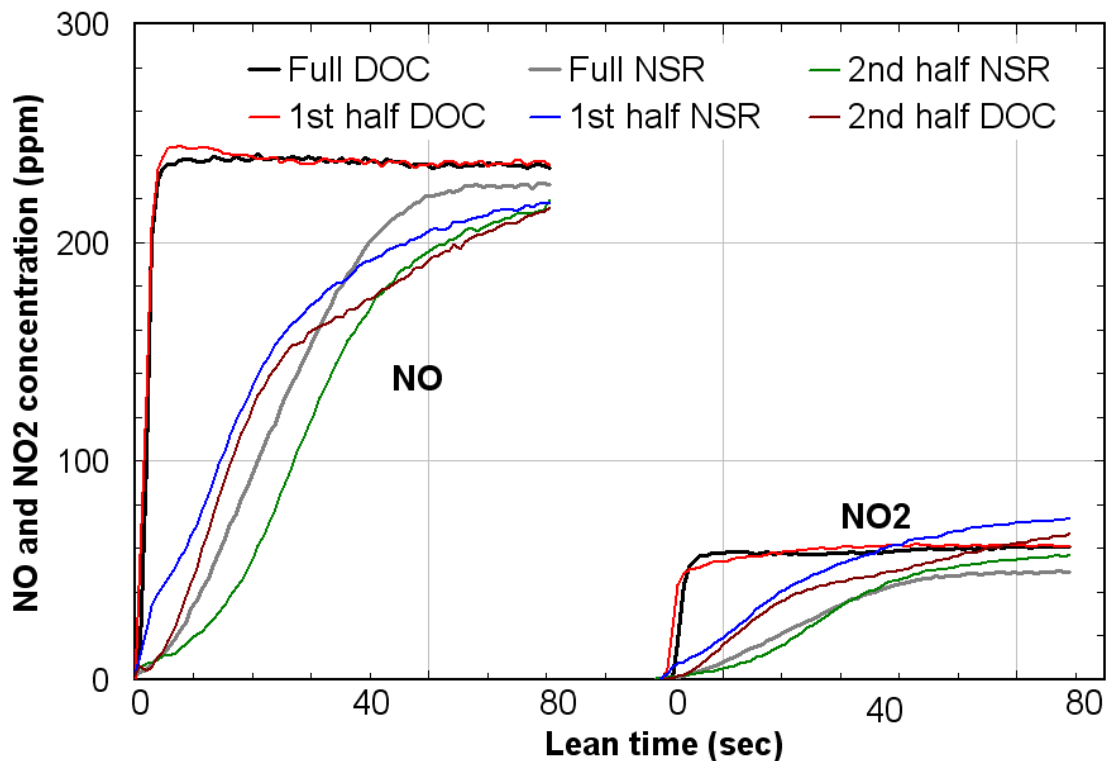
Figure 8.3 NO and NO_2 outlet concentrations obtained at 500°C with group 1 configurations. The lean gas mixtures were 250 ppm NO, 50 ppm NO_2, 10% O_2, 5% CO_2, 5% H_2O, and a balance of N_2. The rich gas mixtures were 1% H_2, 3% CO, and 0.5% C_3H_6, 5% CO_2, 5% H_2O, and a balance of N_2.

Another contributing factor to the differences in performance relates to the amount of NH_3 formed. NH_3 formation during NO_X reduction with H_2 over NSR catalysts has been extensively reported, and NH_3 also acts as a reductant [47-49]. As shown in Figure 8.4 for configuration B, NH_3 was observed at the upstream NSR catalyst outlet and 2nd DOC outlet about 1 to 2 seconds after the onset of the regeneration phase and for each, reached a maximum when the NO_X concentration decreased close to the baseline level. As shown, more NO_X, during the regeneration phase, is observed at the outlet of the 2nd DOC, relative to that at the 1st NSR catalyst outlet, while at the same

time, there is less NH_3 at the 2nd DOC outlet. These data indicate that some of the NH_3 generated on the 1st NSR catalyst is oxidized to NO_X over the downstream DOC, which also means less NH_3 is available for the most downstream NSR catalyst. If the only effect, this should actually lead to decreased performance, indicating that the enhancement observed with the extra NO_2 is somewhat decreased by this impact on the NH_3 generated.
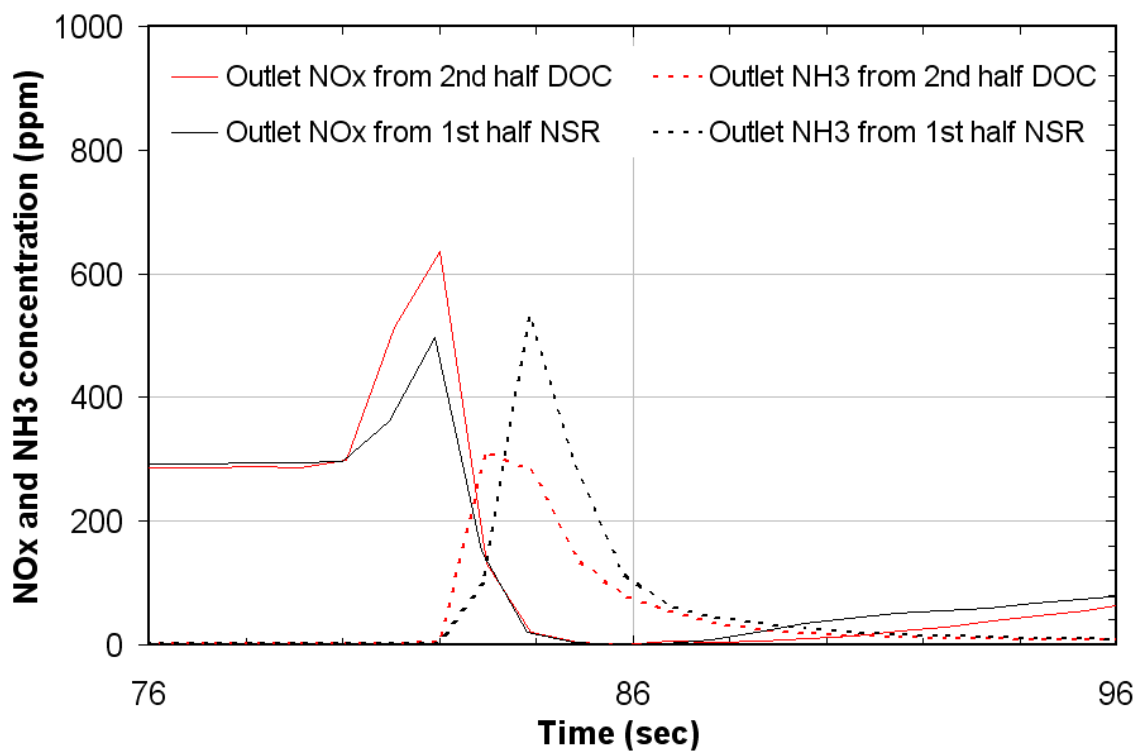
Figure 8.4 NO_X and NH_3 outlet concentrations from the 1st NSR catalyst and 2nd DOC for configuration B of group 1, obtained at 500°C with 1% H_2, 3% CO, and 0.5% C_3H_6 used in the regeneration phase.

Another factor is the changes in reductant concentrations and/or extents of either the WGS or steam reforming reactions. Peak concentration data obtained between each piece of catalyst are listed in Table 8.2. The amount of H_2 at the inlet of the NSR catalyst

213

in configuration A was 1.16%, which is about the same as that at the inlet of the 1st NSR catalyst in configuration B, while the inlet H_2 to the 2nd NSR catalyst in configuration B was 2.2%. The CO shows the opposite trend, with a higher amount of CO at the inlet of the NSR for configuration A relative to the 2nd NSR catalyst in configuration B. The increase in H_2 and decrease in CO indicate that further WGS reaction extents are realized with configuration B. The likely reason for this is that the WGS reaction is inhibited by HCs [50], and by the 2nd DOC there is less HC since more HC would be consumed over the 1st DOC and NSR catalysts, or at least reduced in concentration, as indeed the data listed in Table 8.2 show. With configuration A, only 441 ppm of C_3H_6 were consumed over the upstream DOC while 277 ppm C_3H_6 were consumed over the 1st DOC of configuration B. However, a significant amount of C_3H_6 is also consumed through the NSR catalysts, with only 21 ppm at the outlet of configuration A and 840 ppm at the outlet of the 1st NSR catalyst in configuration B, with a drop to 480 ppm across the next DOC and 0 ppm exiting the 2nd NSR catalyst. Therefore, the 2nd DOC experiences less inhibition and the amount of H_2 formed is higher, possibly leading to more extensive regeneration of the 2nd NSR catalyst. This effect, however, is likely slight since at high temperatures CO, C_3H_6 and H_2 are considered equal in terms of reduction efficacy, although in general H_2 is considered better [20-31]. Furthermore, based solely on the changes in CO and H_2 observed, it would seem that the reduction/regeneration reactions are not limited by H_2 produced through the WGS reaction since the amounts of CO consumed and H_2 formed are similar, and therefore regeneration is not reductant limited. However, since steam reforming is also likely occurring (as discussed in the following paragraph), it is not possible to determine the exact source of the H_2 increase.

Table 8.2 Outlet reductant amounts as a function of temperature and catalyst configurations for group 1, Figure 8.1.

Group 1 (Configuration A)				
Temperature (°C)	Reductant	Inlet DOC	Outlet DOC/Inlet NSR	Outlet NSR
200	CO (%)	3	2.99	2.94
	H_2 (%)	1	0.99	0.82
	C_3H_6 (ppm)	1667	1620	1610
	C_2H_4 (ppm)	0	4	4
	CH_4 (ppm)	0	4	7
350	CO (%)	3	2.9	2.4
	H_2 (%)	1	1.13	0.75
	C_3H_6 (ppm)	1667	1524	1380
	C_2H_4 (ppm)	0	20	9
	CH_4 (ppm)	0	40	25
500	CO (%)	3	2.90	1.65
	H_2 (%)	1	1.16	2.1
	C_3H_6 (ppm)	1667	1226	21
	C_2H_4 (ppm)	0	50	7
	CH_4 (ppm)	0	720	1870

Group 1 (Configuration B)					
Temperature (°C)	Reductant	Inlet 1st DOC	Outlet 1st DOC	Outlet 1st NSR	Outlet 2nd DOC	Out let 2nd NSR
200	CO (%)	3	2.99	2.97	2.93	2.93
	H_2 (%)	1	1	0.9	0.9	0.8
	C_3H_6 (ppm)	1667	1650	1638	1638	1627
	C_2H_4 (ppm)	0	3	4	3	3
	CH_4 (ppm)	0	2	4	6	9
350	CO (%)	3	2.9	2.8	2.6	2.45
	H_2 (%)	1	1.12	0.92	1.35	0.80
	C_3H_6 (ppm)	1667	1550	1520	1430	1350
	C_2H_4 (ppm)	0	15	18	19	25
	CH_4 (ppm)	0	25	18	33	22
500	CO (%)	3	2.99	2.1	1.8	1.55
	H_2 (%)	1	1.15	1.9	2.2	1.8
	C_3H_6 (ppm)	1667	1390	840	480	0
	C_2H_4 (ppm)	0	23	100	43	0
	CH_4 (ppm)	0	250	660	600	1930

As mentioned, H_2 can be produced by steam reforming over these catalysts. C_3H_6 steam reforming using the same DOC and NSR catalyst used in this study has been examined previously, and H_2 was observed via C_3H_6 steam reforming at T > 375ºC [22, 43]. However, C_3H_6 as a reductant proved effective at lower temperatures indicating a direct reaction between C_3H_6 and surface nitrite/nitrate species [22]. As mentioned above, the data listed in Table 8.2 indeed show consumption in C_3H_6 amounts across the DOC and NSR catalysts, with ultimately more consumption observed with configuration B. Some of the increased C_3H_6 consumption with configuration B could be related to the increased amount of NO_X trapped. The surface nitrates or released NO_X could be reduced by the C_3H_6 and since more was trapped with configuration B, more might be consumed.

To further study the improvement observed with the split system, another set of configurations was studied, which are described in Figure 8.1 and labeled as "group 2". It is clear from Figure 8.3 that the outlet amounts of NO and NO_2 from the 2 cm DOC are almost the same as those from the 4 cm DOC, indicating that only the first half, at most, of the DOC is utilized in NO oxidation. Therefore, for group 2, a 2 cm DOC was selected as the upstream DOC in configuration A, while in configuration B, the 2 cm DOC was divided into two equal parts and alternated with NSR samples to make configuration B. The conversions and amount of NO_X trapped and released for these experiments are listed in Table 8.3. It is apparent that NO_X performance is again better with configuration B, with similar trends to what was observed in group 1. The NO_X conversions were 24 and 30% for configurations A and B, respectively. The reasons for such improvement were discussed above. Worth noting is that the outlet NO_2 amounts from the 1st DOC in configuration B was less than that from the larger DOC in configuration A (Figure 8.5).

Table 8.3 Calculated performance characteristics as a function of temperature and catalyst configuration for group 2, as shown in Figure 8.1.

Temperature (ºC)	Group (2)	Time(sec) Lean	Time(sec) Rich	NO_X Trapped (μmoles)	NO_X Released (μmoles)	NO_X Conversion (%)	NH_3 Released (μmoles)
200	Configuration **A**	40	6	41.5	17	22.5	0.94
	Configuration **B** (2nd NSR)	40	6	43	16	24.5	0.64
	Configuration **B** (1st NSR)	40	6	22	8	13	0.54
350	Configuration **A**	100	6	265	6.3	93.5	82
	Configuration **B** (2nd NSR)	100	6	263	5.8	93	109
	Configuration **B** (1st NSR)	100	6	158	29.5	46	77
500	Configuration **A**	80	6	75	23	24	5.6
	Configuration **B** (2nd NSR)	80	6	96	29	30	19.6
	Configuration **B** (1st NSR)	80	6	55	7.4	21	11

In terms of differences in outlet NO_X concentrations between the two configurations, there were differences observed in both NO and NO_2, with both being lower with configuration B. NH_3 formation was also observed and the trend was similar to that observed in Figure 8.4(data not shown for brevity). In terms of H_2 production, the observations were also similar to those discussed above with group 1. As shown in Table 8.4, more H_2 was produced either due to more extensive WGS reaction or C_3H_6 steam reforming. This eventually would lead to more deeply regenerated NSR catalysts, resulting in better NO_X reduction performance.
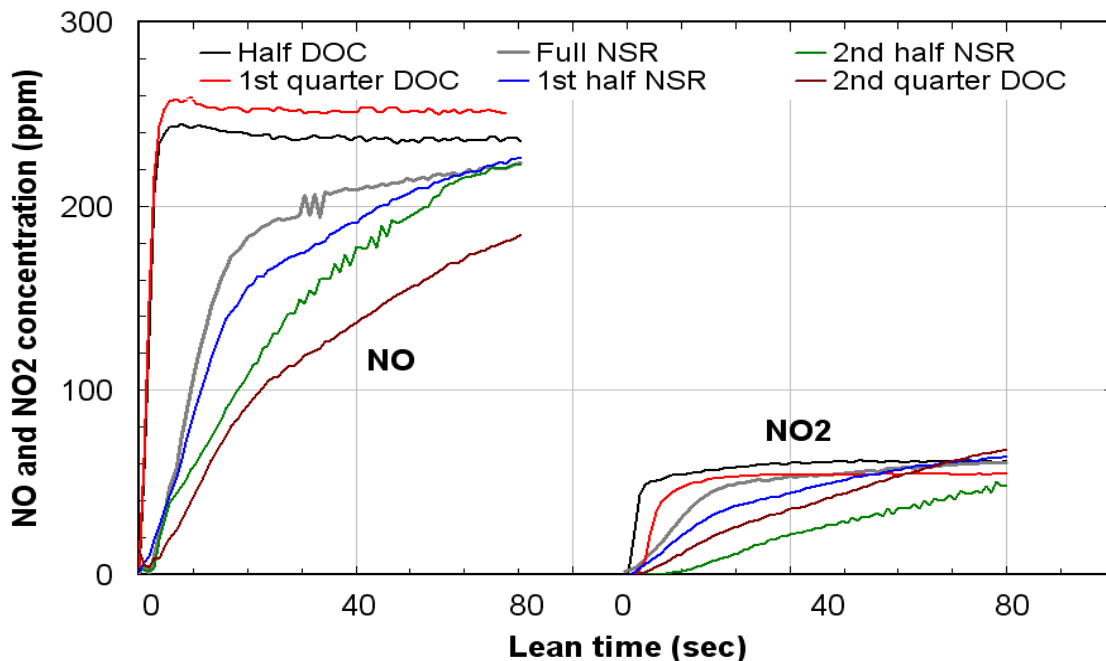
Figure 8.5   NO and NO_2 outlet concentrations obtained at 500°C with group 2 configurations. The lean gas mixtures were 250 ppm NO, 50 ppm NO_2, 10% O_2, 5% CO_2, 5% H_2O, and a balance of N_2. The rich gas mixtures were 1% H_2, 3% CO, and 0.5% C_3H_6, 5% CO_2, 5% H_2O, and a balance of N_2.

CH_4 concentrations were also monitored. They are listed in both Table 8.2 and 8.4. The CH_4 formed is due to C_3H_6 partial decomposition and not due to methanation ($CO + 3H_2 \rightarrow CH_4 + H_2O$). This was confirmed by two experiments, which were performed using a 1 cm DOC followed by a 2 cm NSR catalyst, the first two catalysts in configuration B in group 2. In the first experiment, 3% CO and 1% H_2 was used, while in the second experiment 0.5% C_3H_6 was added to 3% CO and 1% H_2. The CH_4 measured during these two experiments are plotted in Figure 8.6. Only 13 ppm CH_4 was detected in the absence of C_3H_6, indicating that the formed CH_4 during the regeneration period largely originated from C_3H_6 breaking down and not through the methanation reaction.

Table 8.4 Outlet reductant amounts as a function of temperature and catalyst configurations for group 2, as shown in Figure 8.1.

Group 2 (Configuration A)				
Temperature (ºC)	Reductant	Inlet DOC	Outlet DOC/Inlet NSR	Outlet NSR
200	CO (%)	3	2.99	2.93
	H_2 (%)	1	1	0.90
	C_3H_6 (ppm)	1667	1650	1620
	C_2H_4 (ppm)	0	3	4
	CH_4 (ppm)	0	2	8
350	CO (%)	3	2.9	2.5
	H_2 (%)	1	1.12	0.78
	C_3H_6 (ppm)	1667	1550	1400
	C_2H_4 (ppm)	0	15	30
	CH_4 (ppm)	0	25	55
500	CO (%)	3	2.99	1.8
	H_2 (%)	1	1.15	2
	C_3H_6 (ppm)	1667	1390	0
	C_2H_4 (ppm)	0	23	0
	CH_4 (ppm)	0	250	1600

Group 2 (Configuration B)					
Temperature (ºC)	Reductant	Inlet 1st DOC	Outlet 1st DOC	Outlet 1st NSR	Outlet 2nd DOC	Outlet 2nd NSR
200	CO (%)	3	2.95	2.94	2.93	2.88
	H_2 (%)	1	1	0.91	0.91	0.88
	C_3H_6 (ppm)	1667	1640	1638	1637	1620
	C_2H_4 (ppm)	0	3	3	3	3.5
	CH_4 (ppm)	0	1.5	3	3.5	6
350	CO (%)	3	2.89	2.75	2.72	2.3
	H_2 (%)	1	1.1	0.90	1.30	0.88
	C_3H_6 (ppm)	1667	1540	1520	1480	1420
	C_2H_4 (ppm)	0	22	6	13	12
	CH_4 (ppm)	0	30	17	16	10
500	CO (%)	3	2.9	2.1	2.24	1.82
	H_2 (%)	1	1.11	1.7	1.9	1.7
	C_3H_6 (ppm)	1667	1180	750	625	0
	C_2H_4 (ppm)	0	130	55	420	40
	CH_4 (ppm)	0	14	260	50	890
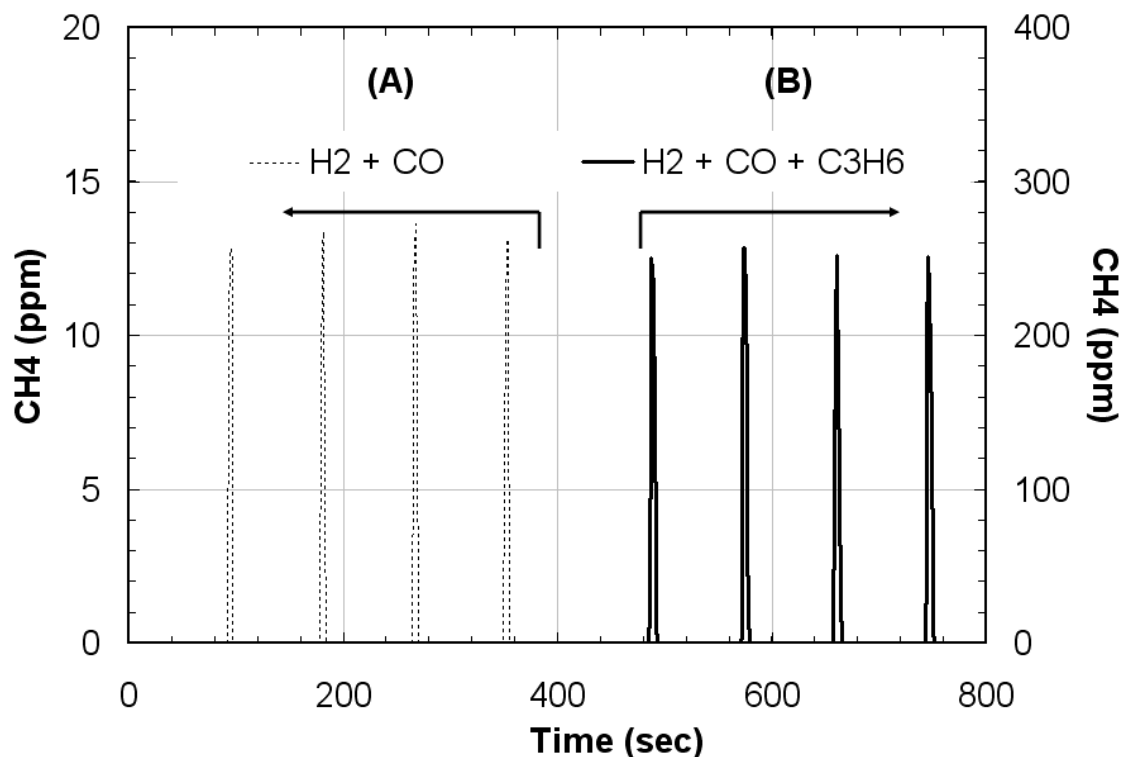
Figure 8.6 CH$_4$ concentrations obtained at 500°C with (A) 1% H$_2$, 3% CO and (B) 1% H$_2$, 3% CO, and 0.5% C$_3$H$_6$ used in the regeneration phase, using a 1 cm DOC followed by a 2 cm NSR catalyst.

8.4.2 Performance at 350ºC

Similar experiments to those at 500°C were also carried out at 350°C to investigate the influence of temperature on the storage and reduction of NO$_X$ as a function of configuration. A summary of the results are also listed in Table 8.1. Again, the NO$_X$ performance improved when the catalysts were in the split configuration. The differences in trapping, in contrast with data at 500°C, were observed from the onset of the lean phase. The amounts trapped, however, were only slightly different, 261 and 267 μmoles, and the amounts released were 3.6 μmoles and 3.3 μmoles for configurations A and B, respectively. The data still show an improvement in overall NO$_X$ performance

220

with the split configuration, though these differences are smaller than those observed at 500°C. These small differences at 350°C compared to 500°C are related to high NO oxidation activity, with a lack of thermodynamic NO_2 limitation, coincident with immediate trapping of the formed NO_2 at 350°C [16], and thus the enhancement with the split configuration is less noticeable. For example, in a previous study [46], only small differences (on order of 2% in the NO_X conversion) were observed in overall NSR performance with NO vs. NO_2 as the inlet NO_X source at 300°C, indicating that NO_X performance is independent of NO_X source in this temperature region. Figure 8.7, again as observed at 500ºC, shows that the amounts NO and NO_2 with the 4 cm and 2 cm DOC samples are the same.
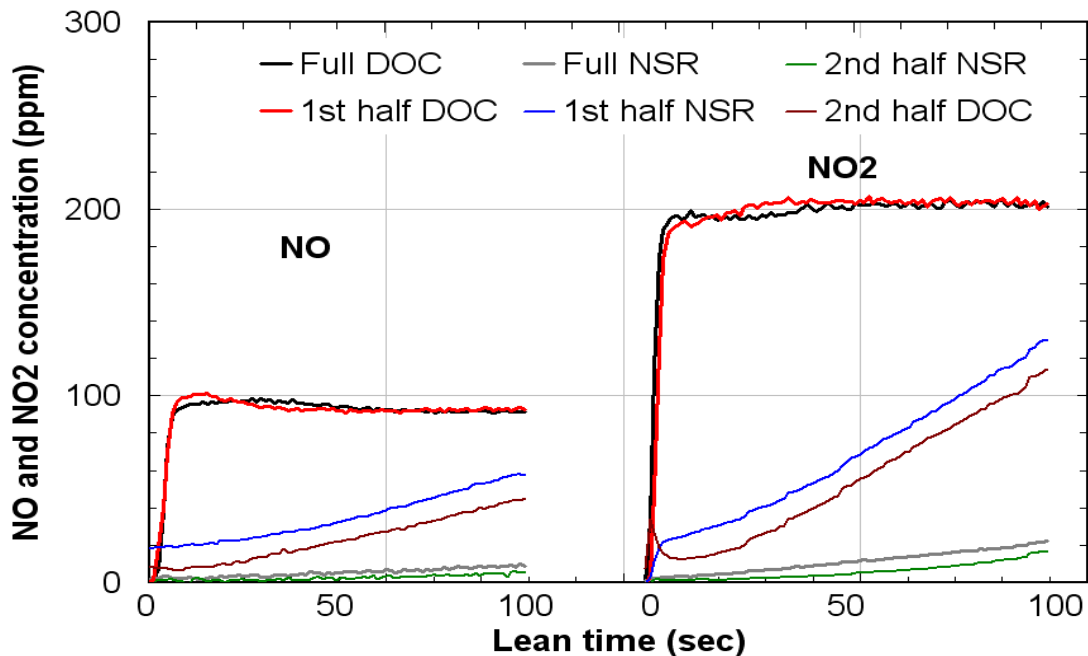
Figure 8.7 NO and NO_2 outlet concentrations obtained at 350°C with group 1 configurations. The lean gas mixtures were 250 ppm NO, 50 ppm NO_2, 10% O_2, 5% CO_2, 5% H_2O, and a balance of N_2. The rich gas mixtures were 1% H_2, 3% CO, and 0.5% C_3H_6, 5% CO_2, 5% H_2O, and a balance of N_2.

Ammonia formation was again observed after the onset of the regeneration phase and reached a maximum when the released NO_X concentration decreased to close to the baseline level. In terms of reductants, again there was an increase in the amounts of inlet H_2, with a decrease in both CO and C_3H_6 to the 2nd half NSR compared with configuration A, as shown in Table 8.2. These smaller differences in H_2 amount, vs the slight decrease in CO and C_3H_6, also lead to the smaller differences observed between these two configurations in group 1 compared to what was observed with the 500ºC data.

NO_X reduction performance was also investigated using configurations A and B in group 2. The detailed NO_X performance data are shown in Table 8.3. It should be mentioned that the trapping performance for both configurations is at first similar, complete, for the first 16 seconds of the lean phase. However, by the end of the lean phase, more NO_X was observed with configuration A at the outlet compared to configuration B. The calculated NO_X conversions were comparable with both configurations. Figure 8.8 compares the outlet NO and NO_2 concentration profiles for each catalyst in group 2. It is apparent that there are now significant differences in the outlet amounts of NO and NO_2 between the DOC for configuration A and the smaller DOC for configuration B. As at 500ºC, the 2nd DOC in configuration B did oxidize some NO. However, NO oxidation over the NSR is also appreciable at 350ºC [16, 45] and apparently this extra NO_2 from the DOC had less impact compared to 500ºC. Comparing the reductant amounts between these two configurations, again there were only small differences, as shown in Table 8.4, which contributes to the comparable performances. Overall, the strong performance at 350ºC normally noted with NSR catalysts [51] makes

any enhancement with the split configuration less noticeable under the conditions of these tests.

Figure 8.8 NO and NO_2 outlet concentrations obtained at 350°C with group 2 configurations. The lean gas mixtures were 250 ppm NO, 50 ppm NO_2, 10% O_2, 5% CO_2, 5% H_2O, and a balance of N_2. The rich gas mixtures were 1% H_2, 3% CO, and 0.5% C_3H_6, 5% CO_2, 5% H_2O, and a balance of N_2.

8.4.3 Performance at 200°C

The NO_X storage and reduction performance was also investigated at 200°C using the configurations described in Figure 8.1. The cycle time was 40 seconds for storage and 6 seconds for regeneration. The outlet NO_X concentrations obtained using configurations A and B in group 1, as described in Figure 8.1, after steady cycle-to-cycle performance had been attained, are shown in Figure 8.9. As shown, complete NO_X uptake was not

achieved. It is the presence of CO and C_3H_6 in the regeneration period that causes the decreased overall NSR catalyst performance, compared with those data at 350 and 500°C.
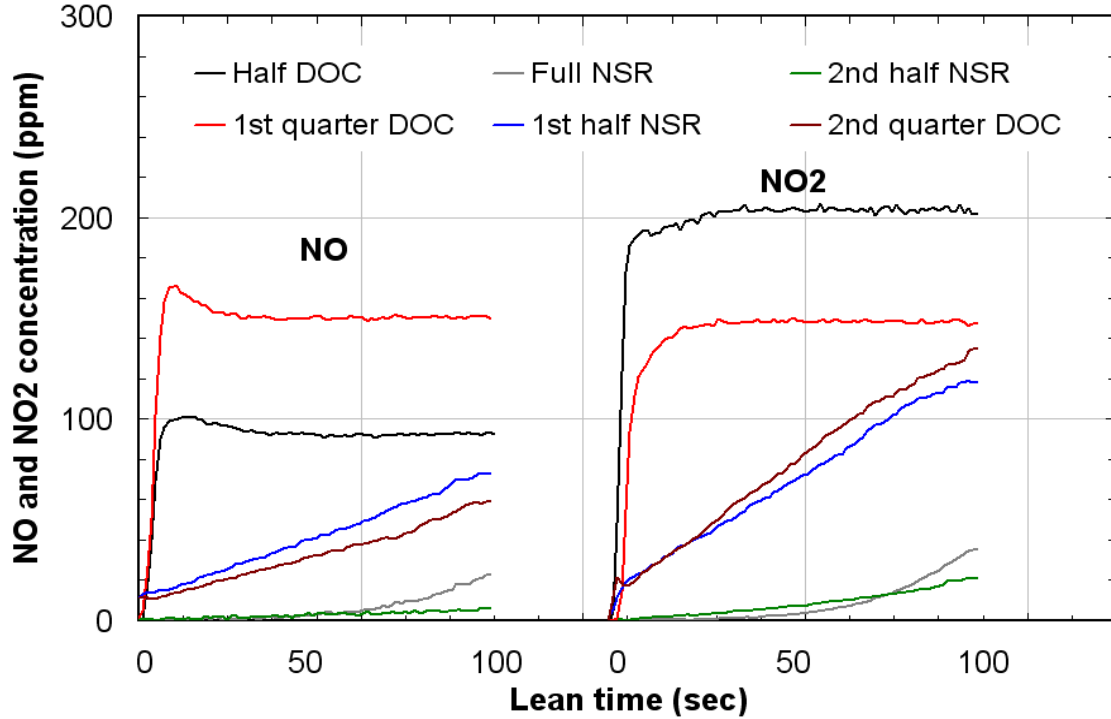

Figure 8.9 NO_X outlet concentrations obtained at 200°C with group 1 configurations. The lean gas mixtures were 250 ppm NO, 50 ppm NO_2, 10% O_2, 5% CO_2, 5% H_2O, and a balance of N_2. The rich gas mixtures were 1% H_2, 3% CO, and 0.5% C_3H_6, 5% CO_2, 5% H_2O, and a balance of N_2.

Worth noting is a second NO_X release peak during the transition from rich to lean, as highlighted in the figure. Such a feature has recently been reported [27, 52-54]. This NO_X release peak originates from the oxidation of strongly bound isocyanate on barium sites [52], formed when CO was used as the reductant in the regeneration period ($Ba(NO3)_2$ + 8CO → $Ba(NCO)_2$ + 6CO_2). These surface isocyanates are readily

224

hydrolyzed by water into NH_3 at T $\geq$ 250°C [27, 52-54], which subsequently acts as a reductant for NO_X reduction. This is consistent with the data in this study, where a second NO_X release peak was not observed during the rich-to-lean transitions at T $\geq$ 350°C. At low temperature ($\sim$ T $\leq$ 250°C), Pt sites are strongly poisoned by CO, leading to decreased hydrolysis of the isocyanates to NH_3. These isocyanates, however, are readily oxidized to NO_X at the onset of the subsequent lean phase [52], and due to the slow NO oxidation kinetics at T $\leq$ 250°C, some of the NO_X is released. Again, this is consistent with the data presented here, where NO_X release was detected at the each rich-to-lean transition at 200°C as shown in Figure 8.9.
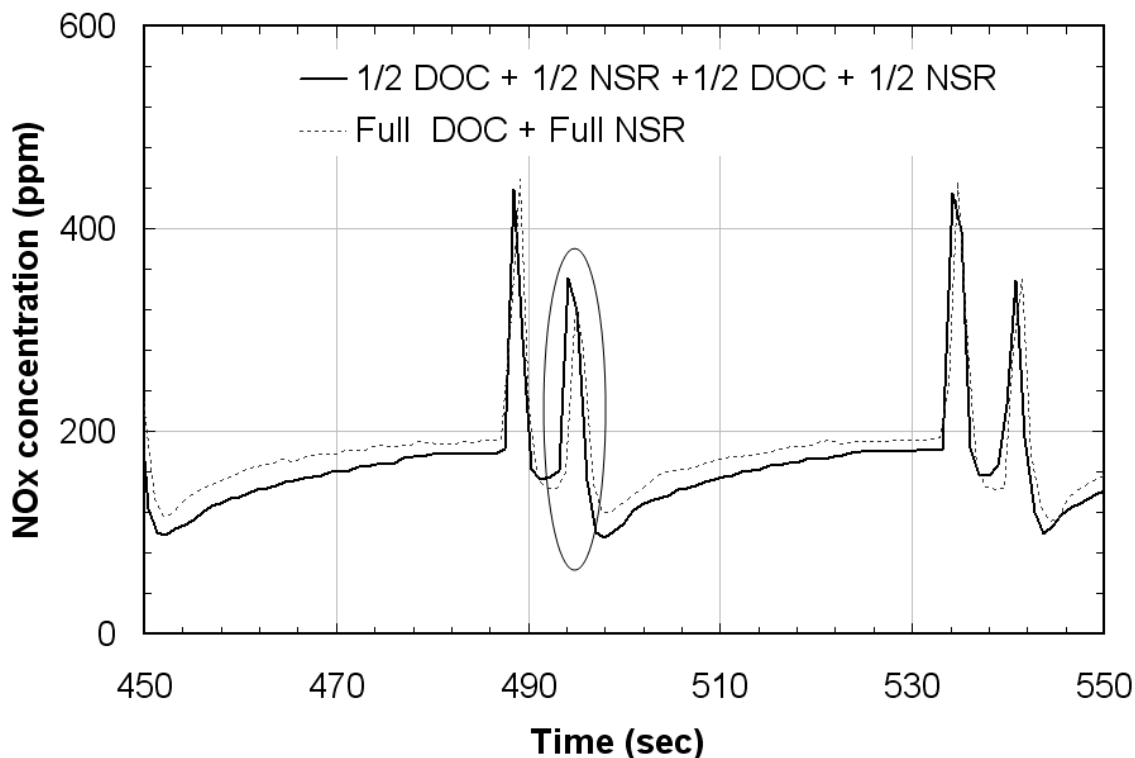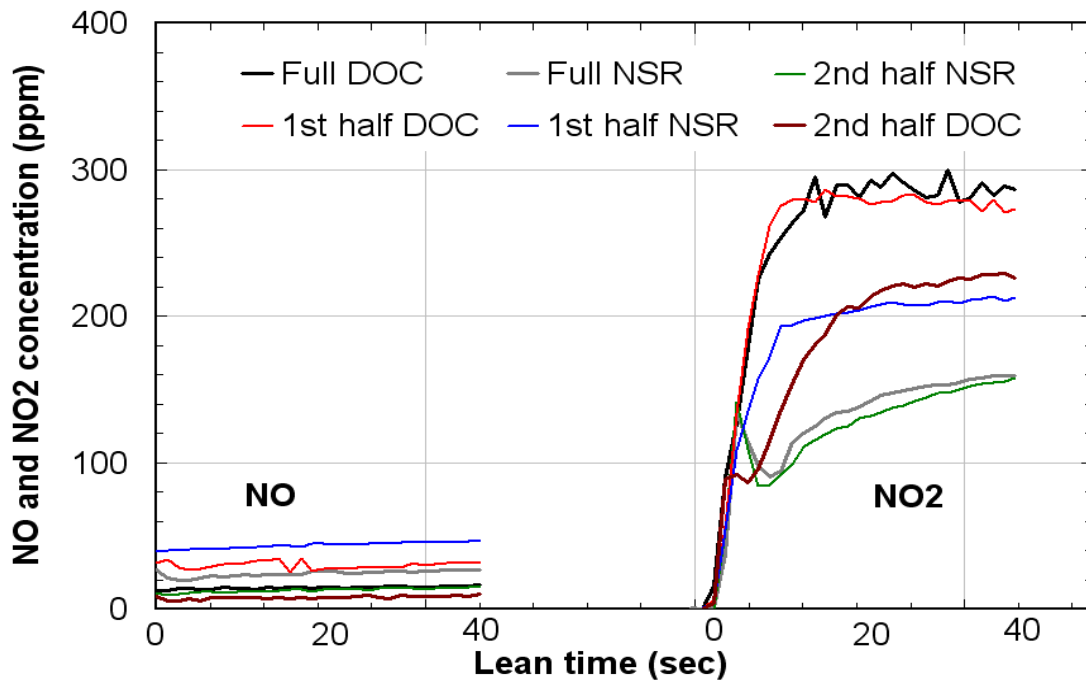

Figure 8.10 NO and NO_2 outlet concentrations obtained at 500°C with group 1 configurations. The lean gas mixtures were 250 ppm NO, 50 ppm NO_2, 10% O_2, 5% CO_2, 5% H_2O, and a balance of N_2. The rich gas mixtures were 1% H_2, 3% CO, and 0.5% C_3H_6, 5% CO_2, 5% H_2O, and a balance of N_2.

Overall, the data clearly show decreased performance at 200°C compared with 350 and 500°C. The conversion of NO to NO_2 was greater than 92% over both configurations, as shown in Figure 8.10, so the poor performance can not be explained by the low NO oxidation rates. It is the presence of CO and HC at low temperature poisoning Pt sites [20, 21] or Ba sites by residual isocyanates (NCO) [27, 31, 54] that causes this poor performance. For example, in a previous study [21] the effects of CO on NSR catalyst performance at 200ºC were characterized, and a key inhibiting effect observed was that CO significantly inhibits the regeneration process by poisoning Pt-catalyzed nitrate decomposition.

Figure 8.11 NO_X outlet concentrations obtained before steady cycle-to-cycle performance was reached at 200°C with 1% H_2, 3% CO, and 0.5% C_3H_6 used in the regeneration phase with group 1 configurations.

In comparing the results obtained at 200°C for the two configurations (group 1), the differences were small and mainly observed in terms of trapping performance. The NO_X conversions were 2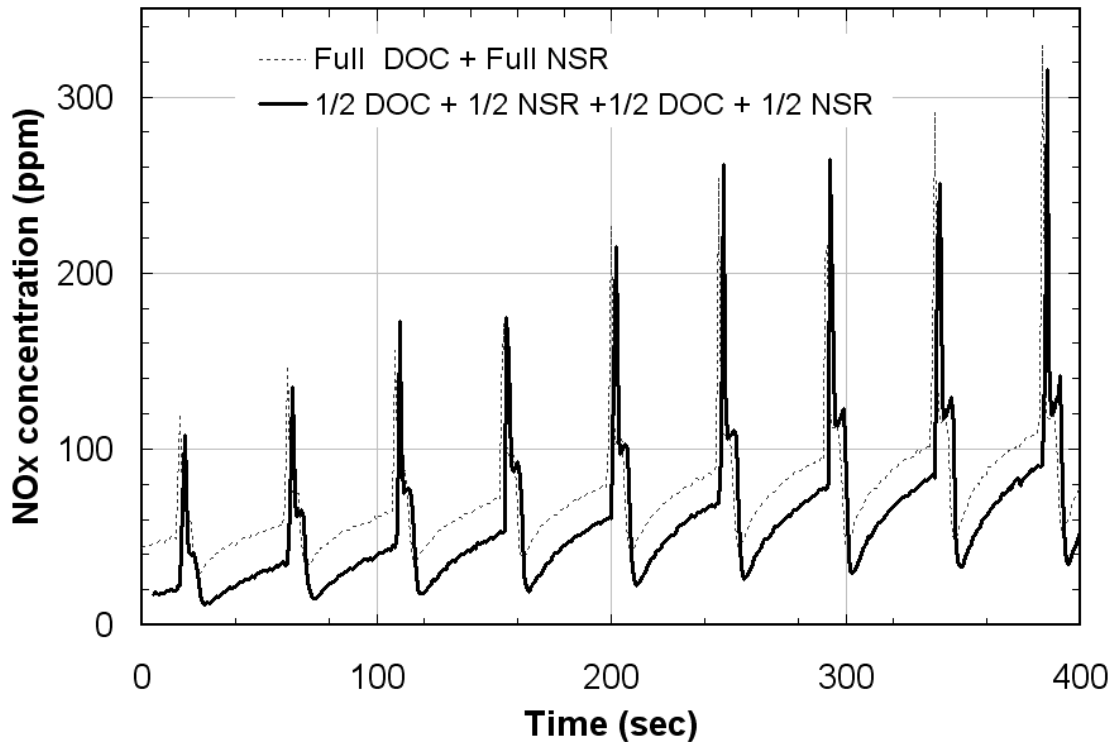7.5 and 29.4% for the two configurations, with the split sample configuration being better. If improved NO oxidation, or an overall larger dose of NO_2, leads to improved performance, but CO poisoning hinders regeneration, the first several cycles of the test should show more significant differences. The first 10 cycles of the test are plotted Figure 8.11.

Another set of experiments, identical to those described above, but using only 1% H_2 as a reductant to isolate the poisoning effects by HCs and CO, was also performed, with the data shown in Figure 8.12. Again, the performance improved with the split configuration.

The slight improvement with configuration B is still due to an overall larger dose of NO_2 for the total NSR catalyst amount. As shown in Figure 8.10, the differences in the NO and NO_2 concentrations are small, but some NO at the outlet of the 1st NSR catalyst in configuration B is oxidized over the 2nd DOC, resulting in more NO_2 for the 2nd NSR catalyst. Little to no WGS or steam reforming is evident at 200°C (Table 8.2) leading to the similar extents of poisoning and therefore similar performance. This is consistent with a previous study [43] where the WGS reaction started at 225°C, but with little H_2 formed, which contributed little to improved performance, while C_3H_6 steam reforming began at T $\geq$ 375°C. Another set of experiments were also carried out using configuration A and B in group 2, to confirm the above findings. The exact same trends were observed and therefore the results are not shown.
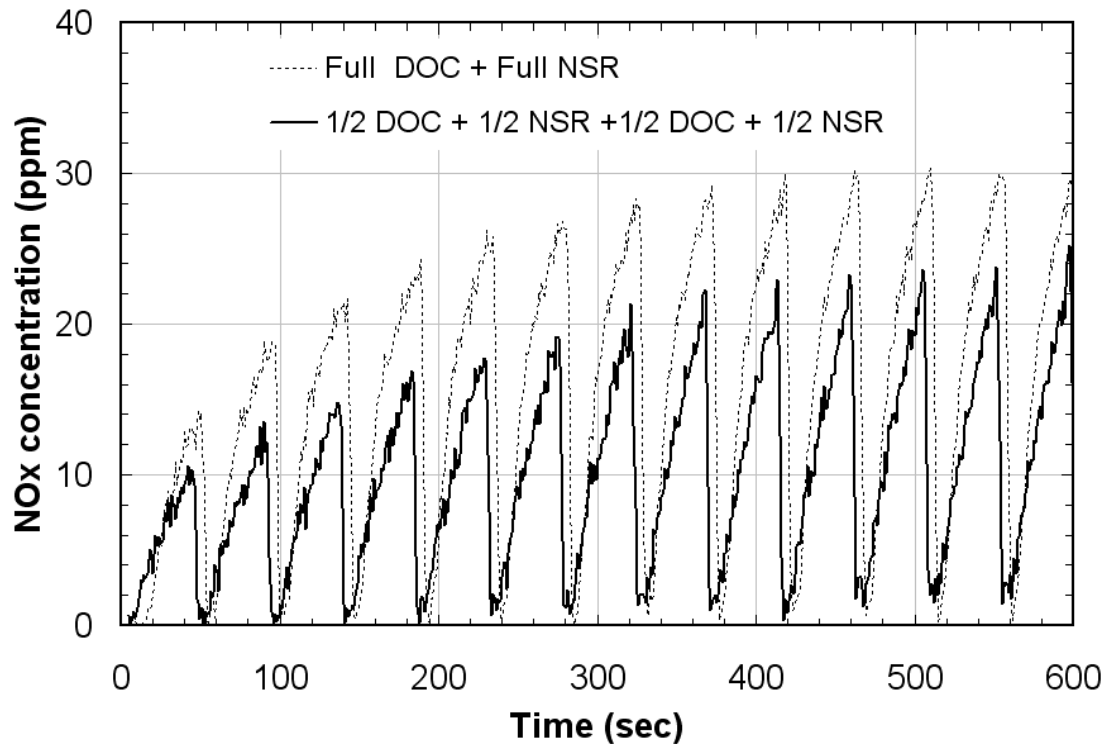
Figure 8.12 NO$_X$ outlet concentrations obtained before steady cycle-to-cycle performance reached at 200°C with 1% H$_2$ used in the regeneration phase with group 1 configurations.

It should be highlighted that it is repeatedly reported in the literature that increasing the amount of NO$_2$ upstream of an NSR catalyst will lead to improved NO$_X$ reduction performance, especially at low temperatures [55, 56]. This is because NO$_2$ is sometimes considered a precursor for nitrate formation, and necessary for the disproportionation reaction [16]. In this study, NO oxidation to NO$_2$ was significant, above 92% at 200°C with the DOC samples used. This clearly indicates that NO oxidation to NO$_2$ is not an issue with the system used in this study at 200°C. However, the performance is still poor. This clearly demonstrates that the poisoning effects of CO and HCs offset any gains that could be realized by higher NO$_2$ amounts. In application

228

diesel exhaust can contain 2-6% CO and 0.3-0.92% hydrocarbons during regeneration [17-19]. Therefore, the NSR catalyst formulations will always be poisoned by CO and HCs at 200°C, which hinders regeneration and ultimately leads to poor catalyst performance.

8.5 Conclusions

In this study, NO_X reduction using two different DOC/NSR configurations was evaluated. Overall performance was improved with the catalysts in a split configuration while maintaining the same overall catalyst volumes (DOC $\rightarrow$ NSR versus DOC $\rightarrow$ NSR $\rightarrow$ DOC $\rightarrow$ NSR). The differences in NO_X conversion were more apparent at the highest temperature tested, 500°C, due to the NSR catalyst being exposed to a larger amount of NO_2 and some of the CO and C_3H_6 being converted to H_2 for better regeneration. At 200°C, there were differences in both NO_X trapping and release for the first several cycles, but then CO poisoning of Pt and Ba sites slowed regeneration to such an extent that the extra NO_2 generated with the split configuration made little difference. At 350°C, little difference in performance was observed under the conditions tested, since NO oxidation is significant, i.e. not kinetically or thermodynamically limited, and the poisoning effects of the CO and HC species are minimal.

8.6 Acknowledgements

229

References

1. L. Gill, P. Blakeman, M. Twigg and A. Walker, Topics in Catalysis 28(2004)1.

2. K. Morita, JSAE Review 24(2003)3.

3. T. Johnson, SAE technical paper series 2006-01-0030

4. B. J. Cooper, and J. E. Thoss, SAE technical paper series 890404.

5. P. Ehrburger, J. F. Brilhac, Y. Drouillot, V. Logie, and P. Gilot, SAE technical Paper 2002011683.

6. S. A. Setiabudi, M. Makkee and J. A. Moulijn, Applied Catalysis B: Environmental 50(2004)185.

7. N. Takahashi, H. Shinjoh, T. Iijima, T. Suzuki, K. Yamazaki, K. Yokota, H. Suzuki, N. Miyoshi, S. Matsumoto, T. Tanizawa, T. Tanaka, S. Tateishi, and K. Kasahara, Catalysis Today 27(1996)63.

8. E. Fridell, M. Skoglundh, B. Westerberg, S. Johansson, and G. Smedler, Journal of Catalysis 183(1999)196.

9. S. Matsumoto, Catalysis Today 29(1996)43.

10. N. Miyoshi, S. Matsumoto, K. Katoh, T. Tanaka, J. Harada, N. Takahashi, K. Yokota, M. Sugiura, and K. Kasahara, SAE technical paper series 950809.

11. M. Crocoll, S. Kureti, and W. Weisweiler, Journal of Catalysis 229(2005)480.

12. B. Westerberg and E. Fridell, Journal of Molecular Catalysis A: Chemical 165 (2001)249.

13. S. Poulston and R. R. Rajaram, Catalysis Today 81(2003)603.

14. E. Fridell, H. Persson, B. Westerberg, L. Olsson, and M. Skoglundh, Catalysis Letters 66(2000)71.

15. W. Bogner, M. Kramer, B. Krutzsch, S. Pischinger, D. Voigtlander, G. Wenningr , F. Wirbeleit, M. Brogan, R. Brisley, and D. Webster, Applied Catalysis B: Environmental 7(1995)153.

16. W. S. Epling, L. E. Campbell, A. Yezerets, N. W. Currier and J. E. Parks, Catalysis Reviews 46(2004)163.

17. S. Huff, B. H. West, J. Parks, M. Swartz, J. Green and R. Graves, SAE technical paper series 2006-01-1416.

18. H. Mahzoul, P. Gilot, J.-F. Brilhac and B. R. Stanmore, Topics in Catalysis 16/17(2001)293.

19. M. Swartz, S. Huff, J. Parks and B. H. West, SAE technical paper series 2006-01-3423.

20. H. Abdulhamid, E. Fridell and M. Skoglundh, Topics in Catalysis 30/31(2004)161.

21. M. AL-Harbi and W. S. Epling, Applied Catalysis B: Environmental 89(2009) 315.

22. M. AL-Harbi, D. Radtke, and W. S. Epling, Applied Catalysis B: Environmental 96(2010)524.

23. M. Konsolakis, and I. V. Yentekakis, Applied Catalysis B: Environmental 29 (2001)103.

24. P. Jozsa, E. Jobson, and M. Larsson, Topics in Catalysis 30/31(2004)177.

25. D. James, E. Fourre´, M. Ishii, and M. Bowker, Applied Catalysis B: Environmental 45(2003)147.

26. S. Poulston, and R. R. Rajaram, Catalysis Today 81(2003)603.

27. T. Lesage, C. Verrier, P. Bazin, J. Saussey, and M. Daturi, Physical Chemistry Chemical Physics 5(2003)4435.

28. Z. Liu and J.A. Anderson, Journal of Catalysis 224(2004)18.

29. C. M. L. Scholz, K. M. Nauta, M. H. J. M. de Croon, and J. C. Schouten, Chemical Engineering Science 63(2008)2843

30. C. M. L. Scholz, B. H. W. Maes, M. H. J. M. de Croon, and J. C. Schouten, Applied Catalysis A: General 332(2007)1.

31. I. Nova, L. Lietti, P. Forzatti, F. Frola, F. Prinetto, and G. Ghiotti, Topics in Catalysis 52(2009)1757.

32. C. Narula, S. Nakouzi, R. Wu, C. Goralski, and L. Allard, Journal of AIChE 47(2001)744.

33. A. Grossale, I. Nova, E. Tronconi, D. Chatterjee and M. Weibel, Journal of Catalysis 256(2008)312.

34. M. AL-Harbi and W.S. Epling, Catalysis Today 130(2009)121.

35. M. C. Sanchez-Sanchez, R. M. N. Yerga, D. I. Kondarides, X. E. Verykios and J. L. G. Fierro, Journal of Physical Chemistry A 114(2010)3873.

36. C. H. Bartholomew, Applied Catalysis A: General 212(2001)17.

37. D. L. Trimm and Z. Ilsen Önsan, Catalysis Reviews 43(2001)31.

38. R. H. Ross, M. W. Roberts and J. M. Thomas, Chemical Society, London, 4(1974)34.

39. T. Montini, L. De Rogatis, V. Gombac, P. Fornasiero and M. Graziani, Applied Catalysis B: Environmental 71(2007)125.

40. W. Faria, L. C. Dieguez and M. Schmal, Applied Catalysis B: Environmental 85(2008)77.

41. J. Barbier and D. Duprez, Applied Catalysis A: General 85(1992)89.

42. C. Resini, L. Arrighi, M. Delgado, M. Vargas, L. J. Alemany, P. Riani, S. Berardinelli, R. Marazza and G. Busca, International Journal of Hydrogen Energy 31(2006)13.

43. M. AL-Harbi, J. Luo, R. Hayes, M. Votsmeier and W. S. Epling, submitted to Journal of Physical Chemistry C.

44. M. Koebel, M. Elsener, and M. Kleemann, Catalysis Today 59(2000)335

45. M. AL-Harbi, W. S. Epling, A. Yezerets, N. W. Currier, H.-Y Chen, and H. Hess, SAE technical paper series 2009-01-0631.

46. M. AL-Harbi and W. S. Epling, Catalysis Letters 130(2009)121.

47. T. Lesage, C. Verrier, P. Bazin, J. Saussey, S. Malo, C. Hedouin, G. Blanchard, and M. Daturi, Topics in Catalysis 30/31(2004)31.

48. A. Lindholm, N.W. Currier, E. Fridell, A. Yezerets, and L. Olsson, Applied Catalysis B: Environmental 75(2007)78.

49. L. Cumaranatunge, S. S. Mulla, A. Yezerets, N. W. Currier, W.N. Delgass, and F. H. Ribeiro, Journal of Catalysis 246(2007)29.

50. L. T. Thompson, Fuel Chemistry Division Preprints 48(2003)321

51. D. Bhatia, R. W. McCabe, M. P. Harold, and V. Balakotaiah, Journal of Catalysis 266(2009)106.

52. J. Luo and W. S. Epling, Applied Catalysis B: Environmental 97(2010)236.

53. J. P. Breen, R. Burch, C. Fontaine-Gautrelet, C. Hardacre, and C. Rioche, Applied Catalysis B: Environmental 81(2008)150.

54. T. Szailer, J. H. Kwak, D. H. Kim, J. C. Hanson, C. H. F. Peden, and J. Szanyi, Journal of Catalysis 239 (2006)51.

55. S. Erkfeldt, E. Jobson, and M. Larsson, Topics in Catalysis 16/17(2001)1.

56. L. Olsson, B. Westerberg, H. Persson, E. Fridell, M. Skoglundh, and B. Anderson, Journal of Physical Chemistry B 103(1999)10433.

Chapter 9

9. Conclusions and Recommendations

9.1 Conclusions

The focus of this research was to provide a systematic and comprehensive understanding of both DOC and NSR catalysts when they are used individually and in series. The extent of inhibition reactions between reactant gases in simulated diesel exhaust was investigated over a monolith-supported DOC. A detailed discussion was provided, explaining why and how this inhibition occurred. Overall, there was inhibition between CO, hydrocarbons, and NO both individually and in mixtures with NO_2. CO was less influenced among the other species because its light-off temperature was lower than that of the other species. DOCs are always placed upstream of NSR, DPF, and SCR catalysts. During the lean phase, or normal diesel exhaust conditions, DOCs can oxidize HCs, CO and NO. During the rich phase, reductants, such as HCs and CO, are available in appreciable amounts (e.g. 2-6% CO and 0.5% HCs) with H_2O. Therefore, the second objective was to investigate H_2 production from both HC steam reforming and water gas shift reactions over a DOC. The results showed that C_3H_6 and dodecane steam reforming started at 375 and 450°C, respectively, whereas the water gas shift reaction started at 225°C. The formed H_2 can be used as a reductant to reduce NO_X species during the rich phase over a downstream NSR catalyst.

For NSR evaluation, investigations included using NO or NO_2 as the NO_X source, different regeneration protocols, and evaluating different reducing agents (hydrocarbons, H_2, or CO). Overall, the performance of catalyst was improved when NO_2 was used as the NO_X source. The primary reason for this improvement is that the monolith is an

integral reactor. With NO_2 as the NO_X source, NO_2 can be readily trapped at the very inlet and along the catalyst length. This results not only in higher trapping amounts, but also in more interaction between reductant and stored NO_X along the catalyst length. The next objective was to study the influence of different regeneration protocols on NSR catalyst performance. Different regeneration times were tested, 4, 8 and 16 seconds with 4, 2, and 1% H_2 as the reductant amounts, respectively, with constant lean times. With longer regeneration times, more nitrite/nitrate decomposition occurred, leading to a cleaner surface for the next lean phase. This led to improved catalyst performance at all temperatures except 500°C, where decomposition was more rapid than reduction so that the significant release of NO_X during the rich phase led to poorer performance. The efficiency of hydrocarbons, H_2, or CO as reducing agents to reduce NO_X species to N_2 was also investigated. At $T \leq 250°C$, H_2 was found best, while at higher temperatures both CO and HCs were comparable to H_2 in regenerating the catalyst. The decreased performance with CO and HCs at 200°C was due to Pt site poisoning and at 250°C was caused by slower kinetics associated with CO and HC activation. Since the onset of propylene steam reforming occurred at 375°C, and with dodecane and m-xylene at even higher temperatures, the relatively good performance with HCs at $T \geq 300°C$ was not due to H_2 production from HC steam reforming. The likely reason is the direct reaction of HCs with NO_X species, as was proved during TPR experiments between NO and propylene.

The performance when both the DOC and NSR catalyst are placed in series was also investigated. The performance was evaluated based on two different configurations. In one configuration, a DOC and NSR catalyst were placed in series whereas in the other

235

configuration, the DOC and NSR catalysts were divided into two equal volumes and placed in alternating series. The results show an improvement in the NO_X performance with the split configuration at all temperatures tested, with small changes at 200°C due to poisoning effects of Pt and Ba sites by CO and hydrocarbons. The reasons for the improved performance with the split configuration were due to more NO_2 being delivered to the downstream NSR, H_2 production from steam reforming and WGS reactions increased, and reduced inhibition of the WGS reaction by hydrocarbons that were consumed over the first DOC and NSR catalysts.

9.2 Recommendations

The ultimate goal of this research was to offer detailed mechanisms, provide further understanding, and determine optimal conditions for the performance of both DOC and NSR catalysts individually, and in series. However, there are still some issues and questions that need to be answered. The following are a number of recommendations proposed for future opportunities:

- Diesel engine exhaust will typically contain SO_2. The extent of inhibition and how the chemistry will differ over DOC catalysts when introducing SO_2 into the inlet gases should be evaluated.

- Along the same concept, what is the effect of thermal aging, arising from the desulphation process, on the performance of the DOC catalyst?

- To better understand NSR chemistry, NO_X trapping, release, and reduction characteristics, and formation of byproducts such as NH_3 and N_2O along the

length of an NSR catalyst when either NO or NO_2 is used as a NO_X source, should be characterized using spatially-resolved capillary-inlet mass spectrometry (SpaciMS). This is especially critical for NO_2 vs NO performance to discern if it is simply NO_2 being trapped better at the front of the catalyst or if other chemistry is significant.

- During our experiments over NSR catalysts, a high amount of NH_3 was formed especially at high operating temperature. Therefore, it is would be beneficial to study the performance improvements with a downstream SCR catalyst in place.

- When the DOC and NSR catalyst are placed in series, what would be the performance of the system after thermal aging? Is the improved performance with the split configuration the same?

- According to the data obtained in this research, CO and HCs can regenerate the NSR catalyst as efficiently as H_2 at T ≥ 300ºC, but not at low temperatures due poisoning of Pt and Ba sites. Therefore, it seems critical to find a catalyst that can preferentially reduce the amount of CO and HCs at low temperature to avoid the downstream poisoning effect and improve overall performance.

Appendix A:

Statistical Analysis and Uncertainties

This experimental study involved many sample calculations to evaluate the performance of the DOC and NSR technologies. Statistical analysis and uncertainty (error) are very important in experimental studies, where they can be used to identify significant errors and hence provide guidance as to where more effort is needed to improve an experiment and assess the significance in the measurements.

Most of statistical analysis, including the one used in this section, is applied when the data are considered to follow a normal distribution. One simple test to check whether the data (sample) follows a normal distribution is using the normal probability plot. In applying this test, two sample sets were chosen; one from the diesel oxidation catalyst and the other from the NO_X storage and reduction catalyst. In the second part of this section, the reproducibility and calculated standard deviation of some selected data for both catalysts are presented. This was to check and ensure that any performed experiment is representative of the mean results. In the last section, the associated error or uncertainty with each measurement (instrument) is provided.

A.1 Normal probability plot

A normal probability plot is a graphical technique to determine if a distribution is approximately normal. When the distribution is close to normal, the plotted points will lie close to a line. Systematic deviations from a line indicate a non-normal distribution.

To apply this test, the output data (response) should be first ordered from smallest to highest. Then, each value is ranked, with the smallest starting with 1. The probability of the data's rank is subsequently calculated with the following equation:

$$P \text{ (rank)} = \frac{(i - 0.5)}{N}$$

where i is the rank of the data and N is the total number of data points.

The next step is finding the expected value of the probability, the **Z-value** that corresponds to each value of "**P**" using a normal probability distribution table. Last, the output data (responses) are plotted against a theoretical expected value of normal distribution in such a way that the points should form an approximate straight line, if it follows a normal distribution. One sample calculation will be provided for one selected data set for each catalyst type.

1. **Diesel Oxidation Catalyst (DOC)**

The sample calculation and normal probability plot is provided for C_3H_6 oxidation. In this set of experiments, C_3H_6 conversions were obtained during a temperature programmed oxidation (TPO) experiment with 1080 ppm C_3H_6, 10 % O_2, 5% CO_2, 5% H_2O, and balance N_2. The conversions (response) along with other calculations are listed in Table A.1

Table A.1 Normal probability plot table for C_3H_6 conversions

Conversion (%)	Rank (i)	P(rank)	Expected Value
0.000	1	0.024	-1.981
5.125	2	0.071	-1.465
10.277	3	0.119	-1.180
15.337	4	0.167	-0.967
20.492	5	0.214	-0.792
25.285	6	0.262	-0.637
30.287	7	0.310	-0.497
35.218	8	0.357	-0.366
40.823	9	0.405	-0.241
45.204	10	0.452	-0.120
50.577	11	0.500	0.005
55.492	12	0.548	0.120
60.449	13	0.595	0.241
65.614	14	0.643	0.366
71.209	15	0.690	0.497
75.831	16	0.738	0.637
80.454	17	0.786	0.792
86.402	18	0.833	0.967
90.575	19	0.881	1.180
95.224	20	0.929	1.465
99.751	21	0.976	1.981
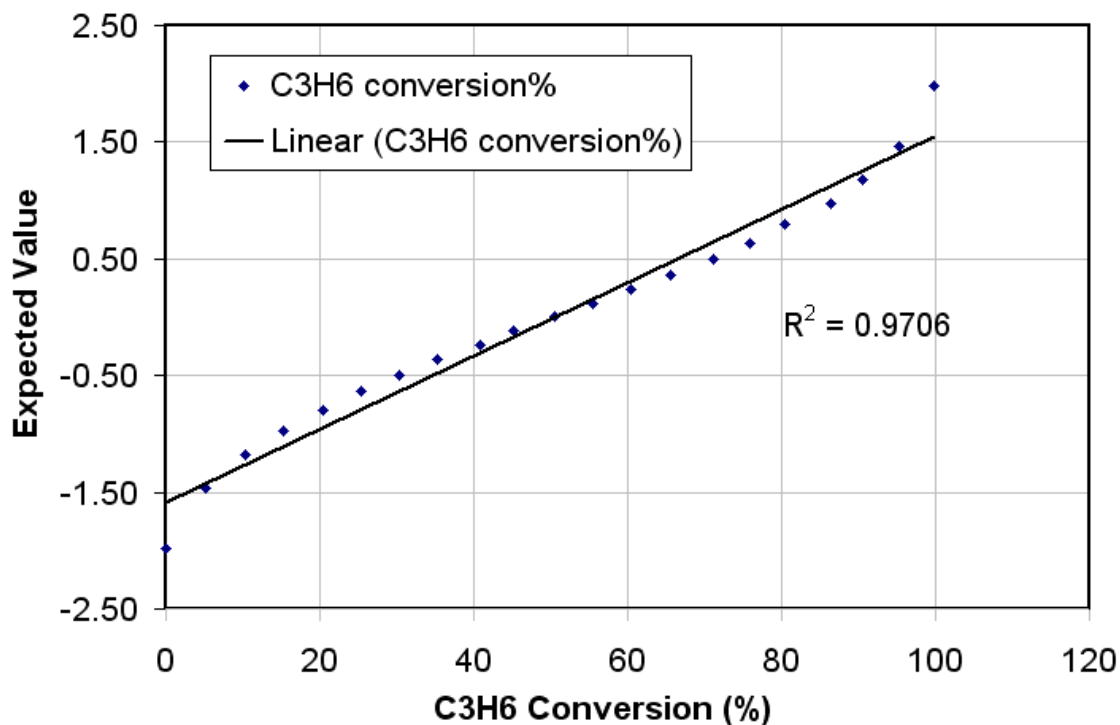
Figure A.1 Normal probability plot for C_3H_6 conversion

The points on this plot form a nearly linear pattern with a correlation coefficient, r = 0.985, the square root of R^2 (the coefficient of determination), which indicates that the normal distribution is a good model for this data set.

2. NO_X storage and reduction (NSR) catalyst

The sample calculation and normal probability plot is provided for the outlet NO_X concentration during the lean phase when H_2 was used as the reducing agent at 300°C. The detailed experiment conditions and flows are listed in Table A.2. The outlet NO_X concentrations along with other calculations are listed in Table A.3.

Table A.2 Details of flow conditions used in the experiments

Flow Conditions	Trapping (lean) phase	Regeneration (rich) phase
Space velocity	25,000 hr^{-1}	25,000 hr^{-1}
Concentrations		
NO	330 ppm	0
O_2	10%	0
CO_2	5%	5%
H_2O	5%	5%
H_2	0	3%
N_2	Balance	Balance
Cycling ratio (sec)	40	4

Table A.3 Normal probability plot table for NOx concentration

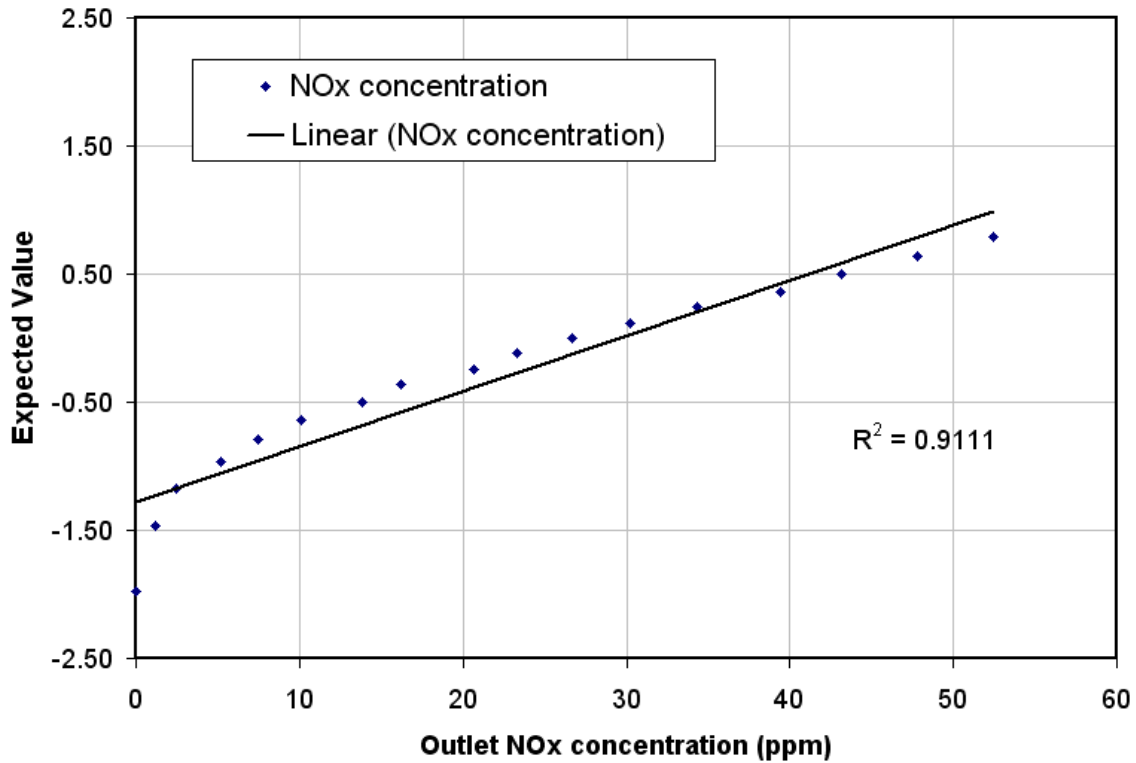| Concentration (ppm)	Rank (i)	P (rank)	Expected Value
0	1	0.024	-1.981
1.178	2	0.071	-1.465
2.441	3	0.119	-1.180
5.160	4	0.167	-0.967
7.443	5	0.214	-0.792
10.081	6	0.262	-0.637
13.868	7	0.310	-0.497
16.182	8	0.357	-0.366
20.642	9	0.405	-0.241
23.311	10	0.452	-0.120
26.692	11	0.500	0.005
30.260	12	0.548	0.120
34.357	13	0.595	0.241
39.414	14	0.643	0.366
43.135	15	0.690	0.497
47.813	16	0.738	0.637
52.410	17	0.786	0.792

Figure A.2 Normal probability plot for outlet NO_X concentration

Again, the points on this plot form a nearly linear pattern with a correlation coefficient r = 0.954, the square root of R^2 (the coefficient of determination), which indicates that the normal distribution is a good model for this data set.

A.2 Reproducibility between repeated experiments

In this section, the reproducibility, via standard deviation measurements, of selected experiments for a DOC and NSR catalyst were performed to ensure no significant variations in the measured performances.

Standard deviation (σ) is a statistical term that measures the dispersion of a set of values about the mean value. If the standard deviation for the data is small, the data values are close to the mean value, while large standard deviation means that the data points are far from the mean. Standard deviation (σ) and mean can be calculated by the following equations:

$$\sigma = \sqrt{\frac{1}{N-1}\sum_{i=1}^{N}(x_i - \bar{x})^2}$$

$$\bar{x} = \frac{x_1 + x_2 + \cdots + x_N}{N} = \frac{1}{N}\sum_{i=1}^{N}x_i$$

Where x is 50% conversion, or amounts of NO_X trapped or released depending on the experiment. $\bar{x}$ is the mean of x.

(1) Diesel oxidation catalyst

In this study, the oxidation of NO, CO, and different types of hydrocarbons was investigated individually and in mixtures with NO_2. Hydrogen production via hydrocarbon steam reforming and water gas shift reactions was also investigated. Table A.4 shows the 50% conversions for the selected experiments and their replicates. The mean and standard deviation for each repeated experiment were calculated and are reported in Table A.4. The repeated experiments of hydrogen production via C_3H_6 steam reforming and the water gas shift reaction during steady state and cycling experiments at 450°C at the middle point of the catalyst (3cm) are shown in Table A.5 along with their mean and standard deviation. Table A.6 shows CO_2 formation obtained during temperature programmed oxidation (TPO) experiments after C_3H_6 steam reforming at

450°C for 180 min and at 2 and 4 cm from the front of catalyst. Again, the mean and standard deviation associated with these experiments were calculated and reported in Table A.6. The detailed experimental descriptions were reported in previous chapters; Chapter 3 for Table A.4 and Chapter 4 for Tables A.5 and A.6.

Table A.4 Statistical analysis for the 50% conversion for the selected repeated set of experiments

Reactants	Experiment (1)	Experiment (2)	Experiment (3)	mean	Standard Deviation (°C)
CO	145	143.8	146.5	145.1	± 1.35
C_3H_6	162	163	162	162	± 1
$CO + C_3H_6$	170.1 [a] 176 [b]	172.2 [a] 177.7 [b]	173.1 [a] 175. 7[b]	171.8 [a] 176.47 [b]	± 1.52 [a] ± 1.04 [b]
$C_3H_6 +$ Dodecane	168 [b] 164.4 c	169.5 [b] 166.3 [c]	167 [b] 165[c]	168.2 [b] 165.3 [c]	± 1.26 [b] ± 0.84 [c]
Dodecane +NO [c]	164	162.2	165	163.7	±1.38
C_3H_6+NO [b]	182	184	182.4	182.8	±0.95
$C_3H_6 + NO + NO_2$ [b*]	198	199.5	197.3	198.3	±1.11

a: the 50% conversion of CO.
b: the 50% conversion of C_3H_6.
c: the 50% conversion of dodecane.
*: a mixture of 200 ppm NO and 200 ppm NO_2.

Table A.5   Statistical analysis for hydrogen production (in ppm) for the selected repeated set of experiments.

Reactants	Experiment (1)	Experiment (2)	Experiment (3)	mean	Standard Deviation (ppm)
C_3H_6 [a]	84	88	86	86	± 2
C_3H_6 [b]	474	480	478	477.3	± 2.36
CO [a]	1005	1010	1007	1007.3	± 2.12
CO [b]	1124	1127.5	1123	1124.8	± 2.32

a: Steady state experiment at 450˚C

b: Cycling experiment at 450˚C

Table A.6   Statistical analysis for CO_2 formation (in ppm) obtained during (TPO) experiments at 2 and 4 cm from the front of catalyst after C_3H_6 steam reforming experiments at 450ºC for 180 min.

Reactants	Experiment (1)	Experiment (2)	Experiment (3)	mean	Standard Deviation (ppm)
C_3H_6 [a]	80.6	82.4	78.5	80.5	± 1.95
C_3H_6 [b]	164	167	169	166.7	± 1.95

a: CO_2 formation at 2 cm

b: CO_2 formation at 4 cm

(2) NO$_X$ storage and reduction catalyst

In this study, the performance of the NO$_X$ storage and reduction catalyst was investigated based on (1) whether the NO$_X$ source was NO or NO$_2$, (2) regeneration time and H$_2$ concentration, and (3) reductant type. For Table A.7, the experiments were repeated three times when either NO or NO$_2$ was the NO$_X$ source at 500°C. In Table A.8, two regeneration protocols; 4 sec rich and 4% H$_2$ and 8 sec rich and 2% H$_2$, were repeated at 400°C. In Table A.9, the reproducibility of the catalyst performance was investigated with either C$_{12}$H$_{26}$ or H$_2$ used as the reductant at 250°C. The lean time was 60 sec and rich time was 10 sec. The detailed experiment descriptions are reported in previous chapters; Chapter 5 for Table A.7, Chapter 6 for Table A.8, and Chapter 7 for Table A.9.

According to the standards deviations listed in the tables, experiments were reproducible and show very little variation in the repeated experiments, as indicated by the small values of standard deviation. For example, H$_2$ production during cycling C$_3$H$_6$ steam reforming experiments was higher than that during steady state experiments over the DOC at 450ºC, as shown in Table A.5. The average H$_2$ formed during cycling experiments was 477.3 ppm (with $\boldsymbol{\sigma} = \pm 2.36$ ppm) whereas 86 ppm (with $\boldsymbol{\sigma} = \pm 2$ ppm) were formed during steady state experiments. Therefore, even if the standard deviation is added/subtracted, these differences are still significant. Table A.9 shows the differences in the NO$_X$ trapping and released when either C$_{12}$H$_{26}$ or H$_2$ was used as the reducing agent at 250ºC. The average NO$_X$ trapped with C$_{12}$H$_{26}$ was 63.2 μmoles (with $\boldsymbol{\sigma} = \pm 0.67$ μmoles) while 82.13 μmoles were trapped (with $\boldsymbol{\sigma} = \pm 0.67$ μmoles) with H$_2$. Again, these differences are significant.

Table A.7 Statistical analysis of the effect of NO_X source (NO or NO_2) on the catalyst performance at 500ºC with 80 sec lean and 4 sec rich. 3% H_2 was used as reducing agent.

Performance (µmoles)	Experiment (1)	Experiment (2)	Experiment (3)	mean	Standard Deviation (µmoles)
NO_X Trapping					
NO	163	166	164	164.3	± 1.2
NO_2	189	192	190.4	190.5	± 1.22
NO_X release					
NO	30.5	33	31	31.5	± 1.2
NO_2	23	26	24	24.3	± 1.3

Table A.8 Statistical analysis of the effect regeneration time on the catalyst performance. Comparison between condition A: 4 sec rich and 4% H_2 and Condition B: 8 sec rich and 2% H_2 at 400ºC.

Performance (µmoles)	Experiment (1)	Experiment (2)	Experiment (3)	mean	Standard Deviation (µmoles)
NO_X Trapping					
A	226	229	227.5	227.5	± 1.2
B	237	239	237.5	237.8	± 0.92
NO_X release					
A	10	12	11	84	± 0.81
B	16	18	16.7	16.9	±0.87

Table A.9 Statistical analysis of the regeneration of a model NO_X storage /reduction catalyst using $C_{12}H_{26}$ and H_2 as the reductant at 250ºC. The lean time was 60 sec and rich time was 10 sec.

Performance (µmoles)	Experiment (1)	Experiment (2)	Experiment (3)	mean	Standard Deviation (µmoles)
NO_X Trapping					
$C_{12}H_{26}$	62.5	64	63	63.2	**± 0.67**
H_2	81.4	83	82	82.13	**± 0.68**
NO_X release					
$C_{12}H_{26}$	18	20	18.5	18.8	**± 0.92**
H_2	7.3	9.8	7.9	8.3	**±1.16**

A.3 Uncertainty with measurements

Every measurement has a degree of error or uncertainty associated with it. Propagating the instrument's error is an important step to check whether the calculated differences between the experiments are significant or not, especially if a high error degree for the instrument is reported. The instruments used in this study can be divided into three categories; namely, the feed delivery system, reactor system, and gas analyzers. The uncertainties associated with each instrument are reported in Table A.10 and were obtained from the associated manuals.

In all experiments, the gas flow rate was greater than 10 L/min, so the listed values are considered small, and therefore their effects are negligible. For the heating

systems and thermocouples, any differences smaller than 2ºC during the experiments were considered insignificant. Uncertainties associated with the gas analyzers were also very small.

Table A.10 Uncertainties associated with instruments

Instrument Type	Associated Uncertainty
Delivery system	
Main feed delivery system	
Mass flowerers	± (2- 4) ml
Water system	
Mass flowerers	± 2.5 ml
Heating System	± 0.8˚C
Hydrocarbon system	
Mass flowerers	± 2.5ml
Heating System	± 0.9˚C
Reactor	
Thermocouples (K-type)	± 1ºC
Gas Analyzers	
FTIR (MKS)	± 0.9 %
Mass spectrometry	± 2-5%
	of the reading

Permissions

Expected completion date	Nov 2010

Introduction

The publisher for this copyrighted material is Springer Science + Business Media. By clicking "accept" in connection with completing this licensing transaction, you agree that the following terms and conditions apply to this transaction (along with the Billing and Payment terms and conditions established by Copyright Clearance Center, Inc. ("CCC"), at the time that you opened your Rightslink account and that are available at any time at http://myaccount.copyright.com).

Limited License

With reference to your request to reprint in your thesis material on which Springer Science and Business Media control the copyright, permission is granted, free of charge, for the use indicated in your enquiry. Licenses are for one-time use only with a maximum distribution equal to the number that you identified in the licensing process.

This License includes use in an electronic form, provided it is password protected or on the university's intranet, destined to microfilming by UMI and University repository. For any other electronic use, please contact Springer at (permissions.dordrecht@springer.com or permissions.heidelberg@springer.com)

The material can only be used for the purpose of defending your thesis, and with a maximum of 100 extra copies in paper.

Although Springer holds copyright to the material and is entitled to negotiate on rights, this license is only valid, provided permission is also obtained from the (co) author (address is given with the article/chapter) and provided it concerns original material which does not carry references to other sources (if material in question appears with credit to another source, authorization from that source is required as well). Permission

free of charge on this occasion does not prejudice any rights we might have to charge for reproduction of our copyrighted material in the future.

Altering/Modifying Material: Not Permitted

However figures and illustrations may be altered minimally to serve your work. Any other abbreviations, additions, deletions and/or any other alterations shall be made only with prior written authorization of the author(s) and/or Springer Science + Business Media. (Please contact Springer at permissions.dordrecht@springer.com or permissions.heidelberg@springer.com)

Reservation of Rights

Springer Science + Business Media reserves all rights not specifically granted in the combination of (i) the license details provided by you and accepted in the course of this licensing transaction, (ii) these terms and conditions and (iii) CCC's Billing and Payment terms and conditions.

Copyright Notice

Please include the following copyright citation referencing the publication in which the material was originally published. Where wording is within brackets, please include verbatim.

"With kind permission from Springer Science+Business Media: <book/journal title, chapter/article title, volume, year of publication, page, name(s) of author(s), figure number(s), and any original (first) copyright notice displayed with material>."

Warranties: Springer Science + Business Media makes no representations or warranties with respect to the licensed material.

Indemnity

You hereby indemnify and agree to hold harmless Springer Science + Business Media and CCC, and their respective officers, directors, employees and agents, from and against any and all claims arising out of your use of the licensed material other than as specifically authorized pursuant to this license.

No Transfer of License

This license is personal to you and may not be sublicensed, assigned, or transferred by you to any other person without Springer Science + Business Media's written permission.

No Amendment Except in Writing

This license may not be amended except in a writing signed by both parties (or, in the case of Springer Science + Business Media, by CCC on Springer Science + Business Media's behalf).

Objection to Contrary Terms

Springer Science + Business Media hereby objects to any terms contained in any purchase order, acknowledgment, check endorsement or other writing prepared by you, which terms are inconsistent with these terms and conditions or CCC's Billing and Payment terms and conditions. These terms and conditions, together with CCC's Billing and Payment terms and conditions (which are incorporated herein), comprise the entire agreement between you and Springer Science + Business Media (and CCC) concerning this licensing transaction. In the event of any conflict between your obligations established by these terms and conditions and those established by CCC's Billing and Payment terms and conditions, these terms and conditions shall control.

Jurisdiction

All disputes that may arise in connection with this present License, or the breach thereof, shall be settled exclusively by the country's law in which the work was originally published.

<div align="center">**ELSEVIER**</div>

WHAT RIGHTS DO I RETAIN AS AN AUTHOR?

As an author, you retain rights for a large number of author uses, including use by your employing institute or company. These rights are retained and permitted without the need to obtain specific permission from Elsevier. These include:

- the right to make copies of the article for your own personal use, including for your own classroom teaching use;
- the right to make copies and distribute copies (including through e-mail) of the article to research colleagues, for the personal use by such colleagues (but not commercially or systematically, e.g. via an e-mail list or list serve);
- the right to post a pre-print version of the article on Internet web sites including electronic pre-print servers, and to retain indefinitely such version on such servers or sites (see also our information onelectronic preprints for a more detailed discussion on these points.);
- the right to post a revised personal version of the text of the final article (to reflect changes made in the peer review process) on the author's personal or institutional web site or server, with a link to the journal home page (on ⇥ elsevier.com);
- the right to present the article at a meeting or conference and to distribute copies of such paper or article to the delegates attending the meeting;
- for the author's employer, if the article is a 'work for hire', made within the scope of the author's employment, the right to use all or part of the information in (any version of) the article for other intra-company use (e.g. training);
- patent and trademark rights and rights to any process or procedure described in the article;
- **the right to include the article in full or in part in a thesis or dissertation (provided that this is not to be published commercially);**
- the right to use the article or any part thereof in a printed compilation of works of the author, such as collected writings or lecture notes (subsequent to publication of the article in the journal); and

- the right to prepare other derivative works, to extend the article into book-length form, or to otherwise re-use portions or excerpts in other works, with full acknowledgement of its original publication in the journal.

Other uses by authors should be authorized by Elsevier through the Global Rights Department (for addresses see Obtaining Permissions), and authors are encouraged to let Elsevier know of any particular needs or requirements.

<u>Source:</u>

http://www.elsevier.com/wps/find/supportfaq.cws_home/rightsasanauthor